The Thesis Committee for Graham Mateau Soto-Kerans
Certifies that this is the approved version of the following Thesis:

Orogen Proximal Sedimentation of a Composite Foreland Basin: Investigation of Permian Foreland Basin Provenance

APPROVED BY
SUPERVISING COMMITTEE:

Scott W. Tinker, Supervisor

Jacob A. Covault, Co-Supervisor

Daniel Stockli

Xavier Janson

Orogen Proximal Sedimentation of a Composite Foreland Basin: Investigation of Permian Foreland Basin Provenance

by

Graham Mateau Soto-Kerans

Thesis

Presented to the Faculty of the Graduate School of

The University of Texas at Austin

in Partial Fulfillment

of the Requirements

for the Degree of

Master of Science in Geological Sciences

The University of Texas at Austin

December, 2018

Acknowledgements

I owe a great deal to Dr. Jacob Covault for introducing me to the world of complex provenance problems. He undertook me as one of his inaugural students after his move from Chevron to the Bureau of Economic Geology (BEG) and I am grateful for his patience throughout this process. Thank you to Dr. Daniel Stockli for instilling knowledge and scientific reason to the world of provenance far beyond the scope I had previously seen, to Dr. Scott Tinker for taking me on as a student during his ever busy schedule as the director of the BEG, and to Xavier Janson for cultivating interest in outcrop geology and making sure I wasn't always at the LA-ICP-MS lab. I would also like to thank the ranchers and landowners of the outcrops I sampled and studied during my research. Specifically, I would like to thank Gordon Buscher of the Boss Ranch, Bruce Blakemore of the Primavera Ranch, and Brad Kelly and Merrill Dana of the Iron Mountain Ranch. Without the collaboration between academic institutions and these generous landowners, this kind of research would not be possible.

This thesis has greatly benefited from the intellectual and laboratory-based support of the Quantitative Clastics Laboratory (QCL) and UT Geo-Thermochronometry Lab. Funding was provided by the QCL, BEG, and University of Texas at Austin, Jackson School of Geosciences. Thank you to the many friends within the graduate school for their research assistance as well as the many productive discussions that this research has benefited from. Finally, thank you to my family and friends for their considerable support whenever it was needed.

Abstract

Orogen Proximal Sedimentation of a Composite Foreland Basin: Investigation of Permian Foreland Basin Provenance

Graham Mateau Soto-Kerans, M.S. Geo. Sci.

The University of Texas at Austin, 2018

Supervisor: Dr. Scott W. Tinker

Co-Supervisor: Dr. Jacob A. Covault

The sedimentary fill of peripheral foreland basins has the potential to preserve a record of the processes of ocean closure and continental collision (e.g., the later phases of the Wilson cycle), as well as the long-term (i.e., 10^7-10^8 yr) sediment-routing evolution associated with these processes. However, the detrital record of these deep-time tectonic processes and the sedimentary response have rarely been documented during an entire cycle of supercontinent assembly. The stratigraphy within the southern margin of the Delaware Basin and Marathon Fold and Thrust Belt captures the record of the Carboniferous-Permian Pangean continental assembly, culminating in the formation of the Permian foreland basins. To evaluate the provenance and sediment-routing evolution of the southern, orogen-proximal region of this foreland-basin system, 1720 new detrital zircon (DZ) U-Pb ages were measured from 13 stratigraphic and paleogeographic-representative samples within the Marathon Fold and Thrust Belt and the Glass Mountains of West Texas. Additionally, 85 separate age core-rim relationships from eight of the

samples further constrain source terranes and sediment routing. Crystallization ages of zircon grains are linked to potential sediment source areas to illuminate provenance and reconstruct sediment-routing pathways. The DZ age spectra from the Marathon region exhibit marked shifts in provenance starting with the Mississippian to Pennsylvanian syn-orogenic record then transitioning to the Permian post-orogenic phase of basin fill. Changes in provenance record the evolution of the collisional margin and its linked proximal foreland. Results from this study demonstrate that the southern orogenic highlands and Gondwanan hinterland regions serve as the dominant sediment source within the proximal (southern) basin. Though extensive paleocurrent and subsurface mapping of the northern portions of the Delaware Basin have yielded sediment input from the north, these distal portions of the Delaware Basin also potentially show a strong southerly sediment source during both syn- and post-orogenic basin filling periods. In the studied area, the appearance of Neoproterozoic—Cambrian zircon grains in the Pennsylvanian Haymond Formation points towards basin inversion and the uplift and exhumation of volcanic units related to Rodinian rifting. Moreover, the upsection decrease in Grenvillian (~1300-920 Ma) and increase in Paleozoic zircons denotes a steady provenance shift from that of dominantly orogenic highland sources to that of sediment sources deeper in the Gondwanan hinterland during tectonic stabilization. The lack of drastic changes in provenance during the early to middle Permian supports the argument for tectonic quiescence within the collisional domain during this time period. Furthermore, the ability to pull multiple ages of zircon crystallization from individual grains demonstrates zircon histories correlative with igneous and metamorphic occurrences within the southern Gondwanan continent, aiding in constraint of a dominant southern source. We supplemented these new data with published DZ geochronologic datasets of regional provenance studies from older and contemporaneous basin filling episodes along the Appalachian-Ouachita suture zone as

well as within the Laurentian cratonic interior. Our results suggest dominant sediment delivery to the Marathon region from the nearby southern orogenic highland; less sediment was delivered from the axial portion of the Ouachita or Appalachian regions suggesting that this area of the basin was not affected by the so-called transcontinental drainage. The provenance evolution of sediment provides insights into how continental collision directs the dispersal and deposition of sediment in the Permian Basin and analogous foreland basins.

Table of Contents

List of Tables

List of Figures

INTRODUCTION

Major tectonic and geologic events, such as ocean closure and continental collision, and the evolution of associated sediment-routing systems, are recorded within the sedimentary fill of foreland basins (Jordan et al., 1988; Decelles and Giles, 1996; Ingersoll, 2012). By recording precise ages of sediment transported at a unique time and place, detrital zircon (DZ) U-Pb geochronology has been shown to be a powerful provenance analysis tool to elucidate hinterland tectonic and erosional processes and associated depositional record (Dickinson, 1988; Fedo et al., 2003; Gehrels, 2012; Gehrels, 2014). Thus, this methodology provides invaluable insights into the geological processes linked to (super-) continental assembly and can help track the complex temporal and spatial evolution of these systems (Graham et al., 1986; Haughton et al., 1991). The Permian Basin is the result of the diachronous collision between the Gondwanan and Laurentian continental plates during the late Mississippian to early Permian, completing the formation of the supercontinent Pangea. This collision led to the inversion of the Laurentian continental margin, over-thrusting of Gondwanan crust, and the formation of several flexural foreland basins and uplifts (King, 1930; King, 1937; Ross, 1986; Yang and Dorobek, 1995; Poole, 2005). The Delaware Basin is the western of two major sub- basins that make up the composite Permian foreland basin. It contains extensive hydrocarbon reservoirs in both conventional deep-water sandstones as well as unconventional shale and carbonate strata. These important resources have motivated numerous studies of the depositional environment and reservoir quality across the basin (Hills, 1984; Harms, 1988; Dutton, 2003; Gardner et al., 2003; Pyles et al., 2010). The Pennsylvanian to middle Permian stratigraphy exposed along the southern margin of the Delaware Basin offers the

unique opportunity to study the geological processes related to late Paleozoic Laurentia-Gondwana continental collision and the foreland basin deposition proximal to the orogenic front.

Provenance studies have been employed to reconstruct the evolution of numerous orogenic systems, such as the Andes or the Himalayas, which still preserve much of both the orogenic hinterland and the marginal basins. In contrast, the Permian Basin represents a more significant challenge as the bulk of the Gondwanan hinterland subsequently rifted away during Mesozoic opening of the Gulf of Mexico (Hatcher et al., 1989; Thomas, 2006; Thomas 2011b). Hence, the sedimentary strata along the southern margin of the Permian Basin offer the potential to help unravel the long-term geological and tectonic evolution of this collisional episode despite the missing or inaccessible hinterland. While the provenance of these sedimentary units has received relatively little attention, several models for the sediment sourcing and routing have been proposed (Kocurek and Kirkland, 1998; Soreghan and Soreghan, 2013). The recent advent of isotopic provenance analysis through DZ U-Pb dating has provided critical process-oriented insights into the linkages between basin formation, hinterland tectonics/unroofing, sediment routing, drainage reorganization, and basin subsidence as read in the basin fill history (Gehrels, 2012; Sharman et al., 2015; Lawton et al., 2016; Thomson et al., 2017). Recent provenance studies have employed DZ U-Pb geochronology in order to interpret sediment sources for the voluminous clastic reservoirs within the Permian Basin (Soreghan and Soreghan, 2013; Anthony, 2015; Xie et al., 2018). These studies identified an unexpected signal of southern sediment provenance (i.e., Peri-Gondwana). However, the sediment-routing scenario continues to be developed. For example, Soreghan and Soreghan (2013) interpret southerly provenance for the Guadalupian section in the northwestern Delaware Basin, but not by a direct feeder system. Rather, sediment was contributed via transcontinental river systems

stemming from the Ouachita and Appalachian regions, which deflated into eolian erg systems ultimately transporting sediment to the Delaware Basin.

We used DZ U-Pb geochronology to define the signal of southern provenance and direct sediment supply from the Marathon Fold and Thrust Belt and Gondwanan hinterland terranes. Moreover, the southern margin of the Delaware Basin comprises strata that document the collisional phases of Pangea; the long-term (10^7-10^8 yr) tectonic processes associated with this supercontinent assembly likely significantly influenced the provenance and sediment-routing evolution of the Delaware Basin.

GEOLOGIC SETTING AND STRATIGRAPHY

The southwestern margin of the Marathon-Ouachita orogenic belt was originally delineated by rifting of the Rodinian continent during late Precambrian—Cambrian time, and Mississippian—Permian diachronous collision of Laurentia and Gondwana resulting in the formation of Pangea (Hatcher et al., 1989; Thomas, 2006; Thomas 2011b). The accretionary margin is one of few that preserves in outcrop the entire complex tectonic history of diachronous continental collision, making it of unique structural interest and the focus of palinspastic reconstruction of numerous studies (Tauvers, 1988; Arbenz et al., 1989; Arbenz, 1989; Muehlberger and Tauvers, 1989; Viele and Thomas, 1989; Cawood et al., 2001; Thomas, 2006; Thomas, 2011a; Thomas, 2011b; Thomas, 2014).

Directly adjacent to the southernmost margin of the Delaware Basin, outcrops of the Marathon region expose the folded and faulted strata of the Marathon Fold and Thrust Belt (Fig. 1, Fig. 2) (McBride, 1989; Muehlberger and Tauvers, 1989; Viele and Thomas, 1989; Hickman et al., 2009). Mostly consisting of deep-water strata, these units were deformed and thrust onto the Laurentian margin as orogenic masses on the leading edge of the Gondwanan continental front (King, 1930; King, 1937; Ross, 1986; Muehlberger and Tauvers, 1989). The continuous piling and loading of these accretionary deposits onto the southern Laurentian margin led to the formation of a massive orogenic wedge, and load-induced flexure in the foreland to the north and northwest (Ross, 1986). Subsequent rapid erosion of these masses resulted in thick accumulations of sediment in the adjacent basins.

IAPETAN RIFTED MARGIN – RODINIAN BREAKUP

Prior to the Assembly of Pangea, Late Precambrian—Cambrian rifting of the Rodinian continent formed the inherited promontories and embayments of southern Laurentia (Fig. 3, Fig. 4) (Arbenz et al., 1989; Cawood et al., 2001; Thomas, 2011b). The

traces of these large-scale features consist of the northwest-trending transform faults (Alabama-Oklahoma and Texas Transforms) and northeast-trending rift segments (Blue Ridge, Ouachita, and Marathon) (Arbenz et al., 1989; Thomas, 2006; Thomas, 2011b). Rifting of the Rodinian supercontinent occurred between ca. 825 Ma and 740 Ma with notable volcanic pulses from 780-540 Ma (Li et al., 2008; Hanson et al., 2016). Stabilization of the new Laurentian continent resulted in passive margin deposition of ~975-1100 m of thin-bedded limestone, shale, chert, and shaly sandstone during the Late Cambrian—Devonian or Early Carboniferous (~170 Myrs) (King, 1978; McBride et al., 1989; Hickman et al., 2009). The interior southern margin of Laurentia contained the Tobosa Basin, a remnant feature of the Rodinian breakup during Neoproterozoic-Cambrian time (Fig. 3) (Walper, 1982; Keller et al., 1983; Arbenz et al., 1989; Li et al., 2008). This region was characterized by weak crustal extension and a low subsidence rate during the lower Paleozoic (Galley, 1958; Horak, 1985).

CONVERGENCE AND COLLISION OF LAURENTIA AND GONDWANA

During the Mississippian-Permian collision of Laurentia and Gondwana, mountain ranges formed across the axial continental divide through growth of orogenic wedges and their thrusting onto the southern margin of the Laurentian continent (Fig. 4, Fig. 5) (Ross, 1986; Poole et al., 2005; Keppie et al., 2008). The combined influences of tectonic stress related to the advancing Marathon Fold and Thrust Belt, and pre-existing lithospheric weakness from the antecedent Tobosa Basin segmented and isolated the Permian Basin along renewed northwest- to north-trending fault zones such as the Puckett-Gray Ranch fault, an intrabasinal uplift known as the Central Basin Platform, and basin-bounding highs as seen in the Diablo Platform, Northwest Shelf, Eastern Shelf and Devils River Uplift (Fig. 6) (Ross, 1986; Yang and Dorobek, 1995; Ewing, 2016). By defining the morphology

of the Permian Basin, these tectonically synthesized, basin-bounding fault zones and basement uplifts altered its structural evolution and subsidence history while simultaneously changing the patterns of foreland deposition (Muehlberger and Tauvers, 1989; Yang and Dorobek, 1995). Here, we describe the Permian Basin as a "composite foreland basin" because of the complex system of tectonic and load-induced flexures that form the separate sub-basins and uplifts, which are not prevalent in all foreland basin systems.

STRATIGRAPHIC RECORD OF THE GLASS MOUNTAINS AND MARATHON FOLD AND THRUST BELT

Situated in the southernmost Delaware Basin, the Glass Mountains and Marathon Fold and Thrust Belt contain outcrops of the entire syn- to early post-collisional stratigraphic section (Fig. 2, Fig. 7) (King, 1930; King, 1937; King, 1978; McBride et al., 1989). The deposits within this region record two stages of sedimentation—pre-collisional passive margin strata of the southern Laurentian continent, which are generally characterized by thin-bedded limestone, shale, chert and shaly sandstone (~975-1100 m over ~170 Myrs), and the rapid accumulation of 4200-5600 m of syn-orogenic strata spanning only 60 Myrs (Fig. 2, Fig. 7) (King, 1937; King, 1978; Flawn et al., 1961; Thomson and McBride, 1964; Hickman et al., 2009; McBride et al., 1989). The Late Mississippian-Early Pennsylvanian Tesnus Formation is a shaly sandstone representing flysch deposits forming submarine fan and channel complexes sourced from the approaching Gondwanan continental terranes (McBride et al., 1989; Hickman et al., 2009). Overlying the Tesnus is the Pennsylvanian age Dimple Limestone and Haymond Formation. The early Pennsylvanian age Dimple Limestone indicates a short period of waning tectonism in which a northern shelf equivalent fed carbonate turbidites southward

(Janson and Hairabian, 2016). Deposited during strong tectonic activity, the sediment source history of the Haymond Formation remains controversial (King, 1958; Denison et al., 1969; McBride et al., 1989; Gleason et al., 2007). The latest Pennsylvanian unit in the system is the Gaptank Formation. Regionally, coarse clastic fluvial and deltaic sediments mark the lower Gaptank. In contrast, the Gaptank in the Glass Mountains is composed of carbonate shelf deposits and phyloid algal mounds, indicative of tectonic quiescence in the region (King, 1937; Janson and Hairabian, 2016). A few miles north of these exposures are the late Paleozoic deposits of the Glass Mountains. The Glass Mountains expose a series of north-northwest prograding mixed carbonate-siliciclastic deposits (Fig. 1, Fig. 2). The 1500-2000 m of Wolfcampian-Guadalupian (Early to Middle Permian) stratigraphy of the Glass Mountains range in depositional setting from Wolfcampian proximal syn-orogenic conglomerates to Guadalupian carbonate reef-rimmed platform and slope (King, 1930; King, 1937; Ross, 1963; Janson and Hairabian, 2016).

PREVIOUS PROVENANCE STUDIES

Long-standing interpretations (Fig. 8) have concluded that the majority of siliciclastic input to the Delaware Basin during middle Permian (Guadalupian) time was sourced from the Ancestral Rocky Mountains (ARM) of central Laurentia. Hull Jr. (1957) suggested that observed arkosic mineralogy of the sandy and silty units of the Artesia and Delaware Mountain group of the Northwest Shelf were evidence of north-to-south transport of sediment from a plutonic-metamorphic source such as the ARM and midcontinent region of Laurentia. Fischer and Sarnthein (1988) emphasized similarities between the Delaware Basin (arid, low latitude, south of the northern trade-wind belt) to the Holocene—Pleistocene of northwest Africa, as well as generally north-south trending paleocurrent data from dunes in the Grand Canyon region during late Paleozoic time to be

evidence of an ARM source for the Delaware Mountain group of the Guadalupe Mountains. Alternatively, Kocurek and Kirkland (1998) suggested that paleogeography and paleowinds would support eolian sediment transport from the Whitehorse Group of the Anadarko Basin, Oklahoma. More recently, through a combination of DZ U-Pb geochronology, compiled paleocurrent data, and paleoclimate data, Soreghan and Soreghan (2013) refuted an ARM source for the Delaware Mountain Group. They documented dominant Paleozoic, Neoproterozoic, and Mesoproterozoic DZ age modes, and minor late Paleoproterozoic ages that would be indicative of an ARM source (Yavapai-Mazatzal ≈ 1825-1600 Ma). Instead, they suggest that measured U-Pb age modes combined with Laurentian paleocurrent data point to a combination of recycled Appalachian/Ouachita derived sources, and Gondwanan and Pan-African terranes south of the Ouachita-Marathon suture. These studies are focused in the Guadalupe Mountains of the northwestern Delaware Basin. Using DZ samples from the central and southern Delaware Basin proper, Anthony (2015), and Xie et al. (2018) suggested sediment sourcing from the Appalachian orogenic belt, Ouachita orogenic belt, and Peri-Gondwanan terranes while also noting a shift in provenance during the middle Permian, suggesting a continental-scale fluvial system spanning from the Appalachian orogenic belt westward across Pangea (Fig. 8). While the Guadalupe Mountains and Delaware Basin proper have been at the epicenter of stratigraphic and provenance studies, detailed work in the Glass Mountains has historically lacked similar treatment. Gleason et al. (2007) analyzed detrital zircons from the Pennsylvanian Haymond Formation of the Marathon Fold and Thrust Belt, suggesting that sources range from the Laurentian Craton, uplifted strata of the remnant ocean basin, Gondwanan crustal sources, and Ouachita sources to the East. Gleason et al. (2007) went further to interpret transport of this sediment as braid deltas and foredelta submarine-ramp environments emanating from the closing Pangean suture zone. The

stratigraphic framework and biostratigraphy of the Glass Mountains are documented by a few (King, 1930; King, 1937; Rathjen, 1993; Haneef et al., 2000; Harris et al., 2000; Lambert et al., 2000; Wardlaw, 2000; Yang and Yancey, 2000; Lambert et al., 2002; Janson and Hairabian, 2016) but detailed provenance history of the clastic record has yet to be completed.

POTENTIAL SEDIMENT SOURCES

Archean and Paleoproterozoic (>1825 Ma)

Detrital zircons older than 1825 Ma could potentially be sourced from the northern extents of the Laurentian craton or from the Amazonian paleo-hinterland of Gondwana. The continent of Amazonia has a multi-stage history of agglutination with both Laurentia, during the assembly of Rodinia (along the Grenvillian margin of Laurentia), and Gondwana during the opening of the Iapetus at around 600 Ma (Sánchez-Bettucci and Rapalini, 2002; Tohver et al., 2002; Cordani et al., 2009). Amazonian basement provinces contain a wide range of Archean and Paleoproterozoic ages. The Amazonian central craton (Fig. 9) contains the Carajás region southwest of the Amazon basin. Basement rocks within Carajás are dated between 3200 and 2600 Ma (Cordani et al., 2009). The Maroni-Itacaiunas province occurs to the north and northeast of the Central-Amazonian province with rocks dated between 2250 and 1950 Ma (Fig. 9) (Cordani et al., 2009). Calc-alkaline, granite-gneiss complexes of the Ventuari-Tapajós and Rio Negro-Juruena provinces formed between 1980 and 1810 Ma (Fig. 9) (Santos et al., 2004; Cordani and Teixeira, 2007; Cordani et al., 2009). These Amazonian provinces were potential sources of Archean and Paleoproterozoic age zircons both during Rodinian (connection with Laurentia) time as well as during the formation of Pangea (connection with the Gondwanan hinterland). Potential sources within the Laurentian continent include the Wyoming and Superior

Provinces (3000 and 2700-2500 Ma) of the northern Laurentian continent (Xie et al., 2018). Grains of 1900-1800 and 1850-1780 Ma from the Penokean Orogen and associated Wisconsin magmatic terrane, and Trans-Hudson Province of the northern Laurentian craton (Fig. 9) were also capable of shedding sediment south toward the Permian Basin (Sims et al., 1989; Beck and Murthy, 1991; Anderson and Morrison, 1992; Holm et al., 2007).

Late Paleoproterozoic (~1825-1578 Ma)

Late Paleoproterozoic aged zircons match closest with the Ancestral Rocky Mountains and Yavapai-Mazatzal (1800-1600 Ma) terranes of central Laurentia (Fig. 9). These basement first-cycle sources were exposed throughout the Pennsylvanian and earliest Permian (Anderson and Morrison, 1992; Anderson et al., 1993; Holm et al., 2007; Giles et al., 2013). These ages have also been documented in detrital zircons from a multitude of basin studies of Paleozoic strata along the Ouachita-Marathon suture zone as well as north and northeast of the Permian Basin, giving the possibility of sediment recycling (Dickinson and Gehrels, 2003; Becker et al., 2005; Becker et al., 2006; Gehrels et al., 2011; Giles et al., 2013; Link et al., 2014; Xie et al., 2016).

Early Mesoproterozoic (~1578-1300 Ma)

Zircons within the early Mesoproterozoic age range are typically representative of the anorogenic igneous activity of the granite-rhyolite province of the central North American plate ranging in age between 1.49 and 1.34 Ga, and spanning from Labrador to California (Fig. 9) (Bickford et al., 1986; Hoffman et al., 1989; Anderson and Morrison, 1992). The Rondonian-San Ignacio province of Amazonia also contains accreted domains of intra-oceanic character, dated between 1550 and 1300 Ma (Geraldes et al., 2001; Santos,

2003; Cordani et al., 2009), granitoids dated between 1520 and 1470 Ma, and the Santa Helena plutonic arc (1450-1420 Ma) (Cordani et al., 2009). Additionally, zircons of this age range are found in other Pennsylvanian and Permian aged basinal strata (Dickinson and Gehrels, 2003; Becker et al., 2005; Becker et al., 2006; Gehrels et al., 2011).

Mesoproterozoic (~1300-920 Ma)

Mesoproterozoic age zircon grains are generally indicative of the Grenville Orogen, present in southern and eastern North America, Mexico, and Gondwana (Fig. 9) (Rainbird et al., 1992; Rainbird et al., 1997; Gillis et al., 2005; Talavera-Mendoza et al., 2005; Soreghan and Soreghan, 2013; Xie et al., 2018). These grains typically make up a significant portion of the DZ population in North American sandstones from Neoproterozoic to Mesozoic (Dickinson and Gehrels, 2003; Moecher and Samson, 2006).

Neoproterozoic to early Cambrian (~920-521 Ma)

Because there are a number of potential sources, the Neoproterozoic to early Cambrian age suite remains contentious regarding provenance within the Permian strata of the Delaware Basin (Soreghan and Soreghan, 2013; Xie et al., 2018). The Appalachian orogenic belt traces the accretion of the (northern) Avalon terrane, (southern) Carolina terrane, and Suwannee (Florida) terrane, which were involved in the collision of Africa and North America during Alleghanian tectonism (Fig. 5, Fig. 9) (Opdyke et al., 1987; Mueller et al., 1994; Heatherington et al., 1996; Wortman et al., 2000; Hibbard et al., 2002; Dickinson and Gehrels, 2009; Park et al., 2010). Specifically, magmatism of 650-550 Ma only occurred in the accreted Avalon, Carolina, and Suwannee terranes (Heatherington et al., 1996).

The Pennsylvanian to Permian strata of the Appalachian Basin generally is thought to capture the erosional history of the Alleghanian orogenic wedge (Becker et al., 2006). Zircon analyses within the Pennsylvanian and Permian strata of the Appalachian foreland basin, however, show these age modes as underrepresented (Becker et al., 2005; Becker et al., 2006).

The exotic terranes associated with the south and southwestern collision of Gondwana are also capable of supplying zircons of this age range. Peri-Gondwanan terranes along the Ouachita-Marathon suture as well as the granitic/plutonic-metamorphic core complexes and Pennsylvanian-Permian strata of the Yucatan/Maya, Coahuila, Oaxaquia, and Mixteca (Acatlán) terranes (Fig. 5, Fig. 9) had been accreted and uplifted by Permian time (Sacks and Secor, 1990; Dickinson and Lawton, 2001; Dickinson and Lawton, 2003; Poole et al., 2005; Soreghan and Soreghan, 2013; Xie et al., 2018). Though all of these now Mexican and Central American terranes are understood to have agglutinated to the Gondwanan continent during the formation of Pangea, timing and positions of the terranes have been up to debate (Dickinson and Lawton, 2001; Murphy et al., 2004; Keppie et al., 2008; Martens et al., 2010; Soreghan and Soreghan, 2013). As stated previously, the Tesnus Formation is a shaly sandstone representing pre-collisional flysch deposits in the form of submarine fan and channel deposits sourced from the approaching Gondwanan continent (McBride et al., 1989; Hickman et al., 2009). The whole of the Mississippian Tesnus was sourced from the Gondwanan continent, yet it does not contain any Neoproterozoic to early Cambrian zircons as have been observed in the Yucatan/Maya, Coahuila, and Mixteca (Acatlán) terranes (Fig. 9).

Rodinian syn-rift volcanic rocks represent the most likely source of sediment that has been overlooked by previous studies. They are situated along the southwestern margin of the Laurentian rifted margin. Rifting of the Rodinian supercontinent occurred between

ca. 825 Ma and 740 Ma with notable volcanic pulses from 780-540 Ma (Fig. 9) (Li et al., 2008; Dickinson and Gehrels, 2009; Hanson et al., 2016). These ancient syn-rift volcanic rocks are restricted to the distal southern Laurentian margin and were subsequently covered by strata deposited along the Laurentian passive margin (King, 1937; Flawn et al., 1961; King, 1978; McBride et al., 1989; Hickman et al., 2009). The abrupt appearance of Neoproterozoic zircons within the Haymond Formation (first syn-orogenic sample) could potentially be representative of incorporation of the ancient Laurentian rifted margin into the Marathon orogenic wedge between the two colliding continents. Additionally, the basement of the Devils River Uplift to the east of the Delaware Basin preserves a portion of the distal Laurentian rifted margin (Fig. 1, Fig. 6). This region contains a succession of Grenvillian-aged basement (1246-1121 Ma Rb/Sr age) (Nicholas et al., 1989; Rodriguez et al., 2017) and a metasedimentary-metavolcanic unit of Cryogenian—Early Cambrian age (Nicholas and Rozendal, 1975; Denison et al., 1977; Nicholas et al., 1989; Thomas, 2011b; Rodriguez et al., 2017).

Paleozoic (~521-263 Ma)

The Appalachian orogenic ranges and related Ordovician—Devonian igneous rocks of the Taconic (490-440 Ma), and Acadian (390-350 Ma) tectonic regions function as potential east and northeast sources for Paleozoic age zircons within the Permian Basin (Hatcher Jr et al., 1989; Park et al., 2010; Gehrels et al., 2011). Portions of the Gondwanan Pan-African regions of Carolina (590-535 Ma) and Suwannee (535-511 Ma), closer to the Appalachian orogenic region, are also potential sources of Paleozoic age zircons (Soreghan and Soreghan, 2013). As for other potential Laurentian Paleozoic sources, Soreghan and Soreghan (2013) point out the possibility of the zircons from the Franklinian orogen of the

arctic Canadian region and its actively eroding clastic wedge (450-370 Ma) (Patchett et al., 2004; Gehrels et al., 2011; Soreghan and Soreghan, 2013).

Geochronological data from Peri-Gondwanan and Pan-African terranes of Mixteca (Acatlán) (480-440 Ma; metamorphic ages of 416-388 Ma) and Yucatan-Maya (418 Ma) closely match the observed DZ U-Pb age modes of the Paleozoic age components throughout the syn- and post-collisional strata of the Marathon Fold and Thrust Belt and southern Delaware Basin (Steiner and Walker, 1996; Keppie, 2004; Gillis et al., 2005; Steiner and Anderson, 2005; Talavera-Mendoza et al., 2005; Keppie et al., 2006; Weber et al., 2006; Keppie et al., 2008; Weber et al., 2008; Martens et al., 2010). The youngest grain ages within this study are <360 Ma, most likely linking them to adjacent volcanic arc activity. The Mississippian Las Delicias Arc of the Coahuila terrane (McKee et al., 1999; Lopez et al., 2001) and Middle Permian East Mexican Arc likely represent the youngest possible volcanic activity within Marathon proximity, and potentially sourced the youngest zircons within the Pennsylvanian—Permian strata of this study.

DETRITAL ZIRCON SAMPLING AND METHODOLOGY

SAMPLING

We collected and analyzed 13 samples across the Marathon Fold and Thrust Belt and Glass Mountains stratigraphic sections (Fig. 1, Fig. 7). Standard mineral separation techniques for all samples proceeded as follows: crushing and grinding of whole-rock samples, water table separation, bromoform heavy liquid separation, Frantz magnetic separation, and methyl iodide heavy liquid separation. Heavy mineral separates were poured onto double sided tape on epoxy resin mounts, zircon grains were then chosen at random for laser ablation-inductively coupled plasma-mass spectrometry (LA-ICP-MS) to obtain U-Pb ages (Hart et al., 2016). In order to ensure representation of grain components comprising >5% of the total sample population is achieved at 95% confidence and ensure accuracy of Maximum Depositional Age (MDA), 120-140 grains were picked in each sample as per Vermeesch (2004).

ANALYTICAL METHODOLOGY

Analyses were run on a PhotonMachine Analyte G.2 excimer laser with a large-volume Helex sample cell and a Thermo Element2 ICP-MS. GJ1 was used as the primary reference standard (Jackson et al., 2004) and Pak1 (in-house zircon standard, 42 Ma) and Plesovice (in-house zircon standard, 337.1 Ma) were used as secondary standards. A 30 mm laser spot was used to ablate ~16 mm deep pits on the upper plane of the un-polished, tape-mounted zircons, producing a depth profile of each analyzed grain. The depth profiling technique enables the resolution of multiple zircon growth zones (Moecher and Samson, 2006) evident from core and rim ages (Stockli, 2013). Analyses were then reduced using Iolite data reduction software and VizualAge (Paton et al., 2011; Petrus and Kamber, 2012). For greater precision, the ages represented in analyses are $^{206}Pb/^{238}U$ ages for zircons

younger than 1200 Ma, and $^{207}Pb/^{206}Pb$ ages for zircons older than 1200 Ma (Gehrels et al., 2008). All ages use 2σ absolute uncertainties, $^{207}Pb/^{206}Pb$ ages are accepted at 100% discordance, and $^{206}Pb/^{238}U$ ages are accepted between >10-30% discordance (Gehrels, 2012). The discordance is calculated using the $^{206}Pb/^{238}U$ and $^{207}Pb/^{235}U$ ages if younger than 1200 Ma and the $^{206}Pb/^{238}U$ and $^{207}Pb/^{206}Pb$ ages if older than 1200 Ma. Mineral separation and LA-ICP-MS analyses were completed at the UT Thermochron facilities at the Jackson School of Geosciences at the University of Texas at Austin (Hart et al., 2016). Data visualization and plotting was performed using DetritalPy (Sharman et al., 2018) python scripts (Fig. 10) (see Appendix). MDA estimates (Fig. 11) were derived using the following rules: Youngest Single Grain (YSG), weighted mean age of youngest cluster of two or more grain ages overlapping age at 1σ (YC1σ (2+)) and weighted mean age of the youngest cluster of three or more grain ages overlapping in age at 2σ (YC2σ (3+)) (Dickinson and Gehrels, 2009). However, for this study we focus on the youngest single grain to emphasize the earliest possible lag time between zircon crystallization and deposition. More information regarding the plotting software and data representation can be found in their respective sections of the Appendix.

CORE-RIM ANALYSIS

Depth profiling of each individual zircon grain yielded 85 concordant core-rim age relationships with three analyzed zircons having multiple concordant rims. This is to say that of the 1720 detrital zircon U-Pb ages, 85 U-Pb age pairs (Fig. 12) were extracted from both an initially formed core of a zircon as well as the anatectic growth rim of secondary igneous or metamorphic activity (Moecher and Samson, 2006; Stockli, 2013). A more comprehensive history of zircon transport and recycling is gleaned by gathering multiple ages from single zircon grains. Specifically, these data help us fingerprint a narrower range

of potential sources by incorporating core-rim age relationships with previously published DZ data within potential sediment source terranes. All core-rim data are from the Permian-age strata of the Glass Mountains, while no such relationships were found from the zircon of the Marathon Fold and Thrust Belt. These analyses cluster into five relative core and rim clusters, each with 1-3 sub-groups (Fig. 12). These core-rim age relationships provide a second constraint on potential sediment source terranes by recording a multi-stage history of tectonic or volcanic activity.

RESULTS

In total, 1720 detrital zircon U-Pb ages were measured in this study. Detrital zircon U-Pb data from the four Marathon Fold and Thrust Belt samples and nine Glass Mountain samples were condensed into seven sample suites (grouped based on multiple samples in the same stratigraphic unit) and are shown as Kernel Density Estimation (KDE) plots, histograms, and cumulative probability density plots of Figure 10. Age data can be found in Tables 1-7 following the Appendix section along with sample locations. Highlighted color-coded groups designate possible detrital zircon source terranes and dominant age range from each source (Fig. 9) (Lawton et al., 2016). On the basis of these possible source ages, detrital zircon U-Pb ages can be separated into six groups: Archean and Paleoproterozoic (>1825 Ma), Late Paleoproterozoic (~1825-1578 Ma), Early Mesoproterozoic (~1578-1300 Ma), Mesoproterozoic (~1300-920 Ma), Neoproterozoic to Early Cambrian (~920-521 Ma), and Paleozoic (~521-263 Ma).

PRE-PERMIAN (MISSISSIPPIAN-PENNSYLVANIAN)

The pre-Permian, syn-orogenic samples of the Marathon Fold and Thrust Belt (Fig. 1, Fig. 10) exhibit two distinct detrital zircon age spectra for the Mississippian Tesnus and the Pennsylvanian Haymond Formations. Tesnus samples are labeled in the Appendix as 13WTX01 and 13WTX02 and will be referred to as TSS1 and TSS2 for simplicity, and Haymond samples, labeled 13WTX03 and 13WTX04 will be referred to as HF1 and HF2. Two samples from massive sandstone beds of the Mississippian Tesnus Formation (n=227) were taken along US Highway 90, east of Marathon, TX, within the Marathon Fold and Thrust Belt (Fig. 1). The DZ U-Pb age spectrum (Fig. 10) exhibits a dominant Mesoproterozoic DZ U-Pb age component (51.1%), with a prominent age peak at ~1037 Ma. There exist minor fractions of detrital zircons of Archean and Paleoproterozoic

(10.6%), Late Paleoproterozoic (14.5%), Early Mesoproterozoic (12.3%), Paleozoic (11%) ages, and a single Neoproterozoic aged zircon of 588 ± 5.7 Ma. Two turbiditic sandstone samples (n=209) from the Pennsylvanian Haymond Formation from along US Highway 90, east of Marathon, TX, exhibit a markedly different detrital zircon age spectrum with Neoproterozoic and Early Cambrian ages totaling 20.6%. The Mesoproterozoic age component continues to dominate and accounts for 36.4% of measured detrital zircons, while the Archean and Paleoproterozoic (14.8%), Late Paleoproterozoic (7.2%), Early Mesoproterozoic (7.7%) and Paleozoic (13.4%) age components remain minor fractions.

EARLY PERMIAN (WOLFCAMPIAN-LEONARDIAN)

The younger, early Permian strata of the Glass Mountains (Fig. 1), north of Marathon, TX, overly the deformed strata of the Marathon Fold and Thrust Belt. Two Wolfcampian samples (n=297) were taken from the conglomeratic Lenox Hills Formation of Leonard Mountain (Fig. 1), and the Leonardian sample was taken from the massive sandstone turbidites of the Skinner Ranch Formation. These samples exhibit less dramatic changes in detrital zircon age distributions. The DZ U-Pb age spectra of the Lenox Hills Formation exhibit minor age components of Archean and Paleoproterozoic (9.4%), Late Paleoproterozoic (5.4%), and Early Mesoproterozoic (5.4%). Paleozoic age zircons make up 16.2% of total DZ U-Pb ages, while the Mesoproterozoic (32.3%) and Neoproterozoic to Early Cambrian (31.3%) age components represent the majority of detrital zircon ages with prominent age peaks at ~1090 Ma and ~524 Ma, respectively. The DZ age spectrum (n=138) of the Skinner Ranch Formation (Leonardian) is similar to that of the Lenox Hills, with age components of Archean and Paleoproterozoic (9.4%), Late Paleoproterozoic (2.2%), Early Mesoproterozoic (5.1%), Mesoproterozoic (30.4%), Neoproterozoic and Early Cambrian (40.6%), and Paleozoic (12.3%).

MIDDLE PERMIAN (GUADALUPIAN)

The middle Permian (Guadalupian) samples were taken from mixed carbonate-clastic turbidites of the Word, Vidrio, and Altuda Formations, north of Marathon, TX, and farthest north of the sampled Glass Mountains section (Fig. 1). The single sample (n=137) of the Word Formation was taken from the turbidite outcrops north of Leonard Mountain, and is lowest in the Guadalupian stratigraphic section. The DZ U-Pb spectra of the Word Formation exhibits an increase in Paleozoic age component (27.7%) and decrease in Neoproterozoic to Early Cambrian age component (28.5%) relative to the Wolfcampian and Leonardian samples. The Mesoproterozoic age component accounts for 24.1% of DZ U-Pb ages, and the early Mesoproterozoic (9.5%), late Paleoproterozoic (5.8%), and Paleoproterozoic and Archean (4.5%) age components maintain minor fractions of the age spectrum. The four Vidrio Formation samples were taken in two separate locations. The first two samples (VSS1 and VSS2; n=276) were taken above the Word sample, north of Leonard Mountain, while the second two samples (VSS3 and VSS4; n=293) were taken from turbidites within Road Canyon, further north of VSS1 and VSS2 (Fig. 1). The compiled age spectra (Fig. 10) exhibit similar components to that of the Word Formation, with high fractions of Paleozoic (27.1%), Neoproterozoic to Early Cambrian (21.6%) and late Mesoproterozoic (26.9%) age components, and low fractions of early Mesoproterozoic (9.5%), late Paleoproterozoic (7.7%), and Paleoproterozoic and Archean (7.2%) age components. The Altuda Formation marks the youngest stratigraphic unit sampled in this study. The sample was taken from a massive sandstone turbidite outcrop just northwest of Gilliand Canyon (King, 1930). The DZ U-Pb age spectrum (n=144) remains similar to the previous Word and Vidrio samples, but with a noticeable enrichment in Paleozoic zircons (34.7%) and relative decrease in amount of late Mesoproterozoic zircons (14.6%).

ZIRCON CORE-RIM AND MDA ANALYSIS

Here we present a group-by-group breakout and interpretation of the five separate core-rim age clusters. Each grouping is separated between other samples on the basis of core age, while intra-sample subgroups have been broken out according to different potential sources correlating to the specific rim age (Fig. 12).

PALEOPROTEROZOIC AND ARCHEAN CORES

Zircon core crystallization ages of Paleoproterozoic and Archean age could have been sourced from a broad range of terranes within and attached to the Laurentian and Gondwanan continents, but specifically the Amazonian terranes of the Gondwanan hinterland (Cordani et al., 2009) and Yavapai-Mazatzal, Wyoming, Superior, and Penokean provinces of northern Laurentia (Anderson and Morrison, 1992). The E1 group of core-rim ages captures potential core ages from Amazonia or Yavapai-Mazatzal, but has much younger rim ages (~600-300 Ma). These rim ages are most likely representative of Peri-Gondwanan or Pan-African origin, suggesting a combined core-rim provenance history of southern or eastern origin. The zircon within E2 (Fig. 12) contains a 1641 ± 33 Ma core with a 921 ± 71 Ma rim. A core of this age would typically be grouped with the Yavapai-Mazatzal province of Laurentia; however, the Grenvillian age rim correlates with the younger Grenville age basement of Oaxaquia as presented by Gillis et al. (2005).

EARLY—MIDDLE MESOPROTEROZOIC CORES

Zircon core-group D falls between the Early—Middle Mesoproterozoic age ranges, a range that could be represented by either the granite-rhyolite provinces of the North American interior craton (Bickford et al., 1986; Hoffman et al., 1989; Anderson and Morrison, 1992), or Amazonian basement and recycled terranes (Geraldes et al., 2001;

Santos, 2003; Cordani et al., 2009). Subgroups D2 and D1 of the plotted core-rim ages (Fig. 12) show concordant rims of Ectasian—Tonian and Tonian—Carboniferous age ranges, respectively. Group D2 contains Grenvillian age rims, which could potentially be related to either Laurentian or Gondwanan activity. Zircons within the subgroup D1 have a broad range of rim ages with the youngest at 343 ± 17 Ma, an age that potentially adheres to volcanic activity or tectonism within the Peri-Gondwanan terranes.

GRENVILLIAN CORES

Grenvillian zircons are ubiquitous in the Neoproterozoic—Mesozoic sandstones of North America (Dickinson and Gehrels, 2003; Moecher and Samson, 2006), impeding provenance interpretations for these detrital age components. However, depth-profiling of zircons from this study (C core groups) presents some quite unique data. The oldest rims of the Grenvillian-core suite are of contemporaneous Grenvillian age, shown in the C3 subgroup (Fig. 12). Provenance of this group is difficult to decipher due to the potential for core and rim generation within a Grenvillian province. However, subgroup C2 displays Grenvillian cores with rims of Neoproterozoic—Middle Paleozoic age. Magmatic overprinting of 650-550 Ma volcanism within rocks of the Avalon, Carolina, and Suwannee terranes (Heatherington et al., 1996; Samson et al., 2005; Moecher and Samson, 2006) could be potential sources for these zircons, but this is less likely for the Suwannee terrane as its DZ age spectra are not well represented by Grenvillian-age zircons (Mueller et al., 1994). A more likely source for these multi-age zircons would be the terranes of Coahuila and Oaxaquia. Lopez et al. (2001) dated Grenvillian and Pan-African rocks within basement terranes of Coahuila and Oaxaquia. Zircon U-Pb analyses of the Grenville rocks presented grains of 1201 ± 60 Ma to 1232 ± 7 Ma with Concordia intercepts at ~580 Ma and Pan-African rocks presented grains of 580 ± 4 Ma. These were interpreted as being

interrelated through melting of the Grenvillian basement during Pan-African age volcanism, giving validity to our visualization of similar core-rim relationships within single zircons (subgroup C2, Fig. 12). Additionally, these ages line up well with volcanism from the rifted Laurentian margin (780-560 Ma), supporting the interpretation that during orogenesis the continental margin would have been included into the accreted wedge. Subgroup C1, which plots within subgroup C2, has rim ages of 422 ± 17 Ma and 432 ± 24 Ma. These rim ages are significant of the Peri-Gondwanan terranes of Mixteca (Acatlán) (480-440 Ma; metamorphic ages of 416-388 Ma) and Yucatan-Maya (418 Ma).

NEOPROTEROZOIC—EARLY PALEOZOIC CORES

Group B contains zircon cores of Neoproterozoic—Early Paleozoic ages and rims of Neoproterozoic—Late Paleozoic ages. The core ages are likely to be of Rodinian volcanic origin (Li et al., 2008) or potentially from Pan-African terranes (Heatherington et al., 1996; Lopez et al., 2001; Samson et al., 2005; Moecher and Samson, 2006). Notably, the top right hand cluster of core-rim ages within group B trend close to the 1:1 line indicating secondary anatectic growth and crystallization, relatively soon after initial crystallization. This kind of growth behavior could be indicative of the first intermittent volcanic pulses following the breakup of Rodinia. On the other hand, the cluster at the bottom left hand corner of group B contain younger cores, which appear to have Pan-African sourcing and a secondary growth related to the younger, Peri-Gondwanan terranes.

PALEOZOIC CORES

Core-rim relationships with purely Paleozoic cores are shown in group A (Fig. 12). These are the youngest core-rim relationships and are almost certainly indicative of the Peri-Gondwanan terrane and/or volcanic arc activity within the Peri-Gondwanan,

Coahuila, or Oaxaquian terranes (Fig. 9). We suggest rim-growth to be indicative of zircon recycling and inclusion in the volcanic arc activity within the Gondwanan hinterland and subsequent transport during the collision of Gondwana and Laurentia.

MAXIMUM DEPOSITIONAL AGES

The youngest zircon grain age or youngest age mode is a powerful method for determining maximum depositional ages (MDAs), particularly in the absence of biostratigraphic age constraints (Dickinson and Gehrels, 2009). This approach is predominantly limited by the generation of new, first-cycle volcanic zircon and their airborne or near-instantaneous fluvial input into the basinal strata. These MDA estimates not only provide invaluable chronostratigraphic control, but also important insights into the presence or absence of local/regional volcanic or plutonic sources as well as erosional lag time constraints (i.e., the difference between MDA and depositional age) for independently dated strata. MDA interpretations by means of the youngest grain ages in a stratigraphic unit have been used to determine the lag time between zircon crystallization and delivery into the sedimentary basin assist with the differentiation of volcanic, plutonic, or recycled and multi-cycle zircons and their sources (e.g., Dickinson and Gehrels, 2009, Xu et al., 2017). While volcanic and plutonic zircons are commonly characterized by lag times of <1 and <20-40 Myrs, respectively, mutli-cycle zircon often exhibit lag times >>50 Myrs.

MDA estimates for the various sampled strata in this study track the record of the youngest zircon grains present in a given sample. Integrating these values with coeval biostratigraphic and sequence stratigraphic information from previous regional studies in the Glass Mountains and Marathon Fold and Thrust Belt provides insight into regional volcanic influence. Specifically, this comparison exhibits the presence of active volcanic

arc magmatism, the unroofing of magmatic belts in the hinterland drainage system, as well as the long-term recycling of pre-contractional sedimentary sequences in the source terrane. Figure 13 displays the MDAs of all 13 samples plotted against their independent best stratigraphic ages, using both the YSG and YC1σ (2+) approaches (Dickinson and Gehrels, 2009, Xu et al., 2017). Here, the independent best stratigraphic ages are based on previous work by biostratigraphic and sequence stratigraphic data collected regionally (Olszewski and Erwin, 2009; Glasspool et al., 2013; Richards, 2013; Nestell et al., in press). The results of this analysis show that volcanic zircons with negligible lag times are not input into the basinal system until the middle Permian (Guadalupian), marking the input and onset of Cordillera or East Mexico arc volcanism at ~260-270 Ma (Dickinson et al., 2000; Dickinson and Lawton, 2001). Prior to middle Permian times, however, no zero-lag-time volcanic zircons were recorded in any of the Pennsylvanian-Permian strata, while minimum lag times deduced from the youngest zircon components are nearly constant at ~30-40 Myrs. Due to correlation between plutonic arc exhumation and calculated lag time, we interpret the zircons with lag times of 30-40 Myrs to have been derived from arc magmatic rocks emplaced along the Gondwanan convergent margin during subduction of the Rheic Ocean in Carboniferous times (Torrez, 1999; Keppie et al., 2008). In summary, based on the differences between true depositional age and zircon-based MDA, there are three dominant sources of zircons in the southern Permian Basin: 1) multi-cycle zircons eroded and recycled from Proterozoic to early Paleozoic Gondwanan or Laurentian strata; 2) plutonic sources erosionally unroofed within the hinterland arc plutonic rocks related to Rheic subduction; and 3) first-cycle volcanic zircons derived from active volcanic arc magmatism in the middle Permian. In particular, the presence of Carboniferous arc magmatic zircons with relatively constant lag times is noteworthy as they unequivocally point to derivation from the Gondwanan convergent margin and to protracted unroofing of

this magmatic arc. Furthermore, however, the presence of these ages suggests essentially continuous Devonian-Carboniferious arc magmatism related to Rheic subduction. This is noteworthy given the sparse record of this magmatism along the Gondwanan margin from Florida, to Yucatan, to NE Mexico, including the Las Delicias Arc (Steiner and Walker 1996; McKee et al., 1999; Lopez et al., 2001; Keppie, 2004; Keppie et al., 2008; Soreghan and Soreghan, 2013).

PROVENANCE EVOLUTION

The detrital zircons from the Marathon Fold and Thrust Belt and Glass Mountains represent a wide range of crystallization ages and a complex history of sediment recycling (Fig. 10). Through comparing the DZ U-Pb signatures with respect to deposition during pre-, syn-, or post-collisional time window, we are able to interpret and reconstruct proximal basin sedimentary evolution during progressive collision. Further, incorporation of other provenance studies regionally helps to establish a broader understanding of how sediment dispersal from the southern orogenic highlands and hinterland influences sediment dispersal during foreland basin formation and fill.

A few key provenance trends can be teased out from the DZ U-Pb analyses in this study: 1) the appearance of Neoproterozoic—Cambrian zircon grains in the Pennsylvanian Haymond Formation points towards basin inversion and the uplift and exhumation of volcanic units related to Rodinian rifting; 2) the upsection decrease in Grenvillian (~1300-920 Ma) and increase in Paleozoic zircons denotes a steady provenance shift from a dominantly orogenic highland source to that of sediment sources deeper in the Gondwanan hinterland; and 3) the lack of drastic changes in provenance during the early to middle Permian supports the argument for tectonic quiescence within the collisional domain during this time period.

MISSISSIPPIAN—PENNSYLVANIAN PROVENANCE EVOLUTION

Previous DZ provenance studies of the Permian Basin focus their efforts on resolving the age spectra of the Delaware Mountain Group, otherwise recognized as the Brushy, Bell, and Cherry Canyon Formations of the Guadalupe Mountains and Delaware Basin proper (Soreghan and Soreghan, 2013; Anthony, 2015; Xie et al., 2018). While results from these studies have made significant contributions to the understanding of

provenance during basin fill of the Delaware Basin, they lack a significant temporal section. Results from this study evaluate the evolutionary component of southern provenance during basin formation and fill. This adds a tie to regional provenance and ability to trace southern input of sediment at any one time by identifying the specific DZ U-Pb signal at a time period.

Tesnus Formation

The Mississippian Tesnus Formation represents flysch deposits of the approaching Gondwanan continental margin and sea floor prior to collision with Laurentia. A wide range of age modes are expressed by the Tesnus DZ spectra (Fig. 10) with a notably high Grenvillian (~1300-920 Ma) age mode and non-existent middle Neoproterozoic-Cambrian (~920-521 Ma) age mode. Because of its presence in the rest of the samples throughout this study, the lack of Neoproterozoic—Cambrian age DZs is conspicuous and deserves special attention. Using the Tesnus as a baseline for provenance evolution helps in understanding provenance shifts within the younger strata of the Marathon fold and thrust belt and Glass Mountains.

Grenville Signature

The Grenville Orogen, present in southern and eastern North America, Mexico, and the Gondwanan continents (Rainbird et al., 1992; Rainbird et al., 1997; Soreghan and Soreghan, 2013), typically makes up a significant portion of the DZ population in North American sandstones from Neoproterozoic to Mesozoic (Dickinson and Gehrels, 2003a; Moecher and Samson, 2006), adding difficulty to resolution of true source for these age modes. Grenvillian zircons within the Tesnus are no different, constituting >50% of the DZ population. However, as stated in a previous section, depth profiling of Grenvillian

zircons can make constraining their original source region possible. Gillis et al. (2005) presented a compilation of DZ U-Pb ages from the Oaxacian crystalline basement terrane and Paleozoic strata of southern Mexico, which showed strong age peaks of 981 Ma and 993 Ma, respectfully. When compared to Grenville ages of southwestern and northeastern North America, the Oaxacian DZ U-Pb ages were consistently younger (<1000 Ma) (Gross et al., 2000; Stewart et al., 2001; Eriksson et al., 2003; Gillis et al., 2005). The most prominent Grenvillian peak within the Tesnus age spectra is 1037 Ma, but due to its nature as comprising pre-collisional deposits, this peak can be defined as being sourced from the Oaxacian terrane.

Paleozoic Signature

Zircons of Paleozoic age are the youngest among Tesnus age spectra with a prominent peak at ~422 Ma. Peri-Gondwanan terranes (Fig. 9) are most suitable because of the pre-collisional nature of the Tesnus Formation. Specifically, the Peri-Gondwanan terranes of Mixteca (Acatlán) (480-440 Ma; metamorphic ages of 416-388 Ma) and Yucatan-Maya (418 Ma) function as the closest match to the DZ U-Pb age modes of the Tesnus age spectra (Steiner and Walker, 1996; Keppie, 2004; Gillis et al., 2005; Steiner and Anderson, 2005; Talavera-Mendoza et al., 2005; Keppie et al., 2006; Weber et al., 2006; Keppie et al., 2008; Weber et al., 2008; Martens et al., 2010). By applying these age domains and collisional timing based on paleogeographic and tectonic reconstructions of the Peri-Gondwanan terranes (Keppie, 2004; Centeno-García et al., 2005; Weber et al., 2008) previous provenance studies argue for initial denudation of the Peri-Gondwanan terranes to be during the middle Permian (Soreghan and Soreghan, 2013; Anthony, 2015; Xie et al., 2018). Alternatively, based on the measured Paleozoic DZ ages from the Tesnus

Formation, denudation and incorporation of sediment from these terranes was likely to have initiated in the Carboniferous, during migration of the Gondwanan continent.

Haymond Formation

Deposited during strong tectonism, the sediment source history of the Haymond Formation remains controversial (Denison et al., 1969; King, 1958; McBride et al., 1989; Gleason et al., 2007). As stated previously, we can effectively use the Tesnus Formation DZ U-Pb age spectra as a baseline for the younger strata sampled and, based on shifts in provenance, we are able to make inferences regarding evolution of the collisional and foreland system. In this case, the Haymond DZ U-Pb age spectra exhibits a marked change in composition with the appearance of the previously absent Neoproterozoic—Cambrian age mode. It is important to note that this is the only significant provenance alteration between the two DZ spectra. This change in provenance denotes the inversion and exhumation of the distal Laurentian margin during Pennsylvanian collision with Gondwana. This defines the Haymond age spectra as a transitional unit between pre- and syn-orogenic units. Such a drastic transition in provenance marks a key finding in terms of understanding the collisional margin evolution and subsequent sediment supply to the Marathon region.

Rifting of the Rodinian supercontinent occurred between ca. 825 Ma and 740 Ma with notable volcanic pulses from 780-540 Ma (Li et al., 2008; Dickinson and Gehrels, 2009; Hanson et al., 2016). Strata deposited along the southern passive margin of Laurentia covered these ancient syn-rift volcanic rocks (King, 1937; Flawn et al., 1961; King, 1978; McBride et al., 1989; Hickman et al., 2009). Thereby, the most viable method to explain inclusion of these volcanic units into younger strata of the Marathon Fold and Thrust Belt (and eventually the southern Delaware Basin) would be through deep-seated uplift of the

continental margin. We propose the formation of a duplex zone between the Gondwanan continent and Laurentian margin, effectively exhuming this material.

EARLY—MIDDLE PERMIAN DEPOSITS: UNROOFING AND TECTONIC QUIESCENCE

The latest syn-orogenic deposits of Wolfcampian age and potentially first post-orogenic deposits of Leonardian age display DZ U-Pb age spectra similar to that of the Pennsylvanian Haymond Formation. We interpret this similarity to be indicative of an ongoing unroofing of the orogenic highlands. The deposition of 4200-5600 m of siliciclastic strata during Wolfcampian time lines up well with the rapid erosion of the massive accreted wedge adjacent to the basin (King, 1937; Flawn et al., 1961; Thomson and McBride, 1964; King, 1978). Additionally, the Leonardian Skinner Ranch Formation is a sandy turbidite facies, much more distal that the Wolfcampian conglomerates, yet still the persistent sediment source appears to remain.

Transfer from the unroofing sequence seen during the Wolfcampian—Leonardian depositional period to that of post-tectonic sediment transport is captured within the Middle Permian deposits, but it is far subtler than the previously observed provenance shifts. Tracking the Grenvillian and Paleozoic DZ U-Pb age components upsection shows this subtle, progressive shift in provenance with a decrease in the Grenvillian age component and increase in the Paleozoic age component (Fig. 10). We interpret this provenance shift to be indicative of the third and final stage of proximal provenance evolution; tectonic quiescence within the collisional domain, and catchment stabilization resulting in sediment sourcing from deeper in the hinterland (Fig. 14). By this point in time, the large orogenic wedge had been denuded to the point that sediment sourcing within the hinterland was possible and could feed the N-NW progradation of the Guadalupian (Middle Permian) deposits on top of the Wolfcampian and Leonardian deposits.

MULTIDIMENSIONAL SCALING OF THE MISSISSIPPIAN—PERMIAN STRATIGARPHY

Multidimensional scaling of the detrital zircon data is employed to semi-quantitatively compare the similarity of the provenance signature of different stratigraphic units and to investigate the provenance evolution through time from before, during, and after continental collision. Intersample MDS plots from this study and others (Fig. 15, Fig. 16) display statistical differences between the DZ U-Pb age spectra with sample clustering indicative of age spectra similarity and samples plotting at distance indicative of a higher degree of dissimilarity. This analysis exhibits abrupt switches and transitions in both the dominant DZ age modes as well as the entire DZ U-Pb age spectrum (Fig. 15). The MDS plot shows three distinct stages of the evolution of the Marathon Fold and Thrust Belt and southern Delaware Basin foreland deposition: 1) pre-collisional deposition of the Tesnus Formation; 2) transition into syn-collisional deposition of the Haymond Formation with Laurentian margin uplift; and 3) tectonic quiescence and hinterland catchment maturity.

The Tesnus Formation samples plot as a distinct grouping that is most dissimilar from the youngest (Guadalupian) post-collisional samples. While KDEs do capture this difference, the MDS analysis more convincingly supports completely different sediment sources. The samples of the Haymond Formation and Wolfcampian-Leonardian samples mark a sharp provenance difference related to the orogenic activity and inversion of the Laurentian passive margin and hence the mixing of Gondwanan and Laurentian margin sources. The shift from the Tesnus Formation to the Haymond Formation appears to be marked by the sudden input of Laurentian margin elements. Subsequently, from the Haymond Formation to the Early Permian Lenox Hills Formation (Wolfcampian) the MDS shows a relative smooth evolutionary trajectory from initial inclusion of the Laurentian passive margin into the orogenic wedge and juvenile sediment dispersal of the orogenic

highlands as displayed in tectonostratigraphic figures 18C and 18D. The Wolfcampian-Leonardian samples cluster together likely reflecting significant unroofing of the orogenic wedge.

In MDS space, the DZ signature of strata deposited during post-collisional tectonic quiescence and their provenance evolution appears to differ strongly from the syn-orogenic trajectory (Fig. 15). The Word, Vidrio, and Altuda Formations appear to plot as a stable provenance shift from oldest to youngest, with the exception of VSS1 plotting closer to the Wolfcampian-Leonardian samples than the stratigraphically older Word (WSS5) sample. These trends and trajectories observed in MDS space are both clear and intuitive and reflect the overall tectonic evolution of the system from convergence, to continental collision, to post-collisional deposition.

DISCUSSION

INTEGRATION OF REGIONAL DELAWARE BASIN PROVENANCE

This provenance study may be unique to the collisional domain and proximal foreland of the Delaware Basin, but it is not the only study within the basin. Soreghan and Soreghan (2013), Anthony (2015), and Xie et al. (2018) each preformed provenance analyses with the use of DZ U-Pb geochronology in the Guadalupe Mountains (northern Delaware Basin) and central/south central Delaware Basin, respectively. Both of these studies focused on testing previous hypotheses for sediment sourcing during the deposition of the Guadalupian-age Delaware Mountain Group (Fig. 16). Here, we compare our collected data from the southern Delaware Basin with that of their data from the central/south central and northern Delaware Basin (Fig. 16, Fig. 17).

Soreghan and Soreghan (2013) used DZ data from the Brushy and Bell Canyon members of the Guadalupe Mountain region to call for sediment sources from the proximal Ouachita foreland as well as sources south of the accreted Ouachita margin. Anthony (2015) used DZ data taken from core in the central and central/southern Delaware Basin, specifically from the Cherry and Bell Canyon members, his interpretation aligns with Soreghan and Soreghan (2013). Our documentation of provenance from coeval deposits from the most southerly portion of the Delaware Basin provides an opportunity to evaluate these interpretations. While potential distal transport of Ouachita regional sources is likely for both of these cases, the importance lies more with volumes contributed. During margin inversion, massive volumes of sediment were shed into the southern Permian Basin (4200-5600m in some places) (King, 1937; Flawn et al., 1961; Thomson and McBride, 1964; King, 1978; McBride et al., 1989; Hickman et al., 2009). This begs the question of where terminal South-North transport of sediment ends and sediment transport from other regions

surrounding the basin begins. Statistical comparison of samples from Soreghan and Soreghan (2013), Anthony (2015), and this study through MDS provide insight into this issue. An intersample comparison between this study, Soreghan and Soreghan (2013), and Anthony (2015) (Fig. 16), highlights the similarities between Guadalupian-age samples from this study (WSS5, VSS1-4, and ALSS1), with that of Anthony (2015) (JCT-4946, JCT-5872, JCT-6068, and JCT-6446). Relative comparison of Soreghan and Soreghan's (2013) Guadalupian-age samples (BcSand, BcSilt, Rader, and Yates) infers a potentially different source. This works well with proximity of samples from Anthony (2015) to the southern margin of the Delaware Basin and northern position of Soreghan and Soreghan's (2013) sample suite. It is important to remember that samples within our study effectively define the southern provenance signal for the entire formation period of the Permian Basin as well as post-collisional deposition of Guadalupian age strata in the southern Delaware Basin. Thus, higher similarity between samples from this study and those from Anthony (2015) and higher dissimilarity with those from Soreghan and Soreghan (2013) indicate a more diverse range of sources in the northern portion of the basin and more pronounced southern signal in some of the central and south central portions of the Delaware Basin (Anthony, 2015). More work is needed, likely from core within the northern portion of the basin and denser upstream sampling of regional sediment feeders from the NW and NE. However, we argue that the Guadalupian section within the southern portion of the basin was being fed almost entirely by proximal Marathon sources as opposed to Ouachita region transport.

MISSISSIPPIAN—PERMIAN TECTONICS

The Marathon Fold and Thrust Belt of West Texas exhibits complex folds, imbricates, duplexes, and refolded structures, making it of particular interest to structural

studies. Pre-tectonic strata of the Laurentian passive margin consisted of variable mechanically weak, thin-bedded intervals and strong chert layers, ultimately leading to the formation of the complex structural features observed in the Marathon Fold and Thrust Belt (Hickman et al., 2009). Many recent studies have documented the unique mechanical stratigraphy and structural style of the fold and thrust belt (DeMis, 1983; Tauvers, 1988; Muehlberger and Tauvers, 1989; Hickman et al., 2009). Our results clearly indicate a temporally significant evolution of the Marathon Fold and Thrust Belt through tracking of sediment provenance evolution of the pre-, syn-, and post-collisional deposits of Mississippian—Permian age. Notably, these tectonostratigraphic units can be broken out into three distinct phases of tectonic evolution and subsequent sediment transport and deposition: 1) pre-tectonic deposition of the Mississippian Tesnus Formation; 2) uplift and exhumation of the passive Laurentian margin and ensuing unroofing of the orogenic wedge; and 3) post-tectonic margin stabilization coupled with catchment maturity and hinterland sediment transport (Fig. 18).

During the early to middle Paleozoic, a relatively thin marine sequence was deposited along the Laurentian passive margin (Fig. 18A), with indication of a north or northwest source of clastic sediment supply (King, 1978; McBride et al., 1989). Meanwhile, Mississippian deposition of the Tesnus formation in the form flysch deposits dominated the clastic record off the coast of the approaching Gondwanan hinterland as displayed by its unique DZ U-Pb age spectra (Fig. 10). These age spectra lacked the entire section of Neoproterozoic-age zircons (Cryogenian—Earliest Cambrian) with the exception of a single grain dated at 588 ± 5.7 Ma. This is a clear indication of the pre-collisional nature of the Tesnus Formation and that, while subduction of the Laurentian oceanic crust was possible, incorporation of even distal portions of the Laurentian marginal sediment was unlikely.

Incorporation of Neoproterozoic-age zircons during the deposition of the Haymond Formation (Fig. 18C) suggests incorporation of the Laurentian rifted margin into the uplifting orogenic wedge during the Pennsylvanian (Fig. 18C). Hickman et al. (2009) noted that the multiple decollement horizons within the pre-tectonic section of Marathon strata led to large-scale duplex zone formation. This idea is bolstered by the appearance of what we interpret to be zircons from the volcanic rocks extruded during Rodinian rifting phases of the Laurentian margin (780-540 Ma). This potential source is unaccounted for by previous regional provenance studies (Soreghan and Soreghan, 2013; Anthony, 2015; Xie et al., 2018). The similarity in DZ U-Pb age spectra of the Wolfcampian—Leonardian strata is indicative of constant unroofing of the accreted orogenic wedge. Knowledge of the sheer volume of sediment deposited over this time interval (King, 1937; Flawn et al., 1961; Thomson and McBride, 1964; King, 1978; McBride et al., 1989; Hickman et al., 2009) combined with our knowledge of a consistent orogenic sediment source leads us to believe that the large volumes of syn-orogenic sediment deposited into the proximal foreland basin are dominated by the orogenic wedge, potentially over long periods of time (~60 Myrs).

The post-tectonic (Guadalupian) stratigraphy of the proximal foreland basin is far more modest and sustained than that of the syn-orogenic deposits (Fig. 18D). The DZ U-Pb age spectra of these samples suggest regional tectonic quiescence, aligning with a change in depositional environment during transgression of the southern margin of the Delaware Basin (King, 1930; Janson and Hairabian, 2016). Upsection increase in Paleozoic ages and decrease in Grenvillian (Mesoproterozoic) ages are indicative of catchment maturation, and drainage stabilization within the Peri-Gondwanan hinterland and potentially deeper into the accreted Pan-African terranes through time. This is also supported by the core-rim relationships extracted through depth-profiling of the

Guadalupian zircons. A few core-rim relationships show Grenvillian cores with Pan-African rims, which suggest that Gondwanan terranes, especially those of Oaxaquia and Coahuila, were likely candidates for sediment supplied to the foreland basin during this time. Of the increasingly sparse Grenvillian-age zircons, a few core-rim relationships exist (Fig. 12) displaying Grenvillian cores with Pan-African rims ranging from 583-422 Ma suggest that Gondwanan terranes, especially that of Oxaquia and Coahuila were likely candidates for sediment supplied to the foreland basin during this time. Finally, the youngest DZ U-Pb age modes within the Guadalupian age spectra are >300 Ma, indicating sediment sourcing from volcanic arc terranes, specifically the Las Delicias arc located within the Coahuila terrane (Lopez et al., 2001).

Provenance studies within the collisional domain and foreland basin have been performed in a variety of basins globally, especially in the Andean and Himalayan regions (DeCelles et al., 1998; Horton et al., 2010; Gehrels et al., 2011; Bande et al., 2012; Colleps et al., 2018). This study effectively resolves a provenance evolution of both spatial and temporal significance within both the collisional domain during continental collision as well as post-collisional sediment dispersal to the resultant foreland basin setting. It is intuitive that the most high-relief, proximal region of the fold-thrust belt would supply the majority of sediment to the adjacent foreland-basin system, and we have demonstrated that is the case in the Glass Mountains of the southern Delaware Basin. Moreover, and curiously enough, there are similarities in the dominant age modes of detrital zircons throughout the basin (e.g. Soreghan and Soreghan, 2013). However, decades of sedimentological and stratigraphic analysis of the depositional fairways suggest a dominant northwest to south paleoflow direction, at least for the Guadalupian strata (Rossen, 1987; Gardner et al., 2003; Pyles et al., 2010). Thus, the ubiquitous provenance signal in the Permian Basin does not necessarily reflect direct sediment input from those initial source areas. Indeed, Soreghan

and Soreghan (2013) and Kocurek and Kirkland (1998), among others, interpret convoluted sediment-routing pathways from initial source to ultimate sink. So, although Permian Basin deposits reflect dominantly southerly provenance, they likely took a more circuitous pathway to deposition, especially in the northwestern Delaware Basin. Future work in the Delaware Basin and beyond should focus on retracing the sediment-routing pathways from predominantly Peri-Gondwanan source terranes to the northern basin margins. Consequently, only through incorporation and baseline use of the earliest pre-collisional strata could we be precise and conclusive in regards to provenance evolution through time. This is not always possible due to gaps in the geologic record, but where possible this effectively traces the culmination of a Wilson cycle.

CONCLUSIONS

By dating the crystallization age of individual zircon grains, we are able to relate regional paleogeography and temporally correlative sediment source terranes to interpret concurrent sediment sourcing and potential transport. By sampling a large vertical section from the syn- and post-orogenic region of the late Paleozoic Delaware Basin, we were able define a characteristic "type section" of provenance from a southern source across a dynamic tectonic system. Provenance changes indicate uplift and exhumation of Neoproterozoic syn-rift volcanic rocks and extension of the sediment-routing system deeper into the Gondwanan hinterland. Here we present 1720 new detrital zircon (DZ) U-Pb ages and 85 separate age core-rim relationships from 13 samples within the Marathon Fold and Thrust Belt and Glass Mountains of West Texas along with published DZ geochronologic datasets of regional provenance studies from older, and contemporaneous basin filling episodes along the Appalachian-Ouachita suture zone as well as within the Laurentian cratonic interior.

Ability to tie these data to basinal sources elevates our understanding of potential source to sink relationships within the basin. By observing these clear trends in provenance, we effectively observed the regional change in provenance of the final stages of a Wilson Cycle-scale continental collision. Similar collisional events are ubiquitous across the geologic record. This work could help to guide others studying sediment sourcing and evolution of the orogenic system of foreland basins.

APPENDIX

PLOTTING SOFTWARE

DetritalPy (Sharman et al., 2018) was employed in plotting all DZ U-Pb data of this study. This Python-based plotting software uses the Jupyter Notebook interface and allows for quick plotting of detrital age distributions using multiple visualization types such as Kernel Density Estimation (KDE) plots, Probability Density Plots (PDP), pie charts, and MDA. Here, we utilize the KDE plots for visualization of a large number of data points and MDA to track transport lag time and volcanic activity in the source regions. We used a Matlab script by Vermeesch (2013) for Multi-Dimensional Scaling (MDS) plots (discussed below). An MDS plot can be seen as a simplification of intersample dissimilarity by plotting pairwise sample comparisons in relation to all samples as opposed to single sample comparison (Vermeesch, 2013). In this way, broad trends can be visualized and interpreted.

DATA REPRESENTATION

A Kernel Density Estimation (KDE) is produced by arranging detrital zircon age measurements along a line and stacking a 'kernel' (e.g., fit of box, triangle, or Gaussian distribution) of a specified width ('bandwidth') on top of them (Vermeesch, 2012). Given a set of n measurements x_i ($I = 1 \rightarrow n$), the KDE can be written as:

$$KDE(x) = \frac{1}{nh}\sum_{i=1}^{n} K\left(\frac{x - x_i}{h}\right)$$

where K is the 'kernel' and h is the 'bandwidth' (Vermeesch, 2012).

Application of KDEs helps to negate probability biases by determining density of measurements as opposed to distribution weighted by analytical precision of measurements as seen in Probability Density Plots (PDPs). However, visual inspection of DZ datasets

through PDPs and KDEs potentially evokes natural bias by a researcher (Satkoski et al., 2013). These plotting methods have great utility when looking at big-picture trends across the sample space and provide a visual aid that represents the data well in publication. However, meticulous inspection of the 1720 DZ ages presented in this study becomes too much information for the human eye to accurately process (Vermeesch, 2013). To correct for this, application of multiple statistical analyses provides inter-sample trend comparisons, which may otherwise be overlooked or misinterpreted. By use of a table of pairwise K-S dissimilarity measurements of a given sample set, Vermeesch (2013) formatted the statistical technique of Multi-Dimensional Scaling (MDS). MDS produces a two dimensional 'map' of points on which samples with similar total DZ age spectra cluster and dissimilar samples plot at distance (Fig. 15, Fig. 16). The output plot can be seen as a simplification of a complex matrix of QQ plots which take each individual sample and compare its similarity along a 1:1 line with each other sample in the study. Q-Q plotting forms an upper triangular matrix of n(n-1)/2 individual plots (where n is the number of samples in a study) whereas MDS gives each sample a unique value in relation to all other samples in the study. Using a dissimilarity metric to plot the points at distance yields a 'map' of points in which points that plot at distance reflect a relatively high dissimilarity and vice versa for those that plot in proximity (Vermeesch, 2013).

SAMPLE LOCATIONS

Sample Name:	Latitude	Longitude
13WTX01 (TSS1):	30.204225°	-102.967016°
13WTX02 (TSS2):	30.204687°	-102.973623°
13WTX03 (HF1):	30.208736°	-102.984907°

13WTX04 (HF2):	30.212437°	-102.988188°
WCSS1:	30.323490°	-103.234193°
WCSS2:	30.323535°	-103.234836°
LSS1:	30.326233°	-103.235566°
WSS5:	30.382164°	-103.231126°
VSS1:	30.381794°	-103.231211°
VSS2:	30.381872°	-103.231476°
VSS3:	30.396649°	-103.243585°
VSS4:	30.396649°	-103.243585°
ALSS1:	30.383844°	-103.304593°

Table 1

TABLES

Sample Name:								207/235		206/238		206/207		Best age		
Grain #	[U] ppm	U/Th	207/235	2σ error	206/238	2σ error	RHO	Age Ma	2σ error	Age (Ma)	2σ error	Age (Ma)	2σ error	(Ma)	2σ error	% Discordance*
13WTX01_1.FIN2	316	1.79	1.76400	0.02100	0.17430	0.00160	0.42524	1032.3	7.7	1035.9	9.0	1034	17	1034.0	17.0	0.2
13WTX01_2.FIN2	21.79	0.87	13.22000	0.20000	0.49920	0.00910	0.21151	2695.0	15.0	2609.0	39.0	2754	22	2754.0	22.0	5.3
13WTX01_3.FIN2	221.5	1.55	4.89400	0.05600	0.32030	0.00430	0.55663	1800.9	9.7	1791.0	21.0	1803	12	1803.0	12.0	0.7
13WTX01_4.FIN2	122.9	1.41	2.60700	0.06100	0.21440	0.00490	0.77241	1306.0	18.0	1252.0	26.0	1434	14	1434.0	14.0	12.7
13WTX01_5.FIN2	34.5	0.76	1.58400	0.05800	0.15690	0.00440	0.40621	963.0	23.0	939.0	25.0	1038	21	1038.0	21.0	9.5
13WTX01_6.FIN2	86.6	0.69	0.54900	0.01300	0.07100	0.00100	0.12401	445.0	8.4	442.4	6.1	456	36	442.4	6.1	0.6
13WTX01_7.FIN2	245.5	1.29	2.12100	0.02600	0.19420	0.00230	0.09801	1155.3	8.3	1144.0	13.0	1181	14	1181.0	14.0	3.1
13WTX01_8.FIN2	8.9	1.36	5.58000	0.20000	0.34600	0.01300	0.14965	1911.0	30.0	1912.0	65.0	1907	45	1907.0	45.0	0.3
13WTX01_9.FIN2	173	1.72	1.64200	0.03100	0.16030	0.00260	0.66220	986.0	12.0	959.0	15.0	1061	16	1061.0	16.0	9.6
13WTX01_10.FIN2	123.4	1.31	3.01400	0.05400	0.23020	0.00330	0.53486	1411.0	14.0	1335.0	17.0	1525	13	1525.0	13.0	12.5
13WTX01_11.FIN2	41.2	1.33	2.47000	0.10000	0.15750	0.00530	0.37654	1261.0	31.0	943.0	30.0	1854	32	1854.0	32.0	49.1
13WTX01_11.FIN2	44.2	1.57	5.22000	0.42000	0.27500	0.02400	0.90890	1850.0	70.0	1560.0	120.0	2198	39	2198.0	39.0	29.0
13WTX01_12.FIN2	27	1.49	1.90100	0.07500	0.18290	0.00440	0.24763	1079.0	26.0	1083.0	24.0	1096	44	1096.0	44.0	1.2
13WTX01_13.FIN2	59.1	1.21	0.54100	0.01900	0.06840	0.00110	0.06736	442.0	12.0	426.6	6.6	541	63	426.6	6.6	3.5
13WTX01_14.FIN2	288	2.52	1.84300	0.02800	0.18020	0.00230	0.15461	1062.3	9.7	1068.0	13.0	1037	18	1037.0	18.0	3.0
13WTX01_15.FIN2	136.7	1.77	3.11000	0.06100	0.24540	0.00400	0.60793	1435.0	15.0	1414.0	21.0	1459	15	1459.0	15.0	3.1
13WTX01_16.FIN2	99.72	1.33	0.51200	0.01100	0.06770	0.00091	0.13066	419.0	7.3	422.3	5.5	418	30	422.3	5.5	0.8
13WTX01_17.FIN2	77.8	1.92	1.83400	0.03900	0.17980	0.00540	0.04680	1057.0	14.0	1066.0	30.0	1048	39	1048.0	39.0	1.7
13WTX01_18.FIN2	265	5.45	1.71900	0.02600	0.17010	0.00310	0.91053	1015.3	9.5	1013.0	17.0	1022	10	1022.0	10.0	0.9
13WTX01_19.FIN2	27.9	0.63	1.09200	0.06800	0.06750	0.00250	0.40974	743.0	32.0	421.0	15.0	1931	73	DISC	DISC	78.2

Table 1

13WTX01_20.FIN2	64.7	2.24	1.90900	0.04800	0.18900	0.00370	0.50378	1083.0	17.0	1116.0	20.0	1032	13	1032.0	13.0	8.1
13WTX01_21.FIN2	147	0.59	4.09500	0.07000	0.28830	0.00430	0.42065	1653.0	14.0	1633.0	21.0	1674	11	1674.0	11.0	2.4
13WTX01_22.FIN2	51.28	1.06	4.16100	0.07300	0.29310	0.00350	0.30572	1665.0	14.0	1657.0	18.0	1678	14	1678.0	14.0	1.3
13WTX01_23.FIN2	84.2	3.23	4.70200	0.08000	0.31530	0.00600	0.65772	1771.0	13.0	1766.0	29.0	1788	13	1788.0	13.0	1.2
13WTX01_24.FIN2	129.2	1.67	2.44700	0.05900	0.19700	0.00480	0.60388	1256.0	17.0	1159.0	26.0	1441	19	1441.0	19.0	19.6
13WTX01_25.FIN2	110.4	0.52	1.69200	0.04400	0.16610	0.00330	0.58636	1005.0	16.0	990.0	18.0	1047	19	1047.0	19.0	5.4
13WTX01_27.FIN2	37.1	0.70	0.50200	0.01800	0.06560	0.00150	0.05662	412.0	12.0	409.3	8.8	442	52	409.3	8.8	0.7
13WTX01_28.FIN2	95.6	0.93	2.54100	0.03300	0.21780	0.00310	0.36927	1283.3	9.4	1270.0	16.0	1316	15	1316.0	15.0	3.5
13WTX01_29.FIN2	187.6	2.21	3.85300	0.03900	0.27970	0.00300	0.57029	1604.9	8.0	1590.0	15.0	1622	10	1622.0	10.0	2.0
13WTX01_30.FIN2	117.9	0.89	4.09600	0.05500	0.28800	0.00300	0.56686	1655.0	11.0	1632.0	15.0	1680	13	1680.0	13.0	2.9
13WTX01_31.FIN2	215	1.10	0.44780	0.00640	0.06073	0.00074	0.21168	375.6	4.5	380.0	4.5	346	25	380.0	4.5	1.2
13WTX01_32.FIN2	111.9	2.05	4.87100	0.04800	0.32670	0.00340	0.50164	1797.9	8.1	1822.0	16.0	1769	10	1769.3	9.6	3.0
13WTX01_33.FIN2	95.5	3.65	2.39700	0.04900	0.21170	0.00370	0.71420	1244.0	14.0	1237.0	20.0	1238	14	1238.0	14.0	0.1
13WTX01_34.FIN2	149.7	1.88	2.75300	0.04000	0.22650	0.00310	0.13446	1342.0	11.0	1316.0	16.0	1387	28	1387.0	28.0	5.1
13WTX01_35.FIN2	276	1.58	2.03700	0.02100	0.19150	0.00150	0.63714	1127.6	7.0	1130.9	8.6	1129	11	1129.0	11.0	0.2
13WTX01_36.FIN2	57.4	1.12	1.94800	0.04400	0.18210	0.00320	0.22057	1097.0	15.0	1078.0	18.0	1124	28	1124.0	28.0	4.1
13WTX01_37.FIN2	126	1.38	17.95000	0.14000	0.58390	0.00500	0.64350	2987.9	7.7	2964.0	20.0	2995	6	2995.1	6.0	1.0
13WTX01_38.FIN2	50.7	2.51	1.52600	0.07900	0.15610	0.00470	0.43194	939.0	32.0	935.0	26.0	973	28	973.0	28.0	3.9
13WTX01_39.FIN2	51.1	1.60	1.88800	0.04400	0.18080	0.00310	0.47107	1077.0	15.0	1071.0	17.0	1080	17	1080.0	17.0	0.8
13WTX01_40.FIN2	255.3	2.04	6.10400	0.08000	0.35770	0.00340	0.76767	1992.0	11.0	1971.0	16.0	2018	10	2017.9	9.6	2.3
13WTX01_41.FIN2	186	1.76	4.26300	0.03900	0.29900	0.00280	0.53926	1687.1	7.9	1686.0	14.0	1696	9	1696.2	9.1	0.6
13WTX01_42.FIN2	31.4	0.73	1.79300	0.07200	0.18110	0.00550	0.14681	1041.0	27.0	1080.0	32.0	957	38	957.0	38.0	12.9
13WTX01_43.FIN2	135.1	0.79	4.91900	0.05500	0.32210	0.00320	0.45493	1804.9	9.5	1800.0	16.0	1801	9	1800.5	9.0	0.0
13WTX01_44.FIN2	6.29	1.12	1.72000	0.11000	0.16170	0.00690	0.26602	1025.0	39.0	965.0	38.0	1145	72	1145.0	72.0	15.7
13WTX01_45.FIN2	258	2.46	1.89800	0.01900	0.18280	0.00170	0.37124	1080.1	6.7	1082.2	9.2	1089	9	1089.2	9.3	0.6
13WTX01_46.FIN2	26.82	0.53	2.02300	0.05600	0.18680	0.00310	0.21781	1126.0	18.0	1104.0	17.0	1170	31	1170.0	31.0	5.6

Table 1

13WTX01_47.FIN2	161.2	2.07	2.09300	0.02100	0.19350	0.00160	0.25477	1146.3	6.8	1140.0	8.8	1155	11	1155.0	11.0	1.3
13WTX01_48.FIN2	95.7	3.32	1.65400	0.04700	0.16080	0.00240	0.32965	990.0	18.0	961.0	13.0	1052	22	1052.0	22.0	8.7
13WTX01_49.FIN2	57.58	0.88	1.89100	0.04100	0.17290	0.00470	0.16372	1078.0	14.0	1028.0	26.0	1157	27	1157.0	27.0	11.1
13WTX01_50.FIN2	52	0.19	0.85600	0.04100	0.08470	0.00420	0.60527	629.0	23.0	528.0	26.0	1008	56	DISC	DISC	47.6
13WTX01_51.FIN2	69.9	1.41	2.04700	0.04500	0.19060	0.00480	0.73211	1131.0	15.0	1125.0	26.0	1137	21	1137.0	21.0	1.1
13WTX01_52.FIN2	183	1.74	1.79700	0.04900	0.17250	0.00370	0.61870	1044.0	18.0	1025.0	20.0	1105	17	1105.0	17.0	7.2
13WTX01_53.FIN2	226.1	1.43	0.59700	0.01200	0.07639	0.00087	0.51474	474.5	7.8	474.5	5.2	492	19	474.5	5.2	0.0
13WTX01_54.FIN2	102.8	0.97	4.74000	0.08200	0.31010	0.00500	0.68854	1773.0	14.0	1741.0	24.0	1806	10	1806.0	10.0	3.6
13WTX01_55.FIN2	83.4	1.28	5.55000	0.06100	0.34600	0.00300	0.46024	1908.8	9.2	1915.0	14.0	1911	9	1911.4	8.9	0.2
13WTX01_56.FIN2	66.3	1.31	1.86800	0.03600	0.17940	0.00290	0.01190	1071.0	12.0	1064.0	16.0	1082	18	1082.0	18.0	1.7
13WTX01_57.FIN2	73	1.51	1.78000	0.02800	0.17270	0.00320	0.12972	1038.0	10.0	1027.0	17.0	1062	27	1062.0	27.0	3.3
13WTX01_58.FIN2	182.1	0.46	1.81800	0.02400	0.17720	0.00240	0.30043	1051.9	8.8	1052.0	13.0	1027	12	1027.0	12.0	2.4
13WTX01_59.FIN2	50.7	3.78	3.98700	0.06300	0.28700	0.00360	0.38974	1633.0	13.0	1626.0	18.0	1643	16	1643.0	16.0	1.0
13WTX01_61.FIN2	59.6	0.91	3.55000	0.10000	0.26000	0.00790	0.77612	1544.0	25.0	1489.0	41.0	1639	21	1639.0	21.0	9.2
13WTX01_62.FIN2	42.8	0.90	2.80700	0.06500	0.24000	0.00460	0.27361	1363.0	16.0	1387.0	24.0	1329	33	1329.0	33.0	4.4
13WTX01_63.FIN2	331	2.93	1.74400	0.01800	0.17140	0.00160	0.44469	1024.5	6.5	1020.0	9.0	1046	11	1046.0	11.0	2.5
13WTX01_64.FIN2	167.6	1.13	4.02900	0.05600	0.29030	0.00440	0.80288	1639.0	11.0	1642.0	22.0	1629	12	1629.0	12.0	0.8
13WTX01_65.FIN2	34.5	3.51	1.75700	0.06000	0.17050	0.00550	0.46120	1028.0	22.0	1014.0	30.0	1083	25	1083.0	25.0	6.4
13WTX01_66.FIN2	123.3	1.07	0.49600	0.01300	0.06453	0.00096	0.25159	408.7	8.6	403.1	5.8	442	30	403.1	5.8	1.4
13WTX01_67.FIN2	96.9	2.22	1.59900	0.03300	0.16030	0.00270	0.26039	969.0	13.0	958.0	15.0	1010	21	1010.0	21.0	5.1
13WTX01_68.FIN2	186	0.88	0.48220	0.00880	0.06389	0.00070	0.22712	399.3	6.0	399.2	4.2	393	24	399.2	4.2	0.0
13WTX01_69.FIN2	59.8	0.61	1.60800	0.04000	0.16670	0.00260	0.29988	972.0	15.0	994.0	14.0	940	27	940.0	27.0	5.7
13WTX01_70.FIN2	168	1.18	0.51800	0.01000	0.06734	0.00072	0.30992	423.3	6.7	420.1	4.3	422	27	420.1	4.3	0.8
13WTX01_71.FIN2	111.8	1.89	5.19500	0.09200	0.33220	0.00590	0.70274	1851.0	15.0	1849.0	29.0	1863	10	1862.7	9.8	0.7
13WTX01_72.FIN2	80.9	0.75	11.22000	0.26000	0.47730	0.00850	0.61435	2540.0	22.0	2515.0	37.0	2550	17	2550.0	17.0	1.4
13WTX01_73.FIN2	76.7	1.01	1.66800	0.04200	0.16650	0.00450	0.47406	996.0	16.0	993.0	25.0	1008	27	1008.0	27.0	1.5

Table 1

13WTX01_74.FIN2	71.1	2.25	1.52600	0.04000	0.15360	0.00260	0.19519	940.0	16.0	921.0	15.0	1000	25	1000.0	25.0	7.9
13WTX01_75.FIN2	81.7	1.83	2.89200	0.05600	0.24200	0.00360	0.05214	1379.0	15.0	1397.0	19.0	1363	25	1363.0	25.0	2.5
13WTX01_76.FIN2	328	2.63	4.14300	0.03300	0.29530	0.00280	0.66536	1663.2	6.6	1668.0	14.0	1653	8	1653.4	8.0	0.9
13WTX01_77.FIN2	213.8	1.79	1.82200	0.02200	0.17460	0.00310	0.40272	1053.1	8.1	1037.0	17.0	1074	17	1074.0	17.0	3.4
13WTX01_78.FIN2	95	0.66	0.47500	0.01400	0.06370	0.00110	0.22081	395.2	9.2	398.3	6.6	401	34	398.3	6.6	0.8
13WTX01_79.FIN2	163	1.26	4.67800	0.04000	0.31580	0.00300	0.58623	1763.8	7.4	1769.0	15.0	1760	7	1760.1	7.0	0.5
13WTX01_80.FIN2	56.23	4.04	3.24300	0.07300	0.24610	0.00490	0.19267	1467.0	17.0	1418.0	25.0	1546	23	1546.0	23.0	8.3
13WTX01_81.FIN2	232	5.87	5.05200	0.06500	0.32190	0.00360	0.79650	1828.0	11.0	1799.0	18.0	1873	9	1872.6	9.2	3.9
13WTX01_82.FIN2	84.9	2.09	1.44100	0.02500	0.14920	0.00190	0.27106	906.0	11.0	896.0	10.0	954	26	954.0	26.0	6.1
13WTX01_83.FIN2	51.3	2.15	1.79000	0.03900	0.17790	0.00440	0.44999	1044.0	15.0	1055.0	24.0	1020	25	1020.0	25.0	3.4
13WTX01_84.FIN2	250	2.44	0.54000	0.01100	0.07100	0.00130	0.47287	438.0	7.1	442.0	7.9	459	52	442.0	7.9	0.9
13WTX01_85.FIN2	70.5	2.88	2.18600	0.05400	0.20330	0.00490	0.17574	1176.0	17.0	1193.0	26.0	1159	23	1159.0	23.0	2.9
13WTX01_86.FIN2	399	2.02	2.68700	0.03800	0.23090	0.00280	0.81872	1324.0	11.0	1339.0	15.0	1297	10	1297.0	10.0	3.2
13WTX01_87.FIN2	44.2	0.80	2.34000	0.16000	0.21000	0.01600	0.80621	1229.0	51.0	1225.0	86.0	1274	31	1274.0	31.0	3.8
13WTX01_88.FIN2	509	7.90	5.84000	0.16000	0.27820	0.00840	0.88547	1952.0	24.0	1582.0	43.0	2353	21	2353.0	21.0	32.8
13WTX01_88.FIN2	29.71	1.63	10.44000	0.32000	0.41800	0.00870	0.46876	2480.0	25.0	2251.0	40.0	2666	17	2666.0	17.0	15.6
13WTX01_89.FIN2	273	7.44	2.09200	0.03700	0.19240	0.00350	0.78441	1148.0	13.0	1134.0	19.0	1177	13	1177.0	13.0	3.7
13WTX01_90.FIN2	49.96	1.48	2.84800	0.08200	0.23790	0.00450	0.24974	1367.0	21.0	1375.0	23.0	1374	34	1374.0	34.0	0.1
13WTX01_91.FIN2	21.95	2.25	1.56000	0.13000	0.15330	0.00470	0.43052	950.0	50.0	919.0	26.0	1073	48	1073.0	48.0	14.4
13WTX01_92.FIN2	39.8	0.97	1.48400	0.04600	0.15460	0.00280	0.03081	929.0	19.0	927.0	16.0	932	40	932.0	40.0	0.5
13WTX01_93.FIN2	413	2.57	2.70000	0.02400	0.22710	0.00220	0.52198	1328.2	6.5	1319.0	12.0	1341	11	1341.0	11.0	1.6
13WTX01_94.FIN2	40.77	1.31	13.22000	0.19000	0.50250	0.00620	0.33912	2694.0	14.0	2630.0	29.0	2747	13	2747.0	13.0	4.3
13WTX01_95.FIN2	170	1.27	1.89900	0.02100	0.18260	0.00160	0.24067	1081.3	7.1	1081.0	8.5	1080	13	1080.0	13.0	0.1
13WTX01_96.FIN2	154.5	1.60	0.56800	0.01200	0.07458	0.00084	0.07775	457.2	7.4	463.7	5.1	421	31	463.7	5.1	1.4
13WTX01_97.FIN2	40.9	0.82	1.63300	0.04800	0.16570	0.00420	0.09414	985.0	19.0	988.0	23.0	1010	42	1010.0	42.0	2.2
13WTX01_98.FIN2	93	1.35	0.57100	0.02500	0.06810	0.00170	0.31476	458.0	16.0	425.0	10.0	592	54	425.0	10.0	7.2

Table 1

13WTX01_99.FIN2	174.1	3.61	1.72200	0.02900	0.16970	0.00170	0.37537	1016.0	11.0	1010.6	9.6	1030	18	1030.0	18.0	1.9
13WTX01_100.FIN2	84.1	1.15	1.58400	0.04800	0.16160	0.00400	0.27184	963.0	19.0	966.0	22.0	976	29	976.0	29.0	1.0
13WTX01_101.FIN2	596	145.00	1.61900	0.02300	0.16160	0.00130	0.58103	979.3	9.6	965.6	7.3	1011	10	1010.6	9.8	4.5
13WTX01_103.FIN2	491	1.39	1.97400	0.02300	0.18260	0.00220	0.62082	1106.4	7.9	1081.0	12.0	1165	12	1165.0	12.0	7.2
13WTX01_105.FIN2	587	10.70	1.85200	0.04000	0.17580	0.00330	0.84267	1063.0	14.0	1044.0	18.0	1114	13	1114.0	13.0	6.3
13WTX01_106.FIN2	503	2.18	2.07200	0.02700	0.19450	0.00250	0.58574	1139.3	9.0	1145.0	14.0	1136	15	1136.0	15.0	0.8
13WTX01_108.FIN2	114.4	1.07	2.17900	0.04300	0.19960	0.00230	0.16899	1174.0	14.0	1173.0	12.0	1178	26	1178.0	26.0	0.4
13WTX01_109.FIN2	86	1.49	3.45700	0.08500	0.26890	0.00660	0.72628	1516.0	19.0	1535.0	33.0	1502	12	1502.0	12.0	2.2
13WTX01_110.FIN2	49.1	0.89	2.97400	0.07300	0.23360	0.00430	0.41186	1400.0	19.0	1353.0	23.0	1465	26	1465.0	26.0	7.6
13WTX01_111.FIN2	423.9	1.58	1.75800	0.01900	0.17160	0.00200	0.37278	1029.9	6.9	1021.0	11.0	1043	12	1043.0	12.0	2.1
13WTX01_112.FIN2	46.8	2.32	3.10600	0.09400	0.23580	0.00430	0.12178	1433.0	23.0	1365.0	23.0	1531	27	1531.0	27.0	10.8
13WTX01_113.FIN2	91.5	1.15	13.98000	0.24000	0.53270	0.00760	0.83619	2747.0	17.0	2759.0	34.0	2739	10	2739.1	9.5	0.7
13WTX01_114.FIN2	52.8	1.56	0.63300	0.02300	0.07930	0.00130	0.23758	496.0	15.0	491.8	8.0	497	54	491.8	8.0	0.8
13WTX01_115.FIN2	200	8.30	1.93100	0.04300	0.18960	0.00410	0.65719	1091.0	15.0	1119.0	22.0	1057	19	1057.0	19.0	5.9
13WTX01_116.FIN2	526	2.01	4.44000	0.02900	0.29860	0.00240	0.59552	1719.7	5.4	1684.0	12.0	1769	7	1768.7	7.3	4.8
13WTX01_117.FIN2	81.6	1.20	1.85300	0.07700	0.17670	0.00380	0.54320	1063.0	28.0	1049.0	21.0	1090	18	1090.0	18.0	3.8
13WTX01_118.FIN2	56	1.19	13.46000	0.20000	0.52040	0.00840	0.65424	2712.0	14.0	2700.0	36.0	2736	8	2736.1	8.2	1.3
13WTX01_119.FIN2	183.9	0.99	3.98900	0.03700	0.28600	0.00310	0.45383	1631.6	7.6	1621.0	16.0	1653	11	1653.0	11.0	1.9
13WTX01_120.FIN2	351	2.78	2.12800	0.03000	0.19600	0.00370	0.52186	1157.6	9.8	1154.0	20.0	1172	15	1172.0	15.0	1.5
13WTX02_1.FIN2	82.5	2.27	2.15200	0.04300	0.18840	0.00390	0.39802	1165.0	14.0	1112.0	21.0	1265	18	1265.0	18.0	12.1
13WTX02_2.FIN2	80.99	0.62	11.61000	0.14000	0.48100	0.00650	0.56713	2574.0	11.0	2531.0	28.0	2616	12	2616.0	12.0	3.2
13WTX02_3.FIN2	21	1.46	0.57100	0.02900	0.07180	0.00260	0.14396	457.0	19.0	447.0	16.0	631	77	447.0	16.0	2.2
13WTX02_4.FIN2	132.6	1.34	4.39400	0.06000	0.29540	0.00370	0.69340	1711.0	11.0	1672.0	17.0	1759	6	1759.3	6.1	5.0
13WTX02_5.FIN2	90.8	0.32	17.31000	0.13000	0.52040	0.00530	0.64979	2953.0	7.7	2700.0	23.0	3136	9	3136.1	9.0	13.9
13WTX02_6.FIN2	51	1.09	2.28600	0.03300	0.19820	0.00270	0.11592	1208.8	9.8	1165.0	14.0	1270	23	1270.0	23.0	8.3

Table 1

13WTX02_8.FIN2	171	1.57	0.56700	0.01000	0.07050	0.00120	0.50926	455.9	6.8	439.4	7.0	566	20	439.4	7.0	3.6
13WTX02_8.FIN2	211.5	3.15	2.03200	0.07300	0.17890	0.00520	0.91985	1125.0	24.0	1061.0	28.0	1268	13	1268.0	13.0	16.3
13WTX02_9.FIN2	240	2.75	1.69600	0.01600	0.16800	0.00130	0.61715	1006.6	5.9	1001.1	7.3	1024	14	1024.0	14.0	2.2
13WTX02_10.FIN2	87	1.43	2.02400	0.05700	0.18690	0.00460	0.71157	1125.0	20.0	1104.0	25.0	1162	23	1162.0	23.0	5.0
13WTX02_11.FIN2	254	1.43	1.43300	0.02200	0.14500	0.00170	0.64645	904.4	8.8	872.6	9.6	995	13	995.0	13.0	12.3
13WTX02_12.FIN2	291	2.90	3.38500	0.03100	0.25850	0.00240	0.57450	1500.6	7.3	1482.0	12.0	1510	11	1510.0	11.0	1.9
13WTX02_13.FIN2	155.4	7.94	11.60700	0.07700	0.49570	0.00430	0.48457	2573.8	6.3	2595.0	18.0	2562	9	2562.1	9.3	1.3
13WTX02_14.FIN2	99.17	1.02	2.16300	0.02700	0.19170	0.00250	0.17977	1168.7	8.6	1130.0	13.0	1235	17	1235.0	17.0	8.5
13WTX02_15.FIN2	87.2	1.75	3.06500	0.04600	0.24440	0.00380	0.65467	1423.0	12.0	1409.0	20.0	1449	15	1449.0	15.0	2.8
13WTX02_16.FIN2	56.6	1.01	0.51100	0.01500	0.06750	0.00110	0.35479	419.0	10.0	420.9	6.5	408	43	420.9	6.5	0.5
13WTX02_17.FIN2	102.5	1.14	0.51800	0.01100	0.06683	0.00089	0.12905	424.6	7.2	417.8	5.2	483	28	417.8	5.2	1.6
13WTX02_18.FIN2	91.2	1.34	3.91000	0.06100	0.27300	0.00420	0.65853	1615.0	13.0	1559.0	22.0	1699	13	1699.0	13.0	8.2
13WTX02_19.FIN2	240.6	2.39	2.09300	0.01900	0.19180	0.00150	0.32968	1146.4	6.2	1131.1	8.2	1174	11	1174.0	11.0	3.7
13WTX02_20.FIN2	746	2.08	2.31700	0.04000	0.16990	0.00290	0.48368	1217.0	12.0	1012.0	16.0	1599	21	1599.0	21.0	36.7
13WTX02_21.FIN2	361	1.86	1.77400	0.01600	0.17320	0.00170	0.48442	1035.9	6.0	1029.4	9.6	1059	10	1059.0	10.0	2.8
13WTX02_22.FIN2	397	1.10	3.18600	0.04500	0.22950	0.00240	0.51626	1453.0	11.0	1332.0	13.0	1643	14	1643.0	14.0	18.9
13WTX02_23.FIN2	380	4.38	1.82600	0.02600	0.16640	0.00190	0.75188	1054.3	9.5	992.0	11.0	1194	10	1194.0	10.0	16.9
13WTX02_24.FIN2	260	1.40	1.96900	0.02100	0.18490	0.00180	0.30169	1104.8	7.1	1093.8	9.9	1133	18	1133.0	18.0	3.5
13WTX02_25.FIN2	63.4	1.23	1.74300	0.03700	0.16650	0.00380	0.39605	1026.0	14.0	996.0	20.0	1073	22	1073.0	22.0	7.2
13WTX02_26.FIN2	166	1.27	0.79100	0.01100	0.09551	0.00096	0.29678	591.3	6.2	588.0	5.7	612	19	588.0	5.7	0.6
13WTX02_27.FIN2	40.5	1.07	1.93700	0.03700	0.18170	0.00260	0.24843	1095.0	13.0	1076.0	14.0	1125	19	1125.0	19.0	4.4
13WTX02_28.FIN2	356	11.42	1.47400	0.01800	0.15080	0.00210	0.57395	919.6	7.5	906.0	12.0	982	11	982.0	11.0	7.7
13WTX02_29.FIN2	114.7	1.50	1.76600	0.02600	0.17120	0.00210	0.53500	1032.5	9.4	1019.0	12.0	1055	20	1055.0	20.0	3.4
13WTX02_30.FIN2	115	2.41	1.70000	0.04900	0.16900	0.00370	0.81450	1007.0	19.0	1006.0	20.0	1017	24	1017.0	24.0	1.1
13WTX02_31.FIN2	66.1	1.77	2.61600	0.05500	0.22540	0.00520	0.58714	1308.0	14.0	1310.0	27.0	1303	22	1303.0	22.0	0.5
13WTX02_32.FIN2	98.7	1.38	2.07100	0.03000	0.18990	0.00270	0.51356	1139.0	10.0	1121.0	15.0	1180	19	1180.0	19.0	5.0

Table 1

13WTX02_33.FIN2	62.2	0.65	1.52200	0.03100	0.15350	0.00250	0.36420	938.0	13.0	923.0	13.0	987	26	987.0	26.0	6.5
13WTX02_34.FIN2	87.7	1.73	1.60000	0.02900	0.15830	0.00260	0.26644	970.0	11.0	947.0	15.0	1032	16	1032.0	16.0	8.2
13WTX02_35.FIN2	55.4	1.60	2.32400	0.05800	0.20700	0.00350	0.54716	1224.0	17.0	1212.0	19.0	1224	21	1224.0	21.0	1.0
13WTX02_36.FIN2	278.1	3.23	0.49300	0.01100	0.06480	0.00120	0.27684	406.9	7.5	404.9	7.1	417	29	404.9	7.1	0.5
13WTX02_37.FIN2	87.9	1.28	1.76700	0.02300	0.17340	0.00210	0.29324	1033.0	8.5	1031.0	12.0	1039	17	1039.0	17.0	0.8
13WTX02_38.FIN2	159.5	2.07	1.67800	0.02400	0.16200	0.00200	0.30892	1001.4	8.8	968.0	11.0	1063	16	1063.0	16.0	8.9
13WTX02_39.FIN2	98.59	0.62	4.55500	0.06300	0.29840	0.00440	0.70976	1740.0	12.0	1683.0	22.0	1816	8	1815.9	8.2	7.3
13WTX02_41.FIN2	405.4	1.92	1.83400	0.04100	0.15330	0.00270	0.79858	1057.0	15.0	919.0	15.0	1373	17	1373.0	17.0	33.1
13WTX02_42.FIN2	500	0.94	2.71000	0.04000	0.22500	0.00500	0.71105	1331.0	11.0	1308.0	26.0	1371	19	1371.0	19.0	4.6
13WTX02_43.FIN2	49.66	0.85	2.26700	0.05200	0.20510	0.00360	0.23105	1201.0	16.0	1202.0	19.0	1216	25	1216.0	25.0	1.2
13WTX02_44.FIN2	131	1.38	2.21600	0.04300	0.19990	0.00290	0.74888	1185.0	13.0	1174.0	15.0	1201	12	1201.0	12.0	2.2
13WTX02_45.FIN2	32.35	0.48	1.83900	0.05400	0.17840	0.00350	0.45870	1057.0	19.0	1058.0	19.0	1042	36	1042.0	36.0	1.5
13WTX02_46.FIN2	211	4.85	0.48240	0.00930	0.06469	0.00073	0.45442	399.3	6.4	404.1	4.4	411	25	404.1	4.4	1.2
13WTX02_47.FIN2	16.83	0.64	1.61500	0.07500	0.15860	0.00670	0.23459	975.0	29.0	948.0	37.0	1099	44	1099.0	44.0	13.7
13WTX02_48.FIN2	165.1	2.15	1.71900	0.02100	0.17090	0.00170	0.46996	1015.1	7.9	1017.2	9.1	1020	11	1020.0	11.0	0.3
13WTX02_49.FIN2	97.2	1.32	2.72400	0.05300	0.22530	0.00330	0.49581	1334.0	15.0	1314.0	16.0	1373	14	1373.0	14.0	4.3
13WTX02_50.FIN2	96	1.55	1.93100	0.04200	0.18670	0.00340	0.51019	1091.0	15.0	1103.0	18.0	1066	22	1066.0	22.0	3.5
13WTX02_51.FIN2	38.33	1.00	1.83400	0.05700	0.17870	0.00340	0.27839	1057.0	20.0	1060.0	19.0	1033	39	1033.0	39.0	2.6
13WTX02_52.FIN2	135.3	1.76	3.63700	0.05100	0.26440	0.00270	0.72481	1557.0	11.0	1512.0	14.0	1634	11	1634.0	11.0	7.5
13WTX02_53.FIN2	167	1.11	4.93100	0.06400	0.32700	0.00580	0.73481	1807.0	11.0	1824.0	28.0	1789	8	1789.1	7.8	2.0
13WTX02_54.FIN2	318.8	2.98	4.99200	0.04000	0.32760	0.00310	0.51401	1817.7	6.8	1827.0	15.0	1819	10	1818.7	9.7	0.5
13WTX02_55.FIN2	147.3	2.46	1.65200	0.02600	0.16690	0.00250	0.66382	992.0	10.0	995.0	14.0	1007	14	1007.0	14.0	1.2
13WTX02_56.FIN2	82.9	1.66	2.70100	0.04900	0.22120	0.00510	0.63252	1332.0	12.0	1288.0	27.0	1407	15	1407.0	15.0	8.5
13WTX02_57.FIN2	65.8	1.94	1.83100	0.06600	0.17540	0.00390	0.66872	1061.0	25.0	1042.0	22.0	1091	26	1091.0	26.0	4.5
13WTX02_58.FIN2	158.3	1.65	2.13400	0.03000	0.19940	0.00210	0.40782	1159.5	9.7	1172.0	11.0	1143	14	1143.0	14.0	2.5
13WTX02_59.FIN2	67	0.56	13.22000	0.13000	0.51890	0.00490	0.54925	2694.8	9.1	2694.0	21.0	2704	9	2703.7	9.1	0.4

Table 1

13WTX02_60.FIN2	90	1.96	2.02400	0.06400	0.19130	0.00410	0.59270	1126.0	21.0	1128.0	22.0	1107	36	1107.0	36.0	1.9
13WTX02_61.FIN2	134	1.49	2.05700	0.04000	0.19170	0.00330	0.45439	1134.0	13.0	1131.0	18.0	1150	15	1150.0	15.0	1.7
13WTX02_62.FIN2	111.2	1.47	3.41300	0.05300	0.26490	0.00330	0.57024	1509.0	12.0	1514.0	17.0	1518	13	1518.0	13.0	0.3
13WTX02_63.FIN2	50.89	1.08	3.59900	0.09000	0.26990	0.00550	0.26738	1548.0	20.0	1540.0	28.0	1606	30	1606.0	30.0	4.1
13WTX02_64.FIN2	215	3.07	1.87600	0.03300	0.18030	0.00310	0.58163	1072.0	12.0	1069.0	17.0	1079	17	1079.0	17.0	0.9
13WTX02_65.FIN2	373	2.99	1.69800	0.02900	0.17030	0.00340	0.80337	1008.0	11.0	1013.0	19.0	1022	15	1022.0	15.0	0.9
13WTX02_66.FIN2	43	1.25	1.50200	0.04300	0.15450	0.00350	0.36216	930.0	17.0	926.0	20.0	939	30	939.0	30.0	1.4
13WTX02_67.FIN2	56.6	1.41	4.03200	0.09200	0.27740	0.00690	0.86297	1638.0	19.0	1577.0	35.0	1716	14	1716.0	14.0	8.1
13WTX02_68.FIN2	121.2	1.15	0.50100	0.01200	0.06600	0.00140	0.31073	412.0	8.2	412.0	8.2	428	26	412.0	8.2	0.0
13WTX02_69.FIN2	180.1	1.56	9.60000	0.11000	0.43690	0.00510	0.77354	2397.0	10.0	2341.0	24.0	2462	8	2462.1	8.2	4.9
13WTX02_70.FIN2	191	1.33	2.90000	0.04600	0.23590	0.00360	0.72352	1381.0	12.0	1365.0	19.0	1400	11	1400.0	11.0	2.5
13WTX02_71.FIN2	431	4.46	2.01800	0.02900	0.18920	0.00310	0.56115	1121.3	9.8	1117.0	17.0	1146	20	1146.0	20.0	2.5
13WTX02_72.FIN2	38	1.93	1.61100	0.03900	0.16310	0.00330	0.04097	973.0	15.0	974.0	18.0	965	43	965.0	43.0	0.9
13WTX02_73.FIN2	77.7	1.68	1.88700	0.05300	0.17960	0.00340	0.29557	1076.0	18.0	1069.0	20.0	1093	24	1093.0	24.0	2.2
13WTX02_74.FIN2	145.3	4.41	1.80400	0.02500	0.17170	0.00240	0.46270	1046.6	9.0	1021.0	13.0	1109	12	1109.0	12.0	7.9
13WTX02_76.FIN2	260.6	1.98	18.81000	0.16000	0.57830	0.00580	0.77451	3032.9	8.4	2941.0	24.0	3101	5	3100.5	4.6	5.1
13WTX02_78.FIN2	267	2.32	0.62900	0.01600	0.07420	0.00130	0.41041	495.3	9.8	461.5	7.9	671	28	461.5	7.9	6.8
13WTX02_78.FIN2	234	1.14	2.37000	0.17000	0.18000	0.01200	0.95718	1225.0	52.0	1066.0	64.0	1528	25	1528.0	25.0	30.2
13WTX02_79.FIN2	446	4.88	1.70000	0.03600	0.16840	0.00410	0.73128	1008.0	14.0	1003.0	22.0	1037	11	1037.0	11.0	3.3
13WTX02_80.FIN2	92.03	0.58	3.53100	0.04900	0.24600	0.00420	0.39638	1534.0	11.0	1418.0	22.0	1718	17	1718.0	17.0	17.5
13WTX02_81.FIN2	194	0.52	1.82300	0.05100	0.17280	0.00410	0.86565	1052.0	18.0	1027.0	22.0	1108	13	1108.0	13.0	7.3
13WTX02_82.FIN2	45.5	0.98	1.91600	0.04100	0.18310	0.00330	0.32065	1087.0	14.0	1084.0	18.0	1102	22	1102.0	22.0	1.6
13WTX02_83.FIN2	28.9	0.68	1.71700	0.05600	0.16580	0.00400	0.19736	1013.0	21.0	988.0	22.0	1100	32	1100.0	32.0	10.2
13WTX02_84.FIN2	351	5.18	1.65300	0.02400	0.16670	0.00200	0.63673	990.6	9.3	994.0	11.0	1002	12	1002.0	12.0	0.8
13WTX02_85.FIN2	146.1	5.59	1.65700	0.02500	0.16680	0.00240	0.27762	993.8	9.7	994.0	13.0	1009	16	1009.0	16.0	1.5
13WTX02_86.FIN2	348	2.38	2.16000	0.03400	0.19910	0.00290	0.70313	1168.0	11.0	1170.0	16.0	1172	13	1172.0	13.0	0.2

Table 1

13WTX02_87.FIN2	125.5	2.49	1.78600	0.02100	0.17470	0.00150	0.38026	1039.9	7.6	1037.9	8.0	1040	13	1040.0	13.0	0.2
13WTX02_88.FIN2	154.9	0.68	13.20000	0.13000	0.53090	0.00460	0.62913	2693.8	9.1	2745.0	19.0	2668	8	2668.0	8.0	2.9
13WTX02_89.FIN2	99.8	1.38	2.74600	0.06300	0.23150	0.00470	0.60680	1340.0	17.0	1342.0	25.0	1367	17	1367.0	17.0	1.8
13WTX02_90.FIN2	78.2	0.94	3.81900	0.08400	0.27920	0.00490	0.45455	1596.0	18.0	1587.0	24.0	1612	20	1612.0	20.0	1.6
13WTX02_91.FIN2	85.5	2.74	1.71200	0.04100	0.16870	0.00340	0.50056	1012.0	16.0	1005.0	19.0	1049	16	1049.0	16.0	4.2
13WTX02_92.FIN2	75.5	1.21	1.86300	0.03000	0.18240	0.00260	0.50365	1069.0	11.0	1080.0	14.0	1066	15	1066.0	15.0	1.3
13WTX02_94.FIN2	127.5	1.59	1.65800	0.04500	0.16560	0.00330	0.47608	992.0	17.0	988.0	19.0	1017	15	1017.0	15.0	2.9
13WTX02_96.FIN2	84.4	0.54	2.10300	0.03900	0.19570	0.00380	0.62480	1149.0	13.0	1152.0	21.0	1167	21	1167.0	21.0	1.3
13WTX02_97.FIN2	179.3	3.43	4.88800	0.04900	0.32540	0.00380	0.46130	1799.8	8.4	1816.0	18.0	1790	9	1790.1	9.2	1.4
13WTX02_99.FIN2	112.5	0.86	4.29300	0.07000	0.30040	0.00450	0.77247	1691.0	14.0	1693.0	22.0	1688	11	1688.0	11.0	0.3
13WTX02_101.FIN2	183.2	1.21	3.34900	0.04000	0.25890	0.00260	0.34469	1492.2	9.3	1484.0	13.0	1512	15	1512.0	15.0	1.9
13WTX02_102.FIN2	133.6	2.11	8.44000	0.19000	0.36170	0.00600	0.50183	2279.0	21.0	1990.0	28.0	2576	20	2576.0	20.0	22.7
13WTX02_103.FIN2	95.5	1.37	1.81600	0.04600	0.16990	0.00360	0.32844	1050.0	17.0	1012.0	20.0	1153	27	1153.0	27.0	12.2
13WTX02_104.FIN2	873	0.76	1.11000	0.06200	0.07011	0.00075	0.02848	754.0	31.0	436.8	4.5	1920	100	DISC	DISC	77.3
13WTX02_105.FIN2	88.5	1.16	2.17100	0.03500	0.19880	0.00330	0.36066	1171.0	11.0	1169.0	18.0	1184	20	1184.0	20.0	1.3
13WTX02_106.FIN2	91.6	1.07	1.66100	0.02900	0.16270	0.00240	0.36629	993.0	11.0	972.0	13.0	1058	16	1058.0	16.0	8.1
13WTX02_107.FIN2	56.3	0.97	0.58400	0.01800	0.07460	0.00120	0.25773	468.0	11.0	463.7	7.4	498	39	463.7	7.4	0.9
13WTX02_108.FIN2	274.1	3.92	3.98800	0.04100	0.29100	0.00320	0.67542	1632.9	8.7	1646.0	16.0	1626	12	1626.0	12.0	1.2
13WTX02_109.FIN2	54.3	0.90	10.17000	0.12000	0.45930	0.00780	0.60579	2450.0	11.0	2436.0	34.0	2478	11	2478.0	11.0	1.7
13WTX02_110.FIN2	78.2	0.60	0.54500	0.01500	0.06935	0.00094	0.11712	440.7	9.6	432.2	5.7	515	40	432.2	5.7	1.9
13WTX02_111.FIN2	198	0.68	3.78000	0.05500	0.28060	0.00460	0.72871	1588.0	12.0	1594.0	23.0	1586	12	1586.0	12.0	0.5
13WTX02_112.FIN2	72.2	0.75	1.61500	0.04000	0.16520	0.00250	0.31850	975.0	16.0	986.0	14.0	972	22	972.0	22.0	1.4
13WTX02_113.FIN2	28.47	0.47	0.59100	0.02600	0.07400	0.00150	0.07555	470.0	17.0	460.2	8.9	562	55	460.2	8.9	2.1
13WTX02_114.FIN2	192.5	2.30	2.05500	0.02900	0.19330	0.00240	0.58327	1135.8	8.8	1139.0	13.0	1121	16	1121.0	16.0	1.6
13WTX02_115.FIN2	28.4	0.90	1.95700	0.07600	0.17850	0.00540	0.65707	1100.0	26.0	1059.0	30.0	1203	21	1203.0	21.0	12.0
13WTX02_116.FIN2	56.1	0.96	3.22700	0.05600	0.25100	0.00400	0.45308	1467.0	13.0	1443.0	21.0	1501	15	1501.0	15.0	3.9

13WTX02_117.FIN2	107	1.19	2.12300	0.06000	0.19840	0.00560	0.67277	1155.0	19.0	1166.0	30.0	1127	22	1127.0	22.0	3.5
13WTX02_119.FIN2	438	1.97	1.94500	0.03300	0.17050	0.00450	0.63656	1096.0	11.0	1015.0	25.0	1281	16	1281.0	16.0	20.8
13WTX02_120.FIN2	80	1.95	2.62700	0.03700	0.22440	0.00440	0.64765	1308.0	10.0	1305.0	23.0	1332	12	1332.0	12.0	2.0

Table 1: 13WTX01 (TSS1) and 13WTX02 (TSS2) sample data.

Table 2

Sample Name:								207/235		206/238		206/207		Best age		
Grain #	[U] ppm	U/Th	207/235	2σ error	206/238	2σ error	RHO	Age Ma	2σ error	Age (Ma)	2σ error	Age (Ma)	2σ error	(Ma)	2σ error	% Discordance*
13WTX03_1.FIN2	94.1	0.58	0.49670	0.00970	0.06637	0.00061	0.23118	409.2	6.6	414.3	3.7	368	22	414.3	3.7	1.2
13WTX03_3.FIN2	188.8	2.69	5.13000	0.07200	0.30860	0.00450	0.95023	1840.0	12.0	1733.0	22.0	2047	6	2046.8	5.6	15.3
13WTX03_6.FIN2	96.1	1.72	1.68600	0.01900	0.17160	0.00150	0.55941	1002.8	7.3	1020.7	8.1	963	11	963.0	11.0	6.0
13WTX03_7.FIN2	54.5	0.96	1.82700	0.02100	0.18310	0.00180	0.45686	1055.8	7.9	1083.5	9.7	1000	13	1000.0	13.0	8.3
13WTX03_8.FIN2	85.4	2.00	7.11200	0.04000	0.41140	0.00260	0.67186	2125.3	5.0	2221.0	12.0	2037	5	2037.1	5.4	9.0
13WTX03_9.FIN2	247	1.49	7.26000	0.13000	0.39090	0.00770	0.96413	2142.0	15.0	2126.0	36.0	2164	6	2163.9	6.1	1.8
13WTX03_10.FIN2	111.4	0.81	4.21600	0.03800	0.30330	0.00130	0.07839	1676.9	7.3	1707.6	6.6	1638	14	1638.0	14.0	4.2
13WTX03_11.FIN2	191.3	6.61	5.75700	0.04900	0.36350	0.00270	0.81006	1939.5	7.3	1998.0	13.0	1879	4	1878.6	4.4	6.4
13WTX03_12.FIN2	415	8.11	1.84990	0.00990	0.18540	0.00110	0.40291	1063.3	3.5	1098.1	5.9	1005	8	1004.9	8.0	9.3
13WTX03_13.FIN2	91.3	1.58	11.50000	0.10000	0.46810	0.00480	0.84561	2564.0	8.4	2475.0	21.0	2718	5	2717.5	4.6	8.9
13WTX03_14.FIN2	119	1.42	0.93800	0.01300	0.11080	0.00120	0.60202	671.4	7.0	677.1	6.7	642	17	677.1	6.7	0.8
13WTX03_15.FIN2	58.6	0.42	1.08300	0.01400	0.12120	0.00170	0.37488	744.5	6.9	737.5	9.7	882	20	737.5	9.7	0.9
13WTX03_16.FIN2	85.6	0.70	4.52000	0.03100	0.32510	0.00220	0.70772	1734.4	5.6	1815.0	11.0	1640	5	1640.1	5.0	10.7
13WTX03_17.FIN2	174.6	0.93	3.48400	0.03600	0.26530	0.00300	0.93333	1522.9	8.1	1516.0	15.0	1625	5	1625.1	5.1	6.7
13WTX03_19.FIN2	212.7	1.24	1.73700	0.01200	0.17140	0.00140	0.53168	1022.2	4.5	1019.6	7.5	1031	8	1030.8	8.1	1.1
13WTX03_21.FIN2	66.9	0.96	2.04700	0.02500	0.19050	0.00190	0.62454	1132.1	8.2	1124.0	10.0	1146	11	1146.0	11.0	1.9
13WTX03_22.FIN2	298	2.98	2.17500	0.02400	0.20190	0.00170	0.63060	1173.5	7.6	1185.6	9.2	1151	12	1151.0	12.0	3.0
13WTX03_23.FIN2	216	2.53	0.78160	0.00770	0.09545	0.00078	0.17406	586.3	4.3	587.7	4.6	579	12	587.7	4.6	0.2
13WTX03_24.FIN2	38.5	1.24	1.32500	0.02000	0.14550	0.00120	0.37150	856.0	8.8	875.5	7.0	935	16	935.0	16.0	6.4
13WTX03_26.FIN2	65.9	1.40	1.68000	0.01800	0.16640	0.00190	0.64084	1002.4	6.9	992.0	10.0	1155	11	1155.0	11.0	14.1
13WTX03_27.FIN2	171.1	0.80	0.88800	0.01100	0.10420	0.00100	0.51192	646.1	6.0	639.0	5.9	672	14	639.0	5.9	1.1
13WTX03_28.FIN2	273	1.67	2.25600	0.02800	0.20920	0.00270	0.90545	1199.1	8.8	1224.0	15.0	1164	7	1164.2	6.5	5.1
13WTX03_29.FIN2	189	2.62	5.10700	0.05700	0.31420	0.00390	0.90887	1836.6	9.5	1761.0	19.0	1925	5	1924.6	4.7	8.5

Table 2

13WTX03_30.FIN2	70.1	0.79	0.52360	0.00880	0.07009	0.00088	0.25927	427.3	5.9	436.6	5.3	491	23	436.6	5.3	2.2
13WTX03_31.FIN2	78.4	0.76	9.20900	0.06800	0.42550	0.00390	0.77636	2358.6	6.8	2287.0	18.0	2514	6	2514.3	5.8	9.0
13WTX03_32.FIN2	124.8	1.90	3.00100	0.04700	0.23600	0.00370	0.90943	1407.0	12.0	1368.0	20.0	1663	7	1663.2	6.5	17.7
13WTX03_33.FIN2	42.2	2.84	0.60700	0.01700	0.07910	0.00200	0.58846	481.0	11.0	491.0	12.0	730	29	491.0	12.0	2.1
13WTX03_34.FIN2	97.6	1.86	1.84400	0.02900	0.18690	0.00230	0.75992	1062.0	10.0	1105.0	13.0	1248	11	1248.0	11.0	11.5
13WTX03_35.FIN2	116	0.70	11.73000	0.14000	0.52080	0.00610	0.91607	2582.0	11.0	2702.0	26.0	2480	8	2479.7	8.3	9.0
13WTX03_36.FIN2	171	1.12	2.67900	0.04500	0.22330	0.00430	0.83897	1321.0	12.0	1298.0	23.0	1370	10	1370.0	10.0	5.3
13WTX03_37.FIN2	399	1.47	0.77450	0.00980	0.09543	0.00086	0.67437	582.1	5.6	587.6	5.1	563	12	587.6	5.1	0.9
13WTX03_38.FIN2	118.3	1.43	0.45600	0.01400	0.05930	0.00110	0.51267	381.0	10.0	371.4	6.8	539	31	371.4	6.8	2.5
13WTX03_39.FIN2	351	1.65	0.54610	0.00860	0.07017	0.00099	0.24291	442.4	5.6	437.2	6.0	471	29	437.2	6.0	1.2
13WTX03_39.FIN2	350.1	1.24	1.12900	0.01600	0.12280	0.00190	0.67639	767.3	7.8	747.0	11.0	831	18	747.0	11.0	2.6
13WTX03_40.FIN2	67.8	1.68	2.27700	0.03000	0.20880	0.00250	0.72603	1204.6	9.4	1222.0	13.0	1162	10	1162.0	10.0	5.2
13WTX03_41.FIN2	30.67	0.84	2.06500	0.03100	0.19190	0.00280	0.24677	1137.0	10.0	1131.0	15.0	1259	15	1259.0	15.0	10.2
13WTX03_42.FIN2	57.1	1.01	2.38700	0.02500	0.21600	0.00170	0.33785	1238.4	7.5	1260.5	8.8	1205	10	1205.3	9.9	4.6
13WTX03_43.FIN2	155.2	1.04	1.66700	0.01800	0.16500	0.00160	0.78951	997.3	6.7	984.6	8.9	1050	9	1049.8	8.6	6.2
13WTX03_44.FIN2	155.1	2.10	0.79490	0.00950	0.09642	0.00059	0.15181	594.4	5.3	593.4	3.5	762	20	593.4	3.5	0.2
13WTX03_45.FIN2	354	29.50	2.11700	0.04500	0.19640	0.00250	0.76474	1154.0	15.0	1156.0	14.0	1143	21	1143.0	21.0	1.1
13WTX03_46.FIN2	131	2.20	0.57050	0.00720	0.07495	0.00096	0.53211	458.1	4.6	465.9	5.8	540	13	465.9	5.8	1.7
13WTX03_48.FIN2	98.31	2.25	2.03100	0.03500	0.19560	0.00360	0.65503	1126.0	12.0	1151.0	20.0	1096	20	1096.0	20.0	5.0
13WTX03_49.FIN2	46.9	1.18	1.59300	0.02400	0.16010	0.00180	0.42925	966.7	9.6	957.0	10.0	1084	15	1084.0	15.0	11.7
13WTX03_50.FIN2	134.2	1.94	0.74400	0.01100	0.09111	0.00081	0.11865	564.4	6.5	562.1	4.8	575	19	562.1	4.8	0.4
13WTX03_51.FIN2	323	1.33	0.41270	0.00480	0.05553	0.00041	0.20451	350.7	3.4	348.4	2.5	370	16	348.4	2.5	0.7
13WTX03_52.FIN2	177	0.85	0.76100	0.01900	0.08960	0.00150	0.45845	574.0	11.0	553.0	9.1	646	28	553.0	9.1	3.7
13WTX03_53.FIN2	416	2.22	0.87450	0.00760	0.10531	0.00083	0.66391	638.5	4.0	645.4	4.8	611	6	645.4	4.8	1.1
13WTX03_54.FIN2	84.8	0.55	6.94500	0.08300	0.35140	0.00380	0.89023	2106.0	11.0	1941.0	18.0	2265	11	2265.0	11.0	14.3
13WTX03_55.FIN2	55.2	0.71	11.52000	0.15000	0.48780	0.00730	0.91895	2565.0	12.0	2560.0	32.0	2654	5	2653.5	5.2	3.5

Table 2

13WTX03_56.FIN2	423	0.87	2.31500	0.02200	0.21220	0.00140	0.05958	1216.6	6.6	1240.4	7.7	1172	19	1172.0	19.0	5.8
13WTX03_57.FIN2	129	1.05	19.22000	0.45000	0.64200	0.01600	0.98931	3049.0	25.0	3191.0	65.0	2963	6	2963.4	5.5	7.7
13WTX03_58.FIN2	337	0.87	0.41810	0.00450	0.05559	0.00048	0.12987	354.6	3.2	348.8	3.0	400	21	348.8	3.0	1.6
13WTX03_59.FIN2	54.2	1.31	0.91200	0.01300	0.10720	0.00120	0.02092	657.5	7.1	657.1	7.0	657	23	657.1	7.0	0.1
13WTX03_61.FIN2	223	1.44	1.89400	0.02400	0.18180	0.00210	0.64231	1079.4	8.1	1077.0	11.0	1072	9	1071.8	9.3	0.5
13WTX03_63.FIN2	197.8	2.54	3.30000	0.01900	0.26410	0.00180	0.62931	1480.8	4.4	1510.9	9.3	1433	7	1432.5	6.5	5.5
13WTX03_64.FIN2	102.3	0.57	0.58670	0.00740	0.07685	0.00085	0.38054	468.6	4.7	477.2	5.1	541	15	477.2	5.1	1.8
13WTX03_65.FIN2	137.5	0.80	0.73900	0.01700	0.09130	0.00160	0.58754	561.7	9.7	562.9	9.3	784	15	562.9	9.3	0.2
13WTX03_66.FIN2	187.9	13.94	1.90700	0.01700	0.18400	0.00150	0.73669	1084.0	6.0	1088.9	8.1	1077	9	1077.0	9.3	1.1
13WTX03_67.FIN2	177	1.13	12.61000	0.11000	0.52650	0.00490	0.80102	2651.3	8.7	2726.0	21.0	2583	6	2583.3	6.0	5.5
13WTX03_68.FIN2	167.2	1.53	0.69140	0.00980	0.08640	0.00110	0.71109	533.4	5.9	534.3	6.3	647	9	534.3	6.3	0.2
13WTX03_69.FIN2	116	3.03	1.85200	0.02400	0.18290	0.00220	0.63632	1063.6	8.6	1084.0	12.0	1023	11	1023.0	11.0	6.0
13WTX03_70.FIN2	205.1	2.69	3.62100	0.02600	0.28000	0.00210	0.61191	1553.9	5.6	1591.0	11.0	1499	7	1499.2	7.0	6.1
13WTX03_74.FIN2	144.2	3.04	0.93000	0.01400	0.10700	0.00150	0.58308	667.2	7.6	655.1	8.9	678	17	655.1	8.9	1.8
13WTX03_75.FIN2	117.8	1.12	1.74500	0.02000	0.17210	0.00210	0.57621	1024.9	7.3	1023.0	12.0	1135	10	1135.0	10.0	9.9
13WTX03_76.FIN2	59.6	0.96	0.46800	0.01100	0.06140	0.00100	0.19766	389.8	7.7	384.3	6.2	552	30	384.3	6.2	1.4
13WTX03_77.FIN2	19.7	0.46	0.64600	0.02100	0.08530	0.00140	0.20595	505.0	13.0	527.7	8.4	644	51	527.7	8.4	4.5
13WTX03_78.FIN2	34.5	0.83	5.20300	0.06900	0.33320	0.00390	0.62911	1854.0	11.0	1853.0	19.0	2073	11	2073.0	11.0	10.6
13WTX03_79.FIN2	273	1.78	0.52420	0.00700	0.06871	0.00066	0.46710	428.3	4.7	428.3	4.0	430	17	428.3	4.0	0.0
13WTX03_81.FIN2	66.6	0.55	3.45800	0.03800	0.26410	0.00320	0.40508	1517.3	8.6	1511.0	16.0	1634	12	1634.0	12.0	7.5
13WTX03_82.FIN2	201.2	7.28	1.16000	0.03100	0.12810	0.00210	0.79368	783.0	14.0	777.0	12.0	1012	21	777.0	12.0	0.8
13WTX03_83.FIN2	47.4	27.80	1.13300	0.02300	0.12660	0.00320	0.36571	771.0	12.0	768.0	18.0	799	24	768.0	18.0	0.4
13WTX03_84.FIN2	122	2.72	23.75000	0.32000	0.63660	0.00900	0.94053	3257.0	13.0	3174.0	36.0	3387	4	3386.8	4.0	6.3
13WTX03_85.FIN2	193.5	2.29	2.03000	0.01400	0.17740	0.00150	0.69193	1126.3	4.9	1052.4	8.0	1464	8	1463.7	7.5	28.1
13WTX03_86.FIN2	118.1	0.88	1.36600	0.01700	0.14330	0.00140	0.48278	874.0	7.3	863.1	7.9	1011	10	1011.0	10.0	14.6
13WTX03_87.FIN2	129.1	0.61	0.41260	0.00640	0.05907	0.00077	0.42128	350.6	4.6	369.9	4.7	456	22	369.9	4.7	5.5

Table 2

13WTX03_88.FIN2	225	2.19	1.78800	0.01600	0.17850	0.00140	0.41930	1040.9	5.9	1058.7	7.9	995	11	995.0	11.0	6.4
13WTX03_89.FIN2	255	2.15	2.28000	0.01900	0.21230	0.00170	0.61088	1206.6	5.8	1242.3	9.0	1139	7	1138.9	7.4	9.1
13WTX03_90.FIN2	178	1.05	0.69850	0.00920	0.08860	0.00130	0.59293	537.7	5.5	547.2	7.8	605	15	547.2	7.8	1.8
13WTX03_91.FIN2	151.1	1.16	1.05400	0.01000	0.12020	0.00099	0.38654	730.8	5.1	731.7	5.7	734	11	731.7	5.7	0.1
13WTX03_92.FIN2	161	2.25	0.86700	0.01300	0.10560	0.00130	0.63233	633.3	6.8	647.3	7.5	579	15	647.3	7.5	2.2
13WTX03_93.FIN2	85.6	0.82	2.64100	0.02700	0.22540	0.00220	0.60824	1311.7	7.5	1310.0	11.0	1389	9	1389.3	8.6	5.7
13WTX03_94.FIN2	32.05	2.86	0.70800	0.01700	0.08890	0.00120	0.01667	543.0	10.0	549.2	6.9	694	29	549.2	6.9	1.1
13WTX03_95.FIN2	44.9	1.88	2.04100	0.05100	0.18790	0.00310	0.69296	1128.0	17.0	1110.0	17.0	1156	23	1156.0	23.0	4.0
13WTX03_96.FIN2	38.3	1.66	1.49200	0.01800	0.15200	0.00220	0.54049	927.6	7.7	912.0	13.0	1071	15	1071.0	15.0	14.8
13WTX03_97.FIN2	30.3	0.92	1.40000	0.02500	0.14950	0.00150	0.17013	888.0	11.0	898.0	8.5	1067	26	1067.0	26.0	15.8
13WTX03_98.FIN2	247	1.28	1.14400	0.02100	0.12750	0.00130	0.17650	774.0	9.7	773.6	7.5	774	32	773.6	7.5	0.1
13WTX03_99.FIN2	135	1.62	14.17000	0.16000	0.55660	0.00580	0.85655	2761.0	10.0	2852.0	24.0	2694	9	2694.3	8.8	5.9
13WTX03_100.FIN2	41.8	0.85	1.37300	0.02500	0.14490	0.00270	0.63173	876.0	11.0	872.0	15.0	975	17	975.0	17.0	10.6
13WTX03_101.FIN2	117.2	1.26	1.77900	0.01700	0.17720	0.00190	0.38276	1038.5	6.5	1052.0	10.0	1013	13	1013.0	13.0	3.8
13WTX03_102.FIN2	196	0.48	0.66490	0.00890	0.08435	0.00094	0.11494	518.2	5.6	522.0	5.6	605	15	522.0	5.6	0.7
13WTX03_103.FIN2	83.9	0.89	0.66600	0.01300	0.08620	0.00120	0.49576	517.7	8.2	532.9	7.1	657	18	532.9	7.1	2.9
13WTX03_104.FIN2	107.9	0.66	0.53360	0.00810	0.07513	0.00082	0.34673	433.9	5.3	466.9	4.9	547	14	466.9	4.9	7.6
13WTX03_105.FIN2	135.4	0.68	1.71700	0.01800	0.17720	0.00140	0.41653	1014.5	6.8	1051.5	7.9	1206	12	1206.0	12.0	12.8
13WTX03_107.FIN2	103.3	0.59	1.55900	0.01800	0.16130	0.00150	0.52162	953.7	7.1	963.7	8.5	1042	13	1042.0	13.0	7.5
13WTX03_108.FIN2	156.6	0.82	1.81500	0.01600	0.17630	0.00220	0.75827	1050.7	5.9	1046.0	12.0	1273	7	1272.7	7.2	17.8
13WTX03_109.FIN2	15.03	1.23	1.25400	0.02800	0.13830	0.00290	0.41369	828.0	12.0	835.0	17.0	1033	27	835.0	17.0	0.8
13WTX03_111.FIN2	67.4	1.60	1.36400	0.01800	0.14420	0.00210	0.58996	873.1	7.8	868.0	12.0	1008	14	1008.0	14.0	13.9
13WTX03_112.FIN2	228	1.25	0.87900	0.01100	0.10140	0.00110	0.53402	639.9	6.1	622.4	6.6	691	15	622.4	6.6	2.7
13WTX03_113.FIN2	151.5	0.59	0.53970	0.00620	0.07015	0.00062	0.23286	438.9	4.3	437.1	3.7	560	13	437.1	3.7	0.4
13WTX03_114.FIN2	32.05	0.53	2.63100	0.04300	0.22290	0.00370	0.42054	1309.0	12.0	1297.0	19.0	1522	18	1522.0	18.0	14.8
13WTX03_115.FIN2	286.6	18.50	2.17500	0.02200	0.17430	0.00230	0.29119	1172.6	7.2	1036.0	13.0	1443	24	1443.0	24.0	28.2

Table 2

13WTX03_116.FIN2	134	1.22	1.70800	0.02000	0.16930	0.00190	0.72204	1011.2	7.7	1010.0	10.0	1135	8	1135.1	8.2	11.0
13WTX03_117.FIN2	60.2	1.41	0.75400	0.01500	0.09620	0.00120	0.40081	571.4	8.1	592.2	6.9	715	22	592.2	6.9	3.6
13WTX03_119.FIN2	55.4	1.69	2.31600	0.04100	0.20930	0.00270	0.64590	1216.0	13.0	1225.0	14.0	1210	18	1210.0	18.0	1.2
13WTX03_120.FIN2	108.2	1.69	2.00100	0.01900	0.19240	0.00150	0.34574	1115.4	6.4	1134.4	8.3	1081	11	1081.0	11.0	4.9
13WTX04_2.FIN2	153.8	1.22	1.64800	0.01700	0.16710	0.00160	0.45455	988.6	6.7	996.2	8.9	965	12	965.0	12.0	3.2
13WTX04_3.FIN2	25.5	1.12	1.72700	0.03300	0.17240	0.00250	0.50505	1017.0	12.0	1025.0	14.0	1102	26	1102.0	26.0	7.0
13WTX04_4.FIN2	136	2.06	13.20000	0.15000	0.52130	0.00530	0.84854	2695.0	11.0	2704.0	23.0	2690	8	2689.9	7.9	0.5
13WTX04_5.FIN2	156	2.54	1.64700	0.01600	0.17040	0.00170	0.58311	988.2	6.2	1014.4	9.2	933	12	933.0	12.0	8.7
13WTX04_6.FIN2	118.8	0.54	0.68370	0.00760	0.08492	0.00076	0.11073	528.9	4.6	525.4	4.5	681	21	525.4	4.5	0.7
13WTX04_7.FIN2	384	0.67	1.36700	0.03300	0.09123	0.00077	0.02594	873.0	14.0	562.8	4.5	1778	46	DISC	DISC	68.3
13WTX04_8.FIN2	374	1.23	0.59000	0.01400	0.07350	0.00130	0.51739	470.7	9.1	457.2	7.7	532	28	457.2	7.7	2.9
13WTX04_9.FIN2	113	1.84	8.49000	0.06000	0.37200	0.00330	0.61313	2284.6	6.4	2039.0	15.0	2610	6	2609.9	6.3	21.9
13WTX04_10.FIN2	181.6	5.07	0.54400	0.01400	0.07220	0.00150	0.46126	440.8	9.0	449.3	8.9	629	33	449.3	8.9	1.9
13WTX04_11.FIN2	75.6	1.28	0.84800	0.01600	0.10170	0.00160	0.23490	624.9	8.8	624.2	9.4	626	30	624.2	9.4	0.1
13WTX04_12.FIN2	96	12.30	0.58600	0.02600	0.07050	0.00190	0.77166	468.0	17.0	439.0	11.0	628	61	439.0	11.0	6.2
13WTX04_12.FIN2	39.25	1.38	13.82000	0.13000	0.51300	0.00490	0.58065	2737.1	8.8	2669.0	21.0	2819	9	2818.7	8.9	5.3
13WTX04_13.FIN2	40	1.36	1.87800	0.02800	0.18050	0.00220	0.55575	1074.0	10.0	1070.0	12.0	1231	13	1231.0	13.0	13.1
13WTX04_14.FIN2	57.2	0.65	2.29200	0.02700	0.21040	0.00200	0.43247	1210.2	8.5	1231.0	11.0	1174	11	1174.0	11.0	4.9
13WTX04_15.FIN2	200.7	0.72	0.53530	0.00720	0.06995	0.00071	0.18215	435.2	4.8	435.9	4.3	550	21	435.9	4.3	0.2
13WTX04_16.FIN2	196	5.40	2.21800	0.07400	0.20230	0.00540	0.59322	1194.0	21.0	1187.0	29.0	1227	39	1227.0	39.0	3.3
13WTX04_17.FIN2	377	0.91	2.11800	0.01900	0.19650	0.00170	0.70812	1154.5	6.1	1156.6	9.0	1155	9	1154.9	9.4	0.1
13WTX04_18.FIN2	254	10.00	0.50920	0.00540	0.06658	0.00051	0.35592	417.8	3.6	415.5	3.1	432	17	415.5	3.1	0.6
13WTX04_19.FIN2	26.1	0.96	1.53400	0.02500	0.15870	0.00250	0.38587	943.1	9.9	949.0	14.0	1017	24	1017.0	24.0	6.7
13WTX04_21.FIN2	74.6	3.13	1.75000	0.01600	0.17250	0.00160	0.43054	1026.8	5.8	1025.8	8.8	1153	12	1153.0	12.0	11.0
13WTX04_22.FIN2	211	1.46	1.58600	0.01200	0.16130	0.00150	0.54312	964.4	4.8	964.1	8.4	1173	9	1173.3	8.7	17.8

Table 2

13WTX04_24.FIN2	349	1.55	1.99400	0.02300	0.19340	0.00260	0.72100	1113.2	7.9	1139.0	14.0	1070	13	1070.0	13.0	6.4
13WTX04_25.FIN2	313	1.76	1.26100	0.02400	0.13590	0.00250	0.92296	827.0	11.0	821.0	14.0	964	10	821.0	14.0	0.7
13WTX04_26.FIN2	153	1.30	0.51610	0.00900	0.06807	0.00064	0.41111	423.9	6.3	424.5	3.8	423	18	424.5	3.8	0.1
13WTX04_27.FIN2	50.5	1.27	1.54100	0.01900	0.15950	0.00180	0.46807	946.2	7.6	954.0	10.0	1028	15	1028.0	15.0	7.2
13WTX04_28.FIN2	94.9	1.14	1.61100	0.02300	0.15540	0.00210	0.56992	974.0	8.9	931.0	12.0	1106	13	1106.0	13.0	15.8
13WTX04_30.FIN2	103	1.28	2.36900	0.02400	0.21670	0.00170	0.35982	1233.1	7.2	1264.2	9.0	1180	12	1180.0	12.0	7.1
13WTX04_31.FIN2	107.2	0.72	0.44250	0.00800	0.06061	0.00072	0.29133	371.8	5.6	379.3	4.4	451	23	379.3	4.4	2.0
13WTX04_32.FIN2	131.6	0.36	1.43100	0.02000	0.15120	0.00240	0.72468	901.7	8.2	907.0	14.0	1083	11	1083.0	11.0	16.3
13WTX04_33.FIN2	166	1.17	3.45000	0.02800	0.27770	0.00240	0.67975	1516.5	6.2	1580.0	12.0	1430	7	1429.7	7.0	10.5
13WTX04_34.FIN2	79.1	1.42	1.93700	0.01800	0.18490	0.00190	0.45736	1093.8	6.2	1094.0	10.0	1209	9	1209.2	8.7	9.5
13WTX04_35.FIN2	515	9.44	0.51690	0.00450	0.06770	0.00310	0.41119	423.1	3.0	422.0	19.0	457	33	422.0	19.0	0.3
13WTX04_35.FIN2	94.3	2.22	2.35500	0.02700	0.21460	0.00280	0.67867	1228.8	8.1	1253.0	15.0	1188	11	1188.0	11.0	5.5
13WTX04_36.FIN2	117.1	0.78	0.78000	0.01700	0.07690	0.00120	0.53130	584.4	9.6	477.5	7.1	1040	47	DISC	DISC	54.1
13WTX04_38.FIN2	31.9	0.76	4.41300	0.04800	0.31660	0.00280	0.38640	1714.2	9.0	1773.0	14.0	1654	11	1654.0	11.0	7.2
13WTX04_39.FIN2	582	12.72	0.82370	0.00730	0.10128	0.00092	0.63654	610.5	4.0	621.9	5.4	571	11	621.9	5.4	1.9
13WTX04_40.FIN2	209	1.26	4.25100	0.06400	0.27490	0.00430	0.87423	1683.0	12.0	1565.0	22.0	1843	8	1843.4	8.3	15.1
13WTX04_41.FIN2	99.7	0.37	0.67700	0.01100	0.08590	0.00130	0.22714	524.5	6.8	531.5	8.0	624	24	531.5	8.0	1.3
13WTX04_42.FIN2	66.2	1.43	1.53600	0.03000	0.15780	0.00250	0.72694	943.0	12.0	944.0	14.0	1129	16	1129.0	16.0	16.4
13WTX04_44.FIN2	264	2.32	1.47000	0.03000	0.14760	0.00270	0.90340	919.0	13.0	887.0	15.0	992	13	992.0	13.0	10.6
13WTX04_45.FIN2	304	2.39	4.48300	0.05600	0.25980	0.00290	0.74557	1727.0	10.0	1489.0	15.0	2029	8	2029.3	8.3	26.6
13WTX04_46.FIN2	246	1.86	3.29200	0.03800	0.24700	0.00370	0.95834	1478.9	9.0	1423.0	19.0	1585	10	1585.0	10.0	10.2
13WTX04_48.FIN2	45.5	0.88	2.68200	0.03500	0.24890	0.00360	0.52585	1323.0	9.8	1432.0	19.0	1198	20	1198.0	20.0	19.5
13WTX04_49.FIN2	11.55	0.17	11.57000	0.19000	0.48100	0.00600	0.47759	2571.0	15.0	2531.0	26.0	2725	12	2725.0	12.0	7.1
13WTX04_50.FIN2	154.7	2.81	4.18100	0.03700	0.30680	0.00240	0.70895	1671.1	7.0	1727.0	12.0	1604	7	1603.8	7.2	7.7
13WTX04_51.FIN2	101.6	1.37	3.65300	0.03500	0.28500	0.00250	0.56746	1560.6	7.7	1616.0	12.0	1496	11	1496.0	11.0	8.0
13WTX04_52.FIN2	184	3.52	0.44400	0.01500	0.05980	0.00190	0.88195	372.0	10.0	375.0	12.0	465	21	375.0	12.0	0.8

Table 2

13WTX04_53.FIN2	128	2.75	1.87000	0.04900	0.18140	0.00280	0.83887	1068.0	17.0	1076.0	15.0	1057	25	1057.0	25.0	1.8
13WTX04_55.FIN2	102.3	1.48	1.69300	0.01900	0.17650	0.00210	0.75111	1005.6	7.3	1048.0	11.0	1141	10	1140.9	9.5	8.1
13WTX04_56.FIN2	66.7	0.62	7.17200	0.07500	0.40340	0.00390	0.59878	2132.2	9.3	2184.0	18.0	2094	9	2093.5	8.8	4.3
13WTX04_57.FIN2	53.4	1.35	1.48500	0.02200	0.15290	0.00190	0.42797	923.7	9.1	917.0	11.0	1050	15	1050.0	15.0	12.7
13WTX04_58.FIN2	259	6.70	0.62350	0.00690	0.07905	0.00095	0.44267	491.9	4.3	490.4	5.7	502	15	490.4	5.7	0.3
13WTX04_59.FIN2	175.9	1.94	3.46200	0.03500	0.25200	0.00310	0.75732	1518.3	8.0	1448.0	16.0	1703	8	1702.5	7.9	14.9
13WTX04_60.FIN2	578	5.59	0.85300	0.02600	0.09580	0.00230	0.01852	626.0	14.0	589.0	14.0	732	67	589.0	14.0	5.9
13WTX04_60.FIN2	87.9	0.52	5.30800	0.06500	0.32590	0.00390	0.49979	1870.0	10.0	1818.0	19.0	1929	11	1929.0	11.0	5.8
13WTX04_61.FIN2	93.9	1.36	2.45300	0.02500	0.21370	0.00210	0.30295	1258.1	7.3	1248.0	11.0	1386	11	1386.0	11.0	10.0
13WTX04_62.FIN2	222.6	1.40	2.59400	0.04100	0.22340	0.00380	0.87125	1298.0	12.0	1303.0	21.0	1472	8	1472.4	8.3	11.5
13WTX04_63.FIN2	414	1.38	1.93500	0.01200	0.18720	0.00130	0.70654	1093.2	4.1	1106.4	6.9	1063	6	1062.9	6.2	4.1
13WTX04_64.FIN2	6.51	54.00	3.64000	0.12000	0.25820	0.00550	0.23445	1565.0	25.0	1480.0	28.0	1792	32	1792.0	32.0	17.4
13WTX04_65.FIN2	739	2.32	0.78520	0.00440	0.09495	0.00057	0.48468	588.4	2.5	584.7	3.4	598	9	584.7	3.4	0.6
13WTX04_66.FIN2	114.3	1.23	0.47880	0.00960	0.06540	0.00100	0.39348	397.0	6.6	408.4	6.1	441	22	408.4	6.1	2.9
13WTX04_67.FIN2	62.2	0.82	1.37100	0.02300	0.14790	0.00220	0.49795	876.0	9.7	889.0	12.0	1064	17	1064.0	17.0	16.4
13WTX04_68.FIN2	135.3	0.88	0.95000	0.01500	0.11060	0.00180	0.49371	678.0	7.7	676.0	11.0	714	18	676.0	11.0	0.3
13WTX04_69.FIN2	225	0.48	2.36300	0.02000	0.21000	0.00180	0.56124	1231.3	6.0	1228.6	9.7	1349	8	1349.3	7.6	8.9
13WTX04_70.FIN2	76.6	1.13	2.03700	0.02000	0.18540	0.00170	0.19400	1127.5	6.6	1097.6	9.2	1217	10	1217.0	10.0	9.8
13WTX04_71.FIN2	107	1.12	2.80800	0.02700	0.24200	0.00220	0.60371	1357.2	7.1	1397.0	11.0	1291	9	1291.1	9.1	8.2
13WTX04_72.FIN2	55.8	1.35	1.96900	0.03000	0.19080	0.00200	0.33465	1101.7	9.3	1125.0	11.0	1053	24	1053.0	24.0	6.8
13WTX04_73.FIN2	257	1.53	1.90800	0.01600	0.18800	0.00150	0.59340	1083.8	5.5	1110.4	7.9	1030	6	1030.4	6.3	7.8
13WTX04_75.FIN2	279	2.59	2.57900	0.03200	0.22620	0.00260	0.63802	1295.1	8.9	1314.0	14.0	1267	12	1267.0	12.0	3.7
13WTX04_76.FIN2	164	1.05	1.66500	0.01700	0.15240	0.00220	0.37917	994.9	6.6	914.0	13.0	1186	22	1186.0	22.0	22.9
13WTX04_77.FIN2	200	0.56	0.75470	0.00870	0.09322	0.00082	0.33777	570.7	5.0	574.5	4.8	568	14	574.5	4.8	0.7
13WTX04_78.FIN2	78.9	1.96	1.52400	0.01900	0.15820	0.00180	0.51425	939.6	7.7	946.0	10.0	1019	18	1019.0	18.0	7.2
13WTX04_79.FIN2	141.1	1.70	3.84800	0.03000	0.28660	0.00220	0.40375	1602.8	6.3	1625.0	11.0	1575	7	1574.8	6.6	3.2

Table 2

13WTX04_80.FIN2	146.8	1.14	0.51320	0.00790	0.06820	0.00066	0.17431	420.4	5.3	425.3	4.0	394	21	425.3	4.0	1.2
13WTX04_81.FIN2	92.9	0.45	0.97800	0.01700	0.11280	0.00120	0.05222	692.1	8.5	688.7	7.1	705	31	688.7	7.1	0.5
13WTX04_84.FIN2	133.4	1.35	2.90300	0.02600	0.23980	0.00220	0.55184	1382.4	6.8	1386.0	12.0	1365	11	1365.0	11.0	1.5
13WTX04_85.FIN2	87.5	0.71	0.48900	0.01300	0.06390	0.00130	0.46206	405.9	9.4	399.3	8.1	544	31	399.3	8.1	1.6
13WTX04_86.FIN2	77	0.80	3.56400	0.02900	0.27190	0.00280	0.65338	1543.1	6.5	1550.0	14.0	1649	10	1648.9	9.8	6.0
13WTX04_87.FIN2	99.6	1.20	3.46900	0.04600	0.25930	0.00300	0.50064	1519.0	10.0	1486.0	15.0	1567	14	1567.0	14.0	5.2
13WTX04_88.FIN2	246.2	1.08	3.92200	0.02700	0.29980	0.00250	0.63646	1617.9	5.6	1690.0	13.0	1519	8	1518.9	7.9	11.3
13WTX04_89.FIN2	145	0.76	6.16200	0.04000	0.38740	0.00240	0.55290	1999.6	5.5	2111.0	11.0	1891	6	1891.4	6.2	11.6
13WTX04_90.FIN2	123.6	1.17	0.66300	0.01000	0.08510	0.00120	0.75405	516.6	5.9	526.3	7.0	600	14	526.3	7.0	1.9
13WTX04_92.FIN2	53.6	0.82	1.33900	0.01700	0.14800	0.00160	0.26216	862.3	7.6	889.8	9.0	1007	14	1007.0	14.0	11.6
13WTX04_94.FIN2	64.8	1.88	1.68600	0.02500	0.17250	0.00240	0.57349	1003.7	9.2	1025.0	13.0	1093	15	1093.0	15.0	6.2
13WTX04_95.FIN2	24.73	0.71	3.37600	0.04600	0.27040	0.00320	0.01853	1498.0	11.0	1543.0	16.0	1611	15	1611.0	15.0	4.2
13WTX04_96.FIN2	42.9	0.66	1.04200	0.02000	0.11970	0.00160	0.52610	724.0	10.0	729.0	9.4	827	19	729.0	9.4	0.7
13WTX04_97.FIN2	177.1	0.38	0.64450	0.00710	0.08530	0.00100	0.62693	505.6	4.5	527.4	6.1	633	14	527.4	6.1	4.3
13WTX04_98.FIN2	167.3	0.81	3.98700	0.04600	0.28060	0.00320	0.83661	1631.1	9.4	1594.0	16.0	1910	7	1910.2	6.7	16.6
13WTX04_99.FIN2	175.9	1.48	6.24400	0.04000	0.39000	0.00260	0.24889	2011.4	5.7	2123.0	12.0	1893	7	1892.8	6.5	12.2
13WTX04_100.FIN2	45.5	1.01	5.64200	0.08000	0.31320	0.00370	0.48498	1922.0	12.0	1756.0	18.0	2196	13	2196.0	13.0	20.0
13WTX04_101.FIN2	56.7	2.14	1.54100	0.04400	0.15910	0.00370	0.55234	944.0	18.0	951.0	21.0	1131	20	1131.0	20.0	15.9
13WTX04_102.FIN2	10.47	0.42	0.67500	0.01900	0.09330	0.00200	0.16894	522.0	11.0	575.0	12.0	595	40	DISC	DISC	3.4
13WTX04_103.FIN2	213	0.83	1.22500	0.02300	0.13230	0.00170	0.59775	812.0	10.0	801.1	9.8	848	14	801.1	9.8	1.3
13WTX04_104.FIN2	156.7	1.61	1.46800	0.01700	0.15360	0.00180	0.70854	917.8	6.9	921.0	10.0	1016	9	1015.7	8.5	9.3
13WTX04_105.FIN2	322	1.31	2.00600	0.02300	0.18800	0.00260	0.39343	1117.4	7.8	1110.0	14.0	1116	19	1116.0	19.0	0.5
13WTX04_106.FIN2	131	0.70	3.65500	0.02700	0.27350	0.00210	0.62254	1561.4	6.0	1558.0	11.0	1671	7	1671.1	7.4	6.8
13WTX04_107.FIN2	126.6	0.86	23.58000	0.14000	0.68310	0.00630	0.71007	3251.0	6.0	3356.0	24.0	3183	6	3183.0	5.8	5.4
13WTX04_109.FIN2	29	0.31	6.42600	0.08000	0.39940	0.00430	0.33911	2035.0	11.0	2166.0	20.0	1909	13	1909.0	13.0	13.5
13WTX04_110.FIN2	154.1	0.52	4.02200	0.02800	0.29510	0.00200	0.57411	1638.4	5.6	1667.1	9.7	1612	8	1611.7	7.7	3.4

Table 2

13WTX04_111.FIN2	285	0.74	0.60900	0.01300	0.07254	0.00067	0.18623	482.3	8.5	451.4	4.0	614	46	451.4	4.0	6.4
13WTX04_113.FIN2	437	14.00	0.77640	0.00970	0.09640	0.00110	0.56432	583.3	5.6	594.3	6.0	553	15	594.3	6.0	1.9
13WTX04_114.FIN2	132.2	1.09	4.57900	0.04000	0.32070	0.00250	0.62599	1745.0	7.3	1793.0	12.0	1693	10	1693.2	9.8	5.9
13WTX04_115.FIN2	36.44	0.71	1.17600	0.03600	0.13560	0.00260	0.42869	789.0	17.0	819.0	15.0	829	30	819.0	15.0	3.8
13WTX04_116.FIN2	217	1.45	5.71800	0.07200	0.32300	0.00360	0.73315	1934.0	11.0	1804.0	17.0	2086	9	2085.8	8.5	13.5
13WTX04_118.FIN2	39.8	1.42	1.48900	0.02600	0.15540	0.00210	0.43424	925.0	11.0	931.0	12.0	1018	17	1018.0	17.0	8.5
13WTX04_119.FIN2	42.5	0.87	10.96000	0.12000	0.46210	0.00580	0.69570	2519.0	10.0	2452.0	25.0	2746	10	2746.1	9.5	10.7
13WTX04_120.FIN2	57.4	1.06	1.90700	0.02600	0.18370	0.00210	0.50141	1082.7	9.0	1087.0	12.0	1072	15	1072.0	15.0	1.4

Table 2: 13WTX03 (HF1) and 13WTX04 (HF2) sample data.

Table 3

Sample Name:								**207/235**		**206/238**		**207/206**		**Best age**			
Grain #	**[U] ppm**	**U/Th**	**207/235**	**2σ error**	**206/238**	**2σ error**	**RHO**	**Age Ma**	**2σ error**	**Age (Ma)**	**2σ error**	**Age (Ma)**	**2σ error**	**(Ma)**	**2σ error**	**% Discordance***	**Rim/Core**
LSS1_1.FIN2	126.9	1.62	0.703	0.019	0.0867	0.0011	0.39582	539	11	535.8	6.7	538	55	535.8	6.7	0.6	
LSS1_2.FIN2	425	3.44	0.636	0.013	0.0803	0.001	0.22199	498.7	8.2	497.8	6.2	500	43	497.8	6.2	0.2	
LSS1_3.FIN2	515	9.61	0.713	0.01	0.08815	0.00088	0.45679	546.3	6.1	544.5	5.2	549	30	544.5	5.2	0.3	
LSS1_4.FIN2	300	1.865	2.062	0.024	0.1923	0.0025	0.73435	1136.2	8.2	1133	13	1145	19	1145.0	19.0	1.0	
LSS1_5.FIN2	39.8		1.402	0.067	0.1458	0.0036	0.2782	885	28	877	20	862	99	862.0	99.0	1.7	
LSS1_6.FIN2	555	2.67	2.04	0.033	0.1911	0.0026	0.80763	1130	11	1127	14	1138	20	1138.0	20.0	1.0	
LSS1_8.FIN2	320	1.087	0.415	0.0092	0.05405	0.00071	0.44193	351.7	6.6	339.3	4.3	446	47	339.3	4.3	3.5	
LSS1_10.FIN2	402	14.7	0.734	0.018	0.0902	0.002	0.37061	558	10	556	12	556	64	556.0	12.0	0.4	
LSS1_11.FIN2	592	1.097	0.6309	0.0091	0.08015	0.00086	0.57308	496.2	5.7	496.9	5.1	484	30	496.9	5.1	0.1	
LSS1_12.FIN2	209.6	1.922	1.636	0.023	0.1647	0.0013	0.425	984	8.6	982.6	7.2	978	25	978.0	25.0	0.5	
LSS1_13.FIN2	254.9	2.459	1.818	0.021	0.1744	0.0014	0.4828	1051	7.6	1036.3	7.8	1070	21	1070.0	21.0	3.1	
LSS1_14.FIN2	47.3	1.709	1.961	0.046	0.186	0.0027	0.37914	1098	16	1099	15	1087	46	1087.0	46.0	1.1	
LSS1_16.FIN2	193	22.5	0.682	0.023	0.0813	0.0014	0.11761	527	14	503.9	8.5	611	80	503.9	8.5	4.4	Rim
LSS1_16.FIN2	394.6	8.15	1.554	0.037	0.1331	0.002	0.45358	951	15	805	12	1294	42	DISC	DISC	15.4	Core
LSS1_17.FIN2	190.2	1.585	0.692	0.029	0.083	0.0018	0.48005	533	17	514	11	596	82	514.0	11.0	3.6	
LSS1_18.FIN2	48.3	1.38	7.02	0.11	0.3818	0.0057	0.55096	2111	14	2083	27	2138	25	2138.0	25.0	2.6	
LSS1_19.FIN2	83.8	1.476	1.715	0.038	0.168	0.0025	0.42807	1012	14	1001	14	1025	42	1025.0	42.0	2.3	
LSS1_20.FIN2	162.8	0.843	1.971	0.033	0.1879	0.0019	0.52216	1104	11	1110	10	1084	29	1084.0	29.0	2.4	
LSS1_21.FIN2	215.5	1.417	1.649	0.029	0.1619	0.002	0.6307	988	11	967	11	1030	25	DISC	DISC	6.1	
LSS1_22.FIN2	462.4	1.294	1.708	0.032	0.1635	0.0027	0.65399	1010	12	976	15	1073	30	DISC	DISC	9.0	
LSS1_23.FIN2	330	2.59	0.942	0.016	0.1093	0.0015	0.63331	672.7	8.3	668.4	8.6	678	30	668.4	8.6	0.6	

Table 3

LSS1_24.FIN2	263	4.05	0.679	0.019	0.085	0.0013	0.35793	525	11	527	7.7	497	57	527.0	7.7	0.4	
LSS1_25.FIN2	296	2.241	1.821	0.025	0.1739	0.0018	0.61586	1052	9	1033.3	9.7	1077	20	1077.0	20.0	4.1	
LSS1_26.FIN2	175.4	3.28	1.828	0.028	0.1777	0.0022	0.54884	1053.9	9.9	1054	12	1051	26	1051.0	26.0	0.3	
LSS1_27.FIN2	111.8	1.274	1.743	0.035	0.1681	0.0024	0.33656	1023	13	1002	13	1067	40	DISC	DISC	6.1	
LSS1_28.FIN2	385	1.828	1.752	0.023	0.1722	0.0022	0.52643	1027	8.5	1024	12	1023	24	1023.0	24.0	0.1	
LSS1_29.FIN2	97.9	1.419	1.198	0.033	0.1094	0.0025	0.55746	797	15	669	14	1174	50	DISC	DISC	16.1	
LSS1_30.FIN2	147.5	2.06	0.754	0.022	0.0918	0.0016	0.21297	569	13	566.2	9.6	567	68	566.2	9.6	0.5	
LSS1_31.FIN2	129.3	1.544	0.764	0.018	0.0937	0.0013	0.20408	576	10	578.4	7.2	561	55	578.4	7.2	0.4	
LSS1_32.FIN2	319.5	6.39	0.688	0.011	0.08519	0.0009	0.43891	532	6.7	527	5.3	547	32	527.0	5.3	0.9	
LSS1_33.FIN2	243.2	14.3	0.715	0.018	0.0875	0.0013	0.28297	547	10	540.9	7.8	560	55	540.9	7.8	1.1	
LSS1_34.FIN2	217.5	1.869	0.648	0.013	0.08153	0.00095	0.35716	506.6	7.7	505.2	5.7	498	41	505.2	5.7	0.3	
LSS1_35.FIN2	434	3.06	1.782	0.047	0.1651	0.0046	0.90233	1034	17	983	25	1149	23	DISC	DISC	14.4	
LSS1_36.FIN2	483.4	6.59	0.501	0.012	0.0627	0.001	0.51811	411.7	8.3	392.3	6.1	508	46	392.3	6.1	4.7	
LSS1_37.FIN2	397	1.648	0.6131	0.0095	0.07731	0.00089	0.5006	484.9	6	479.9	5.4	501	31	479.9	5.4	1.0	
LSS1_38.FIN2	411	5.03	1.139	0.046	0.1112	0.0032	0.77631	769	21	679	19	1021	50	679.0	19.0	11.7	
LSS1_39.FIN2	759	7.1	0.914	0.042	0.1068	0.0036	0.77996	658	22	654	21	662	60	654.0	21.0	0.6	Rim
LSS1_39.FIN2	272	1.227	1.299	0.027	0.1341	0.0018	0.42917	844	12	811	10	929	38	811.0	10.0	3.9	Core
LSS1_40.FIN2	267.1	1.656	4.861	0.056	0.3044	0.0028	0.59218	1794.2	9.7	1712	14	1888	17	DISC	DISC	9.3	
LSS1_41.FIN2	160.3	1.98	3.343	0.041	0.2511	0.0026	0.47377	1489.7	9.6	1444	13	1552	22	DISC	DISC	7.0	
LSS1_42.FIN2	107.7	1.191	3.026	0.055	0.2403	0.0032	0.51953	1413	14	1388	16	1440	30	1440.0	30.0	3.6	
LSS1_43.FIN2	73.8	0.69	2.569	0.053	0.2203	0.0034	0.63247	1291	15	1283	18	1295	32	1295.0	32.0	0.9	
LSS1_44.FIN2	54.4	1.348	6.772	0.098	0.3851	0.0053	0.5436	2083	14	2099	24	2067	25	2067.0	25.0	1.5	
LSS1_45.FIN2	211.2	1.527	0.728	0.015	0.0895	0.0012	0.51841	555.4	9	552.3	7.3	564	39	552.3	7.3	0.6	
LSS1_46.FIN2	54	0.965	2.146	0.043	0.1967	0.0031	0.34552	1161	14	1157	17	1170	44	1170.0	44.0	1.1	
LSS1_47.FIN2	215.3	1.286	3.037	0.041	0.2452	0.0026	0.60776	1415	10	1413	13	1417	21	1417.0	21.0	0.3	

Table 3

LSS1_48.FIN2	162.6	2.39	1.244	0.026	0.1346	0.0017	0.50746	819	12	813.6	9.7	835	39	813.6	9.7	0.7	
LSS1_49.FIN2	176.4	0.743	4.208	0.06	0.2982	0.0035	0.58297	1674	12	1682	17	1662	20	1662.0	20.0	1.2	
LSS1_50.FIN2	422	4.05	0.833	0.03	0.0973	0.0028	0.78354	614	17	598	16	670	50	598.0	16.0	2.6	Rim
LSS1_50.FIN2	89.4	1.482	1.258	0.039	0.1253	0.0023	0.33442	827	17	761	13	1000	61	761.0	13.0	8.0	Core
LSS1_51.FIN2	814	40	0.733	0.033	0.0899	0.0022	0.65265	557	19	555	13	557	73	555.0	13.0	0.4	Rim
LSS1_51.FIN2	299	1.509	1.864	0.028	0.1761	0.0024	0.67385	1067.6	9.9	1045	13	1114	23	DISC	DISC	6.2	Core
LSS1_52.FIN2	545.5	1.606	1.699	0.037	0.1572	0.0037	0.8677	1006	14	941	20	1158	24	DISC	DISC	18.7	
LSS1_53.FIN2	26.5	1.229	0.708	0.038	0.0872	0.0022	0.354	536	22	538	13	490	100	538.0	13.0	0.4	
LSS1_54.FIN2	239.6	3.2	0.64	0.012	0.0806	0.001	0.43514	501.3	7.6	499.6	6.1	502	41	499.6	6.1	0.3	
LSS1_55.FIN2	134	2.87	1.739	0.031	0.1714	0.0021	0.56184	1023	11	1020	11	1027	29	1027.0	29.0	0.7	
LSS1_56.FIN2	157	1.184	2.301	0.047	0.2066	0.0038	0.85581	1210	15	1210	20	1211	21	1211.0	21.0	0.1	
LSS1_57.FIN2	187.4	1.611	1.694	0.068	0.1633	0.0028	0.76445	1003	26	975	16	1101	54	DISC	DISC	11.4	
LSS1_58.FIN2	62.1	2.73	1.37	0.035	0.1449	0.0025	0.46204	874	15	872	14	888	46	888.0	46.0	1.8	
LSS1_59.FIN2	666	8.23	0.743	0.026	0.0932	0.0031	0.53157	564	15	574	18	522	72	574.0	18.0	1.8	Rim
LSS1_59.FIN2	249	3.05	1.924	0.033	0.1839	0.0026	0.76567	1089	12	1088	14	1091	24	1091.0	24.0	0.3	Core
LSS1_60.FIN2	343.6	0.5086	1.205	0.02	0.1324	0.0018	0.35706	802.2	9	801	10	806	36	801	10	0.149588631	
LSS1_61.FIN2	100.3	2.7	2.26	0.057	0.2058	0.0033	0.54762	1198	18	1206	18	1199	48	1199.0	48.0	0.6	
LSS1_62.FIN2	890	68	0.783	0.034	0.0923	0.0033	0.84845	586	19	569	19	658	47	569.0	19.0	2.9	Rim
LSS1_62.FIN2	222.1	3.045	1.543	0.041	0.1576	0.0029	0.65132	946	17	943	16	951	42	951.0	42.0	0.8	Core
LSS1_63.FIN2	180	1.564	1.236	0.043	0.1177	0.0026	0.49908	818	19	717	15	1102	58	717.0	15.0	12.3	
LSS1_64.FIN2	40.2	0.564	12.05	0.2	0.472	0.0072	0.77971	2605	15	2490	31	2704	19	DISC	DISC	7.9	
LSS1_65.FIN2	100	1.55	3.53	0.062	0.2692	0.0039	0.49293	1530	14	1535	20	1529	31	1529.0	31.0	0.4	
LSS1_66.FIN2	653	2.06	0.942	0.015	0.1039	0.0017	0.53803	673.6	7.7	637	10	805	33	637.0	10.0	5.4	
LSS1_67.FIN2	171.4	0.837	0.831	0.019	0.1003	0.0014	0.40703	613	11	616	8.4	598	47	616.0	8.4	0.5	
LSS1_68.FIN2	99.2	2.47	2.336	0.074	0.207	0.0037	0.42351	1221	22	1212	20	1235	57	1235.0	57.0	1.9	

Table 3

LSS1_69.FIN2	216	1.451	5.497	0.074	0.3203	0.0039	0.76083	1898	12	1791	19	2024	16	DISC	DISC	11.5	
LSS1_70.FIN2	128.4	1.169	5.109	0.071	0.3236	0.0035	0.63489	1836	12	1806	17	1875	20	1875.0	20.0	3.7	
LSS1_71.FIN2	221	0.994	0.893	0.025	0.1077	0.0021	0.51403	646	13	659	12	602	53	659.0	12.0	2.0	Rim
LSS1_71.FIN2	290.3	3.85	1.121	0.034	0.126	0.0026	0.60886	762	16	765	15	758	53	765.0	15.0	0.4	Core
LSS1_72.FIN2	251	1.485	1.819	0.028	0.1738	0.0023	0.58651	1051	10	1033	12	1099	27	DISC	DISC	6.0	
LSS1_73.FIN2	157	6.38	7.044	0.082	0.388	0.0044	0.74345	2116	10	2112	20	2123	15	2123.0	15.0	0.5	
LSS1_74.FIN2	313.8	1.732	1.982	0.052	0.1873	0.0047	0.6604	1108	18	1106	26	1119	43	1119.0	43.0	1.2	
LSS1_75.FIN2	242.2	1.23	4.041	0.06	0.2768	0.0034	0.67233	1641	12	1575	17	1731	21	DISC	DISC	9.0	
LSS1_76.FIN2	207	2.33	0.9	0.02	0.1057	0.0014	0.38154	651	11	647.8	8.2	660	46	647.8	8.2	0.5	Rim
LSS1_76.FIN2	117.6	1.535	0.967	0.034	0.113	0.0027	0.39073	686	18	690	15	668	72	690.0	15.0	0.6	Core
LSS1_77.FIN2	217.7	1.981	0.42	0.014	0.0554	0.0011	0.43963	355	10	347.5	6.7	395	79	347.5	6.7	2.1	Rim
LSS1_77.FIN2	168.6	1.895	0.449	0.017	0.0601	0.0011	0.21638	375	12	376	6.4	360	83	376.0	6.4	0.3	Core
LSS1_78.FIN2	103.2	1.888	1.343	0.029	0.1385	0.0018	0.28029	863	13	836	10	928	46	836.0	10.0	3.1	
LSS1_79.FIN2	64.9	0.718	12.8	0.22	0.5015	0.0079	0.71494	2663	16	2619	34	2700	22	2700.0	22.0	3.0	
LSS1_80.FIN2	388	15.6	0.672	0.039	0.0835	0.0023	0.48675	521	23	517	14	530	160	517.0	14.0	0.8	Rim
LSS1_80.FIN2	74.3	2.132	1.566	0.037	0.1536	0.0022	0.36003	954	15	921	12	1028	47	DISC	DISC	10.4	Core
LSS1_81.FIN2	206.1	7.77	3.067	0.034	0.2483	0.002	0.47287	1423.2	8.5	1429	11	1413	20	1413.0	20.0	1.1	
LSS1_82.FIN2	640	42.2	0.798	0.031	0.0967	0.0034	0.67278	595	18	595	20	594	70	595.0	20.0	0.0	Rim
LSS1_82.FIN2	111.8	2.67	6.26	0.14	0.3659	0.0063	0.76946	2009	19	2008	30	2009	23	2009.0	23.0	0.0	Core
LSS1_83.FIN2	317.1	-10	0.779	0.012	0.09568	0.00088	0.45792	584.1	6.8	589	5.2	567	30	589.0	5.2	0.8	
LSS1_84.FIN2	103.8	0.681	1.643	0.029	0.1655	0.0017	0.43403	986	11	987.2	9.6	984	33	984.0	33.0	0.3	
LSS1_86.FIN2	770	12.4	0.743	0.047	0.0875	0.0049	0.72985	563	27	540	29	652	93	540.0	29.0	4.1	Rim
LSS1_86.FIN2	200.8	1.988	9.33	0.13	0.433	0.0059	0.69138	2370	13	2318	27	2419	17	2419.0	17.0	4.2	Core
LSS1_88.FIN2	459	1.578	0.883	0.015	0.0972	0.0014	0.40734	641.7	7.9	598.1	8	799	36	598.1	8	6.794452236	
LSS1_89.FIN2	169	1.668	2.488	0.041	0.2152	0.003	0.74511	1268	12	1256	16	1287	22	1287.0	22.0	2.4	

Table 3

LSS1_90.FIN2	420	4.17	0.946	0.015	0.1109	0.0014	0.60019	675.6	7.9	677.8	7.9	674	29	677.8	7.9	0.3	
LSS1_91.FIN2	78.8	0.738	1.103	0.042	0.1228	0.0025	0.14042	751	21	746	15	756	89	746.0	15.0	0.7	Rim
LSS1_91.FIN2	34.92	0.806	1.248	0.064	0.1356	0.0035	0.28199	818	29	820	20	790	110	820.0	20.0	0.2	Core
LSS1_92.FIN2	196.9	1.249	3.493	0.056	0.2626	0.0034	0.70086	1523	13	1502	17	1554	22	1554.0	22.0	3.3	
LSS1_93.FIN2	440	2.022	0.857	0.013	0.1031	0.0013	0.46122	627.7	7.3	632.7	7.4	609	33	632.7	7.4	0.8	
LSS1_94.FIN2	74.7	1.332	1.992	0.043	0.1895	0.0033	0.52532	1112	15	1118	18	1101	40	1101.0	40.0	1.5	
LSS1_95.FIN2	87.3	1.967	1.973	0.053	0.186	0.0031	0.34827	1104	18	1099	17	1115	53	1115.0	53.0	1.4	
LSS1_96.FIN2	211.9	0.665	1.372	0.027	0.1436	0.002	0.38184	876	12	865	11	900	40	900.0	40.0	3.9	
LSS1_97.FIN2	770	3.23	1.456	0.02	0.1468	0.0017	0.7659	911.3	8.4	882.6	9.3	986	19	DISC	DISC	10.5	
LSS1_98.FIN2	71.6	2.53	0.755	0.031	0.0897	0.0018	0.33135	571	18	554	11	622	86	554.0	11.0	3.0	
LSS1_99.FIN2	274	2.1	0.4666	0.0096	0.0613	0.00082	0.36875	388.1	6.7	383.5	5	403	46	383.5	5.0	1.2	
LSS1_100.FIN2	551	12.4	0.715	0.035	0.0876	0.0035	0.59428	552	23	546	18	589	90	546.0	18.0	1.1	
LSS1_101.FIN2	90.8	0.3946	5.39	0.11	0.3394	0.0059	0.78414	1879	18	1882	29	1883	24	1883.0	24.0	0.1	
LSS1_102.FIN2	221	1.347	1.086	0.033	0.123	0.003	0.53624	745	16	747	17	733	56	747.0	17.0	0.3	
LSS1_103.FIN2	108	1.038	1.876	0.045	0.1788	0.0024	0.50538	1071	16	1060	13	1088	41	1088.0	41.0	2.6	
LSS1_104.FIN2	1276	5.01	1.58	0.028	0.1477	0.003	0.87661	961	11	888	17	1142	22	DISC	DISC	22.2	
LSS1_105.FIN2	597	3.47	1.752	0.026	0.1667	0.0023	0.66042	1026.6	9.7	993	13	1098	24	DISC	DISC	9.6	
LSS1_106.FIN2	237.7	3.87	1.869	0.029	0.1801	0.0026	0.6586	1070	9.8	1067	14	1070	26	1070.0	26.0	0.3	
LSS1_107.FIN2	47.02	1.816	2.066	0.053	0.1925	0.0026	0.5235	1134	18	1134	14	1120	45	1120.0	45.0	1.3	
LSS1_108.FIN2	170	2.03	0.653	0.019	0.076	0.0012	0.28917	509	12	472.3	7.1	673	66	472.3	7.1	7.21021611	
LSS1_109.FIN2	147	1.722	0.406	0.014	0.0544	0.0013	0.26987	344.7	9.7	341.5	7.9	332	73	341.5	7.9	0.9	
LSS1_110.FIN2	187.9	1.699	0.841	0.022	0.094	0.0015	0.31317	620	12	579.1	8.6	764	56	579.1	8.6	6.6	
LSS1_111.FIN2	72.1	0.854	0.862	0.022	0.1023	0.0014	0.22296	630	12	627.4	8.1	619	56	627.4	8.1	0.4	
LSS1_112.FIN2	235	1.82	1.83	0.029	0.1775	0.0022	0.55347	1054	11	1055	11	1055	28	1055.0	28.0	0.0	
LSS1_113.FIN2	226.1	0.7412	3.926	0.065	0.2842	0.0038	0.64954	1617	13	1612	19	1624	23	1624.0	23.0	0.7	

Table 3

LSS1_114.FIN2	79.7	0.959	1.676	0.037	0.1575	0.0024	0.27864	999	15	943	14	1119	48	DISC	DISC	15.7	
LSS1_115.FIN2	308	2.66	0.791	0.017	0.0959	0.0013	0.51244	591.1	9.4	590.5	7.8	587	40	590.5	7.8	0.1	
LSS1_116.FIN2	197	2.26	0.973	0.015	0.1125	0.0011	0.32339	688.8	7.6	687.3	6.6	692	32	687.3	6.6	0.2	
LSS1_117.FIN2	161.6	0.506	0.837	0.018	0.0992	0.0013	0.13836	616.4	9.9	609.7	7.4	626	52	609.7	7.4	1.1	
LSS1_118.FIN2	132.4	1.76	0.887	0.036	0.1022	0.003	0.34392	642	20	627	17	689	86	627.0	17.0	2.3	
LSS1_119.FIN2	231	0.944	1.175	0.017	0.1313	0.0014	0.42741	789.4	8	795.4	7.8	774	29	795.4	7.8	0.8	
LSS1_120.FIN2	0	no value	no value	NAN	no value	NAN	#VALUE!	no value	NAN	no value	NAN	no value	NAN	########	#VALUE!	#VALUE!	
LSS1_121.FIN2	62.8	1.642	1.998	0.05	0.1903	0.0031	0.41649	1111	17	1122	17	1094	45	1094.0	45.0	2.6	
LSS1_122.FIN2	76.7	1.761	6.84	0.12	0.385	0.0062	0.58307	2089	15	2099	29	2087	25	2087.0	25.0	0.6	
LSS1_123.FIN2	343	4.96	0.882	0.014	0.1037	0.0012	0.435	641.2	7.6	636.2	6.9	657	31	636.2	6.9	0.8	
LSS1_124.FIN2	817	7.9	0.716	0.03	0.0882	0.0036	0.66381	547	17	544	21	558	69	544.0	21.0	0.5	Rim
LSS1_124.FIN2	613	3.23	0.831	0.012	0.0998	0.0011	0.2897	613.9	6.5	613.3	6.4	613	33	613.3	6.4	0.1	Core
LSS1_125.FIN2	126.8	0.954	0.358	0.016	0.0498	0.0011	0.071239	310	12	313.2	7	281	99	313.2	7.0	1.0	
LSS1_126.FIN2	604	2.253	4.239	0.085	0.2351	0.0045	0.92187	1678	17	1360	24	2108	14	DISC	DISC	35.5	
LSS1_127.FIN2	401	1.605	1.946	0.027	0.1861	0.0023	0.67227	1095.7	9.3	1100	13	1094	22	1094.0	22.0	0.5	
LSS1_128.FIN2	29.65	1.83	0.73	0.047	0.0858	0.0021	0.28894	549	27	530	12	590	130	530.0	12.0	3.5	
LSS1_129.FIN2	237	2.026	0.384	0.0092	0.05225	0.00066	0.15616	329.1	6.7	328.3	4.1	324	55	328.3	4.1	0.2	
LSS1_130.FIN2	344	0.765	2.041	0.033	0.1755	0.0024	0.58746	1130	12	1042	13	1309	29	DISC	DISC	20.4	
WCSS1_1.FIN2	450.6	2.52	2.694	0.066	0.2099	0.0035	0.56915	1325	18	1228	18	1483	40	DISC	DISC	17.2	
WCSS1_2.FIN2	96.5	0.849	2.033	0.064	0.1907	0.0047	0.8155	1121	22	1124	26	1117	37	1117.0	37.0	0.6	
WCSS1_3.FIN2	72.7	2.39	1.691	0.032	0.1685	0.0024	0.49069	1005	13	1003	13	997	40	997.0	40.0	0.6	
WCSS1_4.FIN2	60.9	1.8	0.612	0.021	0.0772	0.0013	0.032673	484	13	479.5	7.6	482	78	479.5	7.6	0.9	
WCSS1_5.FIN2	190.5	0.6646	0.825	0.014	0.09946	0.00091	0.25567	610.1	7.6	611.2	5.3	602	36	611.2	5.3	0.2	

Table 3

WCSS1_6.FIN2	81.7	1.7	1.779	0.036	0.1747	0.0021	0.24381	1035	13	1038	12	1030	43	1030.0	43.0	0.8	
WCSS1_7.FIN2	615	2.124	0.7368	0.0094	0.0906	0.001	0.43256	560.1	5.5	558.7	6	564	28	558.7	6.0	0.2	
WCSS1_8.FIN2	397.6	9.06	0.756	0.01	0.0923	0.00074	0.41316	571.3	5.8	569	4.4	574	27	569.0	4.4	0.4	
WCSS1_9.FIN2	136.7	0.3982	7.784	0.09	0.4108	0.0043	0.6673	2206	10	2218	20	2192	16	2192.0	16.0	1.2	
WCSS1_10.FIN2	96	2.035	1.863	0.033	0.1809	0.0021	0.48917	1066	12	1072	12	1051	31	1051.0	31.0	2.0	
WCSS1_11.FIN2	301.5	2.133	8.91	0.24	0.3508	0.008	0.95644	2321	25	1936	38	2683	14	DISC	DISC	27.8	
WCSS1_12.FIN2	246.1	0.797	4.475	0.057	0.3065	0.0035	0.66641	1725	10	1723	17	1721	19	1721.0	19.0	0.1	
WCSS1_13.FIN2	266	2.588	2.941	0.036	0.2415	0.0026	0.56457	1390.9	9.2	1394	14	1380	21	1380.0	21.0	1.0	
WCSS1_14.FIN2	414	1.487	1.918	0.022	0.184	0.0017	0.45848	1086.6	7.6	1088.5	9.4	1079	22	1079.0	22.0	0.9	
WCSS1_15.FIN2	534	8.45	1.896	0.021	0.1827	0.0017	0.65043	1080.6	7.4	1081.3	9.4	1081	18	1081.0	18.0	0.0	
WCSS1_16.FIN2	70.4	2.48	7.37	0.12	0.398	0.005	0.48472	2155	15	2159	23	2147	27	2147.0	27.0	0.6	
WCSS1_17.FIN2	601	2.4	0.805	0.043	0.0884	0.0027	0.87788	598	25	546	16	811	55	546.0	16.0	8.7	
WCSS1_17.FIN2	403	0.823	1.62	0.019	0.1629	0.0016	0.59421	977.4	7.5	974.1	8.6	986	21	986.0	21.0	1.2	
WCSS1_18.FIN2	21.41	1.35	11.42	0.3	0.475	0.011	0.80448	2551	24	2502	46	2593	29	2593	29	3.509448515	
WCSS1_19.FIN2	121.5	3.28	2.006	0.042	0.1901	0.0024	0.63575	1115	14	1121	13	1100	32	1100.0	32.0	1.9	
WCSS1_20.FIN2	663	2.115	0.51	0.011	0.063	0.0012	0.071612	418	7.6	393.7	7.3	545	48	393.7	7.3	5.8	
WCSS1_21.FIN2	202.8	6.7	0.732	0.013	0.0897	0.00095	0.33015	557.8	7.9	553.7	5.6	560	39	553.7	5.6	0.7	
WCSS1_22.FIN2	48.5	0.883	0.752	0.029	0.0918	0.0015	0.19023	569	16	565.8	9.1	558	78	565.8	9.1	0.6	
WCSS1_23.FIN2	221	1.423	0.574	0.012	0.07424	0.00083	0.36096	459.6	7.9	461.6	5	434	46	461.6	5.0	0.4	
WCSS1_24.FIN2	78.1	0.2838	0.45	0.018	0.0514	0.0012	0.47503	374	13	322.9	7.6	669	77	322.9	7.6	13.7	Rim
WCSS1_25.FIN2	600	19	0.692	0.019	0.0843	0.0014	0.62564	534	11	521.7	8.2	575	45	521.7	8.2	2.3	Core
WCSS1_25.FIN2	341.1	3.931	0.872	0.016	0.10371	0.00096	0.46792	635.8	8.8	636.1	5.6	628	36	636.1	5.6	0.0	
WCSS1_26.FIN2	210.3	2.421	0.901	0.019	0.1061	0.0013	0.48048	653	10	650.2	7.8	652	41	650.2	7.8	0.428790199	
WCSS1_27.FIN2	133.8	1.21	1.86	0.027	0.18	0.0015	0.30173	1065.3	9.5	1067	8.4	1055	27	1055.0	27.0	1.1	
WCSS1_28.FIN2	75.2	1.449	1.574	0.033	0.1611	0.002	0.38519	959	13	963	11	940	40	940.0	40.0	2.4	

Table 3

WCSS1_29.FIN2	108.6	3.9	1.115	0.049	0.1125	0.0027	0.1306	759	23	687	16	960	100	687.0	16.0	9.5	
WCSS1_29.FIN2	399.5	2.25	1.778	0.027	0.1694	0.0018	0.57833	1036.9	9.8	1008.5	9.7	1090	25	DISC	DISC	7.5	
WCSS1_30.FIN2	2156	55.2	1.264	0.067	0.0982	0.0034	0.95496	827	31	604	20	1478	46	DISC	DISC	27.0	
WCSS1_30.FIN2	479	13.86	6.009	0.062	0.3599	0.0041	0.72547	1976.6	9	1981	19	1964	15	1964	15	0.865580448	Rim
WCSS1_31.FIN2	503	2.94	0.887	0.019	0.1044	0.0013	0.51235	644	11	639.9	7.5	650	42	639.9	7.5	0.6	Core
WCSS1_32.FIN2	230.6	1.328	3.845	0.061	0.2499	0.0043	0.78386	1601	13	1437	22	1823	22	DISC	DISC	21.2	
WCSS1_32.FIN2	194	0.985	5.27	0.15	0.2997	0.0048	0.7486	1861	25	1689	24	2054	37	DISC	DISC	17.8	
WCSS1_33.FIN2	246.3	4.41	2.178	0.025	0.2019	0.0018	0.56873	1173	8.1	1185.1	9.8	1148	20	1148.0	20.0	3.2	
WCSS1_34.FIN2	299	0.769	1.749	0.023	0.1726	0.0015	0.56485	1025.6	8.6	1026.2	8.2	1024	23	1024.0	23.0	0.2	Rim
WCSS1_35.FIN2	146.2	1.176	0.575	0.016	0.07325	0.0009	0.15969	460	10	455.6	5.4	460	64	455.6	5.4	1.0	Core
WCSS1_36.FIN2	31	1.84	2.115	0.065	0.1961	0.0035	0.38298	1151	20	1154	19	1131	58	1131.0	58.0	2.0	Rim
WCSS1_37.FIN2	602	2.346	0.7407	0.0099	0.09086	0.0008	0.58274	562.2	5.7	560.6	4.7	566	23	560.6	4.7	0.3	Core
WCSS1_38.FIN2	50.5	2.36	1.736	0.052	0.1706	0.0029	0.50566	1018	19	1015	16	1013	55	1013.0	55.0	0.2	
WCSS1_39.FIN2	308	5.04	1.907	0.033	0.1837	0.0022	0.6804	1084	12	1087	12	1072	24	1072.0	24.0	1.4	Rim
WCSS1_40.FIN2	196	1.271	0.787	0.017	0.0944	0.0013	0.29684	588.4	9.8	581.5	7.4	626	41	581.5	7.4	1.2	Core
WCSS1_41.FIN2	550	3.52	0.946	0.012	0.10973	0.00085	0.75544	675.4	6.4	671.2	4.9	687	22	671.2	4.9	0.6	
WCSS1_42.FIN2	222	0.833	0.831	0.017	0.0986	0.0011	0.24653	613.2	9.5	606.3	6.3	634	46	606.3	6.3	1.1	
WCSS1_43.FIN2	128.5	1.3	2.327	0.029	0.209	0.0017	0.39441	1219.5	8.8	1223.1	9.2	1212	24	1212.0	24.0	0.9	
WCSS1_44.FIN2	306	2.753	1.767	0.022	0.1692	0.0016	0.4733	1032.7	8	1007.6	8.8	1084	23	DISC	DISC	7.0	
WCSS1_45.FIN2	72.4	2.345	1.758	0.037	0.1733	0.0024	0.43643	1027	14	1030	13	1028	39	1028.0	39.0	0.2	
WCSS1_46.FIN2	53.7	3.01	1.887	0.046	0.1814	0.0028	0.46419	1077	16	1074	15	1071	45	1071.0	45.0	0.3	
WCSS1_47.FIN2	483	2.164	0.751	0.013	0.0924	0.0011	0.31913	568.2	7.5	569.6	6.3	554	38	569.6	6.3	0.2	
WCSS1_48.FIN2	121.3	3.02	2.327	0.043	0.2052	0.0027	0.6957	1220	13	1203	14	1247	26	1247.0	26.0	3.5	
WCSS1_49.FIN2	28.48	1.61	1.739	0.055	0.1724	0.0036	0.38997	1020	20	1024	20	976	65	976.0	65.0	4.9	
WCSS1_50.FIN2	161	1.789	1.769	0.026	0.1745	0.0017	0.37979	1032.6	9.5	1036.7	9.2	1019	29	1019.0	29.0	1.7	

Table 3

WCSS1_51.FIN2	261.2	0.87	17.25	0.18	0.537	0.0055	0.82172	2947	10	2770	23	3070.3	9.8	DISC	DISC	9.8	
WCSS1_52.FIN2	351	1.026	0.5481	0.0082	0.07146	0.00064	0.36614	443.2	5.3	444.9	3.8	425	32	444.9	3.8	0.4	
WCSS1_53.FIN2	240.5	30.1	0.848	0.013	0.10128	0.00089	0.31773	622.7	7.1	621.8	5.2	617	32	621.8	5.2	0.1	
WCSS1_54.FIN2	125.1	1.113	7.208	0.081	0.3859	0.0035	0.52092	2136	10	2103	16	2165	18	2165.0	18.0	2.9	
WCSS1_55.FIN2	262.5	1.572	12.51	0.11	0.5053	0.0045	0.72876	2642.3	8.4	2635	19	2646	11	2646.0	11.0	0.4	
WCSS1_56.FIN2	118	2.69	1.552	0.03	0.16	0.002	0.32424	949	12	957	11	930	42	930.0	42.0	2.9	
WCSS1_57.FIN2	35.5	3.7	1.635	0.052	0.1666	0.0032	0.41365	978	20	992	18	966	60	966.0	60.0	2.7	
WCSS1_58.FIN2	51.81	1.518	1.554	0.04	0.1558	0.0021	0.39229	948	16	933	12	968	50	968.0	50.0	3.6	
WCSS1_59.FIN2	25.8	2.16	1.688	0.067	0.1697	0.0039	0.45783	998	26	1009	22	959	80	DISC	DISC	5.2	
WCSS1_60.FIN2	227	4.06	0.613	0.015	0.0777	0.0011	0.57132	484.6	9.4	482.6	6.7	492	50	482.6	6.7	0.4	
WCSS1_61.FIN2	142.2	1.255	0.87	0.017	0.104	0.0011	0.1464	636	9.5	637.9	6.6	612	47	637.9	6.6	0.3	
WCSS1_62.FIN2	112.7	1.251	13.72	0.19	0.5297	0.0063	0.57678	2729	13	2739	27	2717	20	2717.0	20.0	0.8	
WCSS1_63.FIN2	89.7	0.547	0.693	0.024	0.0875	0.0016	0.27711	532	14	540.6	9.3	486	74	540.6	9.3	1.6	
WCSS1_64.FIN2	159	0.819	4.974	0.076	0.3257	0.0041	0.80648	1814	13	1816	20	1811	16	1811.0	16.0	0.3	
WCSS1_65.FIN2	96	1.083	11.43	0.23	0.4281	0.0075	0.68643	2557	18	2296	34	2765	25	DISC	DISC	17.0	
WCSS1_66.FIN2	53.5	1.443	1.674	0.039	0.1661	0.0022	0.29838	995	15	990	12	1003	44	1003.0	44.0	1.3	
WCSS1_67.FIN2	143	1.553	2.355	0.038	0.2102	0.0024	0.57469	1229	12	1230	13	1220	28	1220.0	28.0	0.8	
WCSS1_68.FIN2	87.5	2.087	2.063	0.036	0.1919	0.0019	0.3817	1134	12	1131	10	1134	34	1134.0	34.0	0.3	
WCSS1_69.FIN2	96.5	1.182	2.377	0.036	0.2106	0.0027	0.52955	1234	11	1231	14	1234	28	1234.0	28.0	0.2	
WCSS1_70.FIN2	297	3.176	4.051	0.045	0.2942	0.003	0.74131	1643.1	9	1662	15	1612	15	1612.0	15.0	3.1	
WCSS1_71.FIN2	282	1.65	1.109	0.033	0.1205	0.002	0.36977	756	16	733	12	809	59	733.0	12.0	3.0	
WCSS1_71.FIN2	203.3	1.551	1.146	0.025	0.1281	0.0018	0.40971	774	12	777	10	753	43	777.0	10.0	0.4	
WCSS1_72.FIN2	244	2.39	1.658	0.032	0.1659	0.0018	0.28748	990	12	989	10	975	33	975.0	33.0	1.4	
WCSS1_73.FIN2	257	1.242	0.601	0.013	0.07724	0.00094	0.34169	478.5	8.8	479.6	5.7	450	49	479.6	5.7	0.2	
WCSS1_74.FIN2	201.5	1.348	0.999	0.016	0.1155	0.0012	0.42894	702.3	8.2	704.5	7.1	686	33	704.5	7.1	0.3	

Table 3

WCSS1_75.FIN2	98.3	1.075	4.092	0.052	0.2925	0.0027	0.60422	1651	10	1654	14	1638	19	1638.0	19.0	1.0	
WCSS1_76.FIN2	420	4.97	0.519	0.011	0.068	0.0011	0.41188	424.2	7.1	423.8	6.9	422	43	423.8	6.9	0.1	
WCSS1_77.FIN2	131.3	1.807	1.367	0.048	0.1414	0.0027	0.32965	873	20	852	15	911	72	DISC	DISC	6.5	
WCSS1_78.FIN2	82.3	0.862	1.639	0.032	0.1641	0.0023	0.40378	982	12	979	13	978	38	978.0	38.0	0.1	
WCSS1_79.FIN2	349	3.194	1.011	0.014	0.1159	0.001	0.39586	708.4	6.9	707	5.9	694	26	707.0	5.9	0.2	
WCSS1_80.FIN2	186.9	1.568	1.351	0.021	0.1381	0.0013	0.34335	866.8	9.2	833.9	7.5	945	32	833.9	7.5	3.8	
WCSS1_81.FIN2	217	5.86	0.823	0.023	0.0961	0.0014	0.43666	609	13	591.3	8.3	666	54	591.3	8.3	2.9	
WCSS1_82.FIN2	178.7	5.04	1.909	0.033	0.1823	0.0021	0.59946	1082	12	1079	11	1092	26	1092.0	26.0	1.2	
WCSS1_83.FIN2	252	2.479	1.776	0.02	0.1739	0.0013	0.37729	1035.6	7.3	1033.6	7.4	1031	23	1031.0	23.0	0.3	
WCSS1_84.FIN2	141.3	2.711	2.803	0.047	0.2327	0.003	0.48806	1355	12	1348	16	1358	29	1358.0	29.0	0.7	
WCSS1_85.FIN2	69.8	1.818	1.511	0.034	0.1556	0.002	0.41569	932	14	932	11	915	42	915.0	42.0	1.9	
WCSS1_86.FIN2	102.5	1.31	4.095	0.066	0.2919	0.0035	0.71768	1650	13	1650	18	1654	21	1654.0	21.0	0.2	
WCSS1_87.FIN2	149.6	1.731	1.863	0.032	0.1773	0.002	0.40982	1066	12	1052	11	1092	35	1092.0	35.0	3.7	
WCSS1_88.FIN2	69.9	3.53	2.154	0.041	0.1989	0.0027	0.5514	1165	13	1169	15	1154	31	1154.0	31.0	1.3	
WCSS1_89.FIN2	106.8	1.446	0.616	0.018	0.0798	0.0011	0.067058	490	10	494.9	6.3	429	68	494.9	6.3	1.0	
WCSS1_90.FIN2	218	2.689	0.631	0.026	0.07003	0.00091	0.49292	493	15	436.3	5.5	791	81	436.3	5.5	11.5	
WCSS1_91.FIN2	101.2	0.81	0.673	0.016	0.0843	0.00097	0.12941	522.9	9.2	521.6	5.7	517	52	521.6	5.7	0.2	
WCSS1_92.FIN2	278	1.651	1.91	0.022	0.1836	0.0017	0.47918	1083.4	7.7	1086.1	9.5	1071	22	1071.0	22.0	1.4	
WCSS1_93.FIN2	281.1	1.142	6.002	0.075	0.356	0.0044	0.70018	1975	11	1963	21	1985	17	1985.0	17.0	1.1	
WCSS1_94.FIN2	302	0.54	1.989	0.031	0.1876	0.002	0.35959	1111	10	1108	11	1110	28	1110.0	28.0	0.2	
WCSS1_95.FIN2	545.7	2.533	2.209	0.029	0.2058	0.0031	0.57738	1183.5	9.2	1206	16	1136	26	DISC	DISC	6.2	
WCSS1_96.FIN2	170.3	0.797	0.81	0.018	0.0949	0.0011	0.23975	603	9.8	584.3	6.5	661	51	584.3	6.5	3.1	
WCSS1_97.FIN2	174	2.3	0.612	0.013	0.07738	0.00074	0.20609	483.4	8.1	480.4	4.4	471	45	480.4	4.4	0.6	
WCSS1_98.FIN2	138.2	2.075	2.216	0.034	0.2011	0.0022	0.63195	1184	11	1181	12	1185	24	1185.0	24.0	0.3	
WCSS1_99.FIN2	680	1.841	0.4466	0.0085	0.05988	0.00073	0.33961	374.6	5.9	374.8	4.5	365	41	374.8	4.5	0.1	

Table 3

WCSS1_100.FIN2	48.3	0.646	0.804	0.034	0.0972	0.0018	0.2964	594	19	598	11	555	86	598.0	11.0	0.7	
WCSS1_101.FIN2	82.7	2.62	1.556	0.033	0.1579	0.0019	0.30134	951	14	945	11	947	43	947.0	43.0	0.2	
WCSS1_102.FIN2	141.1	1.779	0.509	0.012	0.06719	0.00075	0.27159	417.6	7.6	419.1	4.5	393	50	419.1	4.5	0.4	
WCSS1_103.FIN2	174.6	1.109	6.734	0.066	0.3795	0.0038	0.75382	2075.9	8.7	2073	18	2077	14	2077.0	14.0	0.2	
WCSS1_104.FIN2	366	2.9	0.677	0.017	0.0797	0.0017	0.74865	524	11	494	10	647	37	494.0	10.0	5.7	
WCSS1_105.FIN2	47.04	0.971	4.738	0.088	0.3158	0.0048	0.44986	1770	15	1771	23	1775	31	1775.0	31.0	0.2	
WCSS1_106.FIN2	185	0.879	4.219	0.056	0.297	0.0033	0.51932	1676	11	1676	17	1676	24	1676.0	24.0	0.0	
WCSS1_107.FIN2	594	1.683	0.682	0.01	0.08541	0.00085	0.46964	527.4	6.3	528.3	5.1	517	31	528.3	5.1	0.2	
WCSS1_108.FIN2	417.7	1.762	13.05	0.23	0.5168	0.0083	0.92451	2681	17	2683	36	2678	11	2678.0	11.0	0.2	
WCSS1_109.FIN2	142.6	3.151	1.793	0.032	0.1761	0.002	0.54643	1044	12	1045	11	1032	29	1032.0	29.0	1.3	
WCSS1_110.FIN2	311	0.764	0.564	0.022	0.0722	0.0017	0.57271	453	14	449	10	466	69	449.0	10.0	0.9	
WCSS1_111.FIN2	85.19	1.28	4.526	0.059	0.3087	0.0032	0.41851	1734	11	1734	16	1740	24	1740.0	24.0	0.3	
WCSS1_112.FIN2	130.1	1.254	2.229	0.036	0.2034	0.0021	0.42005	1189	11	1193	11	1183	32	1183.0	32.0	0.8	
WCSS1_113.FIN2	308.3	1.105	0.701	0.013	0.0864	0.00092	0.44281	540	7.9	534.1	5.4	560	37	534.1	5.4	1.1	
WCSS1_114.FIN2	70	1.897	0.453	0.015	0.0599	0.001	0.031781	377	11	375.2	6.1	383	78	375.2	6.1	0.5	
WCSS1_115.FIN2	192	0.3119	0.628	0.023	0.0752	0.0015	0.44604	494	14	467.5	9.1	609	70	467.5	9.1	5.4	
WCSS1_116.FIN2	310	2.84	0.797	0.013	0.09707	0.00081	0.52654	594	7.3	597.1	4.8	576	30	597.1	4.8	0.5	
WCSS1_117.FIN2	237.7	1.152	0.828	0.012	0.10041	0.00081	0.37863	611.8	6.5	616.7	4.8	596	28	616.7	4.8	0.8	
WCSS1_118.FIN2	63.1	7.3	1.594	0.038	0.161	0.0022	0.6185	964	15	962	12	966	39	966.0	39.0	0.4	
WCSS1_119.FIN2	580	21.3	0.926	0.014	0.1065	0.0013	0.4683	665.2	7.5	652.1	7.3	712	31	652.1	7.3	2.0	
WCSS1_120.FIN2	305	1.056	0.5701	0.0086	0.07328	0.00063	0.37148	458.2	5.7	455.9	3.8	463	34	455.9	3.8	0.5	
WCSS1_121.FIN2	135.8	1.508	0.675	0.015	0.08473	0.00089	0.36628	522.3	9.3	524.2	5.3	504	47	524.2	5.3	0.4	
WCSS1_122.FIN2	513	2.494	2	0.02	0.1847	0.0014	0.48894	1115	6.6	1092.4	7.4	1166	17	DISC	DISC	6.3	
WCSS1_123.FIN2	595	24	0.8824	0.0096	0.10502	0.00076	0.46656	642.4	5.3	644.8	4.2	640	21	644.8	4.2	0.4	
WCSS1_124.FIN2	327	1.096	0.4771	0.0079	0.06373	0.00059	0.31668	395.5	5.4	398.2	3.6	376	36	398.2	3.6	0.7	

Table 3

WCSS1_125.FIN2	284	11.8	1.942	0.044	0.1855	0.0029	0.86192	1093	15	1096	16	1091	24	1091.0	24.0	0.5	
WCSS1_126.FIN2	333	2.912	1.833	0.029	0.1796	0.0022	0.80938	1056	10	1064	12	1041	20	1041.0	20.0	2.2	
WCSS1_127.FIN2	214	3.18	1.739	0.043	0.1732	0.0033	0.89773	1021	16	1029	18	1002	28	1002.0	28.0	2.7	
WCSS1_128.FIN2	160	1.633	11.89	0.094	0.4832	0.0039	0.57063	2594.9	7.5	2540	17	2642	12	2642.0	12.0	3.9	
WCSS1_129.FIN2	112.2	1.159	13	0.12	0.5108	0.0044	0.80029	2678.4	8.7	2659	19	2698	12	2698.0	12.0	1.4	
WCSS1_130.FIN2	159.7	0.7613	0.816	0.018	0.0973	0.0011	0.15203	605	10	598.4	6.5	624	51	598.4	6.5	1.1	

Table 3: LSS1 and WCSS1 sample data.

Table 4

Sample Name:								207/235		206/238		207/206		Best age			
Grain #	[U] ppm	U/Th	207/235	2σ error	206/238	2σ error	RHO	Age Ma	2σ error	Age (Ma)	2σ error	Age (Ma)	2σ error	(Ma)	2σ error	% Discordance*	Rim/Core
WCSS2_1.FIN2	254	2.106	1.701	0.031	0.1693	0.0028	0.34449	1008	12	1008	16	1071	43	1071.0	43.0	5.9	
WCSS2_2.FIN2	540	1.72	0.723	0.017	0.0903	0.0012	0.45229	552	10	557.2	6.9	590	43	557.2	6.9	0.9	
WCSS2_3.FIN2	219	1.748	1.979	0.028	0.1872	0.0017	0.31948	1108.5	9.3	1106	9.1	1129	29	1129.0	29.0	2.0	
WCSS2_4.FIN2	88.3	0.669	10.83	0.1	0.4762	0.0042	0.52614	2507.9	9	2510	18	2509	15	2509.0	15.0	0.0	
WCSS2_5.FIN2	19.23	-1.4	0.698	0.05	0.0889	0.0018	0.035156	526	30	549	11	390	140	549.0	11.0	4.4	
WCSS2_6.FIN2	348	0.5219	0.908	0.011	0.10323	0.00079	0.35474	655.5	5.7	633.2	4.6	684	23	633.2	4.6	3.4	
WCSS2_7.FIN2	437	15.1	0.946	0.021	0.1097	0.002	0.30115	675	11	671	11	640	52	671.0	11.0	0.6	Rim
WCSS2_7.FIN2	183.9	0.762	2.124	0.048	0.1836	0.003	0.56397	1155	16	1086	16	1237	35	1237.0	35.0	12.2	Core
WCSS2_8.FIN2	431	5.07	1.211	0.021	0.1187	0.0013	0.68542	804.2	9.9	722.9	7.6	970	26	722.9	7.6	10.1	
WCSS2_9.FIN2	170.9	0.6245	0.784	0.02	0.0925	0.0012	0.34355	587	11	570.2	7.2	580	52	570.2	7.2	2.9	Rim
WCSS2_9.FIN2	120.5	0.861	0.863	0.027	0.0996	0.0017	0.38126	630	15	612	10	613	65	612.0	10.0	2.9	Core
WCSS2_10.FIN2	221.9	1.061	0.883	0.013	0.10206	0.0007	0.23244	641.9	6.9	626.4	4.1	633	32	626.4	4.1	2.4	
WCSS2_11.FIN2	61.7	2.77	10.19	0.14	0.4087	0.0049	0.51926	2450	13	2208	22	2603	21	2603.0	21.0	15.2	
WCSS2_12.FIN2	64.5	1.326	0.734	0.03	0.0892	0.0014	0.24553	555	17	550.6	8.3	513	81	550.6	8.3	0.8	
WCSS2_13.FIN2	174	4.75	0.688	0.013	0.08577	0.00085	0.048526	530.7	8.1	530.4	5.1	494	49	530.4	5.1	0.1	
WCSS2_14.FIN2	66	9.2	0.689	0.042	0.0853	0.0028	0.37978	531	27	527	17	520	130	527.0	17.0	0.8	Rim
WCSS2_14.FIN2	111.1	2.74	2.83	0.11	0.2223	0.005	0.55476	1359	30	1294	27	1459	65	1459.0	65.0	11.3	Core
WCSS2_15.FIN2	30	1.35	2.485	0.082	0.2163	0.0038	0.26479	1268	24	1261	20	1260	63	1260.0	63.0	0.1	
WCSS2_16.FIN2	16.09	1.41	0.751	0.053	0.0909	0.0022	0.19547	553	31	560	13	510	140	560.0	13.0	1.3	
WCSS2_17.FIN2	80.7	0.767	0.79	0.023	0.0956	0.0013	0.49505	588	13	588.3	7.7	584	56	588.3	7.7	0.1	
WCSS2_18.FIN2	100	1.169	1.818	0.043	0.1776	0.0019	0.099279	1052	16	1056	11	1043	50	1043.0	50.0	1.2	
WCSS2_19.FIN2	98.8	0.978	8.68	0.14	0.3726	0.0051	0.72712	2302	15	2040	24	2547	20	2547.0	20.0	19.9	

Table 4

WCSS2_20.FIN2	79.4	1.38	2.083	0.047	0.1964	0.0018	0.20982	1143	16	1155.6	9.7	1103	44	1103.0	44.0	4.8	
WCSS2_21.FIN2	35.3	0.902	1.86	0.053	0.1794	0.0029	0.24897	1063	19	1063	16	1045	62	1045.0	62.0	1.7	
WCSS2_22.FIN2	103.5	1.204	0.865	0.025	0.1023	0.0015	0.37624	631	14	627.8	9	617	59	627.8	9.0	0.5	
WCSS2_23.FIN2	376	1.006	0.583	0.01	0.0752	0.00072	0.37178	465.7	6.6	467.4	4.3	442	37	467.4	4.3	0.4	Rim
WCSS2_23.FIN2	207.2	1.58	0.664	0.026	0.0834	0.0017	0.38004	516	16	516	10	489	80	516.0	10.0	0.0	Core
WCSS2_24.FIN2	359	0.907	0.506	0.012	0.06511	0.00074	0.24777	414.7	8.4	406.6	4.5	438	54	406.6	4.5	2.0	
WCSS2_25.FIN2	82.2	1.195	3.586	0.048	0.2707	0.0026	0.39596	1546	10	1544	13	1541	25	1541.0	25.0	0.2	
WCSS2_26.FIN2	189.3	1.719	2.587	0.056	0.2215	0.0036	0.54919	1296	16	1290	19	1322	32	1322.0	32.0	2.4	
WCSS2_27.FIN2	126.5	0.824	0.584	0.014	0.07487	0.00079	0.18107	465.3	9.1	465.3	4.8	458	55	465.3	4.8	0.0	
WCSS2_28.FIN2	152	1.69	0.889	0.019	0.1047	0.0014	0.10698	645	10	641.9	8.1	659	52	641.9	8.1	0.5	
WCSS2_29.FIN2	202.2	1.528	1.898	0.022	0.1853	0.0017	0.17849	1079.8	7.8	1095.5	9.3	1056	27	1056.0	27.0	3.7	
WCSS2_30.FIN2	134	1.87	1.012	0.037	0.1162	0.0023	0.33278	711	20	708	13	706	70	708.0	13.0	0.4	Rim
WCSS2_30.FIN2	102.2	1.068	1.257	0.038	0.1324	0.0019	0.34469	824	17	801	11	878	61	801.0	11.0	2.8	Core
WCSS2_31.FIN2	66.8	0.625	0.669	0.022	0.08412	0.00094	0.022584	517	14	520.6	5.6	481	75	520.6	5.6	0.7	
WCSS2_32.FIN2	273	2.08	1.876	0.03	0.1806	0.0021	0.47058	1071	11	1070	12	1078	30	1078.0	30.0	0.7	Rim
WCSS2_32.FIN2	78.4	1.814	2.07	0.12	0.1934	0.0044	0.007257	1137	41	1140	24	1110	130	1110.0	130.0	2.7	Core
WCSS2_33.FIN2	215	0.976	1.924	0.024	0.1818	0.0013	0.36459	1088	8.3	1076.9	7.1	1101	23	1101.0	23.0	2.2	
WCSS2_34.FIN2	340.9	3.15	3.341	0.026	0.2568	0.0018	0.55413	1490.7	6.3	1473.1	9.1	1498	13	1498.0	13.0	1.7	
WCSS2_35.FIN2	331	1.681	4.416	0.034	0.3042	0.0021	0.50544	1714.5	6.3	1712	10	1701	14	1701.0	14.0	0.6	
WCSS2_36.FIN2	75.9	0.599	0.739	0.022	0.0898	0.0012	0.23003	559	13	554.3	6.8	542	63	554.3	6.8	0.8	
WCSS2_37.FIN2	107.9	1.291	1.909	0.028	0.1829	0.0015	0.20842	1085.2	9.6	1082.4	8.3	1079	31	1079.0	31.0	0.3	
WCSS2_38.FIN2	131.7	0.693	4.619	0.061	0.3104	0.0034	0.19651	1752	11	1742	17	1766	29	1766.0	29.0	1.4	
WCSS2_39.FIN2	344.4	0.638	0.739	0.014	0.0916	0.00074	0.2666	561.2	8.3	565	4.4	553	41	565.0	4.4	0.7	
WCSS2_40.FIN2	669	12.25	0.7612	0.0095	0.09408	0.00071	0.26532	574.3	5.5	579.6	4.2	578	29	579.6	4.2	0.9	
WCSS2_41.FIN2	230	1.572	1.219	0.043	0.1317	0.0028	0.85473	806	20	797	16	852	44	797.0	16.0	1.1	
WCSS2_42.FIN2	179.2	0.735	0.685	0.015	0.08694	0.00095	0.37401	528.5	9.2	537.4	5.6	512	46	537.4	5.6	1.7	

Table 4

WCSS2_43.FIN2	188	0.418	0.901	0.016	0.10678	0.00094	0.22629	650.7	8.7	654	5.5	651	40	654.0	5.5	0.5	
WCSS2_44.FIN2	122.2	1.785	2.12	0.027	0.1957	0.0013	0.20728	1154.2	8.8	1152	6.9	1163	26	1163.0	26.0	0.9	
WCSS2_45.FIN2	501	1.133	0.94	0.017	0.1096	0.0011	0.38401	672.2	8.9	670.2	6.6	669	36	670.2	6.6	0.3	
WCSS2_46.FIN2	98.5	0.547	0.535	0.03	0.06517	0.00091	0.072595	433	20	407	5.5	500	120	407.0	5.5	6.0	
WCSS2_47.FIN2	116.1	1.172	1.394	0.025	0.1455	0.0013	0.1877	886	10	875.4	7.3	869	37	869.0	37.0	0.7	
WCSS2_48.FIN2	506.3	33.7	0.563	0.0081	0.07058	0.00055	0.29432	453	5.2	439.7	3.3	463	31	439.7	3.3	2.9	
WCSS2_49.FIN2	85.7	0.862	13.89	0.14	0.5109	0.0043	0.56805	2742.2	9.4	2662	19	2762	14	2762.0	14.0	3.6	
WCSS2_50.FIN2	102.6	1.32	2.123	0.03	0.1924	0.0015	0.28426	1155.8	9.4	1134.1	8.2	1143	27	1143.0	27.0	0.8	
WCSS2_51.FIN2	108	0.87	0.771	0.02	0.09334	0.00096	0.12888	579	12	575.2	5.7	591	59	575.2	5.7	0.7	
WCSS2_52.FIN2	417	1.422	0.3721	0.0055	0.05094	0.00043	0.23963	320.9	4.1	320.3	2.6	347	34	320.3	2.6	0.2	
WCSS2_53.FIN2	564	9.35	0.731	0.01	0.09031	0.00083	0.28674	556.8	5.9	557.4	4.9	599	30	557.4	4.9	0.1	
WCSS2_54.FIN2	400	2.61	4.007	0.041	0.2888	0.0022	0.66171	1634.6	8.3	1635	11	1683	14	1683.0	14.0	2.9	
WCSS2_55.FIN2	81.6	1.711	1.284	0.031	0.1366	0.0019	0.20702	836	14	825	11	917	53	825.0	11.0	1.3	
WCSS2_56.FIN2	176.5	0.632	0.401	0.011	0.05523	0.00054	0.099445	341.1	7.8	346.5	3.3	337	59	346.5	3.3	1.6	
WCSS2_57.FIN2	429	1.751	14.31	0.12	0.5268	0.0043	0.7528	2769.5	7.6	2730	18	2817.5	8	2817.5	8.0	3.1	
WCSS2_58.FIN2	649	2.63	0.564	0.014	0.0728	0.0015	0.32587	454.1	9.2	452.9	8.8	472	59	452.9	8.8	0.3	Rim
WCSS2_58.FIN2	291	1.585	2.262	0.026	0.1831	0.002	0.29245	1200	8.1	1084	11	1408	25	1408.0	25.0	23.0	Core
WCSS2_59.FIN2	431	2.014	1.649	0.025	0.1657	0.0018	0.57657	988.4	9.8	988	10	973	26	973.0	26.0	1.5	Rim
WCSS2_59.FIN2	167.9	1.565	1.938	0.041	0.1843	0.0022	0.26569	1093	14	1090	12	1064	43	1064.0	43.0	2.4	Core
WCSS2_60.FIN2	162.8	1.309	1.856	0.03	0.1785	0.0021	0.45181	1064	11	1059	11	1030	30	1030.0	30.0	2.8	
WCSS2_61.FIN2	121.3	1.418	3.262	0.05	0.2422	0.003	0.55738	1470	12	1397	16	1505	25	1505.0	25.0	7.2	
WCSS2_62.FIN2	85.4	1.323	1.713	0.045	0.1631	0.0023	0.21153	1015	17	974	13	1023	55	1023.0	55.0	4.8	
WCSS2_63.FIN2	394	2.05	2.734	0.044	0.2206	0.0031	0.45625	1337	12	1285	16	1354	30	1354.0	30.0	5.1	
WCSS2_64.FIN2	138.8	2.72	1.528	0.027	0.1513	0.0014	0.11568	942	11	908	7.7	953	37	953.0	37.0	4.7	
WCSS2_65.FIN2	188.9	0.4949	5.552	0.045	0.3395	0.0025	0.47318	1908	7	1884	12	1894	14	1894.0	14.0	0.5	
WCSS2_66.FIN2	225.7	1.078	0.588	0.012	0.07536	0.00063	0.1607	468.6	7.7	468.3	3.8	451	47	468.3	3.8	0.1	Rim

Table 4

WCSS2_66.FIN2	142.4	1.342	0.927	0.042	0.1087	0.0029	0.039978	665	22	665	17	640	110	665.0	17.0	0.0	Core
WCSS2_67.FIN2	96.5	0.919	1.321	0.035	0.1359	0.0022	0.55329	851	15	821	13	936	46	821.0	13.0	3.5	
WCSS2_68.FIN2	35.7	0.811	2.419	0.071	0.2164	0.0033	0.34771	1242	21	1262	18	1237	57	1237.0	57.0	2.0	
WCSS2_69.FIN2	618	11.2	1.041	0.04	0.1088	0.0019	0.68062	724	20	666	11	961	60	666.0	11.0	8.0	Rim
WCSS2_69.FIN2	411	4.51	1.273	0.028	0.1328	0.0017	0.011761	833	13	803.7	9.9	958	53	803.7	9.9	3.5	Core
WCSS2_70.FIN2	28.2	0.589	23.61	0.3	0.6613	0.0094	0.71522	3254	12	3269	36	3300	17	3300.0	17.0	0.9	
WCSS2_71.FIN2	77.2	0.4263	1.814	0.035	0.184	0.0018	0.14953	1048	13	1088.3	9.6	1046	41	1046.0	41.0	4.0	
WCSS2_72.FIN2	512	1.552	1.587	0.015	0.1642	0.001	0.22969	964.8	6.1	980.1	5.6	1012	21	1012.0	21.0	3.2	
WCSS2_73.FIN2	57.3	2.683	2.135	0.056	0.2008	0.0026	0.51346	1160	17	1179	14	1182	44	1182.0	44.0	0.3	
WCSS2_74.FIN2	182	1.12	5.241	0.048	0.3393	0.0025	0.58945	1858.2	7.8	1883	12	1887	14	1887.0	14.0	0.2	
WCSS2_75.FIN2	228.6	1.34	1.439	0.023	0.1519	0.0019	0.62152	904	9.6	911	11	926	26	926.0	26.0	1.6	
WCSS2_76.FIN2	232	0.95	0.53	0.015	0.06839	0.00095	0.35873	431	10	426.4	5.7	475	63	426.4	5.7	1.1	
WCSS2_77.FIN2	40.6	3.3	1.925	0.065	0.1828	0.0032	0.23703	1086	22	1082	18	1083	71	1083.0	71.0	0.1	
WCSS2_78.FIN2	74.2	0.921	1.861	0.035	0.1802	0.0019	0.21023	1067	12	1068	10	1063	37	1063.0	37.0	0.5	
WCSS2_79.FIN2	96.2	0.436	1.857	0.032	0.18	0.0016	0.33093	1064	11	1066.8	8.5	1056	34	1056.0	34.0	1.0	
WCSS2_80.FIN2	203	1.041	1.834	0.032	0.1768	0.002	0.026282	1056	11	1049	11	1099	38	1099.0	38.0	4.5	
WCSS2_81.FIN2	128	1.754	1.502	0.038	0.1551	0.0024	0.36276	928	15	929	14	922	53	922.0	53.0	0.8	
WCSS2_82.FIN2	206	0.88	1.8	0.024	0.1762	0.0018	0.52666	1045.5	9.1	1046	10	1056	25	1056.0	25.0	0.9	
WCSS2_83.FIN2	89.8	0.823	1.043	0.026	0.1181	0.0015	0.20955	724	13	719.3	8.9	751	59	719.3	8.9	0.6	
WCSS2_84.FIN2	182.6	0.989	0.511	0.012	0.06714	0.00089	0.20299	417.7	8.2	418.8	5.4	422	54	418.8	5.4	0.3	
WCSS2_85.FIN2	133.5	1.673	1.197	0.023	0.131	0.0015	0.14482	797	11	793.2	8.4	826	42	793.2	8.4	0.5	
WCSS2_86.FIN2	356	0.785	0.6004	0.0096	0.0765	0.00084	0.27165	477	6.1	475.2	5	485	38	475.2	5.0	0.4	
WCSS2_87.FIN2	395	1.997	1.131	0.019	0.1222	0.0011	0.26316	767.6	9	743	6.3	834	35	743.0	6.3	3.2	Rim
WCSS2_87.FIN2	169.4	2.194	1.259	0.032	0.1347	0.0017	0.12048	826	14	814.3	9.9	821	49	814.3	9.9	1.4	Core
WCSS2_88.FIN2	173	1.185	0.81	0.014	0.09739	0.00075	0.12283	601	8.1	599.1	4.4	571	40	599.1	4.4	0.3	
WCSS2_89.FIN2	172.2	0.809	0.69	0.014	0.08513	0.00092	0.037669	531.8	8.4	526.6	5.5	502	52	526.6	5.5	1.0	

Table 4

WCSS2_90.FIN2	242.8	4.31	1.202	0.015	0.1318	0.0011	0.3253	800.4	7	797.7	6.5	758	26	797.7	6.5	0.3	
WCSS2_91.FIN2	506	1.517	0.7606	0.0096	0.09215	0.00091	0.33739	573.9	5.6	568.2	5.4	556	27	568.2	5.4	1.0	
WCSS2_92.FIN2	139	1.598	1.572	0.025	0.1587	0.0015	0.1844	958	9.9	949.3	8.3	947	36	947.0	36.0	0.2	
WCSS2_93.FIN2	99.9	1.388	1.842	0.027	0.178	0.0017	0.26156	1060	9.9	1056	9.3	1048	32	1048.0	32.0	0.8	
WCSS2_94.FIN2	501	1.641	0.562	0.012	0.07262	0.00092	0.1995	452.4	7.7	451.9	5.6	447	50	451.9	5.6	0.1	Rim
WCSS2_94.FIN2	99.8	1.423	1.535	0.053	0.1567	0.0033	0.1335	943	21	938	18	936	76	936.0	76.0	0.2	Core
WCSS2_95.FIN2	315	1.097	0.6	0.011	0.07694	0.00078	0.37562	476.7	6.9	477.8	4.6	472	38	477.8	4.6	0.2	
WCSS2_96.FIN2	89.7	0.557	0.386	0.024	0.0519	0.0012	0.08435	329	18	326	7.3	370	140	326.0	7.3	0.9	
WCSS2_97.FIN2	324	0.7377	2.085	0.019	0.1935	0.0013	0.42687	1143	6.2	1140.2	7	1168	17	1168.0	17.0	2.4	
WCSS2_99.FIN2	325	9.45	1.692	0.029	0.1692	0.0027	0.34998	1005	11	1008	15	1014	37	1014.0	37.0	0.6	Rim
WCSS2_99.FIN2	137.2	1.78	3.03	0.055	0.2462	0.0035	0.21615	1414	14	1419	18	1408	39	1408.0	39.0	0.8	Core
WCSS2_100.FIN2	105.5	0.544	3.986	0.05	0.2859	0.0027	0.34181	1630	10	1621	14	1645	23	1645.0	23.0	1.5	
WCSS2_101.FIN2	174	1.28	1.904	0.032	0.1841	0.0025	0.38077	1081	11	1089	14	1049	35	1049.0	35.0	3.8	
WCSS2_102.FIN2	235.4	2.75	0.791	0.013	0.09545	0.00089	0.21193	590.8	7.1	587.6	5.2	579	36	587.6	5.2	0.5	
WCSS2_103.FIN2	562	2.207	12.67	0.14	0.4916	0.0053	0.70863	2654	10	2577	23	2695	14	2695.0	14.0	4.4	
WCSS2_104.FIN2	247.7	15.6	1.762	0.026	0.1725	0.0019	0.34883	1030.6	9.6	1026	10	1027	31	1027.0	31.0	0.1	
WCSS2_105.FIN2	330	2.79	0.795	0.019	0.0934	0.0016	0.20975	593	11	575.7	9.3	649	58	575.7	9.3	2.9	Rim
WCSS2_105.FIN2	242	3.222	0.864	0.021	0.101	0.0013	0.30502	631	11	620.4	7.4	661	50	620.4	7.4	1.7	Core
WCSS2_106.FIN2	170.6	0.965	3.781	0.078	0.2839	0.0055	0.73283	1586	16	1610	28	1556	27	1556.0	27.0	3.5	
WCSS2_107.FIN2	56.4	0.3113	1.021	0.03	0.1172	0.0016	0.23135	711	15	714.4	9.3	684	65	714.4	9.3	0.5	
WCSS2_108.FIN2	125.5	1.114	0.565	0.014	0.07255	0.00066	0.14586	453.2	9.1	451.5	4	464	55	451.5	4.0	0.4	
WCSS2_109.FIN2	133.4	0.4845	0.658	0.019	0.0846	0.001	0.19739	512	12	523.6	6.1	492	69	523.6	6.1	2.3	
WCSS2_110.FIN2	314	3.98	1.773	0.029	0.1737	0.0021	0.40548	1035	11	1033	11	1079	33	1079.0	33.0	4.3	Rim
WCSS2_110.FIN2	176.9	1.686	2.084	0.048	0.1934	0.0034	0.47751	1143	16	1140	18	1177	42	1177.0	42.0	3.1	Core
WCSS2_111.FIN2	83.5	0.748	0.384	0.014	0.05307	0.00071	0.10143	329	10	333.3	4.3	336	80	333.3	4.3	1.3	
WCSS2_112.FIN2	191	0.972	0.537	0.014	0.07048	0.00078	0.32308	436.4	9.1	439	4.7	462	55	439.0	4.7	0.6	

Table 4

WCSS2_113.FIN2	200	0.969	0.411	0.01	0.0564	0.00058	0.025668	348.5	7.2	353.7	3.5	358	56	353.7	3.5	1.5	
WCSS2_114.FIN2	304	0.56	0.714	0.012	0.08904	0.00077	0.26871	546.7	7.2	549.8	4.6	568	37	549.8	4.6	0.6	
WCSS2_115.FIN2	209	0.891	1.805	0.022	0.1754	0.0015	0.32528	1047.3	7.8	1041.7	8.2	1094	24	1094.0	24.0	4.8	
WCSS2_116.FIN2	20.99	1.209	2.18	0.094	0.1817	0.0039	0.36409	1163	30	1075	21	1353	80	1353.0	80.0	20.5	
WCSS2_117.FIN2	439	1.654	0.5185	0.0076	0.0676	0.00057	0.16809	423.7	5.1	421.6	3.4	460	32	421.6	3.4	0.5	
WCSS2_118.FIN2	348	2.166	3.174	0.038	0.256	0.0022	0.49058	1449.9	9.2	1469	11	1445	20	1445.0	20.0	1.7	
WCSS2_119.FIN2	30.53	0.904	1.824	0.067	0.1642	0.003	0.12797	1049	24	980	16	1211	78	1211.0	78.0	19.1	
WCSS2_120.FIN2	148.4	2.859	1.309	0.022	0.1402	0.0011	0.19347	848.3	9.5	846	6.4	858	36	846.0	6.4	0.3	
WCSS2_121.FIN2	83	2.51	3.619	0.061	0.2725	0.0029	0.40269	1555	13	1553	15	1565	29	1565.0	29.0	0.8	
WCSS2_122.FIN2	465	5.14	0.679	0.013	0.08427	0.00091	0.3516	525.9	7.7	522.6	5.7	545	39	522.6	5.7	0.6	
WCSS2_123.FIN2	120.6	0.646	0.619	0.015	0.07778	0.00089	0.19561	487.4	9.4	482.8	5.3	502	55	482.8	5.3	0.9	
WCSS2_124.FIN2	290.4	0.919	0.707	0.013	0.08753	0.00077	0.26313	542.1	7.5	540.9	4.6	538	40	540.9	4.6	0.2	
WCSS2_125.FIN2	427	1.438	0.9031	0.009	0.10716	0.00062	0.09962	653	4.8	656.2	3.6	637	25	656.2	3.6	0.5	
WCSS2_126.FIN2	94.9	1.331	4.632	0.062	0.3137	0.0024	0.43024	1753	11	1759	12	1758	22	1758.0	22.0	0.1	
WCSS2_127.FIN2	131.5	0.591	4.826	0.068	0.2988	0.0034	0.69287	1787	12	1685	17	1922	19	1922.0	19.0	12.3	
WCSS2_128.FIN2	76.3	1.005	1.822	0.038	0.1746	0.0021	0.284	1051	14	1037	11	1095	44	1095.0	44.0	5.3	
WCSS2_129.FIN2	209.9	3.53	0.946	0.016	0.11158	0.00082	0.05639	675.2	8.2	681.8	4.8	672	39	681.8	4.8	1.0	
WCSS2_130.FIN2	128.4	2.034	0.756	0.03	0.0877	0.0017	0.40916	570	17	542	10	687	76	542.0	10.0	4.9	
WCSS2_131.FIN2	73.5	1.101	2.108	0.039	0.1952	0.0019	0.25574	1150	13	1149	10	1157	38	1157.0	38.0	0.7	
WCSS2_132.FIN2	201.3	1.032	6.69	0.065	0.3726	0.0032	0.64248	2071.1	8.5	2041	15	2109	13	2109.0	13.0	3.2	
WCSS2_133.FIN2	117.8	0.735	0.391	0.012	0.054	0.0007	0.24054	334.1	8.6	339	4.3	306	60	339.0	4.3	1.5	
WCSS2_134.FIN2	86.4	1.275	2.149	0.047	0.1998	0.0024	0.14799	1163	15	1174	13	1135	47	1135.0	47.0	3.4	
WCSS2_135.FIN2	106.9	1.633	0.407	0.013	0.05394	0.00074	0.07829	345.3	9.7	338.6	4.5	363	75	338.6	4.5	1.9	
WCSS2_136.FIN2	223	1.333	0.723	0.015	0.08942	0.00088	0.21203	551.1	8.8	552.1	5.2	536	45	552.1	5.2	0.2	
WCSS2_137.FIN2	226.8	1.18	3.494	0.042	0.2664	0.0023	0.4419	1525	9.6	1522	12	1515	22	1515.0	22.0	0.5	
WCSS2_138.FIN2	649	0.658	1.972	0.035	0.1871	0.0031	0.67843	1105	12	1105	17	1092	30	1092.0	30.0	1.2	

Table 4

WCSS2_139.FIN2	194.5	1.406	0.592	0.012	0.07536	0.00062	0.23667	471.2	7.5	468.3	3.7	468	43	468.3	3.7	0.6	
WCSS2_140.FIN2	666	19.8	0.644	0.016	0.0727	0.0015	0.44971	504	10	452.4	8.8	744	53	452.4	8.8	10.2	Rim
WCSS2_140.FIN2	209.5	3.1	0.825	0.025	0.098	0.0016	0.23211	609	14	602.8	9.5	613	66	602.8	9.5	1.0	Core
WCSS2_141.FIN2	98.5	0.7175	3.923	0.071	0.2667	0.0032	0.2917	1617	15	1524	16	1732	34	1732.0	34.0	12.0	Rim
WCSS2_141.FIN2	89	0.7	4.5	0.11	0.2951	0.0057	0.42598	1729	20	1667	29	1789	43	1789.0	43.0	6.8	Core
WCSS2_142.FIN2	67.4	0.572	5.89	0.1	0.3548	0.0042	0.28037	1961	16	1957	20	1944	33	1944.0	33.0	0.7	
WCSS2_143.FIN2	163.3	2.17	1.753	0.031	0.1725	0.0019	0.32439	1027	11	1026	11	998	35	998.0	35.0	2.8	
WCSS2_144.FIN2	88.5	1.17	2.082	0.035	0.1934	0.0017	0.39697	1142	11	1140.6	9.6	1111	32	1111.0	32.0	2.7	
WCSS2_145.FIN2	299.8	0.916	0.7005	0.009	0.08699	0.00061	0.24068	538.6	5.4	537.7	3.6	505	29	537.7	3.6	0.2	
WCSS2_146.FIN2	175	1.24	0.48	0.012	0.06317	0.00072	0.20599	399.2	8.8	394.8	4.4	391	57	394.8	4.4	1.1	

Table 4: WCSS2 sample data.

Table 5

Sample Name:								207/235		206/238		207/206		Best age			
Grain #	[U] ppm	U/Th	207/235	2σ error	206/238	2σ error	RHO	Age Ma	2σ error	Age (Ma)	2σ error	Age (Ma)	2σ error	(Ma)	2σ error	% Discordance *	Rim/Core
VSS4_1.FIN2	22.99	0.836	2.912	0.08	0.0716	0.0015	0.17886	1379	21	445.3	9	3425	51	DISC	DISC	67.7	
VSS4_2.FIN2	210	4.08	0.625	0.013	0.0789	0.0011	0.51136	492.2	8.1	489.2	6.4	492	40	489.2	6.4	0.6	
VSS4_3.FIN2	36.8	0.775	1.864	0.05	0.1788	0.0026	0.33491	1063	18	1060	14	1051	55	1051.0	55.0	0.9	
VSS4_4.FIN2	196.3	1.14	0.778	0.013	0.0929	0.001	0.28818	583.2	7.6	572.5	6	606	37	572.5	6.0	1.8	
VSS4_5.FIN2	520	1.117	0.425	0.01	0.0539	0.00087	0.37847	359.2	7.3	338.4	5.3	486	50	338.4	5.3	5.8	
VSS4_6.FIN2	227.1	1.594	0.48	0.011	0.06394	0.00072	0.37771	397.1	7.3	399.5	4.3	372	46	399.5	4.3	0.6	
VSS4_7.FIN2	33.79	1.187	2.519	0.061	0.2166	0.0029	0.27364	1276	18	1263	15	1285	49	1285.0	49.0	1.7	
VSS4_8.FIN2	147	0.5265	2.33	0.032	0.2067	0.0023	0.31781	1220.1	9.8	1211	12	1233	29	1233.0	29.0	1.8	
VSS4_9.FIN2	290	9.2	2.004	0.065	0.1859	0.0044	0.66849	1115	22	1098	24	1144	49	1144.0	49.0	4.0	Rim
VSS4_9.FIN2	235.1	0.741	2.824	0.043	0.2315	0.003	0.59657	1361	12	1345	15	1383	25	1383.0	25.0	2.7	Core
VSS4_10.FIN2	166	0.663	5.005	0.054	0.3264	0.0027	0.56328	1818.6	9.2	1820	13	1810	17	1810.0	17.0	0.6	
VSS4_11.FIN2	156.9	0.854	0.927	0.024	0.0822	0.002	0.57599	663	13	510	12	1227	49	DISC	DISC	23.1	
VSS4_12.FIN2	544	2.46	0.489	0.018	0.0632	0.0011	0.27736	408	14	395.1	6.7	472	89	395.1	6.7	3.2	Rim
VSS4_12.FIN2	284.3	1.536	0.494	0.014	0.0617	0.001	0.28142	406.8	9.4	385.9	6.2	513	61	385.9	6.2	5.1	Core
VSS4_13.FIN2	543	1.827	0.5538	0.008	0.06047	0.00089	0.029018	447.1	5.2	378.4	5.4	817	43	DISC	DISC	15.4	
VSS4_14.FIN2	742	6.68	0.658	0.03	0.0713	0.0019	0.83104	510	18	444	11	808	58	444.0	11.0	12.9	
VSS4_15.FIN2	853	-70	1.086	0.036	0.1209	0.0029	0.70692	746	17	736	17	776	51	736.0	17.0	1.3	Rim
VSS4_15.FIN2	431	1.201	2.197	0.034	0.2028	0.003	0.6707	1182	12	1190	16	1161	26	1161.0	26.0	2.5	Core
VSS4_16.FIN2	544.4	1.878	1.815	0.018	0.1692	0.0012	0.35972	1050.5	6.5	1007.4	6.6	1146	20	1146.0	20.0	12.1	Rim
VSS4_16.FIN2	388.2	2.392	2.099	0.036	0.1907	0.0024	0.53149	1148	12	1125	13	1185	30	1185.0	30.0	5.1	Core
VSS4_17.FIN2	279	1.609	3.338	0.04	0.2586	0.0021	0.76435	1488.9	9.4	1482	11	1499	19	1499.0	19.0	1.1	

Table 5

VSS4_18.FIN2	163.3	2.107	0.465	0.011	0.06193	0.00065	0.044139	386.4	7.7	387.3	3.9	375	56	387.3	3.9	0.2	
VSS4_19.FIN2	369	1.273	0.965	0.016	0.1131	0.0011	0.22448	685.3	8.1	690.6	6.3	661	37	690.6	6.3	0.8	
VSS4_20.FIN2	212.8	1.192	2.266	0.041	0.2061	0.0026	0.81331	1202	12	1208	14	1188	20	1188.0	20.0	1.7	
VSS4_21.FIN2	127	1.022	0.817	0.019	0.09796	0.00095	0.16605	606	10	602.4	5.6	606	50	602.4	5.6	0.6	
VSS4_22.FIN2	519	3.32	1.785	0.036	0.1671	0.0025	0.28291	1039	13	996	14	1136	42	1136.0	42.0	12.3	
VSS4_23.FIN2	553	0.861	0.4451	0.0079	0.05891	0.00045	0.14119	373.4	5.5	369	2.7	395	40	369.0	2.7	1.2	
VSS4_24.FIN2	259	0.657	0.588	0.014	0.07507	0.00071	0.35039	470.3	9.3	466.6	4.3	483	50	466.6	4.3	0.8	
VSS4_25.FIN2	526	1.078	0.517	0.012	0.06571	0.0007	0.1885	423.8	7.5	410.3	4.2	496	61	410.3	4.2	3.2	
VSS4_26.FIN2	37.3	0.953	2.394	0.061	0.207	0.0026	0.28968	1236	18	1212	14	1269	50	1269.0	50.0	4.5	
VSS4_27.FIN2	149	10.9	1.978	0.049	0.1928	0.0033	0.62135	1107	17	1136	18	1057	49	1057.0	49.0	7.5	Rim
VSS4_27.FIN2	219	1.229	3.057	0.046	0.2498	0.0026	0.54928	1421	12	1437	13	1401	25	1401.0	25.0	2.6	Core
VSS4_28.FIN2	236	1.122	0.583	0.012	0.07297	0.00065	0.29062	465.5	7.6	454	3.9	512	43	454.0	3.9	2.5	
VSS4_29.FIN2	155.8	1.494	2.217	0.029	0.2022	0.0016	0.26532	1184.8	9	1186.8	8.4	1191	27	1191.0	27.0	0.4	
VSS4_30.FIN2	129	1.53	0.604	0.017	0.07809	0.00091	0.13866	478	11	484.6	5.4	435	62	484.6	5.4	1.4	
VSS4_31.FIN2	122.4	0.921	0.841	0.018	0.1013	0.0011	0.42685	618	10	622.1	6.2	603	46	622.1	6.2	0.7	
VSS4_32.FIN2	734	19	0.766	0.014	0.0937	0.0014	0.46368	577.1	8.2	577.6	8.2	583	38	577.6	8.2	0.1	Rim
VSS4_32.FIN2	358	0.837	2.536	0.049	0.1872	0.0029	0.65631	1281	14	1106	16	1589	30	1589.0	30.0	30.4	Core
VSS4_33.FIN2	133	0.728	0.589	0.015	0.0756	0.00091	0.3415	468.7	9.8	469.7	5.5	453	54	469.7	5.5	0.2	
VSS4_34.FIN2	510	1.398	0.4335	0.0087	0.05785	0.00095	0.36177	365.2	6.1	362.5	5.8	391	47	362.5	5.8	0.7	
VSS4_35.FIN2	265.3	0.2914	0.886	0.016	0.1055	0.0011	0.40492	644.9	8.1	646.4	6.6	645	35	646.4	6.6	0.2	
VSS4_36.FIN2	174.1	1.547	1.869	0.027	0.1818	0.0017	0.29391	1068.7	9.6	1076.8	9.2	1050	31	1050.0	31.0	2.6	
VSS4_37.FIN2	169.8	0.603	0.526	0.012	0.06867	0.00075	0.30901	428.1	7.8	428.1	4.5	422	47	428.1	4.5	0.0	
VSS4_38.FIN2	701	2.106	3.147	0.03	0.2401	0.0033	0.66905	1443.6	7.4	1387	17	1535	19	1535.0	19.0	9.6	
VSS4_39.FIN2	69.4	1.32	2.965	0.055	0.2398	0.0034	0.48821	1396	14	1385	17	1430	36	1430.0	36.0	3.1	
VSS4_40.FIN2	69.4	2.42	6	0.11	0.3545	0.0054	0.68434	1974	17	1954	26	2010	24	2010.0	24.0	2.8	

Table 5

VSS4_41.FIN2	341	1.23	0.4553	0.0079	0.06092	0.0005	0.20273	380.4	5.6	381.2	3	377	38	381.2	3.0	0.2	
VSS4_42.FIN2	257.6	1.428	0.4247	0.0097	0.05663	0.00077	0.45098	358.6	6.9	355	4.7	384	47	355.0	4.7	1.0	
VSS4_43.FIN2	234	1.264	0.863	0.014	0.1051	0.0013	0.40373	630.6	7.5	643.8	7.9	598	37	643.8	7.9	2.1	
VSS4_44.FIN2	235	0.884	0.826	0.017	0.0954	0.001	0.2659	609.8	9.5	587.1	5.9	693	45	587.1	5.9	3.7	
VSS4_45.FIN2	234.6	0.792	1.658	0.029	0.1647	0.0017	0.15072	991	11	982.5	9.4	1013	38	1013.0	38.0	3.0	
VSS4_46.FIN2	296.1	7.18	0.4981	0.0099	0.06464	0.0008	0.24121	409.7	6.7	403.7	4.9	432	47	403.7	4.9	1.5	
VSS4_47.FIN2	91.7	1.83	1.551	0.053	0.1611	0.0038	0.32595	948	21	963	21	921	73	921.0	73.0	4.6	Rim
VSS4_47.FIN2	121.8	0.644	3.924	0.095	0.2816	0.0047	0.65501	1616	19	1599	24	1641	33	1641.0	33.0	2.6	Core
VSS4_48.FIN2	258	1.552	3	0.046	0.2459	0.0032	0.55397	1406	12	1417	17	1400	22	1400.0	22.0	1.2	
VSS4_49.FIN2	224.6	1.563	0.514	0.012	0.06447	0.00066	0.023637	420.3	8.2	402.7	4	505	59	402.7	4.0	4.2	
VSS4_50.FIN2	205.5	0.3489	1.775	0.02	0.1746	0.0015	0.43059	1035.5	7.5	1037.2	8.5	1037	23	1037.0	23.0	0.0	
VSS4_51.FIN2	307	2.128	1.761	0.022	0.1748	0.0015	0.54522	1030.2	8.1	1038.1	8.4	1019	22	1019.0	22.0	1.9	
VSS4_52.FIN2	406	3.48	0.97	0.012	0.11376	0.00087	0.5092	688	6.3	694.5	5	669	23	694.5	5.0	0.9	
VSS4_53.FIN2	348	10.82	1.935	0.021	0.1843	0.0016	0.46869	1092.3	7.4	1090.2	8.5	1100	21	1100.0	21.0	0.9	
VSS4_54.FIN2	111.4	2.819	2.719	0.036	0.232	0.002	0.29296	1332.1	9.9	1345	10	1314	27	1314.0	27.0	2.4	
VSS4_55.FIN2	189	1.165	2.535	0.03	0.2231	0.0025	0.54985	1281.2	8.5	1298	13	1261	21	1261.0	21.0	2.9	
VSS4_56.FIN2	118	1.745	2.196	0.033	0.2	0.0019	0.21318	1178	10	1175	10	1192	31	1192.0	31.0	1.4	
VSS4_57.FIN2	242	3.31	2.753	0.037	0.2327	0.0022	0.48787	1342	10	1348	12	1337	24	1337.0	24.0	0.8	
VSS4_58.FIN2	198	1.012	0.528	0.018	0.0683	0.0012	0.11702	430	12	425.9	7	454	78	425.9	7.0	1.0	
VSS4_59.FIN2	405	1.965	0.614	0.016	0.0694	0.0014	0.54888	485	10	432.4	8.4	754	47	432.4	8.4	10.8	
VSS4_60.FIN2	726	1.361	0.874	0.017	0.1016	0.0013	0.40191	637.1	9	623.7	7.7	690	39	623.7	7.7	2.1	
VSS4_61.FIN2	211	1.582	2.989	0.071	0.2431	0.0047	0.91087	1401	18	1401	25	1406	18	1406.0	18.0	0.4	
VSS4_62.FIN2	376	3.493	1.857	0.044	0.1536	0.0038	0.91108	1062	16	920	21	1379	20	1379.0	20.0	33.3	
VSS4_63.FIN2	92.3	0.44	1.77	0.031	0.1748	0.0016	0.31032	1034	12	1038.2	8.6	1025	34	1025.0	34.0	1.3	
VSS4_64.FIN2	365	0.545	0.3953	0.0076	0.05248	0.00062	0.043006	337.8	5.5	329.7	3.8	397	50	329.7	3.8	2.4	

Table 5

VSS4_65.FIN2	90.1	1.92	1.704	0.03	0.1699	0.0019	0.3659	1009	11	1011	10	998	35	998.0	35.0	1.3	
VSS4_66.FIN2	103	2.097	1.923	0.05	0.1768	0.0029	0.35401	1087	18	1049	16	1158	49	1158.0	49.0	9.4	
VSS4_67.FIN2	142.6	0.868	0.761	0.016	0.0902	0.0011	0.17578	573.1	9.2	556.8	6.3	637	47	556.8	6.3	2.8	
VSS4_68.FIN2	482	0.65	0.91	0.011	0.10698	0.00098	0.46666	656.3	5.7	655.1	5.7	662	24	655.1	5.7	0.2	
VSS4_69.FIN2	121.2	0.448	0.531	0.019	0.0681	0.0012	0.18272	430	13	424.3	7	461	80	424.3	7.0	1.3	
VSS4_70.FIN2	156	0.77	0.85	0.016	0.1022	0.0011	0.3001	624.3	8.8	627.2	6.4	617	39	627.2	6.4	0.5	
VSS4_71.FIN2	439	0.6563	3.885	0.05	0.2731	0.0035	0.73898	1609	11	1556	18	1685	17	1685.0	17.0	7.7	
VSS4_72.FIN2	627	0.924	0.374	0.012	0.04966	0.00084	0.19935	322	8.6	312.4	5.1	392	70	312.4	5.1	3.0	
VSS4_73.FIN2	105.9	2.18	3.586	0.068	0.2712	0.0036	0.41573	1545	15	1546	18	1544	34	1544.0	34.0	0.1	
VSS4_74.FIN2	155.9	1.681	1.192	0.058	0.1277	0.0026	0.17792	795	27	774	15	850	110	774.0	15.0	2.6	
VSS4_75.FIN2	147.7	1.555	1.841	0.027	0.1793	0.0015	0.32701	1058.4	9.8	1063.1	8	1048	30	1048.0	30.0	1.4	
VSS4_76.FIN2	301.8	4.58	0.663	0.012	0.08287	0.00092	0.48471	515.5	7.1	513.2	5.5	531	34	513.2	5.5	0.4	
VSS4_77.FIN2	179.3	1.22	2.391	0.027	0.2107	0.0019	0.47161	1238.6	8.2	1232	10	1255	22	1255.0	22.0	1.8	
VSS4_78.FIN2	282.1	0.634	0.412	0.021	0.0537	0.0012	0.23748	350	15	336.9	7.6	420	110	336.9	7.6	3.7	
VSS4_79.FIN2	152.3	1.074	0.651	0.015	0.08166	0.00093	0.17921	507.8	9.1	505.9	5.5	506	52	505.9	5.5	0.4	
VSS4_80.FIN2	440	23.2	0.824	0.014	0.0998	0.0012	0.5754	609.3	7.9	614.3	6.8	595	31	614.3	6.8	0.8	
VSS4_81.FIN2	137.4	1.895	3.011	0.052	0.2428	0.003	0.69999	1407	13	1401	15	1426	23	1426.0	23.0	1.8	
VSS4_82.FIN2	524	0.838	0.523	0.016	0.0679	0.0013	0.31737	427	11	423.3	7.7	450	72	423.3	7.7	0.9	
VSS4_83.FIN2	67	0.778	5.39	0.076	0.3411	0.0035	0.42017	1882	12	1891	17	1880	25	1880.0	25.0	0.6	
VSS4_84.FIN2	26.19	0.587	1.754	0.076	0.1738	0.0047	0.323	1019	28	1032	26	983	87	983.0	87.0	5.0	
VSS4_85.FIN2	335	1.357	2.105	0.064	0.155	0.0055	0.89401	1143	21	926	31	1623	28	1623.0	28.0	42.9	
VSS4_86.FIN2	69.8	0.602	13.09	0.15	0.5043	0.005	0.65417	2685	11	2631	22	2739	17	2739.0	17.0	3.9	
VSS4_87.FIN2	232.7	2.443	2.073	0.033	0.1847	0.0022	0.66474	1138	11	1092	12	1236	23	1236.0	23.0	11.7	
VSS4_88.FIN2	98.7	0.918	1.834	0.029	0.1786	0.0018	0.31056	1056	10	1059.2	9.6	1058	32	1058.0	32.0	0.1	
VSS4_89.FIN2	49.71	0.808	3.387	0.073	0.273	0.0042	0.55931	1497	17	1558	21	1438	37	1438.0	37.0	8.3	

Table 5

VSS4_90.FIN2	63.3	1.296	1.679	0.039	0.1675	0.002	0.30456	996	15	998	11	1002	44	1002.0	44.0	0.4	
VSS4_91.FIN2	132.9	14.5	1.659	0.028	0.1648	0.0021	0.47739	991	11	983	11	1019	32	1019.0	32.0	3.5	
VSS4_92.FIN2	52.3	0.4688	1.82	0.047	0.1772	0.003	0.55158	1050	17	1051	16	1060	44	1060.0	44.0	0.8	
VSS4_93.FIN2	39.2	1.368	2.038	0.049	0.1903	0.0028	0.39331	1123	16	1122	15	1129	45	1129.0	45.0	0.6	
VSS4_94.FIN2	58.19	1.275	1.865	0.046	0.1843	0.0026	0.33719	1065	16	1090	14	1019	50	1019.0	50.0	7.0	
VSS4_95.FIN2	146.6	0.983	0.741	0.017	0.0897	0.0012	0.16896	561.4	9.8	553.9	6.8	598	53	553.9	6.8	1.3	
VSS4_96.FIN2	329	10.9	0.783	0.047	0.0861	0.0031	0.84452	586	27	533	18	810	110	533.0	18.0	9.0	Rim
VSS4_96.FIN2	122.5	1.747	1.779	0.037	0.1745	0.0021	0.25633	1036	13	1036	11	1042	42	1042.0	42.0	0.6	Core
VSS4_97.FIN2	19.91	0.973	1.581	0.068	0.1493	0.0048	0.4139	955	28	895	27	1122	89	1122.0	89.0	20.2	
VSS4_98.FIN2	44.2	1.499	3.957	0.086	0.2794	0.0049	0.63403	1620	18	1587	25	1686	35	1686.0	35.0	5.9	
VSS4_99.FIN2	214	0.844	13.31	0.17	0.5199	0.0067	0.79241	2700	13	2697	28	2716	15	2716.0	15.0	0.7	
VSS4_100.FIN2	169.6	0.999	0.75	0.014	0.09295	0.0009	0.19029	567	8	572.9	5.3	552	43	572.9	5.3	1.0	
VSS4_101.FIN2	330	2.133	4.371	0.043	0.3029	0.0023	0.56697	1705.6	8.1	1705	11	1719	16	1719.0	16.0	0.8	
VSS4_102.FIN2	86	0.898	3.425	0.048	0.2631	0.0022	0.39873	1508	11	1505	11	1524	24	1524.0	24.0	1.2	
VSS4_103.FIN2	598	1.079	0.821	0.019	0.095	0.0015	0.52866	608	11	584.8	8.8	705	44	584.8	8.8	3.8	
VSS4_104.FIN2	55.9	0.3524	0.719	0.026	0.081	0.0012	0.3312	547	16	502.1	7.2	738	76	502.1	7.2	8.2	
VSS4_105.FIN2	268	2.82	0.5117	0.0088	0.06685	0.00053	0.054567	419	5.9	417.1	3.2	431	41	417.1	3.2	0.5	
VSS4_106.FIN2	191.1	1.001	0.783	0.017	0.09411	0.00084	0.050335	585.7	9.4	579.7	4.9	607	49	579.7	4.9	1.0	
VSS4_107.FIN2	1093	4.6	1.323	0.019	0.1282	0.0032	0.67282	855.9	8.1	778	18	1078	38	778.0	18.0	9.1	Rim
VSS4_107.FIN2	118.5	-13.6	1.963	0.04	0.1916	0.0025	0.5375	1101	14	1130	13	1056	34	1056.0	34.0	7.0	Core
VSS4_108.FIN2	272	1.175	0.3933	0.0089	0.05271	0.00055	0.16649	336	6.5	331.1	3.3	376	51	331.1	3.3	1.5	
VSS4_109.FIN2	389	3.56	1.449	0.092	0.1401	0.0068	0.98681	880	41	841	39	985	47	841.0	39.0	4.4	
VSS4_110.FIN2	606	0.981	0.907	0.018	0.0759	0.0016	0.55702	654.8	9.8	471.7	9.6	1363	35	DISC	DISC	28.0	
VSS4_111.FIN2	796	1.04	0.3476	0.009	0.04703	0.00094	0.2441	302.8	6.7	296.3	5.8	365	61	296.3	5.8	2.1	Rim
VSS4_111.FIN2	260	1.527	1.107	0.032	0.1015	0.0018	0.55972	759	17	623	11	1185	51	DISC	DISC	17.9	Core

Table 5

VSS4_112.FIN2	81.2	0.799	6.184	0.072	0.3673	0.003	0.50614	2001.6	9.8	2016	14	1992	18	1992.0	18.0	1.2	
VSS4_113.FIN2	161.8	0.694	0.813	0.015	0.09584	0.0009	0.16159	603.1	8.2	589.9	5.3	649	41	589.9	5.3	2.2	
VSS4_114.FIN2	135	1.756	4.406	0.046	0.3054	0.0025	0.52096	1713.5	9	1718	12	1726	19	1726.0	19.0	0.5	
VSS4_115.FIN2	604	15.8	0.9021	0.0097	0.10756	0.00066	0.22806	652.4	5.2	658.5	3.8	638	24	658.5	3.8	0.9	
VSS4_116.FIN2	307.1	1.363	0.4943	0.0088	0.06458	0.00055	0.1865	408	6.1	403.4	3.4	427	40	403.4	3.4	1.1	
VSS4_117.FIN2	1300	6.95	1.74	0.043	0.1725	0.0038	0.68623	1023	16	1026	21	1027	38	1027.0	38.0	0.1	Rim
VSS4_117.FIN2	161.6	1.099	2.263	0.047	0.2114	0.0023	0.43355	1200	15	1236	12	1137	38	1137.0	38.0	8.7	Core
VSS4_118.FIN2	423	1.316	0.6474	0.0096	0.08183	0.00065	0.26694	506.4	5.9	507	3.9	523	33	507.0	3.9	0.1	
VSS4_119.FIN2	566	3.04	0.39	0.019	0.0526	0.0011	0.24359	334	14	330.7	6.6	360	110	330.7	6.6	1.0	Rim
VSS4_119.FIN2	173.5	0.527	0.432	0.028	0.0584	0.0015	0.0025813	364	20	365.7	9.4	360	160	365.7	9.4	0.5	Core
VSS4_120.FIN2	40.1	1.286	1.841	0.064	0.1786	0.0029	0.4836	1055	23	1059	16	1045	62	1045.0	62.0	1.3	
VSS4_121.FIN2	299.2	1.162	0.541	0.013	0.0708	0.00064	0.22802	438.5	8.7	441	3.9	423	53	441.0	3.9	0.6	
VSS4_122.FIN2	131.3	0.3383	0.907	0.03	0.1	0.0018	0.26626	653	16	614	11	781	68	614.0	11.0	6.0	
VSS4_123.FIN2	72.1	1.015	4.135	0.068	0.296	0.0031	0.48651	1661	13	1671	15	1652	26	1652.0	26.0	1.2	
VSS4_124.FIN2	138	0.519	5.819	0.079	0.3523	0.004	0.85204	1949	12	1944	20	1962	16	1962.0	16.0	0.9	
VSS4_125.FIN2	347	0.758	0.375	0.016	0.0508	0.0011	0.1767	323	12	319.6	6.7	350	100	319.6	6.7	1.1	
VSS4_126.FIN2	69.1	0.955	0.765	0.023	0.0934	0.0013	0.044016	576	14	575.4	7.7	562	73	575.4	7.7	0.1	
VSS4_127.FIN2	224	0.868	1.936	0.024	0.1748	0.0013	0.35527	1092.6	8.3	1038.2	7.4	1204	24	1204.0	24.0	13.8	
VSS4_128.FIN2	213.6	2.118	3.326	0.063	0.2599	0.0039	0.78679	1486	15	1489	20	1494	27	1494.0	27.0	0.3	
VSS4_129.FIN2	45.2	0.711	0.738	0.028	0.0922	0.0014	0.26516	563	16	568.3	8.2	520	77	568.3	8.2	0.9	
VSS4_130.FIN2	432	26	0.467	0.021	0.0619	0.0018	0.33572	388	14	387	11	398	95	387.0	11.0	0.3	Rim
VSS4_130.FIN2	450	6.51	0.911	0.02	0.098	0.0016	0.39647	657	10	602.4	9.5	861	49	602.4	9.5	8.3	Core
VSS4_131.FIN2	209.2	1.601	0.4917	0.0098	0.06515	0.00096	0.24621	405.5	6.7	406.8	5.8	406	50	406.8	5.8	0.3	
VSS4_132.FIN2	362	1.629	0.625	0.027	0.0636	0.0038	0.40509	492	17	398	23	970	120	DISC	DISC	19.1	Rim
VSS4_132.FIN2	353.5	0.991	1.681	0.031	0.1623	0.0026	0.71682	1001	12	969	15	1068	26	1068.0	26.0	9.3	Core

Table 5

VSS4_133.FIN2	268.5	2.947	0.5146	0.0085	0.06801	0.00065	0.2803	421	5.7	424.1	3.9	404	39	424.1	3.9	0.7	
VSS4_134.FIN2	647	6.82	0.3445	0.0079	0.04753	0.00076	0.33019	300.3	6	299.3	4.6	308	52	299.3	4.6	0.3	
VSS4_135.FIN2	558	1.5	2.264	0.034	0.2061	0.0033	0.9323	1199	11	1207	18	1204	21	1204.0	21.0	0.2	
VSS4_136.FIN2	275.5	1.45	2.841	0.04	0.232	0.0024	0.53629	1366	11	1345	12	1398	24	1398.0	24.0	3.8	
VSS4_137.FIN2	71.8	0.2681	1.747	0.058	0.1691	0.0029	0.27012	1022	21	1007	16	1042	66	1042.0	66.0	3.4	
VSS4_138.FIN2	378	0.5962	1.737	0.025	0.1679	0.0019	0.68986	1021.3	9.3	1001	11	1068	22	1068.0	22.0	6.3	
VSS4_139.FIN2	199.7	2.407	0.836	0.015	0.1018	0.0011	0.35535	615.6	8.4	624.8	6.6	575	39	624.8	6.6	1.5	
VSS4_140.FIN2	211.8	0.831	3.968	0.045	0.289	0.0028	0.61767	1626.4	9.2	1636	14	1613	16	1613.0	16.0	1.4	
VSS4_141.FIN2	255	5.83	2.84	0.045	0.2344	0.0029	0.65395	1366	12	1357	15	1377	24	1377.0	24.0	1.5	
VSS4_142.FIN2	98.4	0.837	5.153	0.063	0.3383	0.0036	0.45537	1844	11	1878	17	1807	22	1807.0	22.0	3.9	
VSS4_143.FIN2	211.8	1.588	2.429	0.037	0.2099	0.0025	0.5283	1250	11	1228	13	1289	26	1289.0	26.0	4.7	
WSS5_1.FIN2	181	1.01	4.908	0.088	0.3218	0.0056	0.77771	1802	15	1798	27	1805	30	1805.0	30.0	0.4	
WSS5_2.FIN2	0.1	no value	no value	NAN	no value	NAN	#VALUE!	no value	NAN	no value	NAN	no value	NAN	#VALUE!	#VALUE!	#VALUE!	
WSS5_3.FIN2	293	6.16	0.4776	0.0094	0.06326	0.00058	0.16185	395.6	6.5	395.4	3.5	392	45	395.4	3.5	0.1	
WSS5_4.FIN2	241.5	3.78	0.4188	0.009	0.05594	0.00072	0.3107	354.4	6.5	350.9	4.4	361	47	350.9	4.4	1.0	
WSS5_5.FIN2	220.1	0.71	0.609	0.012	0.07866	0.0007	0.23538	482	7.5	488.1	4.2	437	43	488.1	4.2	1.3	
WSS5_6.FIN2	106.2	2.54	10.76	0.2	0.4137	0.0071	0.81798	2499	18	2230	32	2723	18	2723.0	18.0	18.1	
WSS5_7.FIN2	407.8	1.283	0.743	0.011	0.0895	0.001	0.45862	564	6.8	552.3	6.2	599	34	552.3	6.2	2.1	
WSS5_8.FIN2	862	9.15	1.685	0.026	0.1691	0.0023	0.45059	1002	9.7	1007	13	988	31	988.0	31.0	1.9	Rim
WSS5_8.FIN2	173.5	1.841	2.48	0.056	0.2141	0.0032	0.32595	1265	16	1251	17	1278	45	1278.0	45.0	2.1	Core
WSS5_9.FIN2	654	7.66	1.461	0.074	0.141	0.0042	0.73362	912	31	850	24	1048	72	1048.0	72.0	18.9	Rim
WSS5_9.FIN2	247.9	1.635	2.945	0.039	0.2461	0.0028	0.5299	1393	10	1418	15	1344	24	1344.0	24.0	5.5	Core
WSS5_10.FIN2	934	3.56	0.643	0.01	0.06463	0.00057	0.17724	504.1	6.2	403.7	3.4	979	34	DISC	DISC	19.9	
WSS5_11.FIN2	357	4.19	1.804	0.026	0.1781	0.0017	0.52758	1046.2	9.5	1056.6	9.2	1014	25	1014.0	25.0	4.2	

Table 5

WSS5_12.FIN2	462	8	0.825	0.018	0.0986	0.0018	0.78508	610	10	606	10	623	31	606.0	10.0	0.7	
WSS5_13.FIN2	75.78	1.101	2.1	0.041	0.1975	0.0023	0.25488	1147	13	1162	12	1112	38	1112.0	38.0	4.5	
WSS5_14.FIN2	141.8	1.04	1.912	0.027	0.1828	0.0016	0.44894	1084.9	9.7	1083.4	9.1	1078	27	1078.0	27.0	0.5	
WSS5_15.FIN2	284	1.76	0.558	0.015	0.0726	0.001	0.058725	449.7	9.9	451.9	6	423	65	451.9	6.0	0.5	
WSS5_16.FIN2	36.7	0.789	0.774	0.036	0.0911	0.0028	0.27466	581	21	562	17	630	100	562.0	17.0	3.3	
WSS5_17.FIN2	313	2.63	0.878	0.019	0.1034	0.0012	0.41547	639	10	634.4	7.1	648	44	634.4	7.1	0.7	
WSS5_18.FIN2	178.3	2.56	0.545	0.015	0.0703	0.0013	0.50247	441.2	9.5	438	8	424	51	438.0	8.0	0.7	
WSS5_19.FIN2	426	8.96	0.515	0.01	0.0621	0.0011	0.41042	421.6	6.9	388.4	6.5	593	44	388.4	6.5	7.9	
WSS5_21.FIN2	108.6	1.02	0.506	0.015	0.0663	0.0011	0.4128	414	10	413.6	6.6	383	62	413.6	6.6	0.1	
WSS5_22.FIN2	87.3	0.822	0.549	0.018	0.0711	0.001	0.037342	443	11	442.4	6.3	420	76	442.4	6.3	0.1	
WSS5_23.FIN2	308.7	8.01	1.342	0.034	0.1227	0.0035	0.52436	863	15	746	20	1164	53	746.0	20.0	13.6	
WSS5_24.FIN2	219	1.263	1.891	0.03	0.1738	0.0024	0.61856	1076	10	1033	13	1160	26	1160.0	26.0	10.9	
WSS5_25.FIN2	165.7	1.192	3.39	0.047	0.2564	0.003	0.57841	1500	11	1471	15	1532	22	1532.0	22.0	4.0	
WSS5_26.FIN2	102.3	1.177	1.878	0.029	0.182	0.0021	0.45215	1073	11	1077	11	1056	31	1056.0	31.0	2.0	
WSS5_27.FIN2	198	2.54	0.879	0.018	0.1012	0.0013	0.44291	638.9	9.5	621.5	7.8	688	41	621.5	7.8	2.7	
WSS5_28.FIN2	221.9	1.798	1.689	0.039	0.1664	0.0033	0.55454	1002	15	992	18	1017	42	1017.0	42.0	2.5	
WSS5_29.FIN2	128.6	0.938	0.708	0.028	0.0878	0.0027	0.23357	542	17	542	16	524	98	542.0	16.0	0.0	
WSS5_30.FIN2	257	3.17	1.716	0.029	0.1628	0.0027	0.59771	1012	11	972	15	1094	34	1094.0	34.0	11.2	
WSS5_31.FIN2	152.6	1.49	0.494	0.019	0.0643	0.0015	0.24558	408	12	401.6	8.8	407	83	401.6	8.8	1.6	
WSS5_32.FIN2	257.5	1.154	0.542	0.013	0.06996	0.00088	0.19274	438.9	8.5	435.9	5.3	436	54	435.9	5.3	0.7	
WSS5_33.FIN2	81.5	0.932	3.191	0.055	0.2559	0.003	0.44201	1453	13	1468	15	1418	34	1418.0	34.0	3.5	
WSS5_34.FIN2	445	1.212	0.551	0.014	0.072	0.0017	0.16432	444.8	9.1	448	10	419	68	448.0	10.0	0.7	
WSS5_35.FIN2	130.6	2.6	1.659	0.034	0.1662	0.0036	0.53417	993	13	990	20	994	44	994.0	44.0	0.4	
WSS5_36.FIN2	318.8	0.915	0.867	0.018	0.1021	0.00095	0.27728	633.1	9.6	626.7	5.5	643	43	626.7	5.5	1.0	
WSS5_37.FIN2	244.5	0.712	0.734	0.025	0.0895	0.0024	0.42997	557	15	553	14	554	73	553.0	14.0	0.7	

Table 5

WSS5_39.FIN2	360.4	1.646	2.372	0.023	0.2098	0.0018	0.44559	1233.3	6.8	1227.7	9.6	1236	18	1236.0	18.0	0.7	
WSS5_40.FIN2	157.8	0.995	0.832	0.014	0.10051	0.00085	0.034614	613.3	7.8	617.3	5	582	41	617.3	5.0	0.7	
WSS5_41.FIN2	186.2	1.186	3.976	0.044	0.2851	0.0025	0.33856	1628.4	9	1617	12	1628	20	1628.0	20.0	0.7	
WSS5_42.FIN2	488	2.097	3.202	0.04	0.2538	0.0025	0.68541	1456.4	9.5	1457	13	1444	17	1444.0	17.0	0.9	
WSS5_43.FIN2	1290	1.405	0.4105	0.0069	0.05486	0.00066	0.52358	350.2	5.4	344.3	4.1	379	39	344.3	4.1	1.7	Rim
WSS5_43.FIN2	388	1.894	0.586	0.023	0.0751	0.0012	0.074658	467	15	467	7.4	444	94	467.0	7.4	0.0	Core
WSS5_44.FIN2	228.7	1.116	1.321	0.025	0.1412	0.0021	0.58814	854	11	851	12	848	34	848.0	12.0	0.4	
WSS5_45.FIN2	271	1.27	1.799	0.024	0.1739	0.0016	0.39035	1044.1	8.5	1033.2	8.7	1055	26	1055.0	26.0	2.1	
WSS5_46.FIN2	216	1.954	3.298	0.057	0.2576	0.0031	0.74986	1482	13	1477	16	1484	27	1484.0	27.0	0.5	
WSS5_47.FIN2	243	1.326	1.581	0.025	0.1598	0.0018	0.37305	961.5	9.8	955	10	958	32	958.0	32.0	0.3	
WSS5_48.FIN2	83.5	0.928	0.814	0.022	0.095	0.0015	0.3015	602	12	584.8	8.6	645	57	584.8	8.6	2.9	
WSS5_49.FIN2	208	3.66	2.039	0.038	0.1919	0.0035	0.5734	1129	12	1130	19	1114	33	1114.0	33.0	1.4	
WSS5_50.FIN2	156.3	0.876	0.57	0.013	0.07256	0.0009	0.34439	457.5	8.9	451.5	5.4	469	51	451.5	5.4	1.3	
WSS5_51.FIN2	208.6	1.673	3.438	0.048	0.2616	0.0027	0.76254	1511	11	1498	14	1521	17	1521.0	17.0	1.5	
WSS5_52.FIN2	113.5	1.131	0.772	0.018	0.0928	0.0011	0.050161	580	11	571.8	6.6	588	58	571.8	6.6	1.4	
WSS5_53.FIN2	260	4.78	0.912	0.014	0.1076	0.0011	0.31463	657.2	7.4	658.6	6.3	640	33	658.6	6.3	0.2	
WSS5_54.FIN2	236.7	1.009	0.595	0.017	0.0751	0.0015	0.4267	472	11	466.9	8.9	494	54	466.9	8.9	1.1	
WSS5_55.FIN2	64.9	0.863	0.578	0.021	0.0716	0.0015	0.11701	461	13	445.7	9	507	83	445.7	9.0	3.3	
WSS5_56.FIN2	315.7	1.945	2.703	0.071	0.1956	0.0033	0.568	1328	19	1151	18	1613	40	1613.0	40.0	28.6	
WSS5_57.FIN2	159.2	1.809	1.845	0.03	0.1747	0.0023	0.35286	1062	11	1037	13	1104	35	1104.0	35.0	6.1	
WSS5_58.FIN2	295	0.867	3.769	0.09	0.2603	0.0059	0.68045	1582	19	1490	30	1702	35	1702.0	35.0	12.5	
WSS5_59.FIN2	525	0.7333	0.612	0.011	0.06729	0.00071	0.58321	484.6	7.1	419.8	4.3	786	43	419.8	4.3	13.4	
WSS5_60.FIN2	145	0.846	1.061	0.024	0.1186	0.0016	0.21005	733	12	722.4	9.1	761	53	722.4	9.1	1.4	
WSS5_61.FIN2	231.5	1.626	7.115	0.058	0.3954	0.0029	0.69982	2125.2	7.3	2148	13	2098	11	2098.0	11.0	2.4	
WSS5_62.FIN2	132.3	1.483	0.57	0.023	0.0728	0.0012	0.050793	457	15	453	7.5	446	97	453.0	7.5	0.9	

Table 5

WSS5_63.FIN2	295	3.48	0.668	0.033	0.0835	0.0028	0.39201	516	19	516	17	513	95	516.0	17.0	0.0	Rim
WSS5_63.FIN2	53.8	2.35	2.95	0.18	0.1909	0.0091	0.49217	1389	47	1125	49	1810	100	1810.0	100.0	37.8	Core
WSS5_64.FIN2	81.9	1.06	3.143	0.066	0.2396	0.0036	0.58694	1438	16	1383	19	1511	33	1511.0	33.0	8.5	
WSS5_65.FIN2	267	2.28	0.514	0.019	0.0667	0.0018	0.4498	420	13	416	11	420	76	416.0	11.0	1.0	
WSS5_66.FIN2	331	22	0.534	0.05	0.0694	0.004	0.6343	433	33	432	24	420	150	432.0	24.0	0.2	Rim
WSS5_66.FIN2	148.9	1.567	2.024	0.043	0.1913	0.0023	0.34733	1122	15	1128	12	1101	43	1101.0	43.0	2.5	Core
WSS5_67.FIN2	143.2	0.567	0.712	0.021	0.0876	0.0015	0.41138	544	13	541.1	8.9	533	63	541.1	8.9	0.5	
WSS5_68.FIN2	274.6	2.468	1.887	0.027	0.1866	0.0022	0.57437	1077	10	1103	12	1029	25	1029.0	25.0	7.2	
WSS5_69.FIN2	343.4	2.846	2.044	0.032	0.1909	0.0023	0.47623	1129	11	1126	13	1132	29	1132.0	29.0	0.5	
WSS5_70.FIN2	273	0.674	0.833	0.022	0.0992	0.0019	0.2111	614	12	610	11	630	59	610.0	11.0	0.7	
WSS5_71.FIN2	199.6	0.76	0.557	0.024	0.0718	0.0013	0.23757	448	15	447.2	8.1	428	90	447.2	8.1	0.2	
WSS5_72.FIN2	1.25	0.121	10300	2600	80	19	0.92313	8820	300	25300	1800	5080	43	DISC	DISC	398.0	
WSS5_73.FIN2	171.1	1.183	3.762	0.078	0.2771	0.0066	0.67001	1587	18	1575	33	1597	36	1597.0	36.0	1.4	
WSS5_74.FIN2	72.5	1.385	1.445	0.055	0.1283	0.0032	0.4898	905	23	778	19	1215	66	778.0	19.0	14.0	
WSS5_75.FIN2	164.9	3.91	0.64	0.013	0.08047	0.00077	0.08022	501	7.9	498.9	4.6	499	45	498.9	4.6	0.4	
WSS5_76.FIN2	139	1.373	2.29	0.051	0.2057	0.0038	0.49778	1210	16	1205	20	1200	40	1200.0	40.0	0.4	
WSS5_77.FIN2	90.2	5.78	1.882	0.059	0.1797	0.0049	0.40341	1071	21	1064	27	1080	65	1080.0	65.0	1.5	
WSS5_78.FIN2	202.4	1.032	2.897	0.047	0.223	0.0031	0.81595	1378	12	1297	17	1503	20	1503.0	20.0	13.7	
WSS5_79.FIN2	916	8.51	1.882	0.014	0.181	0.0011	0.45577	1075.6	4.9	1072.1	5.9	1076	14	1076.0	14.0	0.4	
WSS5_81.FIN2	623	1.419	0.579	0.018	0.0744	0.002	0.5871	463	11	462	12	472	54	462.0	12.0	0.2	
WSS5_82.FIN2	88.2	1.77	0.917	0.021	0.1064	0.0014	0.11496	660	12	651.8	8.2	676	53	651.8	8.2	1.2	
WSS5_83.FIN2	114	0.561	0.519	0.015	0.0674	0.001	0.32493	423	10	420.2	6	425	63	420.2	6.0	0.7	
WSS5_84.FIN2	112.5	1.155	1.682	0.053	0.153	0.0038	0.6552	998	20	917	21	1178	49	1178.0	49.0	22.2	
WSS5_85.FIN2	160	1.511	0.877	0.018	0.1043	0.0013	0.29101	638.1	9.8	639.4	7.3	614	45	639.4	7.3	0.2	
WSS5_87.FIN2	128.9	0.646	0.85	0.028	0.079	0.0017	0.36702	625	16	492	11	1132	67	DISC	DISC	21.3	

Table 5

WSS5_88.FIN2	425	0.524	0.46	0.013	0.0556	0.001	0.44793	383.3	9	349	6.4	559	57	349.0	6.4	8.9	
WSS5_89.FIN2	179.8	1.512	3.927	0.062	0.2303	0.0035	0.73923	1619	13	1335	18	2007	20	2007.0	20.0	33.5	
WSS5_90.FIN2	207	0.859	0.84	0.021	0.0981	0.0017	0.46384	617	12	603.3	9.8	649	52	603.3	9.8	2.2	
WSS5_91.FIN2	-0.05	no value	no value	NAN	no value	NAN	#VALUE!	no value	NAN	no value	NAN	no value	NAN	#VALUE!	#VALUE!	#VALUE!	
WSS5_93.FIN2	277.7	1.238	0.495	0.014	0.0634	0.0015	0.50896	406.7	9.8	396.1	9.2	458	57	396.1	9.2	2.6	
WSS5_94.FIN2	62.8	1.486	0.723	0.038	0.0899	0.0027	0.063219	550	22	555	16	520	130	555.0	16.0	0.9	
WSS5_95.FIN2	383	2.184	1.942	0.045	0.1823	0.0041	0.61415	1094	15	1079	23	1114	37	1114.0	37.0	3.1	
WSS5_96.FIN2	103.9	0.943	13.8	0.12	0.5432	0.0041	0.54728	2735.9	8.3	2796	17	2688	13	2688.0	13.0	4.0	
WSS5_97.FIN2	131.8	0.67	1.644	0.05	0.1647	0.0031	0.58113	985	19	983	17	1000	48	1000.0	48.0	1.7	
WSS5_98.FIN2	369.7	4.89	1.894	0.022	0.181	0.0017	0.27882	1078.6	7.7	1072.4	9.2	1085	25	1085.0	25.0	1.2	
WSS5_99.FIN2	361	2.67	1.467	0.053	0.1329	0.0034	0.74621	914	22	804	19	1189	47	804.0	19.0	12.0	
WSS5_100.FIN2	226	1.039	2.056	0.021	0.1934	0.0016	0.22731	1133.2	7	1139.3	8.8	1117	24	1117.0	24.0	2.0	
WSS5_101.FIN2	162.9	1.835	1.658	0.024	0.1669	0.0016	0.38813	991.2	9.1	994.9	8.7	981	29	981.0	29.0	1.4	
WSS5_102.FIN2	103.9	0.972	0.839	0.023	0.1011	0.0012	0.16642	617	13	620.8	6.9	585	59	620.8	6.9	0.6	
WSS5_103.FIN2	145.3	2.48	2.566	0.05	0.1913	0.0029	0.37873	1289	14	1128	16	1567	37	1567.0	37.0	28.0	
WSS5_104.FIN2	191	0.409	0.3505	0.0079	0.04907	0.00053	0.17958	306.7	6.1	308.8	3.2	277	51	308.8	3.2	0.7	
WSS5_105.FIN2	20.73	0.915	0.905	0.085	0.1014	0.0034	0.37714	642	45	622	20	650	180	622.0	20.0	3.1	
WSS5_106.FIN2	261.8	0.4009	0.501	0.014	0.06243	0.00077	0.24	411.8	9.4	390.4	4.7	518	62	390.4	4.7	5.2	
WSS5_107.FIN2	269.9	2.21	0.4878	0.0096	0.06288	0.00071	0.38058	402.8	6.5	393.1	4.3	449	43	393.1	4.3	2.4	
WSS5_108.FIN2	139.3	1.277	0.64	0.013	0.08052	0.00075	0.21795	500.9	8.3	499.2	4.5	494	46	499.2	4.5	0.3	
WSS5_109.FIN2	56	1.141	0.889	0.041	0.0995	0.0021	0.38951	646	21	611	13	757	92	611.0	13.0	5.4	
WSS5_110.FIN2	186	0.85	0.872	0.023	0.1016	0.0016	0.27932	636	12	623.6	9.2	677	57	623.6	9.2	1.9	
WSS5_111.FIN2	129.1	0.743	3.469	0.054	0.2505	0.003	0.43696	1519	12	1441	15	1627	28	1627.0	28.0	11.4	
WSS5_112.FIN2	170	0.933	0.587	0.012	0.06983	0.00068	0.2198	467.9	7.6	435.1	4.1	621	45	435.1	4.1	7.0	
WSS5_113.FIN2	704	13.6	0.932	0.024	0.1011	0.0024	0.31476	668	13	621	14	836	60	621.0	14.0	7.0	Rim

Table 5

WSS5_113.FIN2	290	6.19	1.896	0.038	0.1372	0.0022	0.64683	1081	14	829	12	1631	30	DISC	DISC	23.3	Core
WSS5_114.FIN2	288	0.692	0.399	0.012	0.05152	0.00068	0.16623	340.6	8.3	323.8	4.1	449	64	323.8	4.1	4.9	
WSS5_115.FIN2	911	4.68	1.06	0.019	0.0949	0.0015	0.31062	733	9.5	584.1	8.5	1225	39	DISC	DISC	20.3	Rim
WSS5_115.FIN2	475.9	6.11	1.205	0.023	0.118	0.0019	0.31292	803	10	719	11	1039	42	719.0	11.0	10.5	Core
WSS5_116.FIN2	333	1.791	0.733	0.011	0.08998	0.00078	0.37466	558.1	6.6	555.4	4.6	566	32	555.4	4.6	0.5	
WSS5_117.FIN2	139.3	1.887	0.747	0.029	0.0898	0.0015	0.49281	565	17	554.4	8.9	593	74	554.4	8.9	1.9	
WSS5_118.FIN2	518	1.06	0.537	0.015	0.063	0.0014	0.29697	436.3	9.8	394.1	8.4	670	67	394.1	8.4	9.7	
WSS5_119.FIN2	98.5	0.786	1.586	0.044	0.1609	0.004	0.69287	961	18	961	23	969	49	969.0	49.0	0.8	
WSS5_120.FIN2	107.9	0.566	0.823	0.017	0.09885	0.00092	0.2168	607.8	9.4	607.6	5.4	609	44	607.6	5.4	0.0	
WSS5_121.FIN2	154.5	1.108	6.07	0.055	0.3614	0.003	0.67492	1984.8	8	1988	14	1983	14	1983.0	14.0	0.3	
WSS5_122.FIN2	125.1	0.809	4.002	0.059	0.2897	0.0035	0.49728	1634	12	1640	18	1634	24	1634.0	24.0	0.4	
WSS5_123.FIN2	229.8	1.56	0.41	0.01	0.05496	0.00079	0.33393	348.1	7.4	344.9	4.8	368	52	344.9	4.8	0.9	
WSS5_124.FIN2	416	38	0.529	0.021	0.0706	0.0023	0.57791	430	14	440	14	385	73	440.0	14.0	2.3	Rim
WSS5_124.FIN2	397	16.1	1.499	0.037	0.1375	0.0033	0.73979	929	15	830	19	1173	35	830.0	19.0	10.7	Core
WSS5_125.FIN2	145.2	2.49	2.153	0.037	0.1998	0.003	0.50202	1164	12	1174	16	1161	32	1161.0	32.0	1.1	
WSS5_126.FIN2	144.8	1.495	2.127	0.041	0.1915	0.0037	0.6093	1159	13	1129	20	1224	34	1224.0	34.0	7.8	
WSS5_127.FIN2	3.42	0.169	1100	130	9.1	1.1	0.99757	6960	150	14250	830	5107	19	DISC	DISC	179.0	
WSS5_128.FIN2	174.2	2.494	3.172	0.045	0.2562	0.0034	0.42142	1449	11	1469	17	1424	28	1424.0	28.0	3.2	
WSS5_130.FIN2	326	0.964	0.689	0.019	0.0851	0.0022	0.65259	531	11	526	13	561	47	526.0	13.0	0.9	
WSS5_131.FIN2	67.9	0.872	0.765	0.028	0.0934	0.0018	0.17991	573	16	575	10	550	81	575.0	10.0	0.3	
WSS5_132.FIN2	51.3	1.253	1.32	0.06	0.1252	0.0036	0.64569	844	26	759	21	1055	73	759.0	21.0	10.1	
WSS5_133.FIN2	283	12	0.479	0.019	0.0636	0.0021	0.58642	397	13	397	13	398	70	397.0	13.0	0.0	
WSS5_134.FIN2	170.9	0.962	3.971	0.044	0.2912	0.0033	0.48033	1627.1	9	1649	17	1607	22	1607.0	22.0	2.6	
WSS5_135.FIN2	423	2.603	0.757	0.019	0.0898	0.002	0.56615	573	10	554	12	637	47	554.0	12.0	3.3	
WSS5_137.FIN2	291	1.67	3.283	0.026	0.2582	0.0018	0.51269	1476.3	6.3	1480.5	9.2	1475	14	1475.0	14.0	0.4	

Table 5

WSS5_138.FIN2	73.8	1.437	2.699	0.042	0.2301	0.0024	0.36004	1326	11	1335	13	1313	30	1313.0	30.0	1.7	
WSS5_139.FIN2	360	1.524	0.844	0.04	0.0981	0.0029	0.4871	619	23	603	17	675	96	603.0	17.0	2.6	
WSS5_140.FIN2	115.8	1.212	0.694	0.027	0.081	0.0018	0.13155	534	16	502	11	660	93	502.0	11.0	6.0	
WSS5_141.FIN2	109	1.243	0.858	0.021	0.1024	0.0012	0.2002	627	11	628.3	7.2	611	54	628.3	7.2	0.2	
WSS5_142.FIN2	168.2	0.729	13.89	0.11	0.5312	0.0034	0.58587	2741.5	7.4	2746	14	2741	10	2741.0	10.0	0.2	
WSS5_143.FIN2	210.5	0.703	1.737	0.034	0.1703	0.0029	0.47853	1021	13	1013	16	1040	38	1040.0	38.0	2.6	
WSS5_144.FIN2	284	4.05	2.006	0.045	0.1843	0.004	0.72123	1118	15	1090	22	1177	36	1177.0	36.0	7.4	
WSS5_145.FIN2	140	1.697	3.075	0.036	0.2478	0.0024	0.47356	1424.9	8.9	1427	12	1415	22	1415.0	22.0	0.8	

Table 5: VSS4 and WSS5 sample data.

Table 6

Sample Name:								207/235		206/238		207/206		Best age			
Grain #	[U] ppm	U/Th	207/235	2σ error	206/238	2σ error	RHO	Age Ma	2σ error	Age (Ma)	2σ error	Age (Ma)	2σ error	(Ma)	2σ error	% Discordance*	Rim/Core
VSS1_1.FIN2	66.9	2.231	1.755	0.06	0.1683	0.0035	0.49575	0	22	1002	19	1031	61	1031.0	61.0	2.8	
VSS1_2.FIN2	286	4.56	0.804	0.012	0.097	0.0011	0.2825	598.1	6.5	596.8	6.2	564	34	596.8	6.2	0.2	
VSS1_3.FIN2	317	0.973	0.586	0.014	0.0671	0.001	0.41503	467.4	9	418.7	6.1	674	49	418.7	6.1	10.4	
VSS1_4.FIN2	23.36	0.689	14.88	0.26	0.5438	0.009	0.52488	2806	16	2796	37	2787	28	2787.0	28.0	0.3	
VSS1_5.FIN2	59	2.4	1.88	0.05	0.1737	0.0024	0.35465	1071	18	1032	13	1117	51	1117.0	51.0	7.6	
VSS1_6.FIN2	57.1	2.42	3.69	0.11	0.2464	0.0078	0.51538	1563	23	1417	40	1762	55	1762.0	55.0	19.6	
VSS1_7.FIN2	268.1	1.99	0.765	0.02	0.0931	0.002	0.4995	575	12	573	12	573	51	573.0	12.0	0.3	
VSS1_8.FIN2	504	16.64	12.46	0.26	0.4583	0.0095	0.66613	2635	20	2429	42	2795	27	2795.0	27.0	13.1	
VSS1_9.FIN2	299	1.629	4.075	0.068	0.2902	0.0052	0.68837	1646	14	1641	26	1663	25	1663.0	25.0	1.3	
VSS1_10.FIN2	362	2.77	1.855	0.061	0.1773	0.0056	0.693	1063	22	1050	31	1099	51	1099.0	51.0	4.5	
VSS1_11.FIN2	115	2.15	0.85	0.043	0.0985	0.0045	0.65879	620	23	605	27	706	86	605.0	27.0	2.4	
VSS1_12.FIN2	1080	25.2	0.532	0.027	0.0661	0.0034	0.58889	432	17	412	21	552	94	412.0	21.0	4.6	Rim
VSS1_12.FIN2	197.2	1.838	0.942	0.026	0.103	0.0023	0.48836	673	14	632	13	816	54	632.0	13.0	6.1	Core
VSS1_13.FIN2	56	0.817	1.529	0.046	0.1543	0.0031	0.33395	937	19	925	18	960	65	960.0	65.0	3.6	
VSS1_14.FIN2	81.9	3.74	0.796	0.05	0.0819	0.004	0.34647	590	28	507	24	920	130	507.0	24.0	14.1	
VSS1_15.FIN2	423	1.292	0.773	0.015	0.0938	0.0016	0.43323	580.9	8.3	578.1	9.6	595	40	578.1	9.6	0.5	
VSS1_16.FIN2	193	4.34	1.331	0.055	0.135	0.0054	0.57857	855	24	821	33	981	73	821.0	33.0	4.0	
VSS1_17.FIN2	107.7	1.022	4.116	0.072	0.2806	0.0042	0.47973	1656	14	1594	21	1754	31	1754.0	31.0	9.1	
VSS1_18.FIN2	489	3.01	4.26	0.14	0.2592	0.0071	0.86839	1671	28	1482	37	1946	29	1946.0	29.0	23.8	
VSS1_19.FIN2	72.9	1.445	1.587	0.029	0.1621	0.0019	0.25726	964	12	968	11	967	38	967.0	38.0	0.1	
VSS1_20.FIN2	118	0.832	1.719	0.03	0.1668	0.0022	0.444	1014	11	994	12	1066	34	1066.0	34.0	6.8	
VSS1_21.FIN2	219	9.3	0.666	0.015	0.0824	0.0011	0.26321	517	9	510.6	6.6	551	49	510.6	6.6	1.2	

Table 6

VSS1_22.FIN2	208.2	1.79	7.27	0.25	0.353	0.013	0.80253	2132	31	1949	62	2354	40	2354.0	40.0	17.2	
VSS1_23.FIN2	111.9	2.61	0.794	0.023	0.097	0.0019	0.3479	591	13	597	11	588	65	597.0	11.0	1.0	
VSS1_24.FIN2	433	1.38	0.6283	0.0087	0.08217	0.00091	0.32624	494.5	5.4	509	5.4	432	36	509.0	5.4	2.9	
VSS1_25.FIN2	332.9	1.582	5.508	0.079	0.343	0.0048	0.63911	1901	13	1900	23	1909	22	1909.0	22.0	0.5	
VSS1_26.FIN2	597	1.677	1.819	0.035	0.1716	0.0047	0.62587	1051	13	1020	26	1119	43	1119.0	43.0	8.8	Rim
VSS1_26.FIN2	400.3	4.6	2.434	0.045	0.2127	0.0036	0.5648	1252	13	1243	19	1282	32	1282.0	32.0	3.0	Core
VSS1_27.FIN2	801	2.009	3.26	0.13	0.1447	0.0054	0.4187	1468	31	870	30	2498	72	2498.0	72.0	65.2	Rim
VSS1_27.FIN2	232	2.407	4.36	0.19	0.269	0.011	0.69758	1698	37	1535	54	1923	60	1923.0	60.0	20.2	Core
VSS1_28.FIN2	329	0.933	0.575	0.01	0.074	0.0012	0.30392	460.7	6.5	459.8	7.1	464	44	459.8	7.1	0.2	
VSS1_29.FIN2	200	2.82	0.659	0.025	0.0818	0.0026	0.598	511	15	506	15	527	66	506.0	15.0	1.0	
VSS1_30.FIN2	152	2.3	0.69	0.016	0.0854	0.0012	0.28004	531.4	9.9	528.2	7.2	530	52	528.2	7.2	0.6	
VSS1_31.FIN2	379	10.94	0.595	0.018	0.0707	0.002	0.5348	474	11	440	12	645	62	440.0	12.0	7.2	
VSS1_32.FIN2	295.2	1.442	0.697	0.018	0.0847	0.0017	0.49747	536	11	524	9.8	583	52	524.0	9.8	2.2	
VSS1_33.FIN2	286	4.27	1.036	0.042	0.0937	0.0048	0.51311	720	20	577	28	1201	85	577.0	28.0	19.9	Rim
VSS1_33.FIN2	366	2.636	1.692	0.064	0.1521	0.0053	0.71314	1003	24	912	30	1214	55	1214.0	55.0	24.9	Core
VSS1_34.FIN2	146.9	1.185	4.331	0.067	0.3017	0.004	0.7492	1696	13	1699	20	1689	20	1689.0	20.0	0.6	
VSS1_35.FIN2	215.6	1.444	4.02	0.1	0.2815	0.0065	0.81599	1637	20	1597	33	1688	29	1688.0	29.0	5.4	
VSS1_36.FIN2	246	1.88	0.432	0.023	0.0529	0.0027	0.69047	363	16	332	17	538	95	332.0	17.0	8.5	Rim
VSS1_36.FIN2	158.9	1.181	3.61	0.061	0.2614	0.0053	0.56633	1553	13	1496	27	1640	34	1640.0	34.0	8.8	Core
VSS1_37.FIN2	107	2.05	0.698	0.025	0.0804	0.0024	0.5864	534	15	498	15	675	69	498.0	15.0	6.7	
VSS1_38.FIN2	250.4	2.91	3.284	0.049	0.2588	0.0044	0.55907	1475	12	1485	22	1467	30	1467.0	30.0	1.2	
VSS1_39.FIN2	570	5.62	0.924	0.058	0.0582	0.0056	0.51492	663	31	365	34	1900	140	DISC	DISC	44.9	Rim
VSS1_39.FIN2	192	9.82	3.97	0.15	0.199	0.0071	0.85763	1622	32	1167	38	2287	37	2287.0	37.0	49.0	Core
VSS1_40.FIN2	313	10.34	0.764	0.047	0.0948	0.0062	0.72867	575	28	583	37	515	67	583.0	37.0	1.4	Rim
VSS1_40.FIN2	182.7	1.679	1.631	0.036	0.1615	0.0028	0.47594	980	14	965	15	1023	42	1023.0	42.0	5.7	Core
VSS1_41.FIN2	212.6	0.854	0.877	0.034	0.1047	0.005	0.54168	637	18	641	29	665	91	641.0	29.0	0.6	

Table 6

VSS1_42.FIN2	349	7.7	3.72	0.12	0.2571	0.0087	0.62628	1568	26	1470	44	1707	53	1707.0	53.0	13.9	
VSS1_43.FIN2	105.3	1.918	3.541	0.066	0.278	0.0054	0.61051	1532	15	1579	27	1489	32	1489.0	32.0	6.0	
VSS1_44.FIN2	231	1.933	3.596	0.064	0.2448	0.0047	0.64173	1548	15	1410	24	1736	30	1736.0	30.0	18.8	
VSS1_45.FIN2	238	3.58	0.482	0.014	0.0635	0.0015	0.57795	398.2	9.3	398	9.4	391	53	398.0	9.4	0.1	
VSS1_46.FIN2	173.6	1.86	0.607	0.024	0.074	0.0027	0.61686	479	15	460	16	571	73	460.0	16.0	4.0	
VSS1_47.FIN2	13.6	-237	0.731	0.049	0.0803	0.0032	0.14719	543	28	497	19	700	140	497.0	19.0	8.5	
VSS1_48.FIN2	225	4	1.635	0.077	0.1657	0.0088	0.7812	982	32	985	49	995	70	995.0	70.0	1.0	
VSS1_49.FIN2	226.3	2.54	0.828	0.026	0.1022	0.0029	0.55695	609	14	627	17	530	60	627.0	17.0	3.0	
VSS1_50.FIN2	780	3.37	0.874	0.036	0.0572	0.0028	0.56065	636	19	358	17	1767	76	DISC	DISC	43.7	Rim
VSS1_50.FIN2	328	2.166	0.959	0.027	0.0866	0.0025	0.60712	681	14	535	15	1199	56	DISC	DISC	21.4	Core
VSS1_51.FIN2	254.6	0.843	0.56	0.015	0.0725	0.0017	0.45251	451.6	9.2	451	10	439	58	451.0	10.0	0.1	
VSS1_52.FIN2	415	2.28	0.623	0.019	0.0784	0.0019	0.46565	491	12	488	12	479	65	488.0	12.0	0.6	
VSS1_53.FIN2	170	1.234	0.366	0.015	0.0495	0.0017	0.54847	316	11	311	11	351	82	311.0	11.0	1.6	
VSS1_54.FIN2	179.4	1.705	0.461	0.011	0.0621	0.0011	0.33731	383.4	8	388.1	6.5	326	55	388.1	6.5	1.2	
VSS1_55.FIN2	312	1.945	2.543	0.065	0.1921	0.0049	0.86855	1285	19	1131	26	1541	25	1541.0	25.0	26.6	
VSS1_56.FIN2	91.7	2.24	27.18	0.51	0.6896	0.0095	0.6007	3383	19	3377	36	3383	24	3383.0	24.0	0.2	
VSS1_57.FIN2	167	0.717	0.614	0.018	0.0778	0.0012	0.27304	484	11	482.7	7.3	477	65	482.7	7.3	0.3	
VSS1_58.FIN2	181.4	2.86	2.049	0.044	0.1882	0.0039	0.61852	1130	15	1111	21	1157	37	1157.0	37.0	4.0	
VSS1_60.FIN2	163.8	1.003	0.515	0.012	0.0667	0.00091	0.41738	420.8	7.8	416.2	5.5	426	45	416.2	5.5	1.1	
VSS1_61.FIN2	180	1.554	0.539	0.014	0.0709	0.0016	0.44446	437.5	9.6	441.4	9.4	402	56	441.4	9.4	0.9	
VSS1_62.FIN2	229.5	2.37	0.8	0.025	0.0963	0.002	0.57619	596	14	593	12	622	57	593.0	12.0	0.5	
VSS1_63.FIN2	108.1	1.061	0.807	0.021	0.1021	0.0024	0.36996	599	12	626	14	506	57	626.0	14.0	4.5	
VSS1_64.FIN2	174.1	0.823	0.38	0.018	0.045	0.0022	0.59297	325	13	283	13	639	91	283.0	13.0	12.9	
VSS1_65.FIN2	137.5	0.901	0.666	0.019	0.0824	0.0019	0.41304	518	12	510	11	533	65	510.0	11.0	1.5	
VSS1_66.FIN2	308	2.82	1.473	0.042	0.1413	0.0044	0.57812	917	17	850	25	1097	51	1097.0	51.0	22.5	
VSS1_67.FIN2	151.9	3.38	1.084	0.035	0.1163	0.0036	0.60697	743	17	709	21	874	52	709.0	21.0	4.6	

Table 6

VSS1_68.FIN2	56.1	1.447	0.73	0.027	0.0879	0.0025	0.3306	553	16	543	15	587	82	543.0	15.0	1.8	
VSS1_69.FIN2	178.1	1.884	0.786	0.015	0.0977	0.0022	0.59088	588.7	8.6	600	13	549	40	600.0	13.0	1.9	
VSS1_70.FIN2	201.9	1.216	0.655	0.013	0.0788	0.0013	0.59358	510.5	8	488.5	7.7	626	42	488.5	7.7	4.3	
VSS1_71.FIN2	284	5.53	0.645	0.019	0.0637	0.0017	0.21357	503	12	398	11	1014	51	DISC	DISC	20.9	
VSS1_72.FIN2	123.9	3.577	4.062	0.064	0.2911	0.004	0.51364	1645	13	1646	20	1646	27	1646.0	27.0	0.0	
VSS1_73.FIN2	51.4	0.736	0.833	0.022	0.095	0.0017	0.26465	613	12	584.8	9.9	709	60	584.8	9.9	4.6	
VSS1_74.FIN2	96.7	1.909	4.33	0.15	0.2539	0.0089	0.68718	1693	28	1456	46	2010	50	2010.0	50.0	27.6	
VSS1_75.FIN2	185	2.22	3.1	0.12	0.235	0.011	0.77516	1427	30	1357	56	1557	55	1557.0	55.0	12.8	
VSS1_76.FIN2	104	2	2.722	0.051	0.2208	0.0043	0.49338	1331	14	1285	22	1421	35	1421.0	35.0	9.6	
VSS1_77.FIN2	147.2	1.37	0.303	0.01	0.0423	0.001	0.53547	267.7	8	266.8	6.4	292	61	266.8	6.4	0.3	
VSS1_78.FIN2	52.9	0.967	1.801	0.046	0.1764	0.0035	0.45333	1043	17	1047	19	1036	49	1036.0	49.0	1.1	
VSS1_79.FIN2	65.9	2.429	1.917	0.047	0.1876	0.0038	0.68529	1087	16	1107	21	1065	40	1065.0	40.0	3.9	
VSS1_80.FIN2	391	13.46	0.563	0.016	0.0736	0.002	0.6075	452	10	457	12	424	52	457.0	12.0	1.1	
VSS1_81.FIN2	94.4	3.39	1.801	0.043	0.1742	0.0032	0.48345	1042	15	1035	18	1057	45	1057.0	45.0	2.1	
VSS1_82.FIN2	85.7	1.75	1.595	0.05	0.1635	0.0039	0.72817	961	20	975	22	937	44	937.0	44.0	4.1	
VSS1_83.FIN2	44.93	0.855	1.952	0.049	0.1852	0.0035	0.5278	1096	17	1094	19	1116	44	1116.0	44.0	2.0	
VSS1_84.FIN2	59.3	1.69	6.24	0.15	0.3836	0.0099	0.67013	2002	21	2087	46	1926	41	1926.0	41.0	8.4	
VSS1_85.FIN2	399	7.66	1.271	0.096	0.1224	0.0082	0.79051	824	43	743	47	1057	96	743.0	47.0	9.8	Rim
VSS1_85.FIN2	182.5	1.597	2.277	0.06	0.205	0.0043	0.57373	1202	19	1201	23	1207	45	1207.0	45.0	0.5	Core
VSS1_86.FIN2	62.3	0.96	0.92	0.023	0.105	0.0018	0.32923	661	12	644	10	690	57	644.0	10.0	2.6	
VSS1_87.FIN2	250.4	2.644	1.763	0.034	0.1727	0.003	0.55891	1029	12	1026	17	1036	37	1036.0	37.0	1.0	
VSS1_88.FIN2	239	2.897	0.403	0.02	0.0499	0.0024	0.63306	343	14	314	15	547	86	314.0	15.0	8.5	
VSS1_89.FIN2	808	9.46	0.928	0.022	0.1089	0.0031	0.61478	667	12	666	18	670	51	666.0	18.0	0.1	
VSS1_90.FIN2	157.1	2.67	1.68	0.031	0.169	0.0025	0.53807	1000	11	1006	14	972	35	972.0	35.0	3.5	
VSS1_91.FIN2	74.4	3.11	0.756	0.026	0.0945	0.0023	0.50376	569	15	581	14	499	66	581.0	14.0	2.1	
VSS1_92.FIN2	357	1.818	0.624	0.012	0.0798	0.0015	0.43776	491.2	7.7	494.8	8.7	477	46	494.8	8.7	0.7	

Table 6

VSS1_93.FIN2	107.4	-50	0.825	0.018	0.102	0.0017	0.4715	609.3	9.9	625.6	9.7	554	45	625.6	9.7	2.7	
VSS1_94.FIN2	140.6	2.368	1.571	0.029	0.1613	0.0027	0.52962	957	11	964	15	941	34	941.0	34.0	2.4	
VSS1_95.FIN2	468	1.052	0.565	0.014	0.0575	0.0017	0.48168	455.7	9.3	360	10	978	56	DISC	DISC	21.0	
VSS1_96.FIN2	90.7	1.51	1.788	0.04	0.1761	0.0029	0.46848	1039	15	1045	16	1015	41	1015.0	41.0	3.0	
VSS1_97.FIN2	278	18.9	1.084	0.055	0.1141	0.0053	0.77484	743	27	696	31	890	81	696.0	31.0	6.3	Rim
VSS1_97.FIN2	85.2	2.01	1.475	0.055	0.1494	0.003	0.418	917	22	897	17	958	70	958.0	70.0	6.4	Core
VSS1_98.FIN2	64.8	1.464	1.242	0.043	0.1246	0.0033	0.52658	814	19	762	20	979	61	762.0	20.0	6.4	
VSS1_99.FIN2	741	27.5	1.888	0.077	0.1772	0.0067	0.72593	1072	27	1050	37	1120	57	1120.0	57.0	6.3	Rim
VSS1_99.FIN2	352	9.22	4.81	0.17	0.317	0.01	0.67644	1779	31	1771	50	1798	49	1798.0	49.0	1.5	
VSS1_100.FIN2	28.5	1.83	0.881	0.057	0.102	0.0043	0.39238	634	30	625	25	650	130	625.0	25.0	1.4	
VSS1_101.FIN2	176	2.237	1.66	0.041	0.1504	0.0037	0.5433	990	15	905	21	1185	46	1185.0	46.0	23.6	
VSS1_102.FIN2	426	6.21	2.812	0.078	0.2159	0.0058	0.79988	1359	21	1258	31	1528	36	1528.0	36.0	17.7	
VSS1_103.FIN2	370	1.941	0.3037	0.0088	0.04178	0.00092	0.50041	268.4	6.8	263.8	5.7	300	56	263.8	5.7	1.7	
VSS1_104.FIN2	152.7	2.59	0.612	0.014	0.0785	0.0011	0.36318	483.6	8.8	487	6.4	442	50	487.0	6.4	0.7	
VSS1_105.FIN2	148.9	0.666	0.699	0.016	0.0863	0.0015	0.62895	536.1	9.8	533.6	8.9	529	41	533.6	8.9	0.5	
VSS1_106.FIN2	144	2.15	2.322	0.069	0.2105	0.0053	0.81171	1219	20	1234	27	1189	35	1189.0	35.0	3.8	
VSS1_107.FIN2	81.1	1.795	1.678	0.055	0.1671	0.0048	0.65617	993	21	995	26	986	51	986.0	51.0	0.9	
VSS1_108.FIN2	91.8	4.68	0.407	0.023	0.0405	0.0016	0.54438	345	16	255.9	9.8	960	100	DISC	DISC	25.8	
VSS1_109.FIN2	69.9	2.16	0.417	0.019	0.0551	0.0018	0.51405	353	13	345	11	379	83	345.0	11.0	2.3	
VSS1_110.FIN2	255	0.854	3.046	0.073	0.2453	0.0057	0.59942	1418	19	1412	29	1426	42	1426.0	42.0	1.0	
VSS1_111.FIN2	337	3.85	2.001	0.045	0.1893	0.004	0.68515	1115	15	1116	22	1104	33	1104.0	33.0	1.1	
VSS1_112.FIN2	452	1.979	2.604	0.037	0.2264	0.0031	0.49345	1301	11	1315	16	1263	27	1263.0	27.0	4.1	
VSS1_113.FIN2	193	1.752	3.428	0.06	0.2668	0.004	0.36365	1509	13	1523	20	1475	37	1475.0	37.0	3.3	
VSS1_114.FIN2	167.1	1.644	1.962	0.058	0.1957	0.0062	0.60179	1099	20	1151	33	990	55	990.0	55.0	16.3	
VSS1_115.FIN2	181.1	1.382	2.289	0.054	0.2088	0.0043	0.67949	1208	16	1221	23	1179	35	1179.0	35.0	3.6	
VSS1_116.FIN2	183	1.898	4.08	0.1	0.2882	0.007	0.69794	1647	21	1630	35	1673	35	1673.0	35.0	2.6	

Table 6

VSS1_117.FIN2	699	20.2	0.841	0.043	0.0839	0.004	0.049531	617	24	519	24	990	140	519.0	24.0	15.9	Rim
VSS1_117.FIN2	58	1.451	10.27	0.47	0.448	0.018	0.70898	2452	43	2383	80	2520	58	2520.0	58.0	5.4	Core
VSS1_118.FIN2	89.3	1.016	1.257	0.074	0.1015	0.0046	0.64961	822	33	623	27	1405	90	DISC	DISC	24.2	Rim
VSS1_118.FIN2	24.98	0.645	2.557	0.089	0.2191	0.0057	0.74245	1282	25	1275	30	1295	47	1295.0	47.0	1.5	Core
VSS1_120.FIN2	317.6	2.65	2.298	0.042	0.2065	0.0034	0.71659	1211	12	1209	18	1249	26	1249.0	26.0	3.2	
VSS1_121.FIN2	191	1.723	0.349	0.015	0.0484	0.0018	0.629	303	11	305	11	311	74	305.0	11.0	0.7	
VSS1_122.FIN2	282	1.818	0.892	0.023	0.0916	0.002	0.46855	646	12	565	12	934	51	565.0	12.0	12.5	
VSS1_123.FIN2	34.24	0.885	1.877	0.064	0.1813	0.0055	0.59781	1067	22	1072	30	1057	59	1057.0	59.0	1.4	
VSS1_124.FIN2	300	1.858	1.955	0.043	0.1923	0.0041	0.69304	1098	15	1132	22	1033	32	1033.0	32.0	9.6	
VSS1_125.FIN2	266	1.809	2.102	0.066	0.1835	0.0054	0.81133	1144	21	1084	29	1253	40	1253.0	40.0	13.5	
VSS1_126.FIN2	146.2	1.173	0.744	0.016	0.094	0.0016	0.53733	563.2	9.4	578.6	9.3	491	43	578.6	9.3	2.7	
VSS1_127.FIN2	411	1.96	0.796	0.021	0.0929	0.0021	0.61197	592	12	573	12	664	47	573.0	12.0	3.2	
VSS1_128.FIN2	209.3	1.05	1.865	0.038	0.1789	0.0031	0.59535	1068	13	1060	17	1082	36	1082.0	36.0	2.0	
VSS1_129.FIN2	144.9	0.4896	0.732	0.017	0.0909	0.0011	0.20283	556.3	9.6	560.5	6.5	521	47	560.5	6.5	0.8	
VSS1_130.FIN2	307	12.25	0.842	0.016	0.1011	0.0014	0.50428	619.9	8.9	620.6	8.3	617	36	620.6	8.3	0.1	
VSS1_131.FIN2	250	6.23	1.36	0.091	0.138	0.011	0.70014	867	39	832	65	980	120	832.0	65.0	4.0	Rim
VSS1_131.FIN2	120.1	1.212	2.798	0.063	0.2375	0.0048	0.55929	1352	17	1373	25	1334	38	1334.0	38.0	2.9	Core
VSS1_132.FIN2	333	2.59	6.07	0.25	0.366	0.015	0.93216	1965	38	1994	73	1963	28	1963.0	28.0	1.6	
VSS1_133.FIN2	387	1.868	0.401	0.011	0.0503	0.0011	0.50183	341.2	8.2	316.5	6.8	522	56	316.5	6.8	7.2	
VSS1_134.FIN2	137.9	1.99	0.741	0.014	0.0929	0.0014	0.38238	562	8.2	572.4	8.3	526	42	572.4	8.3	1.9	
VSS1_135.FIN2	111.9	1.815	0.743	0.018	0.0898	0.0016	0.42309	563	10	554.1	9.3	603	50	554.1	9.3	1.6	
VSS1_136.FIN2	197	1.772	0.619	0.02	0.0797	0.0019	0.53181	486	13	494	11	468	64	494.0	11.0	1.6	
VSS1_137.FIN2	362	1.334	0.619	0.015	0.0782	0.0017	0.62202	488.7	9.4	485	10	532	43	485.0	10.0	0.8	
VSS1_139.FIN2	202.1	0.7	0.801	0.022	0.1044	0.0026	0.65701	595	13	640	15	455	48	640.0	15.0	7.6	
VSS1_140.FIN2	107.3	1.446	3.31	0.12	0.2421	0.0085	0.60639	1477	27	1395	44	1631	55	1631.0	55.0	14.5	

Table 6

VSS2_2.FIN2	146	0.971	0.752	0.017	0.0928	0.0014	0.4897	567.6	9.8	571.7	8.4	563	44	571.7	8.4	0.7	
VSS2_3.FIN2	394	2.639	0.466	0.011	0.057	0.0014	0.56894	387.5	7.5	357	8.6	606	48	357.0	8.6	7.9	
VSS2_4.FIN2	193	2.429	4.35	0.09	0.2974	0.007	0.58406	1698	17	1684	36	1747	38	1747.0	38.0	3.6	
VSS2_5.FIN2	125	0.909	0.548	0.013	0.0737	0.0011	0.08282	444.1	8.3	458.1	6.4	388	54	458.1	6.4	3.2	
VSS2_7.FIN2	118.2	0.4478	0.787	0.019	0.0949	0.0014	0.16839	588	11	584.5	8.5	600	58	584.5	8.5	0.6	
VSS2_8.FIN2	189.7	3.12	5.19	0.11	0.3305	0.0063	0.69877	1849	17	1839	30	1876	29	1876.0	29.0	2.0	
VSS2_10.FIN2	299	1.582	3.459	0.066	0.254	0.0052	0.68609	1516	15	1457	27	1596	31	1596.0	31.0	8.7	
VSS2_11.FIN2	201.5	1.602	0.864	0.02	0.0988	0.0022	0.65089	630	11	607	13	719	42	607.0	13.0	3.7	
VSS2_12.FIN2	172	0.64	0.4582	0.009	0.0605	0.0011	0.29913	382.3	6.3	378.4	6.8	407	51	378.4	6.8	1.0	
VSS2_13.FIN2	184.3	2.375	1.68	0.037	0.1635	0.0036	0.64983	1000	14	975	20	1061	39	1061.0	39.0	8.1	
VSS2_14.FIN2	238.1	1.239	0.795	0.02	0.089	0.0022	0.4717	592	11	549	13	767	54	549.0	13.0	7.3	
VSS2_15.FIN2	107.6	1.15	3.065	0.094	0.2342	0.0056	0.76867	1418	24	1355	29	1524	38	1524.0	38.0	11.1	
VSS2_16.FIN2	268	4.88	1.302	0.033	0.1306	0.0032	0.60719	844	14	790	18	1006	45	790.0	18.0	6.4	
VSS2_17.FIN2	282	1.724	3.517	0.076	0.2592	0.0051	0.71849	1526	17	1484	26	1602	28	1602.0	28.0	7.4	
VSS2_18.FIN2	608	2.94	0.967	0.058	0.1061	0.0055	0.64079	670	29	647	32	760	100	647.0	32.0	3.4	
VSS2_19.FIN2	105.4	2.47	0.82	0.023	0.0995	0.0026	0.45201	605	13	611	15	637	59	611.0	15.0	1.0	
VSS2_20.FIN2	645	7.49	0.528	0.012	0.0664	0.0012	0.58116	430.2	7.5	414.6	7	525	42	414.6	7.0	3.6	
VSS2_21.FIN2	43.4	2.513	1.866	0.067	0.1846	0.0062	0.50412	1064	24	1089	33	1019	76	1019.0	76.0	6.9	
VSS2_23.FIN2	106.2	1.567	2.77	0.09	0.2142	0.0064	0.75163	1342	24	1249	34	1545	40	1545.0	40.0	19.2	
VSS2_25.FIN2	130.1	2.01	2.3	0.13	0.204	0.01	0.759	1192	39	1189	54	1238	73	1238.0	73.0	4.0	
VSS2_26.FIN2	104.4	1.357	0.769	0.026	0.0945	0.0033	0.53501	578	16	581	19	548	75	581.0	19.0	0.5	
VSS2_27.FIN2	82.2	0.354	1.872	0.06	0.1766	0.0045	0.61458	1069	20	1047	25	1087	52	1087.0	52.0	3.7	
VSS2_28.FIN2	50.4	0.952	2.808	0.065	0.2414	0.0051	0.56325	1352	17	1392	27	1276	42	1276.0	42.0	9.1	
VSS2_29.FIN2	409	2.45	0.528	0.012	0.0687	0.0013	0.44231	429.7	7.7	428.3	7.9	411	49	428.3	7.9	0.3	
VSS2_30.FIN2	76.5	1.385	0.907	0.03	0.1006	0.0022	0.55783	653	17	618	13	733	61	618.0	13.0	5.4	
VSS2_31.FIN2	358	1.394	0.561	0.016	0.0738	0.0019	0.60862	450	10	459	11	384	52	459.0	11.0	2.0	

Table 6

VSS2_32.FIN2	405	5.34	1.324	0.069	0.128	0.0058	0.68517	851	30	775	33	1031	75	775.0	33.0	8.9	Rim
VSS2_32.FIN2	221.4	2.22	2.453	0.082	0.2043	0.0078	0.83679	1253	24	1196	42	1347	42	1347.0	42.0	11.2	Core
VSS2_33.FIN2	209.9	3.09	0.559	0.021	0.0732	0.0024	0.65136	447	14	455	15	391	65	455.0	15.0	1.8	
VSS2_34.FIN2	245.2	1.064	2.319	0.034	0.2116	0.003	0.7059	1217	11	1237	16	1157	22	1157.0	22.0	6.9	
VSS2_35.FIN2	64.4	2.45	1.951	0.054	0.1773	0.0042	0.41481	1093	18	1051	23	1171	51	1171.0	51.0	10.2	
VSS2_36.FIN2	97.1	2.04	1.959	0.054	0.1857	0.004	0.63947	1096	19	1097	22	1066	46	1066.0	46.0	2.9	
VSS2_37.FIN2	296	3.64	0.551	0.022	0.0691	0.0024	0.58608	447	14	431	14	482	74	431.0	14.0	3.6	
VSS2_38.FIN2	403	7.13	2.101	0.069	0.1816	0.0065	0.70242	1143	23	1072	35	1272	53	1272.0	53.0	15.7	
VSS2_39.FIN2	184	1.33	3.81	0.12	0.2861	0.0092	0.73819	1598	23	1621	48	1530	46	1530.0	46.0	5.9	
VSS2_40.FIN2	361	1.135	0.5724	0.0096	0.0739	0.001	0.45455	458.8	6.2	459.7	6.2	418	35	459.7	6.2	0.2	
VSS2_41.FIN2	46.9	1.139	0.52	0.019	0.0675	0.0013	0.23059	422	13	420.9	7.9	386	77	420.9	7.9	0.3	
VSS2_42.FIN2	417	9.08	0.816	0.022	0.0936	0.0021	0.65496	604	12	577	12	692	48	577.0	12.0	4.5	
VSS2_43.FIN2	341	4.41	0.596	0.031	0.0749	0.0033	0.56976	472	20	465	20	481	99	465.0	20.0	1.5	Rim
VSS2_43.FIN2	343	3.7	0.862	0.036	0.0933	0.0029	0.62266	632	20	574	17	822	72	574.0	17.0	9.2	Core
VSS2_44.FIN2	556	2.883	3.672	0.072	0.2803	0.0061	0.68637	1561	16	1590	30	1521	31	1521.0	31.0	4.5	
VSS2_45.FIN2	124	3.84	2.459	0.08	0.2202	0.0068	0.61307	1256	24	1279	36	1212	54	1212.0	54.0	5.5	
VSS2_46.FIN2	110.5	1.202	4.594	0.092	0.3234	0.0065	0.70706	1743	17	1804	32	1667	29	1667.0	29.0	8.2	
VSS2_47.FIN2	151.7	2.48	3.61	0.12	0.2858	0.0088	0.70141	1540	26	1615	44	1432	47	1432.0	47.0	12.8	
VSS2_48.FIN2	353	1.66	0.633	0.011	0.0815	0.0013	0.33732	498	7.3	505.1	7.7	448	42	505.1	7.7	1.4	
VSS2_50.FIN2	219.3	0.932	0.915	0.015	0.1081	0.0016	0.40227	658.7	8.2	661.4	9.4	639	38	661.4	9.4	0.4	
VSS2_51.FIN2	318	2.8	4.64	0.16	0.288	0.011	0.81052	1744	28	1623	53	1896	39	1896.0	39.0	14.4	
VSS2_52.FIN2	246.4	1.992	3.003	0.052	0.2594	0.0043	0.55669	1405	13	1486	22	1290	30	1290.0	30.0	15.2	
VSS2_53.FIN2	187	1.672	3.153	0.086	0.2522	0.0073	0.74475	1440	22	1446	37	1440	38	1440.0	38.0	0.4	
VSS2_54.FIN2	321	1.091	12.44	0.59	0.485	0.023	0.79276	2617	45	2532	99	2701	51	2701.0	51.0	6.3	
VSS2_55.FIN2	376	18	0.849	0.031	0.0891	0.0045	0.64753	621	17	549	27	911	87	549.0	27.0	11.6	
VSS2_56.FIN2	138.3	1.172	0.618	0.026	0.0778	0.0018	0.2523	487	16	483	11	496	88	483.0	11.0	0.8	

Table 6

VSS2_57.FIN2	140	6.8	0.578	0.043	0.0676	0.0028	0.61739	460	28	422	17	670	150	422.0	17.0	8.3	Rim
VSS2_57.FIN2	27.49	1.048	1.964	0.076	0.1864	0.0043	0.29162	1103	28	1106	25	1092	84	1092.0	84.0	1.3	Core
VSS2_58.FIN2	387	6.25	0.615	0.015	0.0733	0.0015	0.61228	486.4	9.3	455.8	8.9	628	51	455.8	8.9	6.3	
VSS2_59.FIN2	258	2.3	2.078	0.038	0.2047	0.0039	0.6942	1139	13	1199	21	1042	31	1042.0	31.0	15.1	
VSS2_60.FIN2	581	2.223	3.897	0.096	0.276	0.0061	0.65904	1609	20	1569	31	1678	34	1678.0	34.0	6.5	
VSS2_61.FIN2	449	0.888	0.456	0.011	0.0571	0.001	0.53829	380.5	7.9	358	6.1	518	47	358.0	6.1	5.9	
VSS2_62.FIN2	163	4.34	2.419	0.042	0.2213	0.0039	0.57336	1247	12	1287	21	1176	33	1176.0	33.0	9.4	
VSS2_63.FIN2	130.4	2.69	4.64	0.18	0.299	0.011	0.71045	1744	32	1679	56	1846	51	1846.0	51.0	9.0	
VSS2_64.FIN2	335	11.2	3.31	0.15	0.206	0.0086	0.93251	1467	36	1203	46	1901	29	1901.0	29.0	36.7	
VSS2_65.FIN2	717	17.93	0.561	0.011	0.0701	0.0013	0.52109	452.7	7.7	436.4	8.1	547	43	436.4	8.1	3.6	
VSS2_66.FIN2	105.8	1.021	0.993	0.03	0.1154	0.0034	0.59455	696	15	703	19	670	58	703.0	19.0	1.0	
VSS2_68.FIN2	118	2.39	0.938	0.03	0.1109	0.0033	0.48873	670	16	677	19	639	68	677.0	19.0	1.0	
VSS2_69.FIN2	37.2	0.951	0.698	0.034	0.0869	0.0028	0.53128	532	20	536	17	494	85	536.0	17.0	0.8	
VSS2_70.FIN2	102.8	0.848	1.741	0.034	0.1712	0.0032	0.37581	1021	13	1018	17	1017	44	1017.0	44.0	0.1	
VSS2_71.FIN2	141.5	3.621	1.971	0.043	0.1906	0.0035	0.66604	1102	14	1124	19	1035	34	1035.0	34.0	8.6	
VSS2_72.FIN2	170.9	1.605	2.996	0.064	0.2461	0.0041	0.58441	1404	16	1417	21	1377	34	1377.0	34.0	2.9	
VSS2_73.FIN2	490	3.63	1.761	0.052	0.1727	0.0064	0.85562	1025	20	1024	35	1061	36	1061.0	36.0	3.5	
VSS2_74.FIN2	133.3	1.568	0.642	0.018	0.0795	0.0018	0.36438	503	11	493	11	522	62	493.0	11.0	2.0	
VSS2_75.FIN2	327	7.12	4.87	0.11	0.3175	0.0083	0.81338	1789	20	1779	39	1798	28	1798.0	28.0	1.1	
VSS2_76.FIN2	55.8	1.247	0.623	0.036	0.0755	0.0035	0.4937	491	23	469	21	600	120	469.0	21.0	4.5	Rim
VSS2_76.FIN2	38.4	0.831	1.186	0.077	0.1268	0.0061	0.48213	788	36	769	35	840	130	769.0	35.0	2.4	Core
VSS2_77.FIN2	371.9	1.81	2.08	0.032	0.1946	0.0029	0.51622	1141	11	1146	15	1127	30	1127.0	30.0	1.7	
VSS2_78.FIN2	224	1.749	1.448	0.09	0.1437	0.007	0.7744	903	38	864	39	999	84	999.0	84.0	13.5	Rim
VSS2_78.FIN2	46.6	1.923	3.06	0.1	0.2445	0.0068	0.63818	1417	26	1408	35	1426	48	1426.0	48.0	1.3	Core
VSS2_79.FIN2	707	14.35	1.424	0.027	0.1415	0.0027	0.75734	897	11	852	15	1025	24	1025.0	24.0	16.9	
VSS2_80.FIN2	546	6.02	0.5503	0.009	0.07181	0.00091	0.65378	444.5	6	446.9	5.5	438	28	446.9	5.5	0.5	

Table 6

VSS2_82.FIN2	402.7	3.96	0.571	0.016	0.0743	0.0019	0.76859	457	10	462	11	424	43	462.0	11.0	1.1	
VSS2_83.FIN2	327	0.86	0.615	0.018	0.0726	0.002	0.56868	484	11	451	12	642	54	451.0	12.0	6.8	
VSS2_84.FIN2	520	0.867	0.578	0.014	0.0706	0.0015	0.4569	462.6	8.8	439.3	9.3	582	54	439.3	9.3	5.0	
VSS2_85.FIN2	124	1.31	3.64	0.052	0.2784	0.0034	0.58377	1556	11	1582	17	1524	23	1524.0	23.0	3.8	
VSS2_86.FIN2	173.9	1.341	6.8	0.28	0.383	0.014	0.70611	2066	39	2077	67	2086	54	2086.0	54.0	0.4	
VSS2_87.FIN2	91.5	2.695	2.03	0.059	0.1863	0.004	0.66807	1121	20	1101	22	1169	39	1169.0	39.0	5.8	
VSS2_88.FIN2	346	3.01	3.73	0.16	0.268	0.011	0.66771	1566	33	1524	56	1627	62	1627.0	62.0	6.3	
VSS2_89.FIN2	328	1.508	0.952	0.019	0.1103	0.0022	0.50757	677.4	9.9	674	13	691	43	674.0	13.0	0.5	
VSS2_90.FIN2	53.5	3.51	1.887	0.046	0.1752	0.003	0.43718	1073	16	1040	16	1138	50	1138.0	50.0	8.6	
VSS2_91.FIN2	125	1.8	0.398	0.016	0.0533	0.0018	0.5365	339	12	334	11	370	74	334.0	11.0	1.5	
VSS2_92.FIN2	199.2	1.525	0.516	0.022	0.0662	0.003	0.402	423	15	413	18	479	96	413.0	18.0	2.4	
VSS2_93.FIN2	296	5	0.512	0.019	0.0665	0.0025	0.69494	417	13	414	15	425	62	414.0	15.0	0.7	
VSS2_94.FIN2	115.6	1.186	3.74	0.12	0.291	0.0083	0.57789	1571	26	1643	42	1474	53	1474.0	53.0	11.5	
VSS2_95.FIN2	158	0.871	6.2	0.15	0.3365	0.0089	0.76807	1999	22	1865	43	2147	31	2147.0	31.0	13.1	
VSS2_96.FIN2	346	1.377	0.624	0.014	0.059	0.0016	0.54651	491.1	8.7	369	9.9	1116	50	DISC	DISC	24.9	
VSS2_97.FIN2	604	4.89	1.65	0.14	0.0833	0.0033	0.62302	960	54	519	21	2110	130	DISC	DISC	45.9	
VSS2_98.FIN2	92.3	1.718	3.467	0.072	0.2722	0.0063	0.5258	1515	16	1549	32	1473	42	1473.0	42.0	5.2	
VSS2_99.FIN2	133.4	0.754	1.293	0.038	0.118	0.0024	0.43152	840	17	719	14	1190	55	719.0	14.0	14.4	
VSS2_100.FIN2	91	1.446	1.841	0.031	0.1773	0.0025	0.49902	1058	11	1052	14	1088	32	1088.0	32.0	3.3	
VSS2_101.FIN2	371	1.326	0.537	0.032	0.0569	0.0035	0.55907	434	21	357	21	890	120	357.0	21.0	17.7	
VSS2_102.FIN2	265	12	0.883	0.05	0.1037	0.007	0.69428	640	27	635	41	700	100	635.0	41.0	0.8	Rim
VSS2_102.FIN2	86.9	1.397	1.517	0.06	0.1413	0.0033	0.45695	930	24	851	19	1146	75	1146.0	75.0	25.7	Core
VSS2_103.FIN2	81.6	0.865	4.361	0.081	0.3195	0.0052	0.6327	1701	15	1786	26	1620	27	1620.0	27.0	10.2	
VSS2_104.FIN2	142.9	3.05	1.771	0.034	0.1805	0.0029	0.57163	1032	12	1069	16	974	34	974.0	34.0	9.8	
VSS2_105.FIN2	204	1.375	0.768	0.014	0.0963	0.0013	0.40224	577.1	8.1	592.5	7.6	526	40	592.5	7.6	2.7	
VSS2_106.FIN2	224.2	1.056	0.792	0.023	0.0971	0.0025	0.55216	589	13	597	15	573	56	597.0	15.0	1.4	

Table 6

VSS2_107.FIN2	409	7.64	1.725	0.056	0.1703	0.0055	0.67929	1013	21	1012	30	1039	52	1039.0	52.0	2.6	
VSS2_108.FIN2	143.9	2.578	5.26	0.24	0.306	0.0092	0.73277	1852	35	1717	45	2027	49	2027.0	49.0	15.3	
VSS2_109.FIN2	361	17.4	0.524	0.02	0.0674	0.0026	0.69641	425	14	420	16	475	65	420.0	16.0	1.2	
VSS2_110.FIN2	95.4	1.249	1.487	0.038	0.1435	0.0036	0.56569	921	15	863	20	1075	47	1075.0	47.0	19.7	
VSS2_111.FIN2	325	2.9	3.74	0.11	0.2696	0.0078	0.66452	1577	24	1536	39	1628	46	1628.0	46.0	5.7	
VSS2_112.FIN2	117.6	2.34	1.652	0.053	0.1649	0.0042	0.61702	985	20	985	24	980	55	980.0	55.0	0.5	
VSS2_113.FIN2	135.8	7.14	1.591	0.063	0.1436	0.0064	0.43605	961	24	863	36	1205	89	1205.0	89.0	28.4	Rim
VSS2_113.FIN2	64.7	5.27	1.895	0.064	0.1818	0.0052	0.26706	1076	23	1076	29	1083	78	1083.0	78.0	0.6	Core
VSS2_114.FIN2	111.1	1.437	0.526	0.019	0.0564	0.002	0.62996	427	12	353	12	862	66	353.0	12.0	17.3	
VSS2_115.FIN2	347	2.36	1.129	0.03	0.0921	0.0025	0.57461	764	14	568	15	1400	49	DISC	DISC	25.7	
VSS2_116.FIN2	326.8	1.398	2.879	0.045	0.2143	0.0027	0.55637	1374	12	1251	14	1570	26	1570.0	26.0	20.3	
VSS2_117.FIN2	305	12.3	0.4903	0.0088	0.0645	0.001	0.48545	405.2	6.1	402.8	6.4	427	40	402.8	6.4	0.6	
VSS2_118.FIN2	173.4	2.316	2.721	0.066	0.2358	0.005	0.73223	1329	18	1363	26	1286	33	1286.0	33.0	6.0	
VSS2_119.FIN2	179	11.7	2.405	0.045	0.22	0.0043	0.56578	1243	14	1280	23	1185	37	1185.0	37.0	8.0	
VSS2_120.FIN2	169	1.924	0.524	0.014	0.0703	0.001	0.37253	426.5	9.1	437.6	6.3	369	54	437.6	6.3	2.6	
VSS2_121.FIN2	493	2.37	0.358	0.018	0.043	0.0021	0.36668	310	14	271	13	560	110	271.0	13.0	12.6	
VSS2_122.FIN2	196.2	1.394	5.78	0.25	0.348	0.013	0.57896	1935	39	1919	59	1970	66	1970.0	66.0	2.6	
VSS2_123.FIN2	255	1.033	0.992	0.017	0.1153	0.0017	0.57506	701.8	7.9	703	10	714	29	703.0	10.0	0.2	
VSS2_124.FIN2	615	7.35	0.625	0.016	0.0606	0.0013	0.64193	493	10	378.9	7.6	1068	41	DISC	DISC	23.1	
VSS2_125.FIN2	170	1.315	0.908	0.026	0.1077	0.002	0.40611	654	14	659	12	640	64	659.0	12.0	0.8	
VSS2_126.FIN2	229	1.004	3.128	0.066	0.2546	0.0055	0.68935	1436	16	1460	28	1418	32	1418.0	32.0	3.0	
VSS2_127.FIN2	226	4.24	3.57	0.15	0.2246	0.0094	0.78811	1536	34	1302	50	1898	49	1898.0	49.0	31.4	
VSS2_129.FIN2	237.4	2.369	2.837	0.047	0.236	0.0044	0.42876	1364	13	1365	22	1361	35	1361.0	35.0	0.3	
VSS2_130.FIN2	98.1	1.031	1.551	0.034	0.1558	0.0031	0.48379	949	14	933	17	982	45	982.0	45.0	5.0	
VSS2_132.FIN2	108.9	0.526	0.665	0.026	0.0759	0.0019	0.64048	514	16	471	11	716	66	471.0	11.0	8.4	
VSS2_133.FIN2	310	3.19	1.03	0.056	0.1013	0.0068	0.68323	715	29	619	40	1107	97	619.0	40.0	13.4	

Table 6

VSS2_134.FIN2	233	1.59	0.587	0.03	0.0521	0.002	0.45651	467	20	327	12	1212	94	DISC	DISC	30.0	
VSS2_135.FIN2	199.6	1.454	0.529	0.016	0.068	0.002	0.55934	430	11	424	12	456	60	424.0	12.0	1.4	
VSS2_136.FIN2	309	1.248	3.412	0.053	0.2658	0.0049	0.61875	1508	13	1521	26	1481	30	1481.0	30.0	2.7	
VSS2_137.FIN2	222	4.4	0.787	0.03	0.096	0.0044	0.60657	589	17	589	26	585	78	589.0	26.0	0.0	
VSS2_138.FIN2	44.3	1.376	1.781	0.042	0.1628	0.0028	0.37359	1034	16	972	15	1156	47	1156.0	47.0	15.9	
VSS2_139.FIN2	315	4.87	0.605	0.024	0.0675	0.0019	0.47724	476	15	421	11	706	73	421.0	11.0	11.6	
VSS2_140.FIN2	94	0.751	0.412	0.014	0.0513	0.0012	0.29528	349	10	322.4	7.3	494	76	322.4	7.3	7.6	

Table 6: VSS1 and VSS2 sample data.

Table 7

Sample Name:								207/235		206/238		207/206		Best age			
Grain #	[U] ppm	U/Th	207/235	2σ error	206/238	2σ error	RHO	Age Ma	2σ error	Age (Ma)	2σ error	Age (Ma)	2σ error	(Ma)	2σ error	% Discordance*	Rim/Core
ALSS1_1.FIN2	220.4	0.954	0.84	0.016	0.0978	0.0014	0.51425	617.9	9	601.5	8	671	38	601.5	8.0	2.7	
ALSS1_2.FIN2	104.5	5.6	0.339	0.02	0.0426	0.0022	0.53594	298	14	271	13	490	110	271.0	13.0	9.1	
ALSS1_3.FIN2	91	3.459	6.91	0.24	0.3612	0.0085	0.72062	2090	31	1984	40	2189	43	2189.0	43.0	9.4	
ALSS1_4.FIN2	949	8.6	1.37	0.022	0.1101	0.0019	0.7918	874.9	9.2	673	11	1416	23	673.0	11.0	23.1	
ALSS1_5.FIN2	76.6	2.044	0.708	0.026	0.0642	0.0021	0.60749	542	16	401	13	1178	64	401.0	13.0	26.0	
ALSS1_6.FIN2	455	2.369	2.403	0.049	0.2069	0.0029	0.37772	1241	15	1212	16	1285	40	1285.0	40.0	5.7	
ALSS1_8.FIN2	201.1	3.096	2.608	0.077	0.1713	0.0054	0.70074	1299	21	1017	29	1797	41	1797.0	41.0	43.4	
ALSS1_9.FIN2	227.7	2.259	2.696	0.056	0.2163	0.005	0.764	1324	15	1261	27	1437	28	1437.0	28.0	12.2	
ALSS1_10.FIN2	50.4	0.93	0.559	0.051	0.0657	0.0057	0.61246	447	32	410	34	650	160	410.0	34.0	8.3	Rim
ALSS1_10.FIN2	130.8	3.85	3.339	0.073	0.2342	0.0054	0.5824	1489	17	1356	28	1694	38	1694.0	38.0	20.0	Core
ALSS1_11.FIN2	232.4	2.403	1.799	0.076	0.176	0.0056	0.57546	1037	27	1043	31	1016	65	1016.0	65.0	2.7	
ALSS1_12.FIN2	218.9	0.794	0.503	0.024	0.0659	0.0027	0.63815	409	16	411	16	393	80	411.0	16.0	0.5	
ALSS1_13.FIN2	140.3	0.941	9.66	0.39	0.394	0.016	0.84635	2384	39	2126	75	2636	38	2636.0	38.0	19.3	
ALSS1_14.FIN2	505	2.02	9.18	0.25	0.379	0.011	0.74878	2344	25	2063	50	2613	32	2613.0	32.0	21.0	
ALSS1_15.FIN2	154.3	2.049	2.862	0.047	0.2292	0.0024	0.58642	1369	13	1330	13	1435	25	1435.0	25.0	7.3	
ALSS1_16.FIN2	93.5	3.18	0.611	0.023	0.0762	0.0027	0.68659	482	15	475	16	530	64	475.0	16.0	1.5	
ALSS1_17.FIN2	181.1	1.687	0.84	0.015	0.0991	0.0012	0.39148	618.9	8	608.8	7	649	37	608.8	7.0	1.6	
ALSS1_19.FIN2	241.5	1.803	0.417	0.012	0.0572	0.0015	0.45575	355.1	9.2	358.3	9.2	339	64	358.3	9.2	0.9	
ALSS1_20.FIN2	236.1	2.78	1.801	0.075	0.1613	0.0072	0.65003	1039	26	961	39	1235	69	1235.0	69.0	22.2	
ALSS1_21.FIN2	369	2.06	0.594	0.023	0.0728	0.003	0.56365	473	14	453	18	585	77	453.0	18.0	4.2	Rim
ALSS1_21.FIN2	171	4.98	0.805	0.018	0.0972	0.0018	0.45617	598	10	598	10	603	47	598.0	10.0	0.0	Core
ALSS1_22.FIN2	311	30.1	0.412	0.02	0.0545	0.0023	0.3831	349	15	342	14	400	110	342.0	14.0	2.0	Rim

Table 7

ALSS1_22.FIN2	131.7	12.6	0.447	0.017	0.0613	0.0015	-0.11191	375	12	383.3	8.9	330	100	383.3	8.9	2.2	Core
ALSS1_22.FIN2	27.9	2.3	0.66	0.053	0.0828	0.0034	-0.039304	511	32	513	20	460	200	513.0	20.0	0.4	Core
ALSS1_23.FIN2	326	17.96	0.531	0.029	0.0591	0.0018	0.425	431	19	370	11	770	100	370.0	11.0	14.2	
ALSS1_24.FIN2	106.3	1.512	4.095	0.098	0.2856	0.0039	0.61598	1651	20	1618	19	1691	37	1691.0	37.0	4.3	
ALSS1_25.FIN2	77.3	4.84	5.01	0.23	0.326	0.017	0.56169	1795	42	1810	82	1800	85	1800.0	85.0	0.6	
ALSS1_27.FIN2	367	1.125	0.581	0.01	0.0706	0.0011	0.63007	464.4	6.6	439.6	6.5	593	33	439.6	6.5	5.3	
ALSS1_28.FIN2	68.1	21.6	0.367	0.017	0.0515	0.0021	0.47737	316	13	323	13	291	91	323.0	13.0	2.2	
ALSS1_29.FIN2	96.7	1.587	5.67	0.15	0.347	0.01	0.63792	1919	23	1913	50	1940	42	1940.0	42.0	1.4	
ALSS1_30.FIN2	181.9	1.532	0.918	0.034	0.1066	0.0036	0.66338	657	18	652	21	682	62	652.0	21.0	0.8	
ALSS1_31.FIN2	163.4	6.82	0.816	0.014	0.09802	0.00095	0.32885	604.9	7.8	602.7	5.6	622	34	602.7	5.6	0.4	
ALSS1_32.FIN2	397	3.87	0.325	0.013	0.0456	0.0017	0.53985	285	10	287	10	250	72	287.0	10.0	0.7	
ALSS1_33.FIN2	203.1	1.882	0.4967	0.0084	0.06564	0.00081	0.3025	409.5	5.5	409.8	4.9	407	39	409.8	4.9	0.1	
ALSS1_34.FIN2	398	0.915	0.523	0.013	0.06684	0.00083	0.39896	427.6	8.2	417.1	5	479	51	417.1	5.0	2.5	
ALSS1_35.FIN2	322	5.38	2.29	0.19	0.158	0.0093	0.81831	1201	59	945	52	1705	94	1705.0	94.0	44.6	Rim
ALSS1_35.FIN2	89.7	1.727	5.88	0.12	0.3314	0.005	0.59236	1956	17	1844	24	2079	29	2079.0	29.0	11.3	Core
ALSS1_36.FIN2	238	4.84	1.965	0.071	0.1867	0.0071	0.60401	1096	24	1099	38	1113	61	1113.0	61.0	1.3	
ALSS1_37.FIN2	155.6	3.19	1.113	0.049	0.1104	0.0049	0.63169	759	24	674	28	1029	75	674.0	28.0	11.2	
ALSS1_38.FIN2	78.3	2.554	1.263	0.036	0.1177	0.0023	0.25853	825	16	717	13	1112	56	717.0	13.0	13.1	
ALSS1_39.FIN2	211.9	1.272	0.377	0.012	0.0419	0.0013	0.72891	323.8	9.1	264.4	7.8	776	48	264.4	7.8	18.3	
ALSS1_40.FIN2	124.3	1.467	0.816	0.016	0.0939	0.0016	0.39563	605.7	9.1	578.6	9.2	705	44	578.6	9.2	4.5	
ALSS1_41.FIN2	273	2.655	2.481	0.075	0.2061	0.0053	0.75879	1261	23	1206	28	1362	38	1362.0	38.0	11.5	
ALSS1_43.FIN2	412	1.01	0.775	0.037	0.0909	0.0045	0.55667	580	22	561	26	665	95	561.0	26.0	3.3	
ALSS1_44.FIN2	117.9	1.522	3.73	0.11	0.2641	0.0075	0.68259	1574	23	1508	38	1654	43	1654.0	43.0	8.8	
ALSS1_45.FIN2	104.1	1.783	3.88	0.09	0.2766	0.0057	0.71271	1603	19	1572	29	1663	31	1663.0	31.0	5.5	
ALSS1_46.FIN2	806	21.4	0.476	0.016	0.064	0.0019	0.25065	395	11	400	12	389	83	400.0	12.0	1.3	
ALSS1_47.FIN2	97.5	1.115	11.83	0.13	0.4771	0.0048	0.68291	2589	11	2513	21	2652	15	2652.0	15.0	5.2	

Table 7

ALSS1_48.FIN2	145.3	1.532	6.88	0.25	0.3345	0.0073	0.8226	2078	31	1856	35	2306	32	2306.0	32.0	19.5	
ALSS1_49.FIN2	757	3.15	0.4499	0.009	0.05681	0.00097	0.63206	376.5	6.3	356.1	5.9	511	36	356.1	5.9	5.4	
ALSS1_50.FIN2	1420	24.9	0.449	0.034	0.0547	0.0028	0.77331	376	24	343	17	580	110	343.0	17.0	8.8	Rim
ALSS1_50.FIN2	216.3	1.838	1.637	0.078	0.1379	0.0045	0.76841	982	30	833	26	1332	60	833.0	26.0	15.2	Core
ALSS1_50.FIN2	87	0.809	3.3	0.13	0.2494	0.0056	0.53461	1478	30	1435	29	1520	63	1520.0	63.0	5.6	Core
ALSS1_51.FIN2	192.7	1.689	1.739	0.023	0.1717	0.0021	0.51792	1022.9	8.8	1021	11	1027	25	1027.0	25.0	0.6	
ALSS1_52.FIN2	206.1	2.438	5.663	0.048	0.348	0.0026	0.63769	1924.8	7.3	1925	12	1922	12	1922.0	12.0	0.2	
ALSS1_53.FIN2	274.8	1.101	3.758	0.062	0.2747	0.0041	0.77915	1582	13	1564	21	1606	20	1606.0	20.0	2.6	
ALSS1_54.FIN2	454	1.716	2.076	0.055	0.1934	0.0051	0.89118	1137	18	1139	28	1144	23	1144.0	23.0	0.4	
ALSS1_55.FIN2	301	9.14	0.2781	0.0099	0.0375	0.0011	0.10405	248.8	7.9	237.4	6.9	364	86	237.4	6.9	4.6	Rim
ALSS1_55.FIN2	645	6.67	1.532	0.041	0.1479	0.0032	0.83927	944	17	889	18	1066	31	1066.0	31.0	16.6	Core
ALSS1_56.FIN2	281	1.71	3.696	0.075	0.2582	0.0049	0.72608	1565	16	1479	25	1689	26	1689.0	26.0	12.4	
ALSS1_57.FIN2	92	3.26	0.399	0.039	0.0479	0.0038	0.66812	338	28	301	23	590	160	301.0	23.0	10.9	Rim
ALSS1_57.FIN2	25.34	2.121	0.526	0.04	0.0678	0.0021	0.32733	422	26	423	13	370	140	423.0	13.0	0.2	Core
ALSS1_58.FIN2	35.37	1.968	1.658	0.052	0.1575	0.0046	0.44456	990	20	944	25	1092	65	1092.0	65.0	13.6	
ALSS1_59.FIN2	233	5.01	0.504	0.035	0.0659	0.0035	0.48362	412	23	411	21	410	130	411.0	21.0	0.2	Rim
ALSS1_59.FIN2	196.9	3.315	0.997	0.034	0.1047	0.0027	0.74829	700	18	641	16	886	47	641.0	16.0	8.4	Core
ALSS1_60.FIN2	125.8	0.568	0.906	0.024	0.1067	0.0023	0.55639	652	13	653	13	633	50	653.0	13.0	0.2	
ALSS1_61.FIN2	201	3.31	1.871	0.032	0.1807	0.0033	0.60997	1070	12	1070	18	1068	31	1068.0	31.0	0.2	
ALSS1_62.FIN2	103	0.83	1.817	0.037	0.1729	0.0023	0.42202	1050	13	1027	12	1088	37	1088.0	37.0	5.6	
ALSS1_63.FIN2	186	1.38	0.84	0.018	0.1025	0.0013	0.37626	619.6	9.9	629.1	7.9	566	45	629.1	7.9	1.5	
ALSS1_64.FIN2	178	3.04	1.248	0.079	0.1097	0.0061	0.52909	819	36	670	36	1250	120	670.0	36.0	18.2	Rim
ALSS1_64.FIN2	96.5	2.452	1.698	0.047	0.1654	0.0029	0.62602	1003	17	986	16	1035	43	1035.0	43.0	4.7	Core
ALSS1_65.FIN2	489	2.71	0.736	0.03	0.0848	0.0031	0.75434	557	17	524	19	691	58	524.0	19.0	5.9	
ALSS1_66.FIN2	428	5.21	0.731	0.014	0.0907	0.0015	0.73618	557	8.7	559.2	8.7	543	32	559.2	8.7	0.4	
ALSS1_67.FIN2	135	3.113	2.612	0.036	0.2219	0.0023	0.64901	1302	10	1292	12	1328	22	1328.0	22.0	2.7	

Table 7

ALSS1_68.FIN2	13.69	1.86	0.684	0.057	0.0774	0.0033	0.094684	534	39	480	19	710	190	480.0	19.0	10.1	
ALSS1_69.FIN2	235	0.862	0.47	0.015	0.0524	0.001	0.42804	390	10	329.4	6.3	748	61	329.4	6.3	15.5	
ALSS1_70.FIN2	470	3.379	3.645	0.058	0.2452	0.0042	0.85523	1558	13	1412	22	1760	16	1760.0	16.0	19.8	
ALSS1_71.FIN2	300.8	2.8	0.505	0.018	0.0655	0.0023	0.69911	414	13	408	14	451	59	408.0	14.0	1.4	
ALSS1_72.FIN2	103.3	1.458	0.932	0.033	0.1061	0.0036	0.45874	667	18	649	21	726	73	649.0	21.0	2.7	
ALSS1_73.FIN2	150.1	1.75	1.484	0.043	0.1381	0.0038	0.37864	922	18	833	21	1128	65	833.0	21.0	9.7	
ALSS1_74.FIN2	236.3	0.883	0.594	0.016	0.0666	0.0012	0.54676	472	10	415.7	7.5	750	49	415.7	7.5	11.9	
ALSS1_75.FIN2	602	4.04	0.493	0.023	0.0642	0.0032	0.64853	403	15	400	20	457	82	400.0	20.0	0.7	
ALSS1_76.FIN2	129	3.93	0.612	0.021	0.0794	0.0025	0.45311	484	13	492	15	441	77	492.0	15.0	1.7	
ALSS1_77.FIN2	201	2.09	4.067	0.064	0.2952	0.0044	0.52535	1646	13	1666	22	1623	28	1623.0	28.0	2.6	
ALSS1_78.FIN2	36.5	1.697	0.461	0.026	0.0592	0.0021	0.45422	382	18	370	13	460	100	370.0	13.0	3.1	
ALSS1_79.FIN2	189.4	1.595	3.238	0.042	0.2492	0.0024	0.51977	1465	10	1434	12	1509	22	1509.0	22.0	5.0	
ALSS1_80.FIN2	125.6	1.328	4.433	0.092	0.2932	0.0043	0.47037	1715	17	1656	22	1785	35	1785.0	35.0	7.2	
ALSS1_81.FIN2	205.4	1.78	2.18	0.045	0.1884	0.004	0.47155	1175	14	1112	22	1286	43	1286.0	43.0	13.5	
ALSS1_82.FIN2	267	4.45	1.088	0.049	0.0951	0.0042	0.59194	742	24	584	25	1267	75	584.0	25.0	21.3	
ALSS1_84.FIN2	223	1.385	0.836	0.013	0.1004	0.0011	0.31187	617.9	6.9	616.7	6.2	615	34	616.7	6.2	0.2	
ALSS1_85.FIN2	222.5	1.996	4.085	0.05	0.2925	0.0032	0.54853	1651	10	1653	16	1649	22	1649.0	22.0	0.2	
ALSS1_86.FIN2	55.2	0.428	5.24	0.18	0.32	0.011	0.68732	1843	29	1783	53	1938	48	1938.0	48.0	8.0	
ALSS1_87.FIN2	105.9	2.8	10.95	0.28	0.4553	0.0079	0.89515	2509	25	2416	35	2588	22	2588.0	22.0	6.6	
ALSS1_89.FIN2	219.6	2.217	0.844	0.037	0.0965	0.0037	0.51946	616	20	593	22	696	82	593.0	22.0	3.7	
ALSS1_90.FIN2	230.6	1.338	3.675	0.081	0.2508	0.005	0.73884	1562	18	1440	25	1724	28	1724.0	28.0	16.5	
ALSS1_91.FIN2	414	14.24	0.748	0.05	0.0821	0.0038	0.60955	562	29	508	23	770	110	508.0	23.0	9.6	
ALSS1_92.FIN2	47.7	0.969	2.032	0.037	0.187	0.0022	0.090552	1123	13	1105	12	1166	41	1166.0	41.0	5.2	
ALSS1_93.FIN2	138	1.239	0.834	0.015	0.0986	0.0013	0.53501	615.3	8.4	606.3	7.7	638	37	606.3	7.7	1.5	
ALSS1_94.FIN2	278.6	4.69	0.716	0.028	0.0698	0.0029	0.53332	550	16	435	18	1050	79	435.0	18.0	20.9	
ALSS1_96.FIN2	93.6	1.668	1.461	0.055	0.1376	0.0051	0.70063	913	23	829	28	1110	60	829.0	28.0	9.2	

Table 7

ALSS1_97.FIN2	499	3.84	2.507	0.064	0.2162	0.0049	0.67924	1267	19	1260	26	1284	40	1284.0	40.0	1.9	
ALSS1_98.FIN2	75.5	1.29	0.872	0.028	0.1035	0.003	0.56431	639	17	634	17	654	73	634.0	17.0	0.8	
ALSS1_99.FIN2	561	1.02	0.51	0.016	0.0554	0.0017	0.53475	416	11	347	10	838	62	347.0	10.0	16.6	
ALSS1_100.FIN2	436	0.698	0.521	0.011	0.0681	0.0016	0.35876	425.5	7.2	424.8	9.5	422	57	424.8	9.5	0.2	
ALSS1_101.FIN2	283	2.31	0.607	0.025	0.0706	0.0027	0.53101	479	16	439	16	665	84	439.0	16.0	8.4	
ALSS1_102.FIN2	238.5	4.03	2.72	0.11	0.1682	0.0067	0.81119	1323	28	999	37	1917	45	1917.0	45.0	47.9	
ALSS1_103.FIN2	133.9	9.58	1.34	0.046	0.1242	0.0028	0.548	859	20	754	16	1147	57	754.0	16.0	12.2	
ALSS1_104.FIN2	80	1.948	2.162	0.048	0.1973	0.0037	0.38586	1167	15	1160	20	1191	48	1191.0	48.0	2.6	
ALSS1_105.FIN2	445	3.5	3.85	0.1	0.2803	0.0048	0.79644	1596	21	1591	24	1607	32	1607.0	32.0	1.0	
ALSS1_106.FIN2	97.3	0.657	1.565	0.037	0.1627	0.0028	0.32879	956	15	971	16	929	49	929.0	49.0	4.5	
ALSS1_107.FIN2	338	4.06	0.907	0.029	0.1042	0.0036	0.54582	655	16	638	21	709	72	638.0	21.0	2.6	
ALSS1_108.FIN2	200.7	1.002	0.823	0.018	0.0978	0.0015	0.29168	608	9.9	601.3	8.8	624	49	601.3	8.8	1.1	
ALSS1_109.FIN2	294	3.66	1.877	0.03	0.1858	0.0027	0.61381	1072	11	1098	15	1025	28	1025.0	28.0	7.1	
ALSS1_110.FIN2	497	31.9	0.996	0.023	0.1046	0.0023	0.61474	700	12	641	14	905	43	641.0	14.0	8.4	
ALSS1_111.FIN2	977	253	0.4841	0.0074	0.06315	0.00069	0.42268	400.5	5	394.7	4.2	438	32	394.7	4.2	1.4	
ALSS1_112.FIN2	547	6.48	0.403	0.011	0.0541	0.0014	0.56156	343.5	7.7	339.4	8.6	365	54	339.4	8.6	1.2	
ALSS1_114.FIN2	209	1.627	0.3913	0.0091	0.0547	0.00089	0.35478	334.5	6.7	343.2	5.5	277	50	343.2	5.5	2.6	
ALSS1_115.FIN2	838	11.91	0.466	0.01	0.0561	0.0012	0.59196	387.7	6.9	351.5	7.1	610	41	351.5	7.1	9.3	
ALSS1_116.FIN2	466	2.656	0.445	0.011	0.0543	0.0012	0.58067	373.3	7.5	341	7.4	580	44	341.0	7.4	8.7	
ALSS1_117.FIN2	295	1.894	0.492	0.035	0.0544	0.0038	0.68977	404	23	341	23	790	110	341.0	23.0	15.6	Rim
ALSS1_117.FIN2	337	1.871	0.75	0.026	0.0879	0.0044	0.75012	567	15	542	26	685	70	542.0	26.0	4.4	Core
ALSS1_118.FIN2	279	4.09	0.704	0.013	0.0846	0.0014	0.507	540	8	523.5	8.1	602	41	523.5	8.1	3.1	
ALSS1_119.FIN2	288	1.714	0.809	0.016	0.0965	0.0018	0.52519	600.3	9	594	11	626	41	594.0	11.0	1.0	
ALSS1_120.FIN2	250	5.52	0.361	0.02	0.0456	0.0022	0.4881	311	15	287	14	490	110	287.0	14.0	7.7	
ALSS1_121.FIN2	181.9	0.622	1.392	0.064	0.1373	0.005	0.49509	879	28	834	30	1034	85	834.0	30.0	5.1	
ALSS1_122.FIN2	144.2	2.293	0.824	0.02	0.096	0.0016	0.45399	609	11	590.8	9.7	679	47	590.8	9.7	3.0	

Table 7

ALSS1_123.FIN2	62.4	1.467	5.77	0.21	0.342	0.013	0.6126	1928	33	1888	62	1977	61	1977.0	61.0	4.5	
ALSS1_124.FIN2	143.4	1.54	0.843	0.025	0.0976	0.0023	0.36211	619	13	600	13	697	58	600.0	13.0	3.1	
ALSS1_125.FIN2	206	1.989	0.761	0.025	0.0807	0.0023	0.39492	576	15	500	14	885	72	500.0	14.0	13.2	
ALSS1_126.FIN2	100.8	2.05	0.581	0.032	0.075	0.0042	0.61133	466	21	465	25	460	100	465.0	25.0	0.2	
ALSS1_127.FIN2	148.8	3.1	0.97	0.052	0.1099	0.0058	0.35335	679	26	674	35	730	110	674.0	35.0	0.7	
ALSS1_128.FIN2	496	0.657	1.172	0.068	0.1092	0.0064	0.65103	780	32	666	37	1155	92	666.0	37.0	14.6	Rim
ALSS1_128.FIN2	182	2.2	2.36	0.18	0.189	0.014	0.71622	1210	56	1109	77	1420	120	1420.0	120.0	21.9	Core
ALSS1_129.FIN2	570	5.42	1.447	0.025	0.1486	0.003	0.63251	907	11	895	18	943	34	943.0	34.0	5.1	
ALSS1_131.FIN2	369	2.53	0.771	0.017	0.0964	0.0022	0.72806	578.4	9.9	593	13	515	41	593.0	13.0	2.5	
ALSS1_133.FIN2	984	2.92	2.536	0.048	0.2206	0.0036	0.67838	1280	14	1284	19	1266	28	1266.0	28.0	1.4	
ALSS1_134.FIN2	392	1.4	0.551	0.016	0.0686	0.0015	0.61983	445	10	427.7	8.8	527	50	427.7	8.8	3.9	
ALSS1_135.FIN2	146.8	2.56	0.437	0.024	0.056	0.0021	0.34263	367	17	351	13	450	110	351.0	13.0	4.4	Rim
ALSS1_135.FIN2	362	1.252	0.537	0.012	0.07	0.0015	0.45266	436	8.1	436.1	9.2	421	52	436.1	9.2	0.0	Core
ALSS1_136.FIN2	417.2	3.09	0.497	0.011	0.0628	0.0012	0.53455	409.3	7.6	392.7	7.1	490	45	392.7	7.1	4.1	
ALSS1_137.FIN2	347.3	1.68	0.574	0.011	0.0699	0.0014	0.37479	459.6	7.3	435.3	8.7	583	47	435.3	8.7	5.3	
ALSS1_138.FIN2	293.9	3.63	1.306	0.042	0.1238	0.0041	0.57288	842	18	751	23	1089	59	751.0	23.0	10.8	
ALSS1_139.FIN2	200	4.57	1.56	0.046	0.1572	0.0052	0.53356	948	18	939	29	968	64	968.0	64.0	3.0	
ALSS1_140.FIN2	39.47	2.331	2.213	0.059	0.1981	0.0032	0.19473	1180	19	1167	18	1179	57	1179.0	57.0	1.0	
VSS3_1.FIN2	32.3	0.682	1.727	0.047	0.1713	0.0035	0.34672	1014	17	1018	19	993	55	993.0	55.0	2.5	
VSS3_2.FIN2	102.8	1.041	3.984	0.099	0.2841	0.006	0.53053	1623	20	1609	30	1633	42	1633.0	42.0	1.5	
VSS3_3.FIN2	119.7	1.758	1.635	0.025	0.1659	0.0019	0.39804	983	10	989	11	945	32	945.0	32.0	4.7	
VSS3_4.FIN2	246	1.707	1.916	0.075	0.1608	0.0067	0.91483	1077	27	957	37	1342	31	1342.0	31.0	28.7	
VSS3_5.FIN2	127.7	2.6	2.539	0.066	0.2193	0.0048	0.63614	1282	19	1280	26	1286	40	1286.0	40.0	0.5	
VSS3_6.FIN2	350	4.2	0.3933	0.007	0.05372	0.0006	0.20545	336.3	5.1	337.3	3.7	308	42	337.3	3.7	0.3	
VSS3_7.FIN2	228.7	3	0.375	0.019	0.0496	0.0022	0.65458	322	14	312	14	374	97	312.0	14.0	3.1	

Table 7

VSS3_8.FIN2	196	1.83	2.24	0.21	0.153	0.013	0.95777	1147	64	909	74	1683	51	1683.0	51.0	46.0	
VSS3_9.FIN2	620	2.18	0.582	0.019	0.0734	0.0018	0.6385	464	12	456	11	476	54	456.0	11.0	1.7	
VSS3_10.FIN2	218	1.83	3.369	0.04	0.2594	0.0032	0.53243	1495.6	9.3	1486	16	1500	23	1500.0	23.0	0.9	
VSS3_11.FIN2	167.2	1.58	0.558	0.014	0.0718	0.0016	0.27918	450	9.2	446.5	9.7	453	61	446.5	9.7	0.8	
VSS3_13.FIN2	98.9	3.51	2.067	0.045	0.1965	0.0038	0.58696	1137	16	1156	21	1095	40	1095.0	40.0	5.6	
VSS3_14.FIN2	289.2	1.41	0.868	0.02	0.1013	0.0025	0.67341	634	11	623	14	678	44	623.0	14.0	1.7	
VSS3_16.FIN2	157	4.11	1.719	0.038	0.1699	0.004	0.55305	1012	14	1010	22	1004	43	1004.0	43.0	0.6	
VSS3_17.FIN2	240.7	1.65	1.793	0.035	0.1777	0.0037	0.58473	1040	13	1053	20	1005	37	1005.0	37.0	4.8	
VSS3_18.FIN2	146.3	2.932	2.086	0.037	0.1941	0.0031	0.48505	1143	12	1143	17	1136	35	1136.0	35.0	0.6	
VSS3_19.FIN2	328	4.17	1.761	0.036	0.1715	0.0035	0.52285	1029	14	1019	19	1056	38	1056.0	38.0	3.5	
VSS3_20.FIN2	255.5	1.227	0.913	0.039	0.104	0.0038	0.59246	653	20	637	22	696	77	637.0	22.0	2.5	
VSS3_21.FIN2	338	1.055	0.766	0.026	0.0919	0.0027	0.32066	576	15	566	16	620	81	566.0	16.0	1.7	
VSS3_22.FIN2	195	1.235	1.449	0.047	0.1431	0.004	0.68685	905	20	861	22	1002	53	1002.0	53.0	14.1	
VSS3_23.FIN2	84	0.657	13.98	0.25	0.56	0.01	0.57279	2747	18	2860	43	2666	28	2666.0	28.0	7.3	
VSS3_24.FIN2	654	9.79	2.023	0.033	0.1821	0.0032	0.61216	1121	11	1078	17	1213	29	1213.0	29.0	11.1	
VSS3_25.FIN2	102.2	0.992	0.531	0.016	0.0681	0.0017	0.45842	431	11	424	10	457	62	424.0	10.0	1.6	
VSS3_26.FIN2	192.9	2.007	0.799	0.024	0.0966	0.0026	0.31313	595	14	594	15	592	72	594.0	15.0	0.2	
VSS3_28.FIN2	250.9	19.1	0.846	0.02	0.1004	0.0022	0.50868	621	11	616	13	633	50	616.0	13.0	0.8	
VSS3_29.FIN2	296	1.399	7.82	0.33	0.2597	0.0098	0.78455	2192	38	1484	50	2956	40	2956.0	40.0	49.8	
VSS3_30.FIN2	335.1	20.92	0.3857	0.0092	0.05203	0.00092	0.49988	330.4	6.7	326.9	5.6	348	48	326.9	5.6	1.1	
VSS3_31.FIN2	326	1.647	0.4965	0.008	0.06548	0.00088	0.48252	408.8	5.5	408.8	5.3	405	34	408.8	5.3	0.0	
VSS3_32.FIN2	48.9	0.795	1.993	0.062	0.1886	0.0062	0.61223	1110	21	1110	34	1116	58	1116.0	58.0	0.5	
VSS3_33.FIN2	415	9.2	0.987	0.024	0.1109	0.0025	0.58403	696	12	678	14	754	45	678.0	14.0	2.6	
VSS3_34.FIN2	314	3.37	2.025	0.053	0.1795	0.0039	0.69843	1119	18	1063	21	1225	36	1225.0	36.0	13.2	
VSS3_35.FIN2	269.3	3.87	19.74	0.65	0.546	0.015	0.84499	3065	33	2798	65	3251	28	3251.0	28.0	13.9	
VSS3_36.FIN2	550	1.376	0.587	0.017	0.0668	0.002	0.48999	467	11	416	12	725	64	416.0	12.0	10.9	

Table 7

VSS3_37.FIN2	620	80	0.533	0.026	0.0702	0.0035	0.69364	433	17	437	21	416	86	437.0	21.0	0.9	Rim
VSS3_37.FIN2	51.2	0.592	3.74	0.19	0.276	0.011	0.71255	1574	40	1571	57	1578	69	1578.0	69.0	0.4	Core
VSS3_38.FIN2	289	1.223	0.771	0.02	0.0837	0.0022	0.54913	578	11	518	13	824	53	518.0	13.0	10.4	
VSS3_39.FIN2	100.7	1.525	4.227	0.091	0.2988	0.0057	0.55738	1677	18	1684	28	1672	36	1672.0	36.0	0.7	
VSS3_40.FIN2	1105	8.48	1.727	0.089	0.1561	0.0083	0.53799	1013	33	933	46	1200	100	1200.0	100.0	22.3	Rim
VSS3_40.FIN2	404	2.07	2.9	0.12	0.2336	0.009	0.74389	1375	32	1351	47	1418	53	1418.0	53.0	4.7	Core
VSS3_41.FIN2	127	1.342	1.793	0.035	0.1773	0.0032	0.53978	1041	13	1055	18	1014	37	1014.0	37.0	4.0	
VSS3_42.FIN2	766	4.21	3.3	0.1	0.1987	0.005	0.71362	1473	23	1166	27	1939	37	1939.0	37.0	39.9	
VSS3_43.FIN2	276.8	1.52	0.81	0.018	0.0986	0.002	0.57084	601	10	606	12	582	43	606.0	12.0	0.8	
VSS3_44.FIN2	286	2.26	2.256	0.036	0.1994	0.0026	0.71073	1197	12	1172	14	1244	22	1244.0	22.0	5.8	
VSS3_45.FIN2	417	3.67	0.3862	0.0098	0.0534	0.0013	0.49132	330.6	7.2	335.1	8	310	55	335.1	8.0	1.4	
VSS3_46.FIN2	151.5	1.449	4.89	0.1	0.3159	0.0062	0.65713	1795	17	1771	31	1832	29	1832.0	29.0	3.3	
VSS3_47.FIN2	192.6	1.44	4.043	0.076	0.2871	0.0043	0.55854	1645	16	1626	21	1671	35	1671.0	35.0	2.7	
VSS3_48.FIN2	267	2.85	1.306	0.065	0.1051	0.0075	0.70111	847	28	644	43	1442	82	644.0	43.0	24.0	Rim
VSS3_48.FIN2	91.8	2	2.105	0.047	0.1752	0.0034	0.65881	1152	15	1040	19	1362	35	1362.0	35.0	23.6	Core
VSS3_49.FIN2	380	4.04	1.774	0.045	0.1743	0.0045	0.57074	1031	17	1034	25	1041	49	1041.0	49.0	0.7	
VSS3_50.FIN2	1095	1.918	0.531	0.012	0.0564	0.0014	0.43923	431.8	7.9	353.5	8.6	880	52	353.5	8.6	18.1	
VSS3_51.FIN2	566	1.095	0.916	0.02	0.1061	0.0017	0.49627	659	11	649.8	9.7	695	42	649.8	9.7	1.4	
VSS3_52.FIN2	156	1.577	1.785	0.053	0.1607	0.0043	0.71127	1035	20	959	24	1210	44	1210.0	44.0	20.7	
VSS3_53.FIN2	170.4	14.45	4.26	0.14	0.2964	0.0071	0.57565	1683	29	1672	35	1710	50	1710.0	50.0	2.2	
VSS3_54.FIN2	309.2	2.32	1.773	0.041	0.1655	0.0036	0.57822	1032	15	990	19	1140	41	1140.0	41.0	13.2	
VSS3_55.FIN2	607	1.957	0.528	0.012	0.0591	0.0012	0.46116	429.1	8.1	369.9	7.5	764	50	369.9	7.5	13.8	
VSS3_56.FIN2	709	3.2	0.3999	0.005	0.05533	0.00058	0.48442	341.3	3.6	347.1	3.5	305	27	347.1	3.5	1.7	
VSS3_57.FIN2	1170	1.89	0.627	0.028	0.05	0.0019	0.59077	492	17	315	12	1427	72	DISC	DISC	36.0	
VSS3_58.FIN2	386	3.3	0.598	0.015	0.0707	0.0019	0.55709	474.3	9.7	440	11	640	53	440.0	11.0	7.2	
VSS3_59.FIN2	372.2	1.071	3.226	0.066	0.2547	0.0052	0.60823	1465	16	1464	27	1478	36	1478.0	36.0	0.9	

Table 7

VSS3_60.FIN2	132.5	1.027	6.452	0.088	0.3763	0.0049	0.45008	2038	12	2058	23	2022	26	2022.0	26.0	1.8	
VSS3_61.FIN2	264.6	1.01	0.926	0.031	0.1066	0.0023	0.62818	664	16	653	13	706	54	653.0	13.0	1.7	
VSS3_62.FIN2	118.1	1.212	0.883	0.024	0.1039	0.0018	0.12196	643	14	637	10	675	71	637.0	10.0	0.9	
VSS3_63.FIN2	172	1.647	1.727	0.03	0.1676	0.0031	0.63538	1017	11	998	17	1070	31	1070.0	31.0	6.7	
VSS3_64.FIN2	151	1.373	2.155	0.027	0.1983	0.002	0.45807	1165.6	8.7	1166	11	1177	23	1177.0	23.0	0.9	
VSS3_65.FIN2	148.9	1.808	0.79	0.018	0.0933	0.0019	0.49494	590	10	575	11	662	50	575.0	11.0	2.5	
VSS3_66.FIN2	219	8.4	14.75	0.35	0.53	0.014	0.73983	2793	22	2745	61	2842	33	2842.0	33.0	3.4	
VSS3_67.FIN2	81	1.828	2.825	0.043	0.2382	0.0031	0.47621	1360	12	1378	16	1341	29	1341.0	29.0	2.8	
VSS3_68.FIN2	407	5.82	0.553	0.011	0.0714	0.001	0.50691	446.1	6.9	444.3	6.3	451	39	444.3	6.3	0.4	
VSS3_69.FIN2	242	1.047	6.82	0.18	0.377	0.011	0.58052	2083	24	2055	52	2129	47	2129.0	47.0	3.5	
VSS3_70.FIN2	140	0.829	0.592	0.013	0.076	0.001	0.31559	470.7	8.5	472.4	6.1	462	48	472.4	6.1	0.4	
VSS3_71.FIN2	540	0.993	0.816	0.025	0.0774	0.0017	0.69903	604	14	480	10	1122	45	480.0	10.0	20.5	
VSS3_72.FIN2	588	0.866	0.562	0.021	0.0718	0.0018	0.56185	452	13	447	11	486	71	447.0	11.0	1.1	
VSS3_73.FIN2	193.8	3.57	2.161	0.033	0.197	0.0022	0.54626	1167	10	1159	12	1193	25	1193.0	25.0	2.8	
VSS3_74.FIN2	38.8	1.576	1.542	0.044	0.1468	0.0026	0.47604	943	18	882	15	1089	49	1089.0	49.0	19.0	
VSS3_75.FIN2	333	0.893	0.3768	0.0079	0.05027	0.0007	0.42113	324.3	5.8	316.2	4.3	384	44	316.2	4.3	2.5	
VSS3_76.FIN2	119.7	0.81	0.794	0.022	0.0994	0.0022	0.42559	591	12	610	13	521	58	610.0	13.0	3.2	
VSS3_77.FIN2	174	1.137	0.503	0.013	0.0663	0.0012	0.47413	412.5	9	413.6	7	398	52	413.6	7.0	0.3	
VSS3_78.FIN2	271.3	1.78	2.465	0.065	0.2119	0.0045	0.62933	1256	19	1238	24	1294	40	1294.0	40.0	4.3	
VSS3_79.FIN2	127	0.867	0.707	0.021	0.0859	0.0018	0.51203	541	13	531	10	577	57	531.0	10.0	1.8	
VSS3_80.FIN2	94	2.58	1.892	0.041	0.1791	0.0029	0.73752	1075	14	1062	16	1110	29	1110.0	29.0	4.3	
VSS3_81.FIN2	330	1.54	2.242	0.055	0.2048	0.0049	0.67304	1191	17	1200	26	1175	39	1175.0	39.0	2.1	
VSS3_82.FIN2	52.99	0.3252	0.839	0.024	0.1011	0.0015	0.2174	618	13	620.7	8.5	564	64	620.7	8.5	0.4	
VSS3_83.FIN2	79.9	2.276	3.421	0.081	0.247	0.0046	0.55531	1505	19	1422	24	1629	38	1629.0	38.0	12.7	
VSS3_84.FIN2	266.9	1.46	0.802	0.016	0.0978	0.0014	0.3863	597.2	9.2	602.4	8.4	572	45	602.4	8.4	0.9	
VSS3_85.FIN2	263	1.261	0.522	0.0085	0.06816	0.00083	0.41391	425.9	5.7	425	5	418	35	425.0	5.0	0.2	

Table 7

VSS3_86.FIN2	133.9	2.302	1.713	0.023	0.171	0.002	0.32617	1012.1	8.4	1017	11	996	28	996.0	28.0	2.1	
VSS3_87.FIN2	439	4.66	1.302	0.058	0.1091	0.0038	0.68075	844	26	667	22	1338	65	667.0	22.0	21.0	Rim
VSS3_87.FIN2	290	3.32	1.416	0.065	0.1242	0.005	0.65609	893	28	754	29	1251	70	754.0	29.0	15.6	Core
VSS3_87.FIN2	189.5	3.312	1.638	0.074	0.1507	0.0061	0.72275	983	28	904	34	1156	76	1156.0	76.0	21.8	Core
VSS3_88.FIN2	202	0.869	0.816	0.015	0.0991	0.0012	0.44356	604.6	8.1	608.8	6.9	563	37	608.8	6.9	0.7	
VSS3_89.FIN2	75.4	1.183	1.962	0.037	0.1853	0.0025	0.36383	1101	13	1096	14	1099	38	1099.0	38.0	0.3	
VSS3_90.FIN2	249	8.7	0.513	0.01	0.06651	0.00084	0.45153	419.4	7.1	415	5.1	419	41	415.0	5.1	1.0	
VSS3_91.FIN2	577	1.213	0.357	0.018	0.049	0.0023	0.36312	309	13	308	14	320	110	308.0	14.0	0.3	Rim
VSS3_91.FIN2	490	0.835	0.391	0.017	0.0513	0.0017	0.60177	334	12	322	10	354	82	322.0	10.0	3.6	Core
VSS3_92.FIN2	236	0.99	0.36	0.016	0.0501	0.0014	0.39773	311	12	314.8	8.4	269	87	314.8	8.4	1.2	
VSS3_93.FIN2	944	3.74	0.556	0.01	0.04704	0.0009	0.63241	448.2	6.5	296.3	5.5	1327	33	DISC	DISC	33.9	
VSS3_94.FIN2	270.5	4	1.69	0.11	0.1305	0.0056	0.77497	997	42	790	32	1465	78	790.0	32.0	20.8	
VSS3_95.FIN2	110.7	2.043	5.55	0.14	0.3335	0.006	0.5946	1904	22	1853	29	1946	37	1946.0	37.0	4.8	
VSS3_96.FIN2	343	2.279	0.438	0.011	0.0593	0.0011	0.55029	367.9	7.7	371	6.9	315	48	371.0	6.9	0.8	
VSS3_97.FIN2	589	4.92	0.521	0.011	0.0658	0.0013	0.4859	425.2	7.5	410.4	7.9	474	47	410.4	7.9	3.5	
VSS3_98.FIN2	35.5	10.4	0.834	0.034	0.0999	0.0023	0.21407	615	18	613	14	583	82	613.0	14.0	0.3	
VSS3_99.FIN2	470	1.87	0.78	0.025	0.0955	0.0029	0.35749	585	14	588	17	552	78	588.0	17.0	0.5	
VSS3_100.FIN2	166.1	1.814	2.778	0.055	0.2308	0.0045	0.58333	1350	14	1338	23	1343	34	1343.0	34.0	0.4	
VSS3_101.FIN2	98.9	1.469	0.69	0.026	0.0807	0.0031	0.53987	533	16	499	19	652	75	499.0	19.0	6.4	
VSS3_102.FIN2	136	1.147	3.058	0.053	0.2439	0.0034	0.47228	1422	14	1406	18	1422	32	1422.0	32.0	1.1	
VSS3_103.FIN2	311	1.47	0.389	0.013	0.0514	0.0015	0.48859	332.6	9.3	322.7	9.4	374	69	322.7	9.4	3.0	
VSS3_104.FIN2	215	0.832	0.536	0.013	0.0699	0.0012	0.43535	434.6	8.2	436.6	7.6	392	48	436.6	7.6	0.5	
VSS3_105.FIN2	356	0.995	1.873	0.059	0.1741	0.0039	0.35787	1069	21	1034	21	1115	61	1115.0	61.0	7.3	
VSS3_106.FIN2	182	2.161	1.976	0.034	0.1862	0.0028	0.59897	1105	12	1100	15	1096	29	1096.0	29.0	0.4	
VSS3_107.FIN2	354	1.87	0.5385	0.0084	0.06979	0.00076	0.31934	436.9	5.5	434.8	4.6	420	35	434.8	4.6	0.5	
VSS3_108.FIN2	406	10.69	0.918	0.023	0.1081	0.0033	0.4451	660	12	661	19	623	68	661.0	19.0	0.2	

Table 7

VSS3_109.FIN2	287	1.225	0.558	0.013	0.07094	0.00099	0.40846	449.5	8.6	441.8	5.9	453	48	441.8	5.9	1.7	
VSS3_110.FIN2	379	2.11	0.839	0.016	0.0982	0.0015	0.57011	617.3	8.7	603.6	8.8	646	37	603.6	8.8	2.2	
VSS3_111.FIN2	101	1.589	1.49	0.043	0.1443	0.0028	0.44546	924	17	869	16	1028	54	1028.0	54.0	15.5	
VSS3_112.FIN2	525	0.94	4.789	0.08	0.3061	0.005	0.85626	1780	14	1720	25	1840	16	1840.0	16.0	6.5	
VSS3_113.FIN2	167	4.31	3.018	0.067	0.1991	0.0033	0.41808	1409	17	1170	18	1774	39	1774.0	39.0	34.0	
VSS3_114.FIN2	103	1.359	4.063	0.084	0.283	0.0043	0.60541	1642	17	1605	21	1674	30	1674.0	30.0	4.1	
VSS3_115.FIN2	185.7	1.403	0.571	0.013	0.07074	0.0007	0.44646	457.7	8.3	441.1	4.1	508	45	441.1	4.1	3.6	
VSS3_116.FIN2	32.5	0.781	3.339	0.093	0.2542	0.005	0.69192	1486	22	1459	26	1505	42	1505.0	42.0	3.1	
VSS3_117.FIN2	374	5.9	2.105	0.042	0.1934	0.0026	0.73385	1149	14	1139	14	1157	26	1157.0	26.0	1.6	
VSS3_118.FIN2	131.7	2.295	1.516	0.046	0.1317	0.0027	0.54245	935	19	797	15	1260	52	797.0	15.0	14.8	
VSS3_119.FIN2	134.2	2.976	2.482	0.054	0.218	0.0051	0.62152	1264	16	1269	27	1270	39	1270.0	39.0	0.1	
VSS3_120.FIN2	128.3	1.263	2.194	0.037	0.1975	0.0031	0.64891	1177	12	1161	17	1199	28	1199.0	28.0	3.2	
VSS3_121.FIN2	66.2	0.554	0.868	0.022	0.1037	0.0015	0.29998	632	12	635.7	8.7	593	55	635.7	8.7	0.6	
VSS3_122.FIN2	299	2.94	0.566	0.013	0.0655	0.0013	0.50249	454.2	8.3	408.9	7.7	664	48	408.9	7.7	10.0	
VSS3_123.FIN2	199.8	3.639	1.606	0.028	0.1577	0.0023	0.63717	971	11	943	13	1028	28	1028.0	28.0	8.3	
VSS3_124.FIN2	39.65	3.313	0.591	0.025	0.0749	0.0016	0.18893	469	16	465.4	9.3	483	86	465.4	9.3	0.8	
VSS3_125.FIN2	174	2.116	2.875	0.055	0.2365	0.0034	0.71746	1372	14	1368	18	1380	26	1380.0	26.0	0.9	
VSS3_126.FIN2	181.5	2.057	0.575	0.019	0.0746	0.0015	0.56633	459	12	463.8	8.9	425	59	463.8	8.9	1.0	Rim
VSS3_126.FIN2	120.7	2.104	0.93	0.035	0.0982	0.0025	0.48556	667	18	604	14	878	70	604.0	14.0	9.4	Core
VSS3_127.FIN2	137.6	1.148	1.879	0.036	0.1799	0.0026	0.54211	1071	13	1066	14	1081	32	1081.0	32.0	1.4	
VSS3_128.FIN2	542	0.9	0.503	0.017	0.04699	0.00086	0.28082	413	12	296	5.3	1111	72	296.0	5.3	28.3	
VSS3_129.FIN2	472	3.467	4.035	0.077	0.2557	0.0042	0.89093	1641	15	1467	21	1875	16	1875.0	16.0	21.8	
VSS3_130.FIN2	392	2.289	5.546	0.043	0.3397	0.0026	0.61881	1907	6.7	1887	12	1931	12	1931.0	12.0	2.3	
VSS3_131.FIN2	83.9	2.039	0.496	0.013	0.0645	0.001	0.26403	407.5	9	402.9	6.2	427	59	402.9	6.2	1.1	
VSS3_132.FIN2	203.1	1.057	0.4384	0.0079	0.05812	0.00056	0.15593	368.5	5.5	364.2	3.4	399	43	364.2	3.4	1.2	
VSS3_133.FIN2	244	1.072	0.787	0.015	0.0953	0.0015	0.49452	589.2	8.8	586.7	8.6	583	40	586.7	8.6	0.4	

Table 7

VSS3_134.FIN2	172	4.24	2.903	0.038	0.2391	0.0028	0.46424	1381	10	1381	15	1385	25	1385.0	25.0	0.3	
VSS3_135.FIN2	94.4	1.25	4.512	0.076	0.3136	0.0048	0.73142	1730	14	1757	24	1700	24	1700.0	24.0	3.4	
VSS3_136.FIN2	482	1.833	3.386	0.064	0.2403	0.0054	0.79581	1499	14	1386	28	1673	25	1673.0	25.0	17.2	
VSS3_137.FIN2	910	1.237	0.861	0.031	0.075	0.0024	0.68157	626	17	466	15	1258	55	466.0	15.0	25.6	
VSS3_138.FIN2	179.4	3.1	4.76	0.13	0.3162	0.0073	0.64113	1771	24	1768	36	1790	39	1790.0	39.0	1.2	
VSS3_139.FIN2	99.4	0.724	1.361	0.047	0.144	0.0031	0.4794	867	20	866	17	862	64	862.0	64.0	0.5	
VSS3_140.FIN2	395	2.44	3.42	0.11	0.2793	0.0095	0.75843	1503	25	1581	48	1404	48	1404.0	48.0	12.6	

Table 7: ALSS1 and VSS3 sample data.

FIGURES

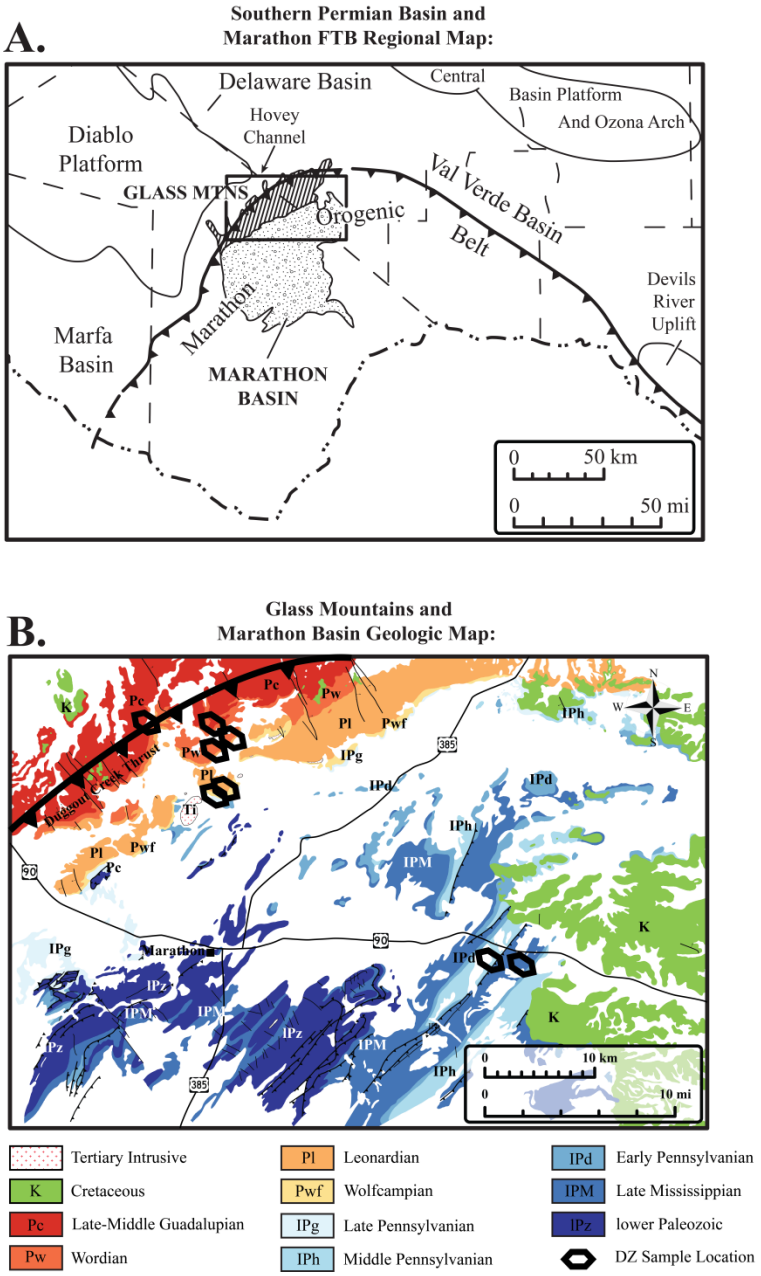

Figure 1: A. Regional map of the Glass Mountains and Marathon Basin in relation to Guadalupian paleogeography of the Permian Basin (from Hickman, 2009). B. Associated modern geologic map of the Marathon Region with sample locations.

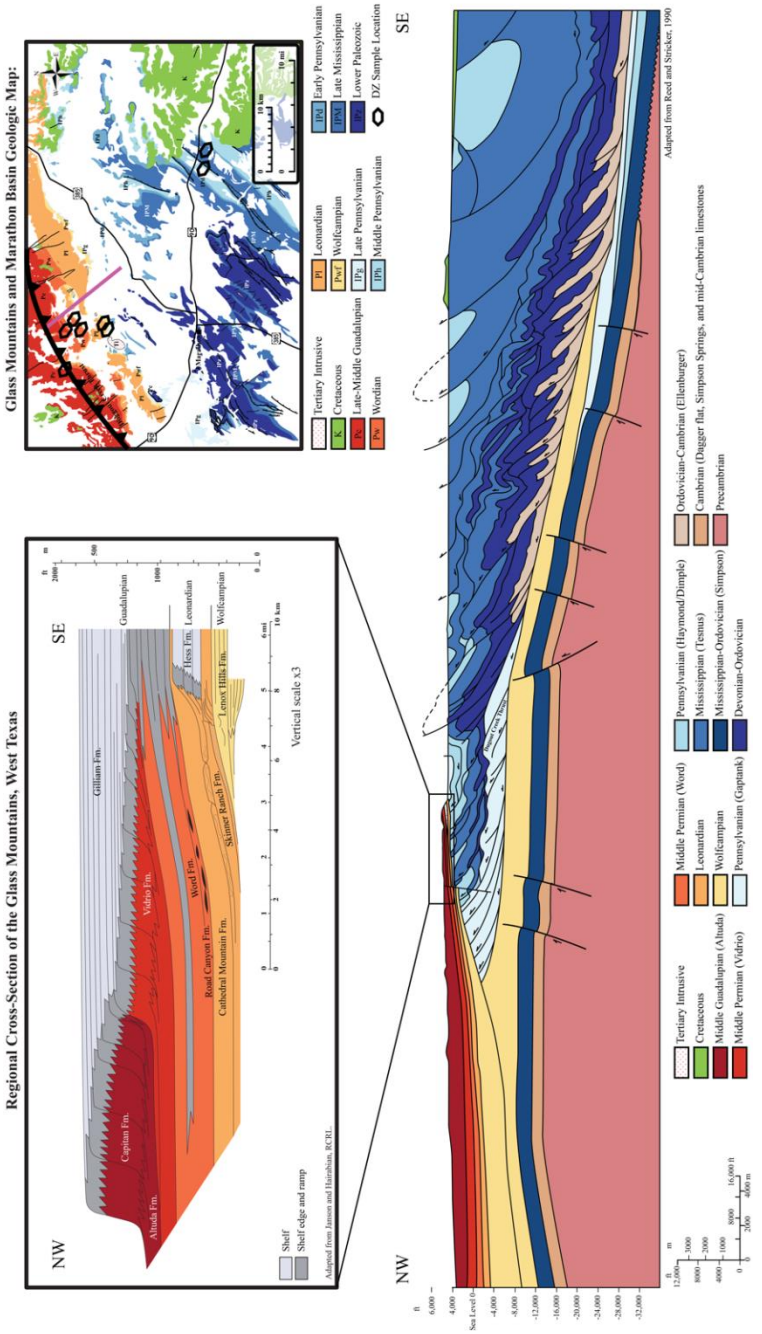

Figure 2: Cross section of the Glass Mountains study area displaying N-NW progradation of Wolfcamp-Guadalupian stratigraphic units during basin formation and fill (Janson and Hairabian, 2016) and structural cross section of the broader Marathon Region derived from multiple well and seismic ties (Strickler and Reed, 1990).

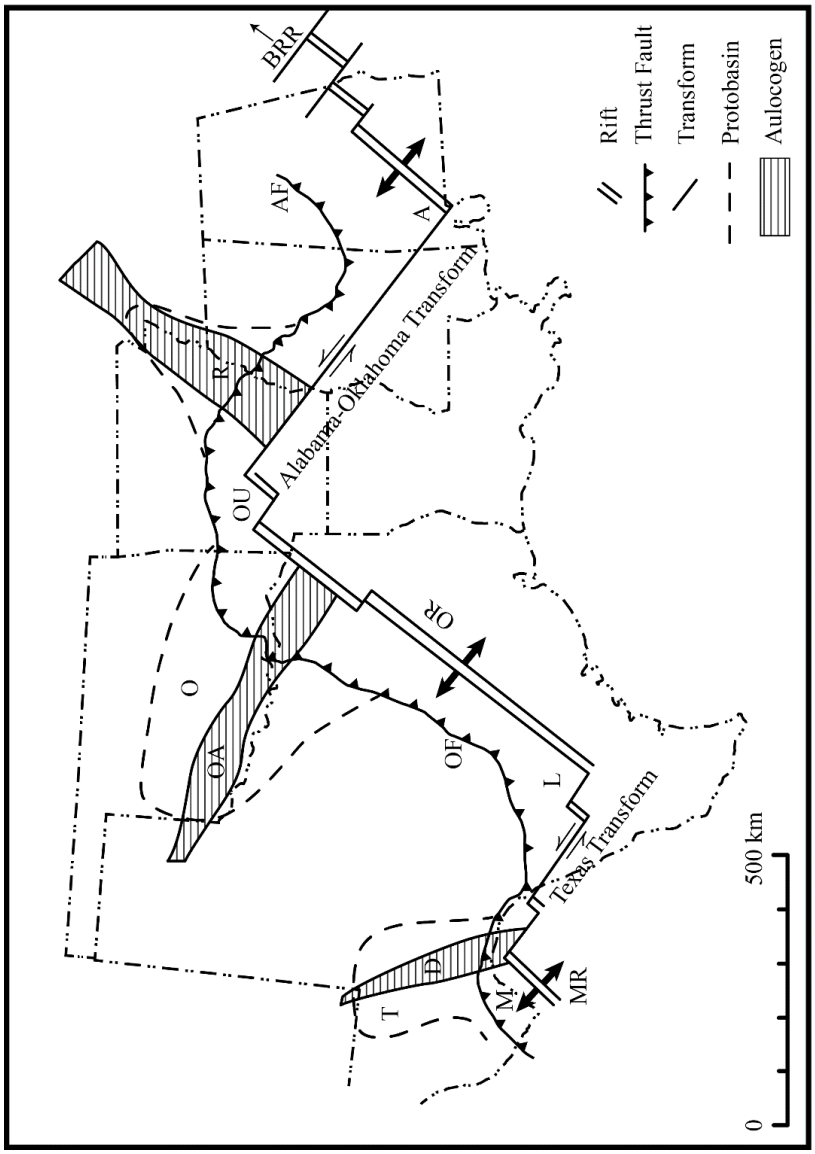

Figure 3: Late Precambrian to Middle Cambrian rift-transform breakup of Rodinia, subsequent thrust belt formation during Mississippian-Permian collision of Laurentia and Gondwana. A = Alabama promontory, AF = late Paleozoic Appalachian thrust front, BRR = Blue Ridge Rift, D = Delaware aulacogen, L = Llano (or Texas) promontory, M = Marathon embayment, MR = Marathon Rift, O = Oklahoma Basin (early Paleozoic), OA = Oklahoma aulacogen, OF = late Paleozoic Ouachita thrust front, OR = Ouachita Rift, OU = Ouachita embayment, R = Redfoot rift (with early Paleozoic Mississippi Valley Basin, T = Tobosa Basin (early Paleozoic). From Arbenz, 1989 and Thomas et al., 2002.

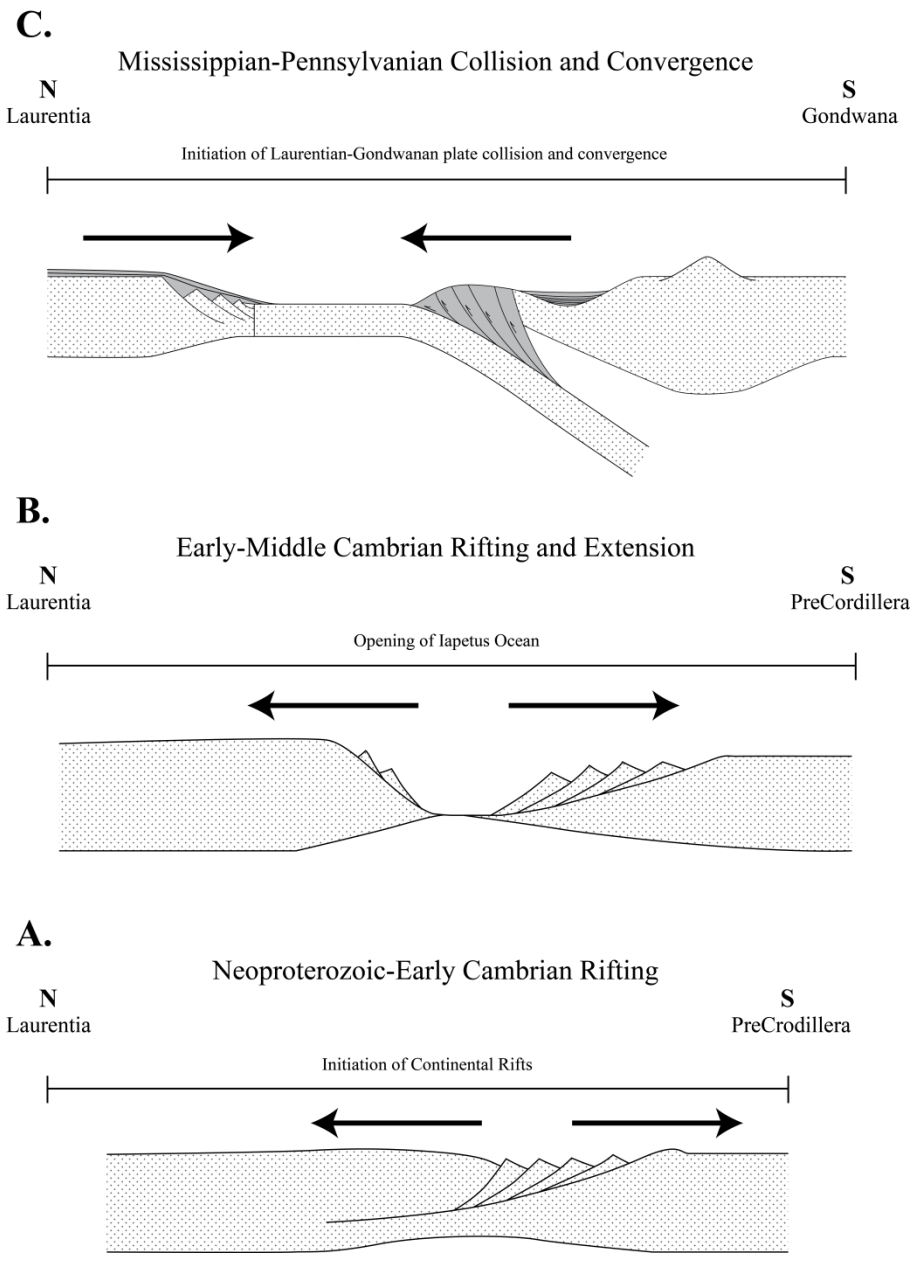

Figure 4: Schematic cross section of Rodinian breakup and subsequent collision and convergence of Laurentia and Gondwana during the formation of Pangea. A. Initial rifting of the Rodinian continent during Neoproterozoic-Early Cambrian time. B. Early-Middle Cambrian rifting and opening of the Iapetus Ocean. C. Initiation of collision and convergence of the Laurentian and Gondwanan continents during the formation of Pangea. Adapted from Thomas, 2011b.

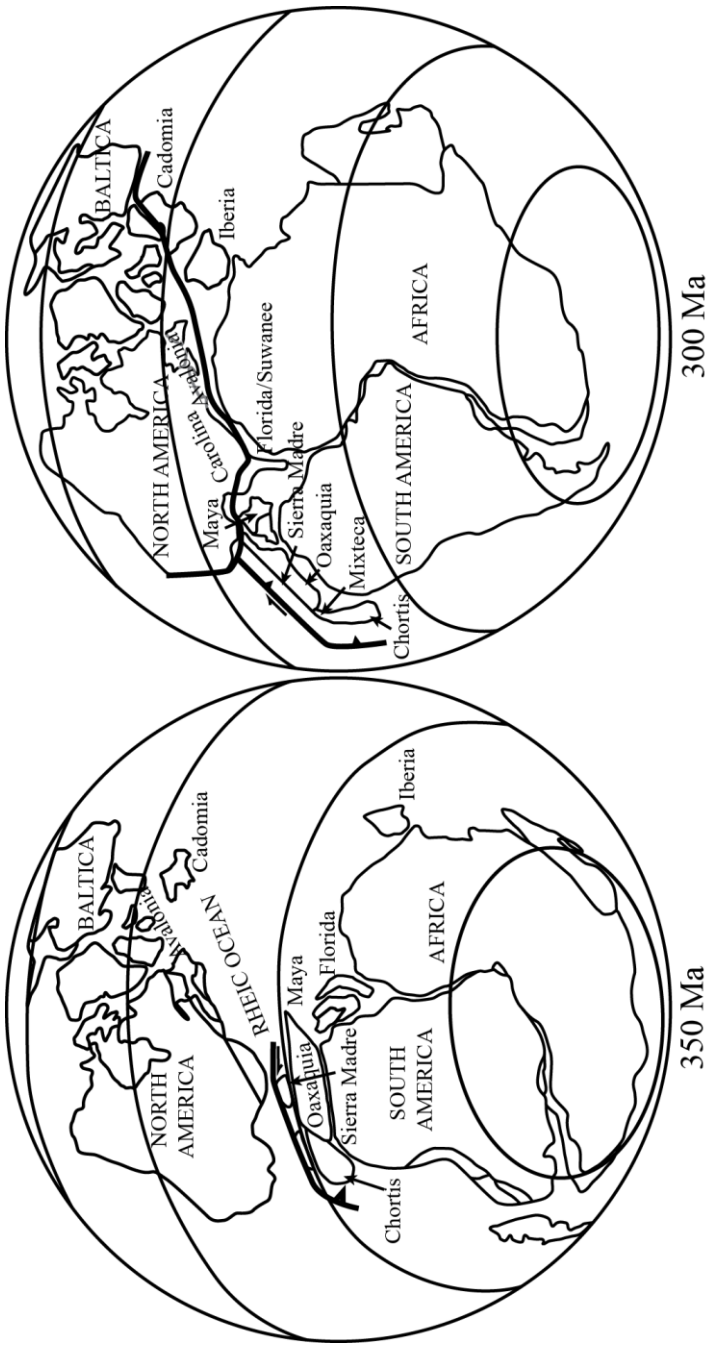

Figure 5: Paleogeographic reconstructions showing Laurentian, Gondwanan, and African continental pieces during Carboniferous reconstruction on the active pacific margin with subduction beneath the Mixteca (Acatlán) and Oaxaquia terranes (A.), and Permian age construction of Pangea during continental collision of Laurentia and Gondwana (adapted from Keppie et al., 2008).

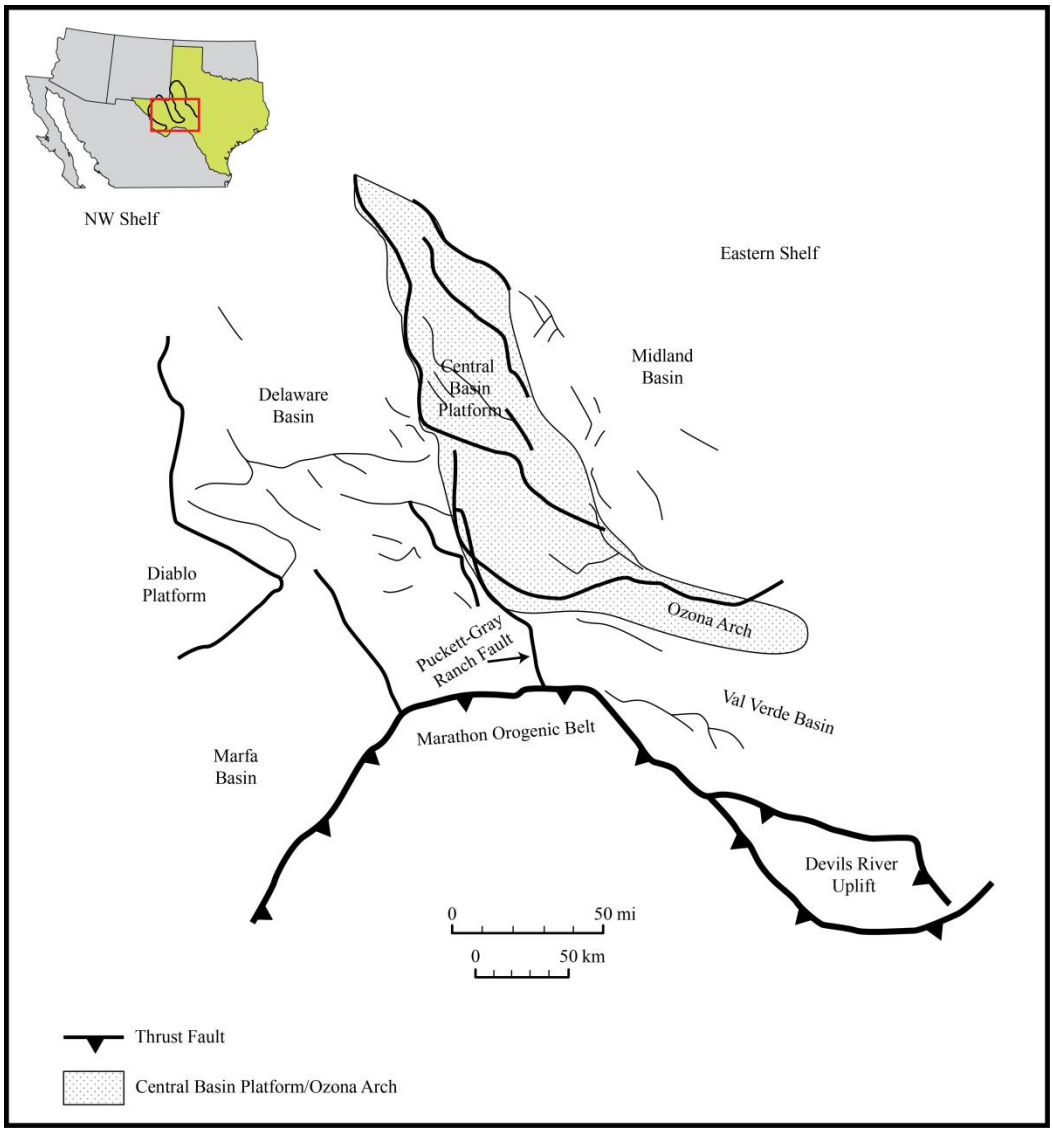

Figure 6: Mapped structural features of the Permian Basin region. Adapted from Yang and Dorobek, 1995.

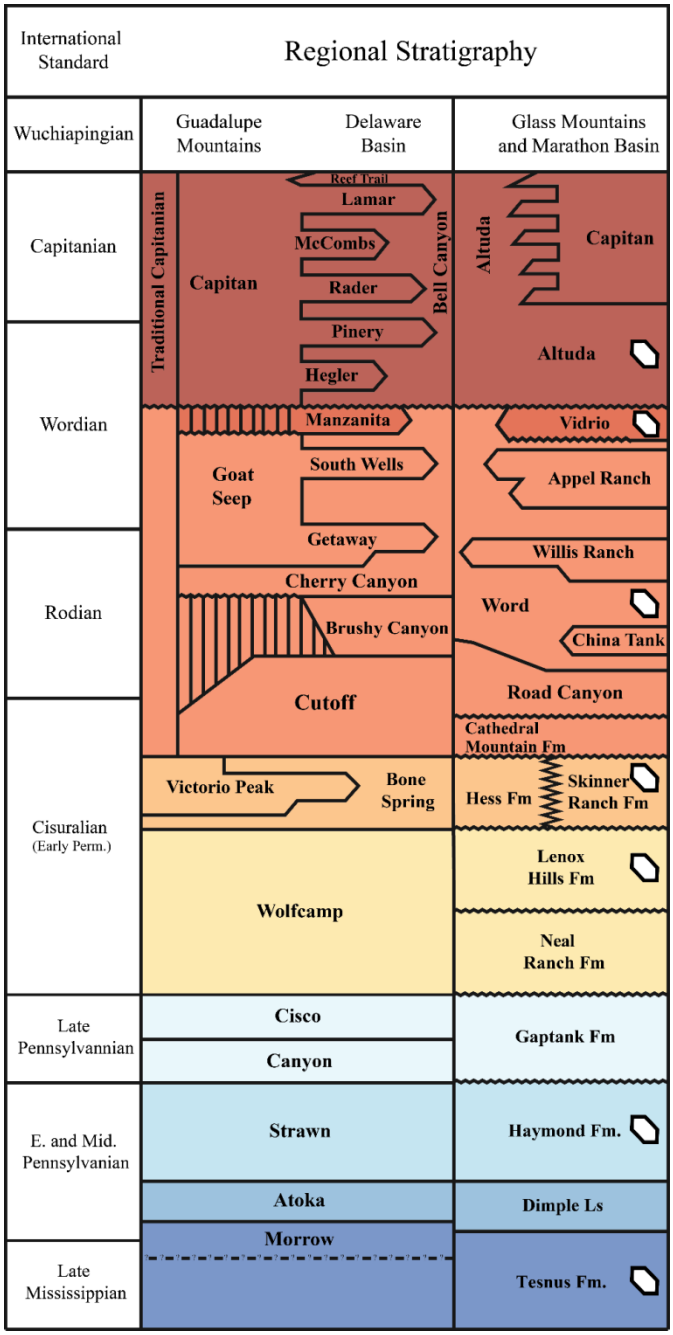

Figure 7: Stratigraphic column of the Guadalupe Mountains, Delaware Basin, and Glass Mountains and Marathon Basin (this study). Detrital zircon sample locations are denoted by white symbols within stratal intervals. Adapted from Barnaby et al. (2004), Olszewski and Erwin (2009), and Nestell et al. (in press).

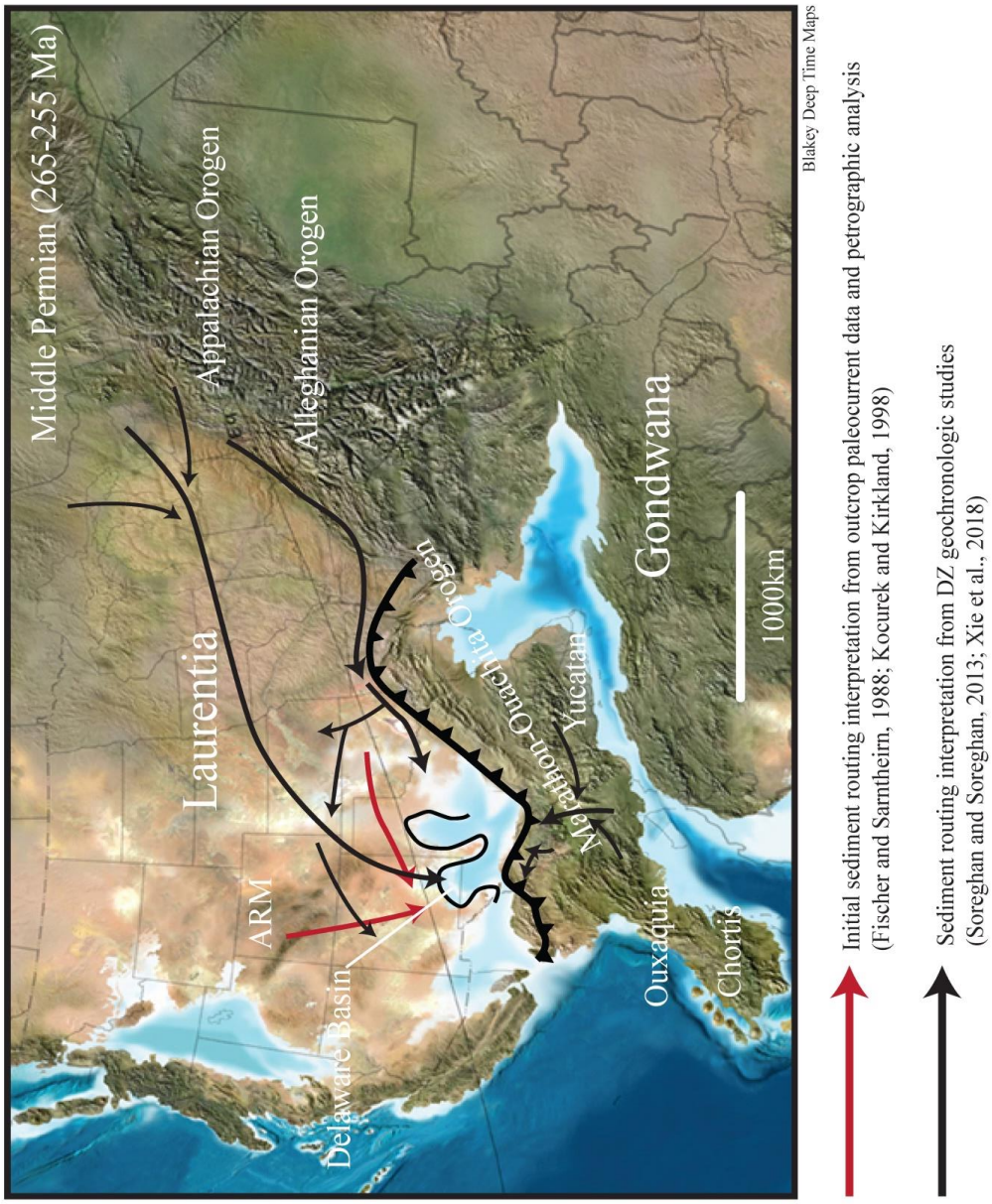

Figure 8: Paleogeographic map of the Laurentian and Gondwanan continents during the middle Permian. Arrows indicate sediment routing interpretations by previous studies within the Delaware Basin.

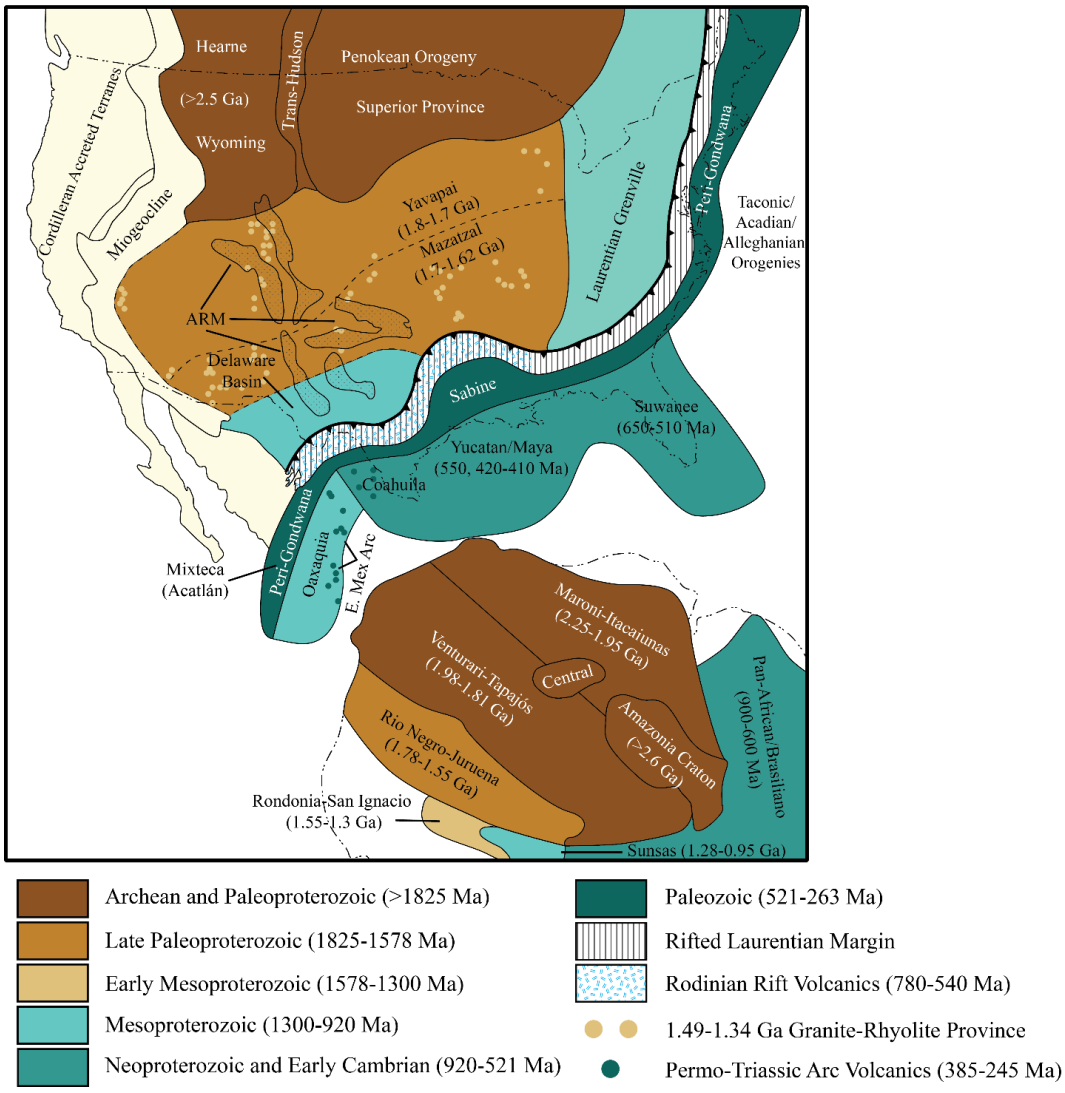

Figure 9: Map depicting main basement age provinces of North America and accreted terranes capable of shedding sediment to the Permian Basin. Adapted from Lawton et al., 2016.

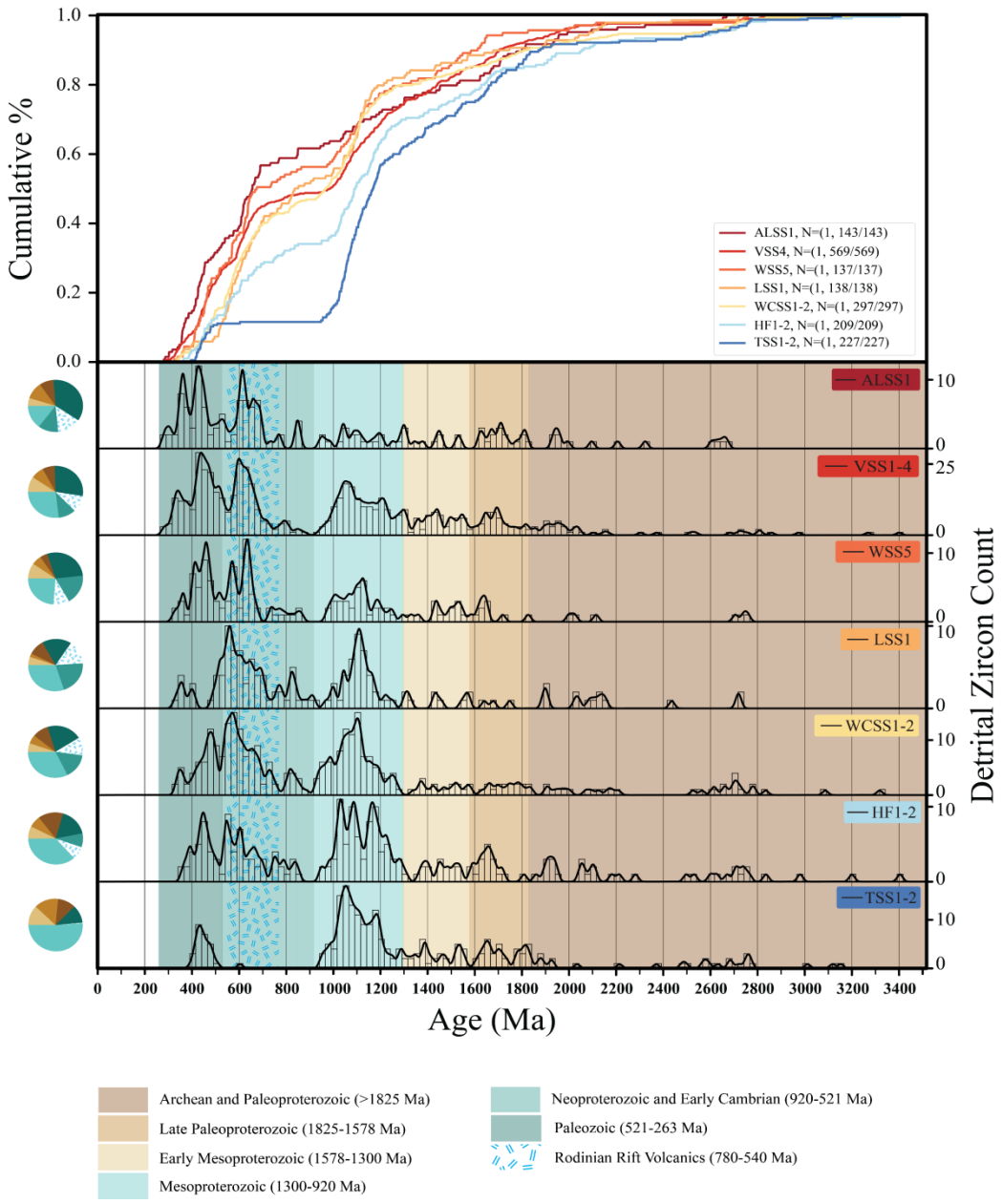

Figure 10: Cumulative probability density plot and non-uniform kernel density estimation plots of each sample suite analyzed in this study. Highlighted color-coded groups designate broad-scale potential detrital zircon source terranes and dominant age range from each source (Fig. 9) (Lawton et al., 2016).

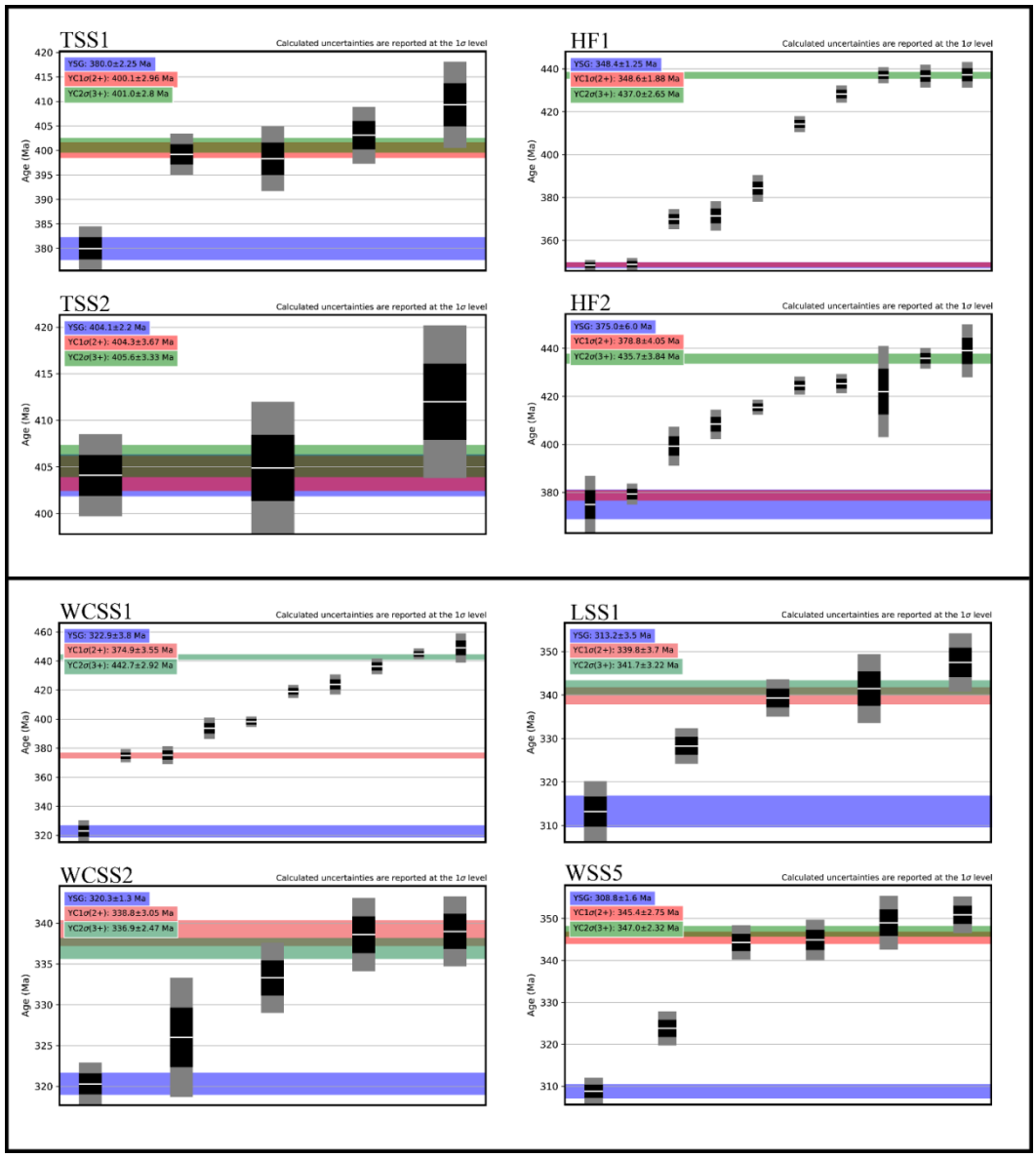

Figure 11: Maximum depositional ages taken from DZ U-Pb data for each stratigraphic unit within this study. Youngest Single Grain (YSG), weighted mean age of youngest cluster of two or more grain ages overlapping age at 1σ (YC1σ (2+)) and weighted mean age of the youngest cluster of three or more grain ages overlapping in age at 2σ (YC2σ (3+)) (Dickinson and Gehrels, 2009).

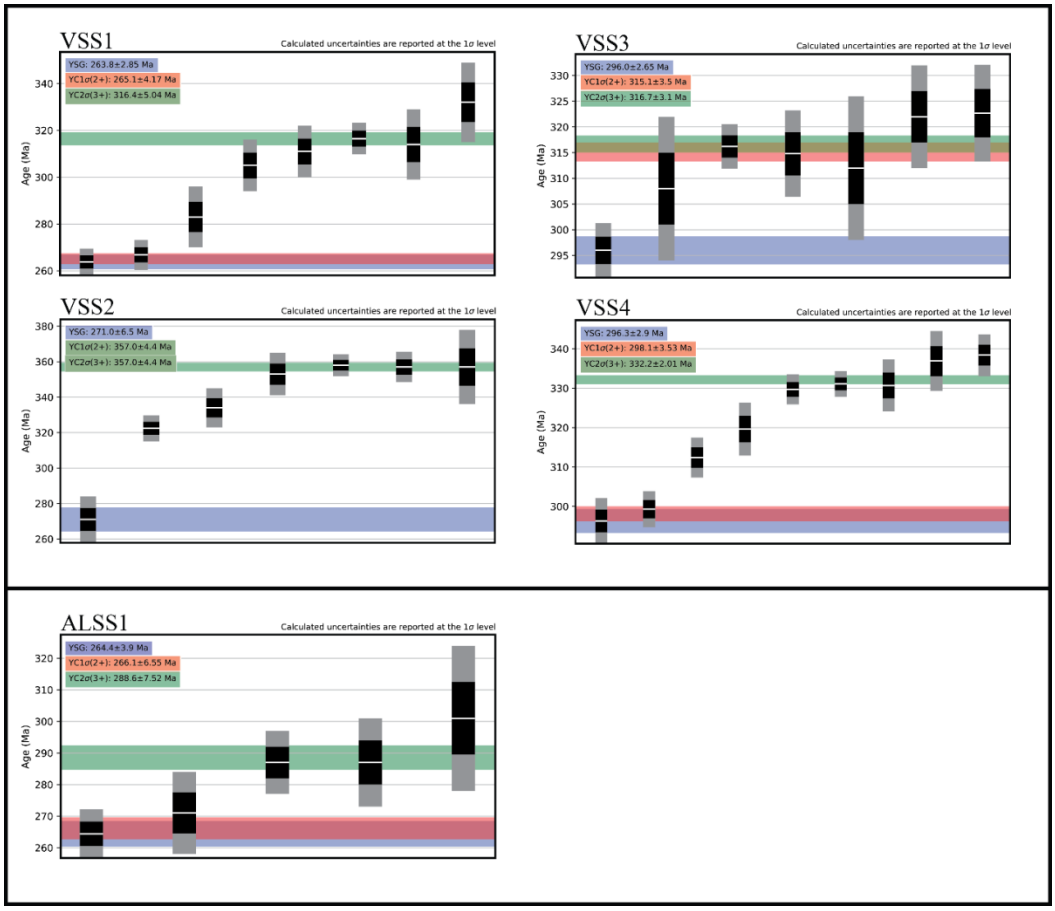

Figure 11 ct.: Maximum depositional ages taken from DZ U-Pb data for each stratigraphic unit within this study. Youngest Single Grain (YSG), weighted mean age of youngest cluster of two or more grain ages overlapping age at 1σ (YC1σ (2+)) and weighted mean age of the youngest cluster of three or more grain ages overlapping in age at 2σ (YC2σ (3+)) (Dickinson and Gehrels, 2009).

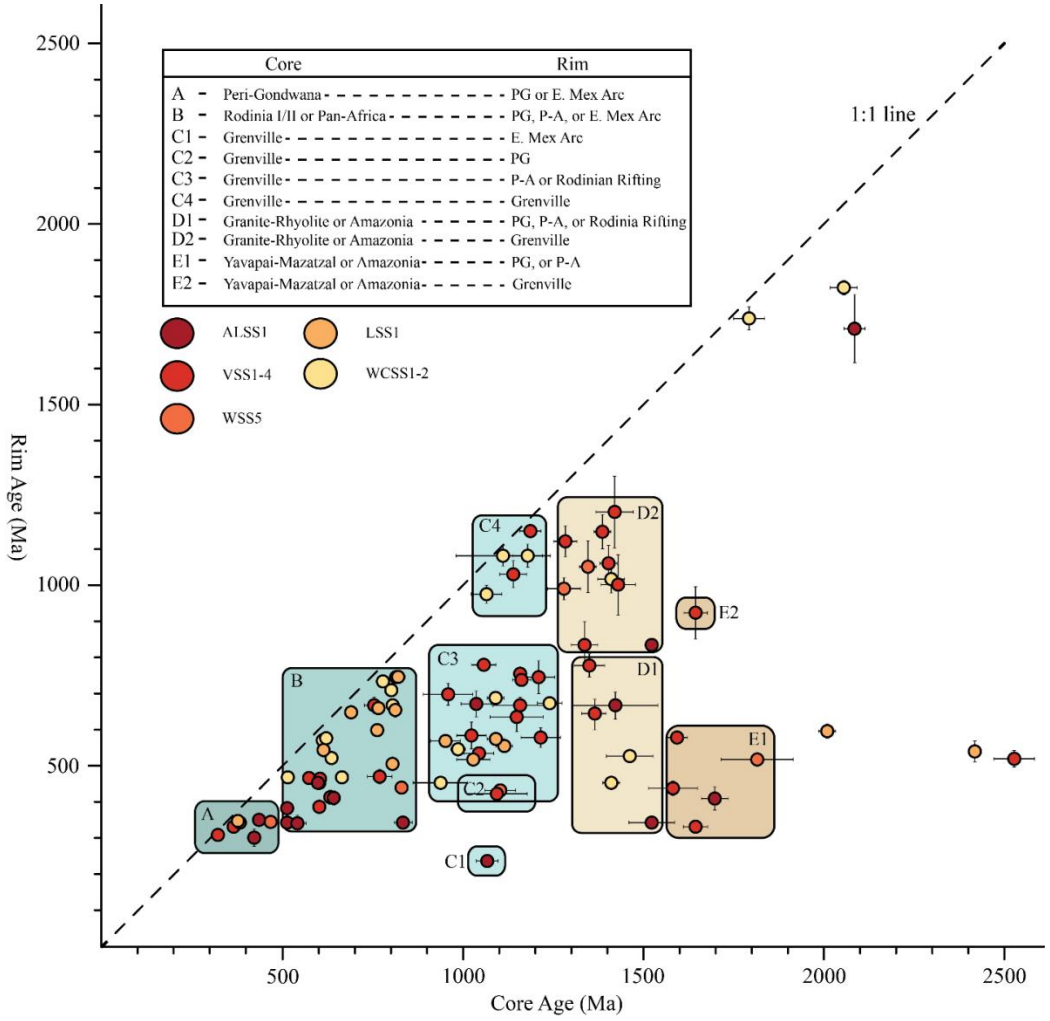

Figure 12: Plot of measured core and rim ages produced from U-Pb age measurements of detrital zircon depth profiles. Alphabetic and numerically labeled boxes group together interpreted source terranes based on core-rim relationships. A grain plotting close to the 1:1 line is indicative of similar crystallization age of core and rim components.

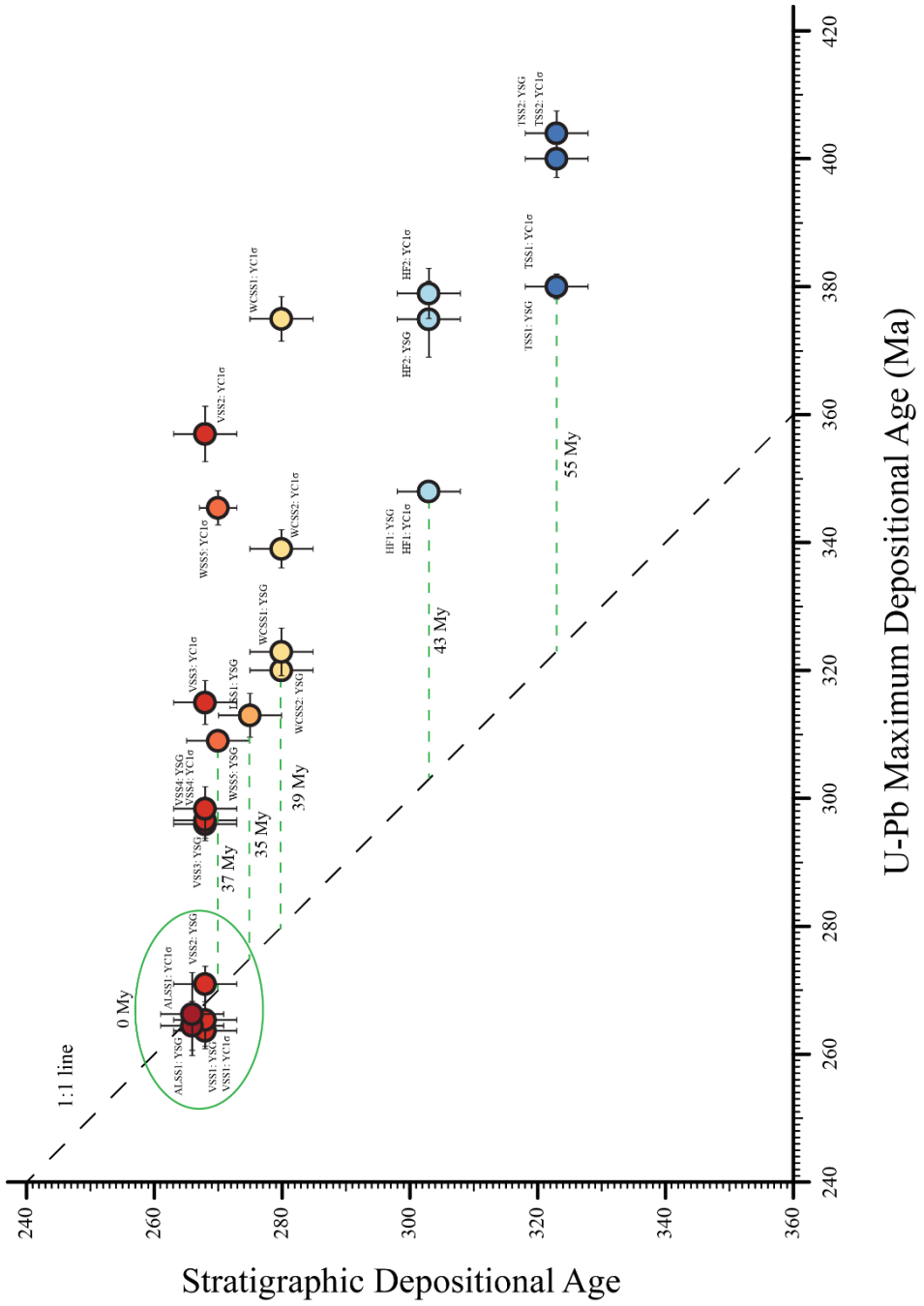

Figure 13: Maximum depositional age from DZ U-Pb vs. stratigraphic depositional age from publication (Olszewski and Erwin, 2009; Glasspool et al., 2013; Richards, 2013; Nestell et al., in press).

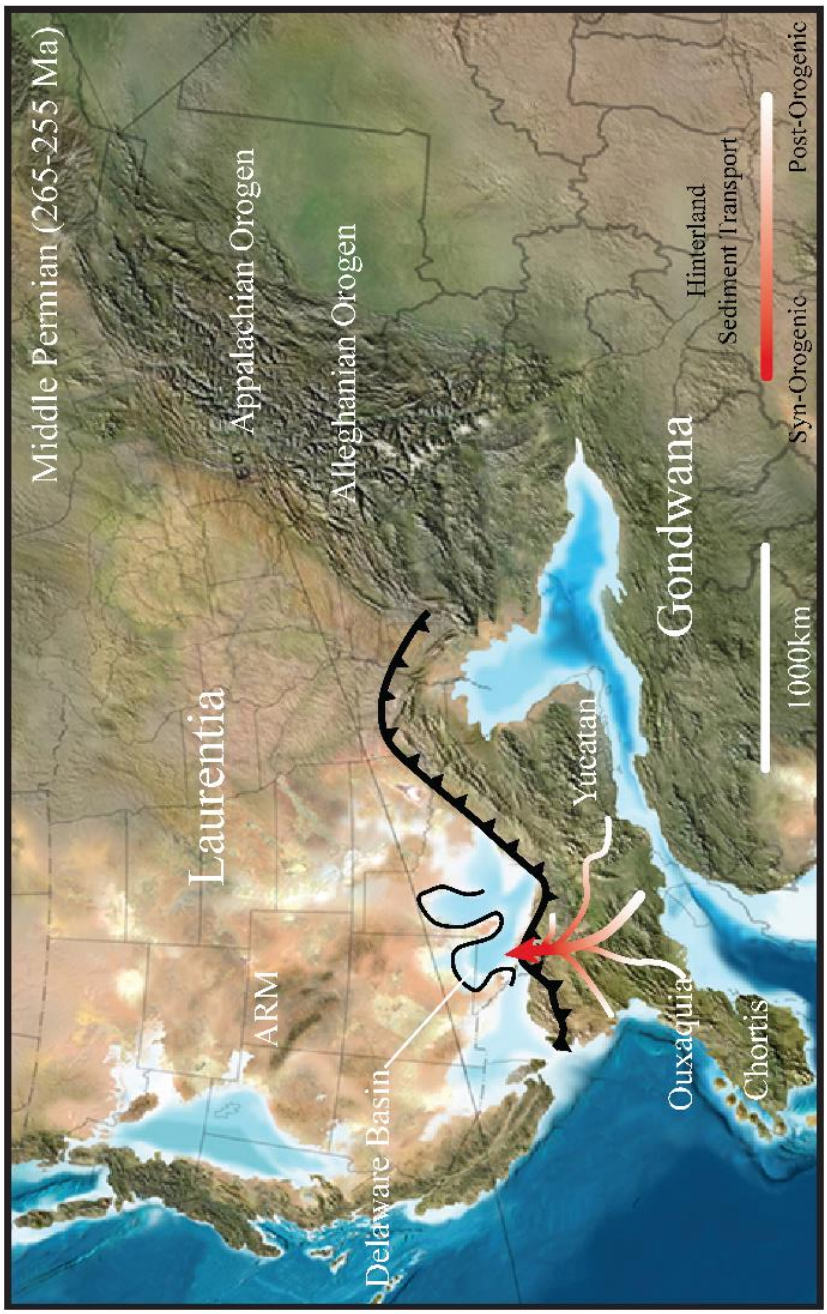

Figure 14: Paleogeographic map of the Laurentian and Gondwanan continents during the middle Permian. This study's interpretation of dominant sediment supply to the Delaware Basin, coupled with timing of drainage system sourcing sediment from deeper within the Gondwanan hinterland.

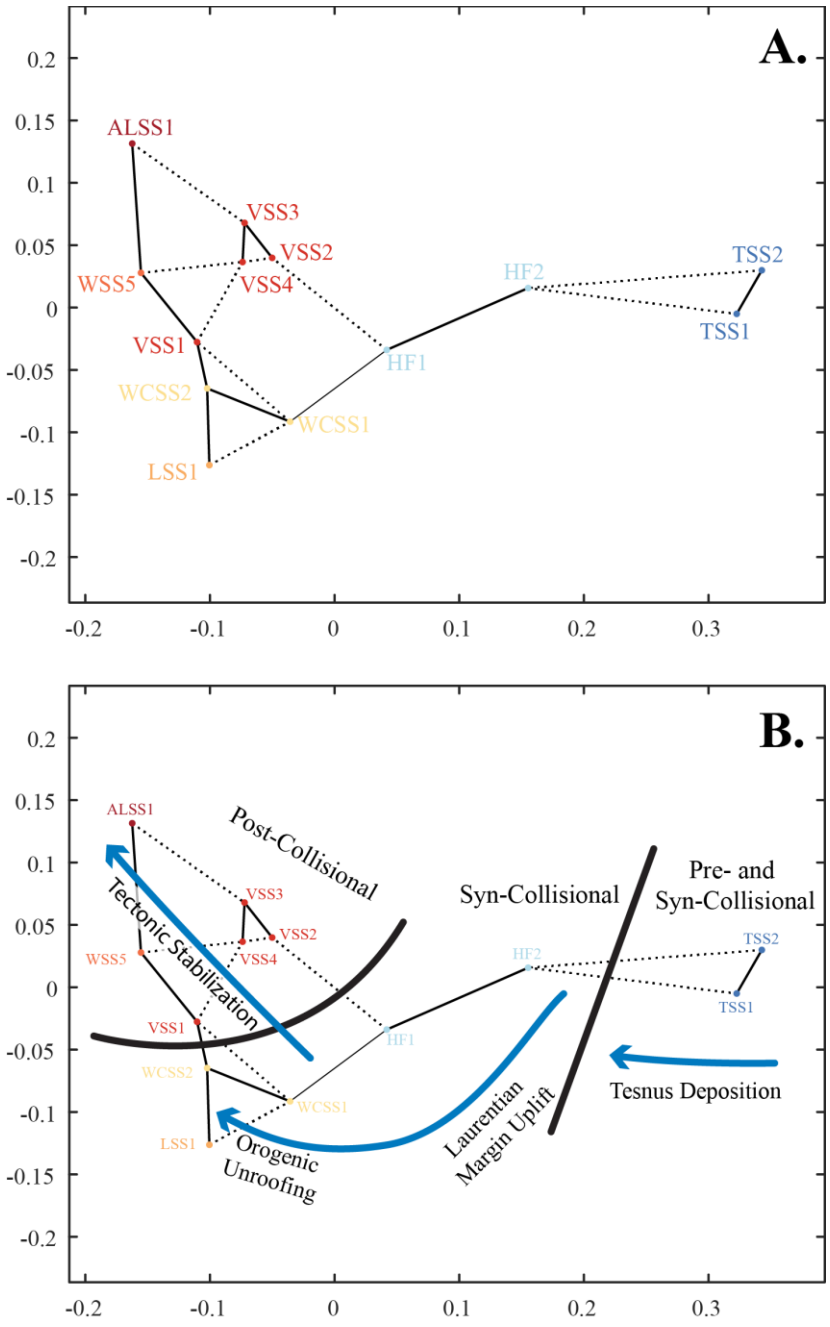

Figure 15: MDS map of study samples. A. Uninterpreted MDS map showing the relative dissimilarity of samples. B. Interpreted MDS map of samples, dark black lines show transition in pre-, syn-, and post-collisional stages while blue arrows represent specific stages of sediment supply and regional processes. MDS formatted using Vermeesch (2013) Matlab code.

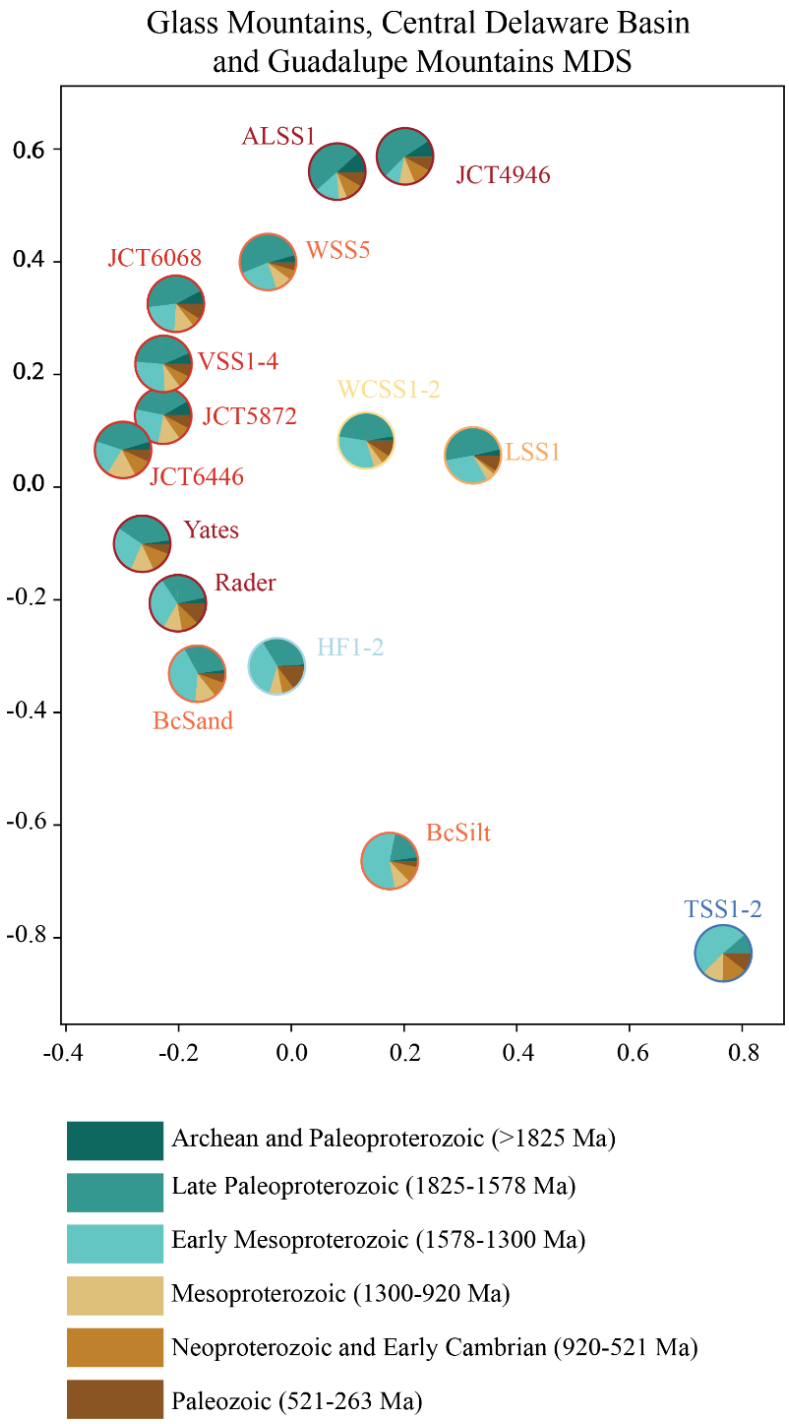

Figure 16: MDS map from all Delaware Basin samples. Data compiled from this study, Soreghan and Soreghan, 2013, and Anthony, 2015.

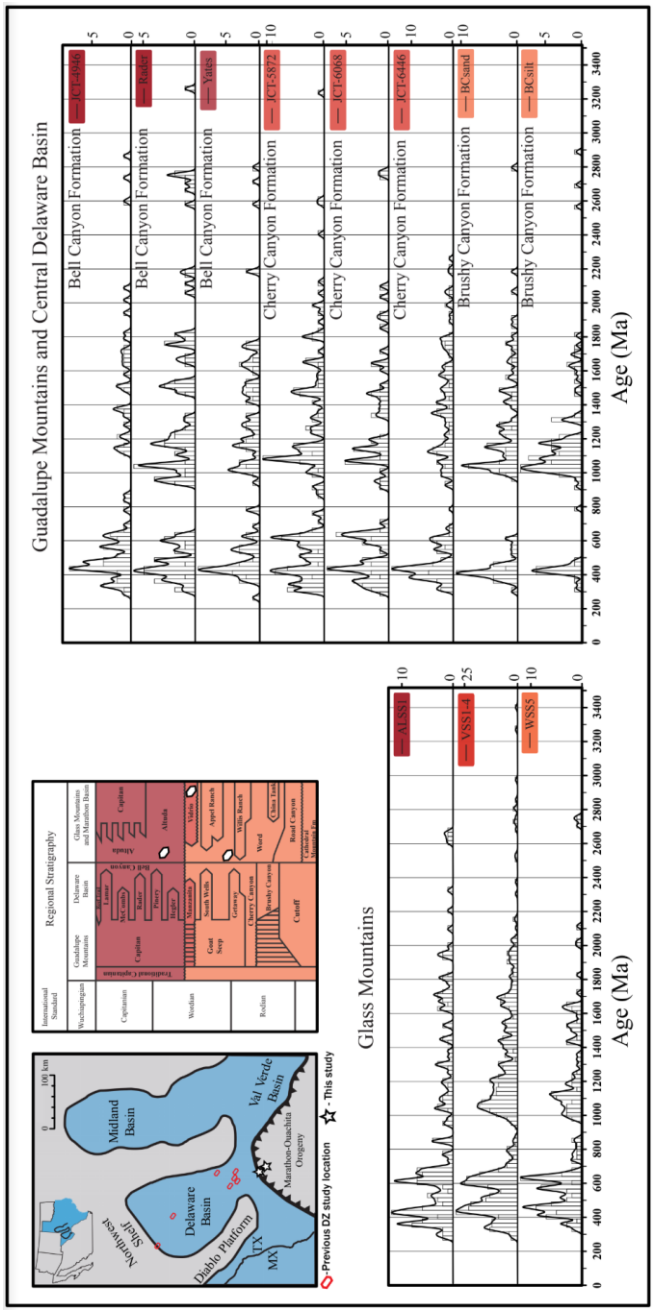

Figure 17: Intersample comparison of detrital zircon age spectra from coeval units across the Delaware Basin. Glass Mountains data from this study and Guadalupe Mountains and Central Delaware Basin data compiled from Soreghan and Soreghan (2013), and Anthony (2015).

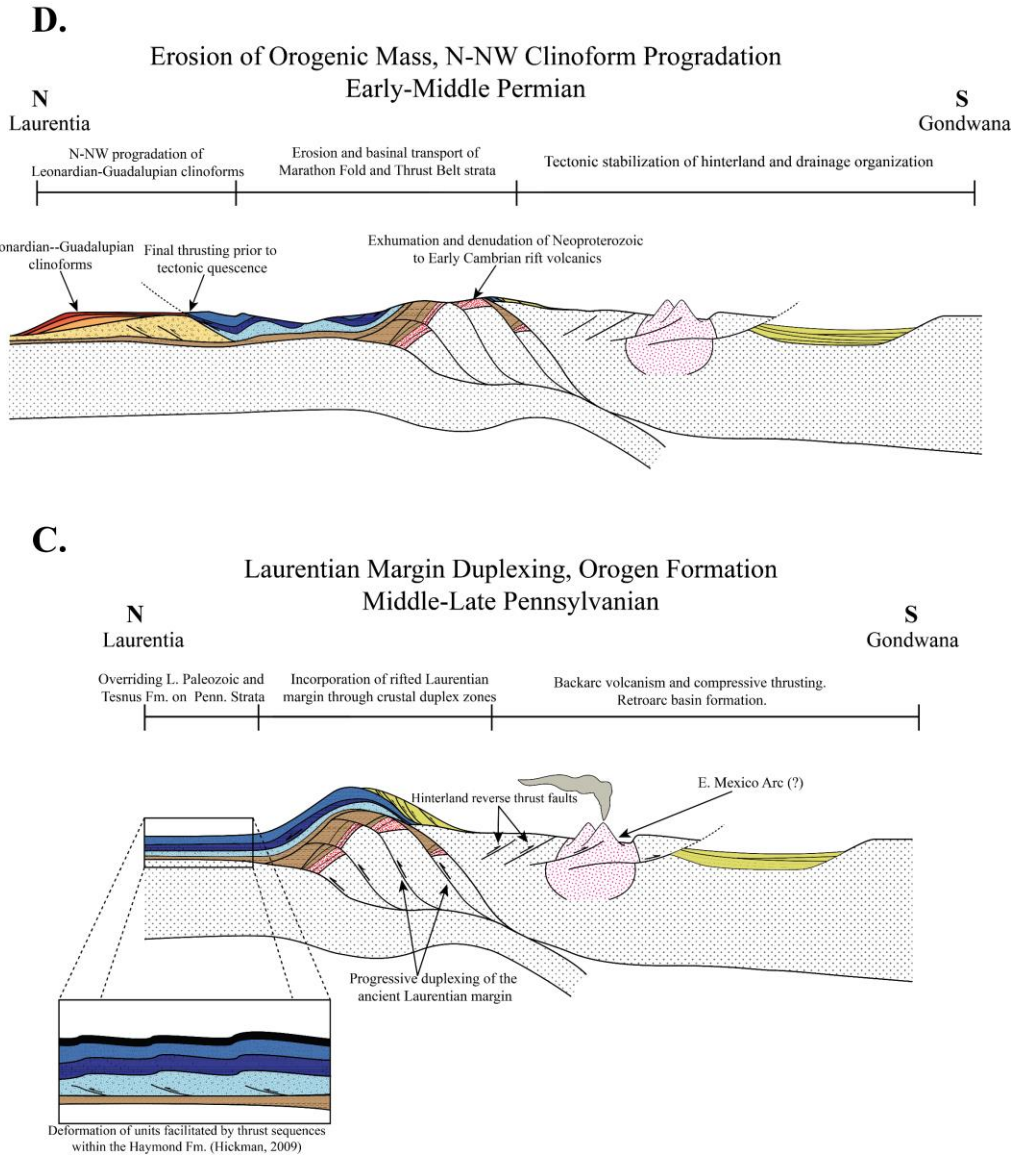

Figure 18: Tectonostratigraphic reconstruction of the evolving Laurentian-Gondwanan margin throughout the Mississippian-middle Permian based on DZ U-Pb data. A. Pre-collisional deposition of Tesnus Formation on the leading edge of approaching Gondwanan continent, deposition of thin-bedded limestone, shale, and chert. B. Initial deposition of the Haymond Formation during continental collision. C. Collision of Laurentia and Gondwana, incorporation of rifted Laurentian crust through crustal duplexing. D. Post-collisional figure representing tectonic quiescence, sediment supply from deeper within the Gondwanan hinterland, supporting progradation of stable clinoforms along the southern margin of the Delaware Basin.

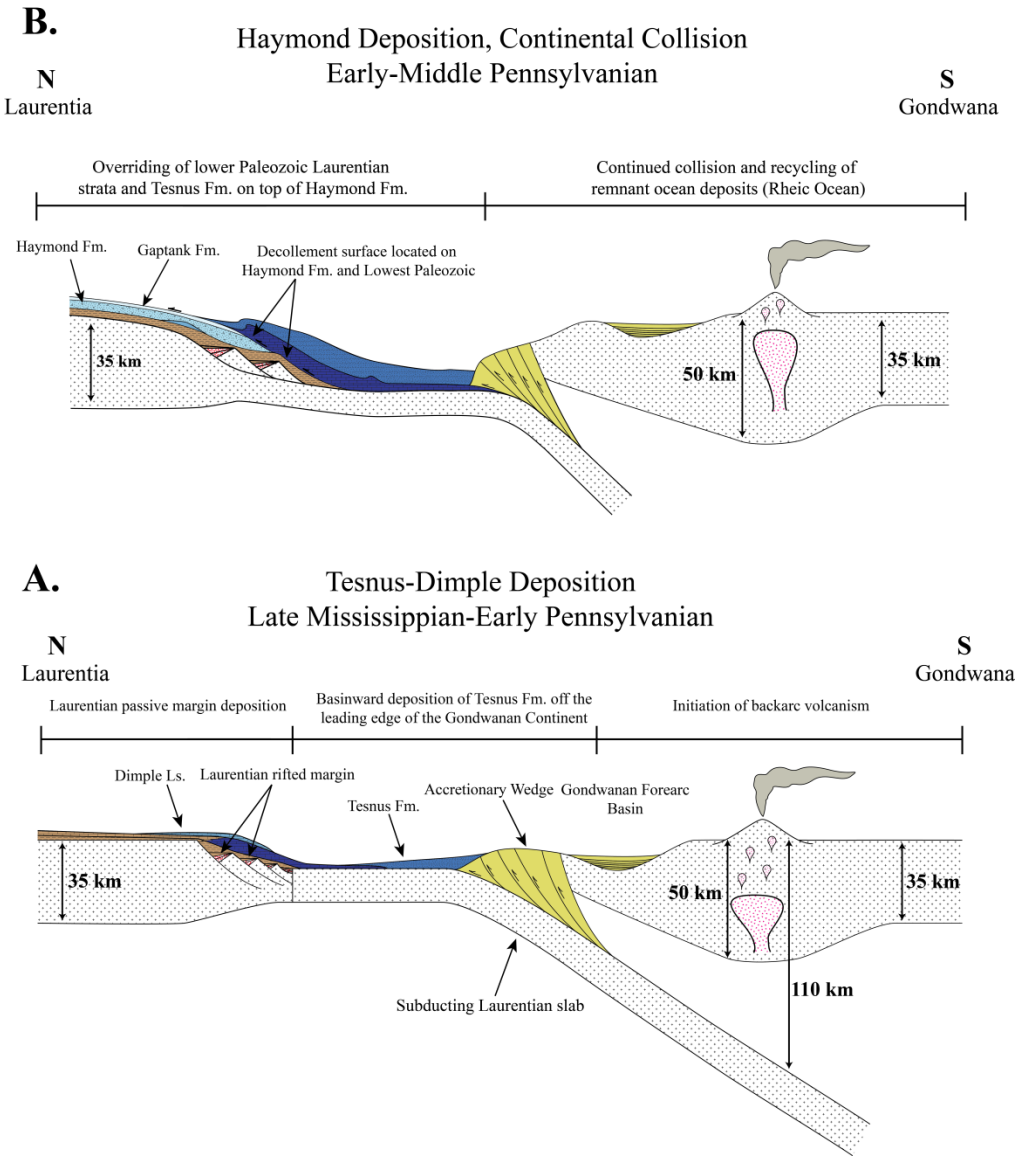

Figure 18 ct: Tectonostratigraphic reconstruction of the evolving Laurentian-Gondwanan margin throughout the Mississippian-middle Permian based on DZ U-Pb data. A. Pre-collisional deposition of Tesnus Formation on the leading edge of approaching Gondwanan continent, deposition of thin-bedded limestone, shale, and chert. B. Initial deposition of the Haymond Formation during continental collision. C. Collision of Laurentia and Gondwana, incorporation of rifted Laurentian crust through crustal duplexing. D. Post-collisional figure representing tectonic quiescence, sediment supply from deeper within the Gondwanan hinterland, supporting progradation of stable clinoforms along the southern margin of the Delaware Basin.

REFERENCE CITED

Anderson, J., Bender, E., Anderson, R., Bauer, P., Robertson, J., Bowring, S., . . . Grambling, J. (1993). Transcontinental Proterozoic provinces. *The Geology of North America, 2*, 171-334.

Anderson, J., & Morrison, J. (1992). The role of anorogenic granites in the Proterozoic crustal development of North America *Developments in Precambrian Geology* (Vol. 10, pp. 263-299): Elsevier.

Anthony, J. M. (2015). *Provenance of the Middle Permian, Delaware Mountain Group: Delaware basin, southeast New Mexico and West Texas.* Texas Christian University.

Arbenz, J., Hatcher, R., Thomas, W., & Viele, G. (1989). Ouachita thrust belt and Arkoma basin. *The Appalachian-Ouachita Orogen in the United States*, 621-634.

Arbenz, J. K. (1989). The Ouachita system. *The geology of North America—An overview: Geological Society of America, The Geology of North America, v. A*, 371-396.

Bande, A., Horton, B. K., Ramírez, J. C., Mora, A., Parra, M., & Stockli, D. F. (2012). Clastic deposition, provenance, and sequence of Andean thrusting in the frontal Eastern Cordillera and Llanos foreland basin of Colombia. *Bulletin, 124*(1-2), 59-76.

Barnaby, R. J., Oetting, G. C., & Gao, G. (2004). Strontium isotopic signatures of oil-field waters: Applications for reservoir characterization. *Aapg Bulletin, 88*(12), 1677-1704.

Beck, J. W., & Murthy, V. R. (1991). *Evidence for continental crustal assimilation in the Hemlock Formation flood basalts of the early Proterozoic Penokean Orogen, Lake Superior region*: US Department of the Interior, US Geological Survey.

Becker, T. P., Thomas, W. A., & Gehrels, G. E. (2006). Linking late Paleozoic sedimentary provenance in the Appalachian basin to the history of Alleghanian deformation. *American Journal of Science, 306*(10), 777-798.

Becker, T. P., Thomas, W. A., Samson, S. D., & Gehrels, G. E. (2005). Detrital zircon evidence of Laurentian crustal dominance in the lower Pennsylvanian deposits of the Alleghanian clastic wedge in eastern North America. *Sedimentary Geology, 182*(1-4), 59-86.

Bickford, M., Van, W., & Zietz, I. (1986). Proterozoic history of the midcontinent region of North America. *Geology, 14*(6), 492-496.

Capaldi, T. N., Horton, B. K., McKenzie, N. R., Stockli, D. F., & Odlum, M. L. (2017). Sediment provenance in contractional orogens: The detrital zircon record from modern rivers in the Andean fold-thrust belt and foreland basin of western Argentina. *Earth and Planetary Science Letters, 479*, 83-97.

Cawood, P. A., McCausland, P. J., & Dunning, G. R. (2001). Opening Iapetus: constraints from the Laurentian margin in Newfoundland. *Geological Society of America Bulletin, 113*(4), 443-453.

Centeno-García, E., Gehrels, G., & Talavera-Mendoza, O. (2005). *Zircon provenance of Triassic (Paleozoic?) turbidites from central and western Mexico: Implications for the early evolution of the Guerrero arc [abs.]*. Paper presented at the Geological Society of America Abstracts with Program.

Colleps, C. L., McKenzie, N. R., Stockli, D. F., Hughes, N. C., Singh, B. P., Webb, A. A. G., . . . Horton, B. K. (2018). Zircon (U-Th)/He Thermochronometric Constraints on Himalayan Thrust Belt Exhumation, Bedrock Weathering, and Cenozoic Seawater Chemistry. *Geochemistry, Geophysics, Geosystems, 19*(1), 257-271.

Cordani, U. G., & Teixeira, W. (2007). Proterozoic accretionary belts in the Amazonian Craton. *Geological Society of America Memoirs, 200*, 297-320.

Cordani, U. G., Teixeira, W., D'Agrella-Filho, M., & Trindade, R. (2009). The position of the Amazonian Craton in supercontinents. *Gondwana Research, 15*(3-4), 396-407.

DeCelles, P. G., Gehrels, G. E., Quade, J., & Ojha, T. (1998). Eocene-early Miocene foreland basin development and the history of Himalayan thrusting, western and central Nepal. *Tectonics, 17*(5), 741-765.

DeCelles, P. G., & Giles, K. A. (1996). Foreland basin systems. *Basin research, 8*(2), 105-123.

DeMis, W. D. (1983). Geology of the Hell's Half Acre, Marathon Basin, Texas.

Denison, R., Burke, W., Otto, J., Hetherington, E., & Stone, C. (1977). *Age of igneous and metamorphic activity affecting the Ouachita foldbelt.* Paper presented at the Symposium on the geology of the Ouachita Mountains.

Denison, R. E., Kenny, G. S., BURKE JR, W. H., & HETHERINGTON JR, E. A. (1969). Isotopic ages of igneous and metamorphic boulders from the Haymond Formation (Pennsylvanian), Marathon Basin, Texas, and their significance. *Geological Society of America Bulletin, 80*(2), 245-256.

Dickinson, W. R. (1985). Interpreting provenance relations from detrital modes of sandstones *Provenance of arenites* (pp. 333-361): Springer.

Dickinson, W. R. (1988). Provenance and sediment dispersal in relation to paleotectonics and paleogeography of sedimentary basins *New perspectives in basin analysis* (pp. 3-25): Springer.

Dickinson, W. R., & Gehrels, G. E. (2003). U–Pb ages of detrital zircons from Permian and Jurassic eolian sandstones of the Colorado Plateau, USA: paleogeographic implications. *Sedimentary Geology, 163*(1-2), 29-66.

Dickinson, W. R., & Gehrels, G. E. (2009). Use of U–Pb ages of detrital zircons to infer maximum depositional ages of strata: a test against a Colorado Plateau Mesozoic database. *Earth and Planetary Science Letters, 288*(1-2), 115-125.

Dickinson, W. R., & Lawton, T. F. (2001). Carboniferous to Cretaceous assembly and fragmentation of Mexico. *Geological Society of America Bulletin, 113*(9), 1142-1160.

Dickinson, W. R., & Lawton, T. F. (2003). Sequential intercontinental suturing as the ultimate control for Pennsylvanian Ancestral Rocky Mountains deformation. *Geology, 31*(7), 609-612.

Dickinson, W. R., Soreghan, M., & Gehrels, G. (2000). Geodynamic interpretation of Paleozoic tectonic trends oriented oblique to the Mesozoic Klamath-Sierran continental margin in California. *SPECIAL PAPERS-GEOLOGICAL SOCIETY OF AMERICA*, 209-246.

Dickinson, W. R., & Suczek, C. A. (1979). Plate tectonics and sandstone compositions. *Aapg Bulletin, 63*(12), 2164-2182.

Dutton, S. P., Flanders, W. A., & Barton, M. D. (2003). Reservoir characterization of a Permian deep-water sandstone, East Ford field, Delaware basin, Texas. *Aapg Bulletin, 87*(4), 609-627.

Eriksson, K. A., Campbell, I. H., Palin, J. M., & Allen, C. M. (2003). Predominance of Grenvillian magmatism recorded in detrital zircons from modern Appalachian rivers. *The Journal of Geology, 111*(6), 707-717.

Ewing, T., 2016, Texas Through Time: Lone Star Geology, Landscapes, and Resources, The University of Texas at Austin, Bureau of Economic Geology Udden Series No. 6, 431 p.:

Fedo, C. M., Sircombe, K. N., & Rainbird, R. H. (2003). Detrital zircon analysis of the sedimentary record. *Reviews in Mineralogy and Geochemistry, 53*(1), 277-303.

Fischer, A. G., & Sarnthein, M. (1988). Airborne silts and dune-derived sands in the Permian of the Delaware Basin. *Journal of Sedimentary Research, 58*(4), 637-643.

Galley, J. E. (1958). Oil and geology in the Permian basin of Texas and New Mexico: North America.

Gardner, M. H., Borer, J. M., Melick, J. J., Mavilla, N., Dechesne, M., & Wagerle, R. N. (2003). Stratigraphic process-response model for submarine channels and related features from studies of Permian Brushy Canyon outcrops, West Texas. *Marine and Petroleum Geology*, *20*(6-8), 757-787.

Gehrels, G. (2011). Detrital zircon U-Pb geochronology: Current methods and new opportunities. *Tectonics of sedimentary basins: Recent advances*, 45-62.

Gehrels, G. (2014). Detrital zircon U-Pb geochronology applied to tectonics. *Annual Review of Earth and Planetary Sciences*, *42*, 127-149.

Gehrels, G., Kapp, P., DeCelles, P., Pullen, A., Blakey, R., Weislogel, A., . . . McQuarrie, N. (2011). Detrital zircon geochronology of pre-Tertiary strata in the Tibetan-Himalayan orogen. *Tectonics*, *30*(5).

Gehrels, G. E., Blakey, R., Karlstrom, K. E., Timmons, J. M., Dickinson, B., & Pecha, M. (2011). Detrital zircon U-Pb geochronology of Paleozoic strata in the Grand Canyon, Arizona. *Lithosphere, 3*(3), 183-200.

Gehrels, G. E., Valencia, V. A., & Ruiz, J. (2008). Enhanced precision, accuracy, efficiency, and spatial resolution of U-Pb ages by laser ablation–multicollector–inductively coupled plasma–mass spectrometry. *Geochemistry, Geophysics, Geosystems*, *9*(3).

Geraldes, M. C., Van Schmus, W. R., Condie, K. C., Bell, S., Teixeira, W., & Babinski, M. (2001). Proterozoic geologic evolution of the SW part of the Amazonian Craton in Mato Grosso state, Brazil. *Precambrian Research, 111*(1-4), 91-128.

Giles, J. M., Soreghan, M. J., Benison, K. C., Soreghan, G. S., & Hasiotis, S. T. (2013). Lakes, loess, and paleosols in the Permian Wellington Formation of Oklahoma, USA: implications for paleoclimate and paleogeography of the Midcontinent. *Journal of Sedimentary Research, 83*(10), 825-846.

Gillis, R. J., Gehrels, G. E., Ruiz, J., & de Dios Gonzaléz, L. A. F. (2005). Detrital zircon provenance of Cambrian–Ordovician and Carboniferous strata of the Oaxaca terrane, southern Mexico. *Sedimentary Geology, 182*(1-4), 87-100.

Glasspool, I., Wittry, J., Quick, K., Kerp, H., & Hilton, J. (2013). A preliminary report on a Wolfcampian age floral assemblage from the type section for the Neal ranch Formation in the Glass Mountains, Texas. *The Carboniferous–Permian Transition. New Mexico Museum of Natural History and Science Bulletin, 60*, 98-102.

Gleason, J. D., Gehrels, G. E., Dickinson, W. R., Patchett, P. J., & Kring, D. A. (2007). Laurentian sources for detrital zircon grains in turbidite and deltaic sandstones of the Pennsylvanian Haymond Formation, Marathon assemblage, west Texas, USA. *Journal of Sedimentary Research, 77*(11), 888-900.

Graham, S., Tolson, R., DeCelles, P., Ingersoll, R., Bargar, E., Caldwell, M., . . . Handschy, J. (1986). Provenance modeling as a technique for analyzing source terrane evolution and controls on foreland sedimentation. *Foreland basins, 8*, 425-436.

Gross, E. L., Stewart, J. H., & Gehrels, G. E. (2000). Detrital zircon geochronology of Neoproterozoic to Middle Cambrian miogeoclinal and platformal strata: Northwest Sonora, Mexico. *Geofísica Internacional, 39*(4), 295-308.

Haneef, M., Rohr, D., & Wardlaw, B. (2000). A deep water turbidity origin for the Altuda Formation (Capitanian, Permian), Northwest Glass Mountains, Texas. *Smithsonian Contributions to Earth Sciences, 32*, 319-332.

Hanson, R. E., Roberts, J. M., Dickerson, P. W., & Fanning, C. M. (2016). Cryogenian intraplate magmatism along the buried southern Laurentian margin: Evidence from volcanic clasts in Ordovician strata, Marathon uplift, west Texas. *Geology, 44*(7), 539-542.

Harms, J., Williamson, C., & Mazzullo, S. (1988). Deep-water density current deposits of the Delaware Mountain Group, Delaware Basin. *The Geologic Evolution of the Permian Basin: SEPM, Permian Basin Section*, 34-36.

Harris, M., Lehrmann, D., & Lambert, L. (2000). *Comparison of the depositional environments and physical stratigraphy of the Cutoff Formation (Guadalupe Mountains) and the Road Canyon Formation (Glass Mountains): Lowermost Guadalupian (Permian) of West Texas.* Paper presented at the The Guadalupian symposium, Smithsonian contributions to the Earth sciences.

Hart, N. R., Stockli, D. F., & Hayman, N. W. (2016). Provenance evolution during progressive rifting and hyperextension using bedrock and detrital zircon U-Pb geochronology, Mauléon Basin, western Pyrenees. *Geosphere, 12*(4), 1166-1186.

Hatcher Jr, R. D., Thomas, W. A., & Viele, G. W. (1989). *The Appalachian-Ouachita Orogen in the United States*: Geological Society of America.

Haughton, P., Todd, S., & Morton, A. (1991). Sedimentary provenance studies. *Geological Society, London, Special Publications, 57*(1), 1-11.

Heatherington, A., Mueller, P., & Nutman, A. (1996). Neoproterozoic magmatism in the Suwannee terrane: Implications for terrane correlation. *Geological Society of America Special Papers, 304*, 257-268.

Hibbard, J. P., Stoddard, E. F., Secor, D. T., & Dennis, A. J. (2002). The Carolina Zone: overview of Neoproterozoic to Early Paleozoic peri-Gondwanan terranes along the eastern flank of the southern Appalachians. *Earth-Science Reviews, 57*(3-4), 299-339.

Hickman, R. G., Varga, R. J., & Altany, R. M. (2009). Structural style of the Marathon thrust belt, west Texas. *Journal of Structural Geology, 31*(9), 900-909.

Hills, J. M. (1984). Sedimentation, tectonism, and hydrocarbon generation in Delaware basin, west Texas and southeastern New Mexico. *Aapg Bulletin, 68*(3), 250-267.

Hoffman, P. F., Bally, A., & Palmer, A. (1989). Precambrian geology and tectonic history of North America. *The geology of North America—an overview*, 447-512.

Holm, D., Anderson, R., Boerboom, T., Cannon, W., Chandler, V., Jirsa, M., . . . Van Schmus, W. (2007). Reinterpretation of Paleoproterozoic accretionary boundaries of the north-central United States based on a new aeromagnetic-geologic compilation. *Precambrian Research, 157*(1-4), 71-79.

Horak, R. L. (1985). Trans-Pecos tectonism and its affects on the Permian Basin. *Structure and Tectonics of Trans-Pecos Texas: Midland, Texas, West Texas Geological Society*, 81-87.

Horton, B. K., Saylor, J. E., Nie, J., Mora, A., Parra, M., Reyes-Harker, A., & Stockli, D. F. (2010). Linking sedimentation in the northern Andes to basement configuration, Mesozoic extension, and Cenozoic shortening: Evidence from detrital zircon U-Pb ages, Eastern Cordillera, Colombia. *Bulletin, 122*(9-10), 1423-1442.

Hull Jr, J. P. (1957). Petrogenesis of Permian Delaware Mountain Sandstone, Texas and New Mexico. *Aapg Bulletin, 41*(2), 278-307.

Ingersoll, R. V. (2011). Tectonics of sedimentary basins, with revised nomenclature. *Tectonics of sedimentary basins: Recent advances*, 1-43.

Ingersoll, R. V., Kretchmer, A. G., & Valles, P. K. (1993). The effect of sampling scale on actualistic sandstone petrofacies. *Sedimentology, 40*(5), 937-953.

Jackson, S. E., Pearson, N. J., Griffin, W. L., & Belousova, E. A. (2004). The application of laser ablation-inductively coupled plasma-mass spectrometry to in situ U–Pb zircon geochronology. *Chemical Geology, 211*(1-2), 47-69.

Janson, X., and Hairabian, A., 2016, Guadalupian Stratigraphy and Slope Systems in the Southern Delaware Basin, Glass Mountains: RCRL Annual Sponsors Field Trip Guidebook, p. 79.

Jordan, T. E., Flemings, P. B., & Beer, J. A. (1988). Dating thrust-fault activity by use of foreland-basin strata *New perspectives in basin analysis* (pp. 307-330): Springer.

Keller, G., Lidiak, E., Hinze, W., & Braile, L. (1983). The role of rifting in the tectonic development of the midcontinent, USA *Developments in Geotectonics* (Vol. 19, pp. 391-412): Elsevier.

Keppie, J. D. (2004). Terranes of Mexico revisited: A 1.3 billion year odyssey. *International Geology Review*, *46*(9), 765-794.

Keppie, J. D., Dostal, J., Murphy, J. B., & Nance, R. D. (2008). Synthesis and tectonic interpretation of the westernmost Paleozoic Variscan orogen in southern Mexico: From rifted Rheic margin to active Pacific margin. *Tectonophysics*, *461*(1-4), 277-290.

Keppie, J. D., Nance, R., Fernández-Suárez, J., Storey, C. D., Jeffries, T. E., & Murphy, J. B. (2006). Detrital zircon data from the Eastern Mixteca Terrane, Southern Mexico: evidence for an Ordovician—Mississippian continental rise and a Permo-Triassic clastic wedge adjacent to Oaxaquia. *International Geology Review*, *48*(2), 97-111.

King, P. B. (1930). *The geology of the Glass Mountains, Texas*: University of Texas at Austin.

King, P. B. (1937). *Geology of the Marathon region, Texas* (2330-7102). Retrieved from

King, P. B. (1958). Problems of Boulder Beds of Haymond Formation, Marathon Basin, Texas: DISCUSSION. *Aapg Bulletin*, *42*(7), 1731-1734.

King, P. B. (1978). Tectonics and sedimentation of the Paleozoic rocks in the Marathon region, west Texas. *Tectonics and Paleozoic facies of the Marathon geosyncline, West Texas: Society of Economic Paleontologists and Mineralogists, Permian Basic Section, Publication*(78-17), 5-38.

Kocurek, G., & Kirkland, B. L. (1998). Getting to the source: aeolian influx to the Permian Delaware basin region. *Sedimentary Geology*, *117*(3-4), 143-149.

Lambert, L. L., Lehrmann, D. J., Harris, M. T., Wardlaw, B., Grant, R., & Rohr, D. (2000). *Correlation of the Road Canyon and Cutoff formations, West Texas, and its relevance to establishing an international Middle Permian (Guadalupian) series.* Paper presented at the The Guadalupian Symposium. Smithsonian Contributions to the Earth Sciences.

Lambert, L. L., Wardlaw, B. R., Nestell, M. K., & Nestell, G. P. (2002). Latest Guadalupian (middle Permian) conodonts and foraminifers from West Texas. *Micropaleontology*, 343-364.

Lawton, T., Pindell, J., Beltran-Triviño, A., Juárez-Arriaga, E., Molina-Garza, R., & Stockli, D. (2015). Late Cretaceous-Paleogene Foreland Sediment-Dispersal Systems in Northern and Eastern Mexico: Interpretations From Preliminary Detrital-Zircon Analysis. *American Association of Petroleum Geologists Search and Discovery, article 30423*.

Li, Z.-X., Bogdanova, S., Collins, A., Davidson, A., De Waele, B., Ernst, R., . . . Jacobs, J. (2008). Assembly, configuration, and break-up history of Rodinia: a synthesis. *Precambrian Research, 160*(1-2), 179-210.

Link, P. K., Mahon, R. C., Beranek, L. P., Campbell-Stone, E. A., & Lynds, R. (2014). Detrital zircon provenance of Pennsylvanian to Permian sandstones from the Wyoming craton and Wood River Basin, Idaho, USA. *Rocky Mountain Geology, 49*(2), 115-136.

Lopez, R., Cameron, K., & Jones, N. W. (2001). Evidence for Paleoproterozoic, Grenvillian, and Pan-African age Gondwanan crust beneath northeastern Mexico. *Precambrian Research, 107*(3-4), 195-214.

Martens, U., Weber, B., & Valencia, V. A. (2010). U/Pb geochronology of Devonian and older Paleozoic beds in the southeastern Maya block, Central America: Its affinity with peri-Gondwanan terranes. *Bulletin, 122*(5-6), 815-829.

McBride, E., Hatcher, R., Thomas, W., & Viele, G. (1989). Stratigraphy and sedimentary history of pre-Permian Paleozoic rocks of the Marathon uplift. *The Geology of North America, 2*, 603-620.

McKee, J. W., Jones, N. W., Anderson, T. H., Bartolini, C., Wilson, J., & Lawton, T. (1999). Late Paleozoic and early Mesozoic history of the Las Delicias terrane, Coahuila, Mexico. *SPECIAL PAPERS-GEOLOGICAL SOCIETY OF AMERICA*, 161-190.

Moecher, D. P., & Samson, S. D. (2006). Differential zircon fertility of source terranes and natural bias in the detrital zircon record: Implications for sedimentary provenance analysis. *Earth and Planetary Science Letters, 247*(3-4), 252-266.

Muehlberger, W., & Tauvers, P. (1989). Marathon fold-thrust belt, west Texas. *The Appalachian–Ouachita orogen in the United States: Boulder, Colorado, Geological Society of America, 2*, 673-680.

Mueller, P. A., Heatherington, A. L., Wooden, J. L., Shuster, R. D., Nutman, A. P., & Williams, I. S. (1994). Precambrian zircons from the Florida basement: A Gondwanan connection. *Geology, 22*(2), 119-122.

Murphy, J. B., Pisarevsky, S. A., Nance, R. D., & Keppie, J. D. (2004). Neoproterozoic—Early Paleozoic evolution of peri-Gondwanan terranes: implications for Laurentia-Gondwana connections. *International Journal of Earth Sciences, 93*(5), 659-682.

Nicholas, R., Waddell, D., Hatcher, R., Thomas, W., & Viele, G. (1989). The Ouachita system in the subsurface of Texas, Arkansas, and Louisiana. *The Appalachian-Ouachita Orogen in the United States*, 661-672.

Nicholas, R. L., & Rozendal, R. A. (1975). Subsurface positive elements within Ouachita foldbelt in Texas and their relation to Paleozoic cratonic margin. *Aapg Bulletin, 59*(2), 193-216.

Olszewski, T. D., & Erwin, D. H. (2009). Change and stability in Permian brachiopod communities from western Texas. *Palaios, 24*(1), 27-40.

Opdyke, N. D., Jones, D. S., MacFadden, B. J., Smith, D. L., Mueller, P. A., & Shuster, R. D. (1987). Florida as an exotic terrane: Paleomagnetic and geochronologic

investigation of lower Paleozoic rocks from the subsurface of Florida. *Geology, 15*(10), 900-903.

Park, H., Barbeau Jr, D. L., Rickenbaker, A., Bachmann-Krug, D., & Gehrels, G. (2010). Application of foreland basin detrital-zircon geochronology to the reconstruction of the southern and central Appalachian orogen. *The Journal of Geology, 118*(1), 23-44.

Patchett, P., Embry, A., Ross, G., Beauchamp, B., Harrison, J., Mayr, U., . . . Spence, G. (2004). Sedimentary cover of the Canadian Shield through Mesozoic time reflected by Nd isotopic and geochemical results for the Sverdrup Basin, Arctic Canada. *The Journal of Geology, 112*(1), 39-57.

Paton, C., Hellstrom, J., Paul, B., Woodhead, J., & Hergt, J. (2011). Iolite: Freeware for the visualisation and processing of mass spectrometric data. *Journal of Analytical Atomic Spectrometry, 26*(12), 2508-2518.

Petrus, J. A., & Kamber, B. S. (2012). VizualAge: A novel approach to laser ablation ICP-MS U-Pb geochronology data reduction. *Geostandards and Geoanalytical Research, 36*(3), 247-270.

Poole, F. G., Perry, W. J., Madrid, R. J., & Amaya-Martínez, R. (2005). Tectonic synthesis of the Ouachita-Marathon-Sonora orogenic margin of southern Laurentia: Stratigraphic and structural implications for timing of deformational events and plate-tectonic model. *Geological Society of America Special Papers, 393*, 543-596.

Pyles, D. R., Jennette, D. C., Tomasso, M., Beaubouef, R. T., & Rossen, C. (2010). Concepts learned from a 3D outcrop of a sinuous slope channel complex: Beacon Channel Complex, Brushy Canyon Formation, West Texas, USA. *Journal of Sedimentary Research, 80*(1), 67-96.

Rainbird, R. H., Hearnan, L. M., & Young, G. (1992). Sampling Laurentia: Detrital zircon geochronology offers evidence for an extensive Neoproterozoic river system originating from the Grenville orogen. *Geology, 20*(4), 351-354.

Rainbird, R. H., McNicoll, V., Theriault, R., Heaman, L., Abbott, J., Long, D., & Thorkelson, D. (1997). Pan-continental river system draining Grenville Orogen recorded by U-Pb and Sm-Nd geochronology of Neoproterozoic quartzarenites and mudrocks, northwestern Canada. *The Journal of Geology, 105*(1), 1-17.

Rathjen, J. D. (1993). Microfacies and depositional environment of the Word Formation (Permian) Glass Mountains, Texas. *Geological Society of America, Abstracts with Programs;(United States), 25*(CONF-9303212--).

Reed, T., & Strickler, D. (1990). *Structural geology and petroleum exploration of the Marathon thrust belt, West Texas.* Paper presented at the Marathon Thrust Belt: Structure, Stratigraphy, and Hydrocarbon Potential. In: Higgins, L.(Ed.),, West Texas Geological Society and Permian Basin Section SEPM Field Seminar May 10e12.

Richards, B. C. (2013). Current status of the International Carboniferous time scale. *The Carboniferous-Permian Transition, Bulletin, 60*, 348-353.

Rodriguez, E., Dickerson, P., & Stockli, D. (2017). *New Zircon U-Pb Age Constrain of the Origin of Devil's River Uplift (SW Texas) and Insights into the Late Proterozoic and Paleozoic Evolution of the Southern Margin of Laurentia.* Paper presented at the AGU Fall Meeting Abstracts.

Ross, C. A. (1986). Paleozoic evolution of southern margin of Permian basin. *Geological Society of America Bulletin, 97*(5), 536-554.

Rossen, C., & Sarg, J. (1987). Sedimentology and regional correlation of a basinally restricted deepwater siliciclastic wedge: Brushy Canyon Formation-Cherry Canyon Tongue (Lower Guadalupian), Delaware basin. *AAPG (Am. Assoc. Pet. Geol.) Bull.;(United States), 71*(CONF-870606-).

Sacks, P. E., & Secor, D. T. (1990). Kinematics of late Paleozoic continental collision between Laurentia and Gondwana. *Science, 250*(4988), 1702-1705.

Samson, S. D., D'Lemos, R. S., Miller, B. V., & Hamilton, M. A. (2005). Neoproterozoic palaeogeography of the Cadomia and Avalon terranes: constraints from detrital zircon U–Pb ages. *Journal of the Geological Society, 162*(1), 65-71.

Sánchez-Bettucci, L., & Rapalini, A. E. (2002). Paleomagnetism of the Sierra de Las Animas Complex, southern Uruguay: its implications in the assembly of western Gondwana. *Precambrian Research, 118*(3), 243-265.

Santos, J. d. (2003). Geotectônica dos escudos das Guianas e Brasil-Central. *Geologia, Tectônica e Recusrsos Minerais do Brasil (texto, mapas & SIG). Brasília, Serviço Geológico do Brasil–CPRM/MME*, 169-226.

Satkoski, A. M., Wilkinson, B. H., Hietpas, J., & Samson, S. D. (2013). Likeness among detrital zircon populations—An approach to the comparison of age frequency data in time and space. *Bulletin, 125*(11-12), 1783-1799.

Sharman, G. R., Graham, S. A., Grove, M., Kimbrough, D. L., & Wright, J. E. (2015). Detrital zircon provenance of the Late Cretaceous–Eocene California forearc: Influence of Laramide low-angle subduction on sediment dispersal and paleogeography. *Bulletin, 127*(1-2), 38-60.

Sharman, G. R., Sharman, J. P., & Sylvester, Z. detritalPy: A Python-based Toolset for Visualizing and Analyzing Detrital Geo-Thermochronologic Data. *The Depositional Record*.

Sims, P., Schmus, W. V., Schulz, K., & Peterman, Z. (1989). Tectono-stratigraphic evolution of the Early Proterozoic Wisconsin magmatic terranes of the Penokean Orogen. *Canadian Journal of Earth Sciences, 26*(10), 2145-2158.

Soreghan, G. S., & Soreghan, M. J. (2013). Tracing Clastic Delivery To the Permian Delaware Basin, USA: Implications For Paleogeography and Circulation In Westernmost Equatorial PangeaTRACING CLASTIC DISPERSAL TO THE WESTERNMOST PANGEAN SUTURE. *Journal of Sedimentary Research, 83*(9), 786-802.

Steiner, M., & Walker, J. D. (1996). Late Silurian plutons in Yucatan. *Journal of Geophysical Research: Solid Earth, 101*(B8), 17727-17735.

Steiner, M. B., & Anderson, T. (2005). Pangean reconstruction of the Yucatan Block: Its Permian, Triassic, and Jurassic geologic and tectonic history. *SPECIAL PAPERS-GEOLOGICAL SOCIETY OF AMERICA, 393*, 457.

Stewart, J. H., Gehrels, G. E., Barth, A. P., Link, P. K., Christie-Blick, N., & Wrucke, C. T. (2001). Detrital zircon provenance of Mesoproterozoic to Cambrian arenites in the western United States and northwestern Mexico. *Geological Society of America Bulletin, 113*(10), 1343-1356.

Stockli, D. F. (2013). Unlocking provenance secrets from single detrital zircons by U-Pb and trace-element depth-profile laser-ablation-split-stream ICP-MS analysis and (U-Th). *He double dating: Geological Society of America Abstracts with Programs, 45*(7), 0.

Talavera-Mendoza, O., Ruiz, J., Gehrels, G. E., Meza-Figueroa, D. M., Vega-Granillo, R., & Campa-Uranga, M. F. (2005). U–Pb geochronology of the Acatlán Complex and implications for the Paleozoic paleogeography and tectonic evolution of southern Mexico. *Earth and Planetary Science Letters, 235*(3-4), 682-699.

Tauvers, P. R. (1988). Basement-influenced deformation in the Marathon fold-thrust belt, west Texas. *The Journal of Geology, 96*(5), 577-590.

Thomas, W. A. (2006). Tectonic inheritance at a continental margin. *GSA today, 16*(2), 4-11.

Thomas, W. A. (2011a). Detrital-zircon geochronology and sedimentary provenance. *Lithosphere, 3*(4), 304-308.

Thomas, W. A. (2011b). The Iapetan rifted margin of southern Laurentia. *Geosphere, 7*(1), 97-120.

Thomas, W. A. (2014). A mechanism for tectonic inheritance at transform faults of the Iapetan margin of Laurentia. *Geoscience Canada, 41*(3), 321-344.

Thomas, W. A., Astini, R. A., & Bayona, G. (2002). Ordovician collision of the Argentine Precordillera with Gondwana, independent of Laurentian Taconic orogeny. *Tectonophysics, 345*(1-4), 131-152.

Thomson, A., & McBride, E. F. (1964). *Summary of the geologic history of the Marathon geosyncline.* Paper presented at the Permian Basin Section-SEPM Field Trip Symposium and Guidebook Publication.

Thomson, K. D., Stockli, D. F., Clark, J. D., Puigdefàbregas, C., & Fildani, A. (2017). Detrital zircon (U-Th)/(He-Pb) double-dating constraints on provenance and foreland basin evolution of the Ainsa Basin, south-central Pyrenees, Spain. *Tectonics, 36*(7), 1352-1375.

Tohver, E., Van der Pluijm, B., Van der Voo, R., Rizzotto, G., & Scandolara, J. (2002). Paleogeography of the Amazon craton at 1.2 Ga: early Grenvillian collision with the Llano segment of Laurentia. *Earth and Planetary Science Letters, 199*(1), 185-200.

Vermeesch, P. (2004). How many grains are needed for a provenance study? *Earth and Planetary Science Letters, 224*(3-4), 441-451.

Vermeesch, P. (2012). On the visualisation of detrital age distributions. *Chemical Geology, 312*, 190-194.
Vermeesch, P. (2013). Multi-sample comparison of detrital age distributions. *Chemical Geology, 341*, 140-146.
Viele, G., Thomas, W., & Hatcher, R. (1989). Tectonic synthesis of the Ouachita orogenic belt. *The Appalachian-Ouachita orogen in the United States: Boulder, Colorado, Geological Society of America, Geology of North America, 2*, 695-728.
Walper, J. L. (1982). Plate tectonic evolution of the Fort Worth Basin.
Wardlaw, B. R. (2000). *Guadalupian conodont biostratigraphy of the Glass and Del Norte Mountains.* Paper presented at the The Guadalupian Symposium.
Weber, B., Schaaf, P., Valencia, V. A., Iriondo, A., & Ortega-Gutiérrez, F. (2006). Provenance ages of late Paleozoic sandstones (Santa Rosa Formation) from the Maya Block, SE México: implications on the tectonic evolution of western Pangea. *Revista mexicana de ciencias geológicas, 23*(3), 262-276.
Weber, B., Valencia, V. A., Schaaf, P., Pompa-Mera, V., & Ruiz, J. (2008). Significance of provenance ages from the Chiapas Massif Complex (southeastern Mexico): redefining the Paleozoic basement of the Maya Block and its evolution in a peri-Gondwanan realm. *The Journal of Geology, 116*(6), 619-639.
Wortman, G. L., Samson, S. D., & Hibbard, J. P. (2000). Precise U-Pb zircon constraints on the earliest magmatic history of the Carolina terrane. *The Journal of Geology, 108*(3), 321-338.
Xie, X., Anthony, J. M., & Busbey, A. B. (2018). Provenance of Permian Delaware Mountain Group, central and southern Delaware Basin, and implications of sediment dispersal pathway near the southwestern terminus of Pangea. *International Geology Review*, 1-20.
Xie, X., O'Connor, P. M., & Alsleben, H. (2016). Carboniferous sediment dispersal in the Appalachian–Ouachita juncture: Provenance of selected late Mississippian sandstones in the Black Warrior Basin, Mississippi, United States. *Sedimentary Geology, 342*, 191-201.
Xu, J., Stockli, D. F., & Snedden, J. W. (2017). Enhanced provenance interpretation using combined U–Pb and (U–Th)/He double dating of detrital zircon grains from lower Miocene strata, proximal Gulf of Mexico Basin, North America. *Earth and Planetary Science Letters, 475*, 44-57.
Yang, K.-M., & Dorobek, S. L. (1995). The Permian basin of west Texas and New Mexico: tectonic history of a" composite" foreland basin and its effects on stratigraphic development. *Stratigraphic evolution of foreland basins: SEPM Special Publication, 52*, 149-174.
Yang, Z., & Yancey, T. (2000). Fusulinid biostratigraphy and paleontology of the Middle Permian (Guadalupian) strata of the Glass Mountains and Del Norte Mountains, west Texas. *Smithsonian Contributions to the Earth Sciences, 32*, 185-259.